Heinrich Heine
Universität
Düsseldorf

Metalloproteins as Sustainable Biocatalysts

Enhancement and Characterization of Different Systems for Effective Catalytic Applications

Inaugural-Dissertation

zur Erlangung des Doktorgrades der
Mathematisch-Naturwissenschaftlichen Fakultät der
Heinrich-Heine-Universität Düsseldorf

vorgelegt von
Steffen Mielenbrink
aus Wuppertal

Düsseldorf, Juni 2021

aus dem Institut für Physikalische Biologie
der Heinrich-Heine-Universität Düsseldorf

Gedruckt mit der Genehmigung der
Mathematisch-Naturwissenschaftlichen Fakultät der
Heinrich-Heine-Universität Düsseldorf

Referent: Jun.-Prof. Dr. Ingrid Span
Korreferent: Prof. Dr. Matias Zurbriggen

Tag der mündlichen Prüfung: 23.07.2021

Contents

Zusammenfassung

Metalloproteine vereinigen die Reaktivität von Metallen mit der Selektivität der Proteinumgebung. Hierbei können verschiedene Übergangsmetalle, wie beispielsweise Eisen und Kupfer, ähnliche biologische Rollen erfüllen, die von Elektronentransport bis hin zu Redox-Katalyse reichen. Evolutionär betrachtet, spielten Eisen-Schwefel-Proteine (Fe-S-Proteine) eine dominante Rolle in einer Zeit, bevor die Sauerstoffkonzentration anstieg. Die höhere Konzentration an Sauerstoff in der Luft führte dazu, dass die sauerstoffempfindlichen Kofaktoren teilweise von anderen Übergangsmetallen, wie Kupfer, ersetzt wurden. Trotzdem spielen Fe-S-Proteine, wie auch Kupferproteine, weiterhin eine zentrale Rolle in der Übertragung von Elektronen und der Katalyse von Redox-Prozessen. Die vorliegende Arbeit befasst sich mit der Untersuchung von Struktur und Funktion natürlich vorkommender Eisen- und Kupfer-haltigen Enzymen, sowie der Herstellung und Charakterisierung von artifiziellen Kobalt-Schwefel-Proteinen (Co-S-Proteinen). Der Fokus liegt insbesondere auf der Assemblierung natürlicher Fe-S- und artifizieller Co-S-Kofaktoren und ihrem Einbau in eine Proteinumgebung. Das Ziel ist es, die Funktionsweise natürlicher Redox-Katalysatoren zu verstehen und artifizielle Biokatalysatoren mit verbesserten Eigenschaften für biotechnologische Anwendungen herzustellen.

Der erste Artikel (Mielenbrink *et al.* (2020) Maturation of Fe–S Cluster Containing Proteins) beschreibt die systematische Untersuchung unterschiedlicher Maturierungsstrategien für verschiedene [4Fe-4S]-Proteine *in vitro* und *in vivo*. Bisher ist der Einfluss unterschiedlicher Strategien auf die Maturierung von Fe-S-Proteinen nicht detailiert untersucht worden. Hierzu wurde die Vollständigkeit des Cluster-Einbaus verschiedenster *in vivo* Syteme mit denen der auf Apo-Proteine angewendeten *in vitro* Methoden verglichen. Dazu zählen Expressionssysteme mit erhöhter Fe-S-Cluster Assemblierungsaktivität und chemische sowie semienzymatische Rekonstitution. Unsere Studien konnten zeigen, dass die erfolgreiche Synthese von Fe-S-Proteinen stark von der Maturierungsstrategie abhängen kann. Das zeigt, wie wichtig es ist, kein allgemeines Protokoll für die Entwicklung von Fe-S-Proteinen zu nutzen, um ein optimales Ergebnis aus der Herstellung von Fe-S-Proteinen zu erzielen. Hierdurch konnte die Isolierung des radical SAM-Enzyms ThnB, welches bisher nur *in vitro* maturiert werden konnte, entscheidend verbessert werden. Unsere Studien leisten darüber hinaus einen systematischen Beitrag zu der Entwicklung von Fe-S-Proteinen als nachhaltige Biokatalysatoren.

Der zweite Artikel (Mielenbrink *et al.* (2021) Co–S Cluster Assembly in Fe–S Proteins) präsentiert die erste *in vitro* Maturierung künstlicher Co-S-Cluster in verschiedenen Fe-S-Proteinen, sowie deren Cluster-Transfer-Interaktionen mit Zielproteinen. Künstliche Co-S-Proteine stehen im Verdacht zur effektiven biokatalytischen Gewinnung von Wasserstoff als Energiequelle genutzt werden zu können. Dazu wurde bakterielles Fe-S-Cluster-Gerüstprotein IscU aus verschiedenen Organismen verwendet, Co-S-Cluster *in vitro* mittels chemischer und semienzymatischer Rekonstitution zu assemblieren. Die spektroskopischen Eigenschaften dieser Cluster wurden charakterisiert und mit spektroskopischen Daten aus der Literatur verglichen, um Hinweise auf das Vorhandensein eines künstlichen Co-S-Clusters in IscU zu finden. Darüber hinaus wurden Punktmutationen dazu verwendet, den zusammengeset-

zten Co-S-Cluster für eine längere Zeit unter aeroben Bedingungen zu stabilisieren. In diesem Artikel präsentieren wir erste Hinweise dafür, dass Co-S-Cluster erstmalig in eine Proteinumgebung eingebaut wurden. Elektronenabsorptionsspektroskopie (EAS), Zirkulardichroismusspektroskopie (CD) und Massenspektrometrie mit induktiv gekoppeltem Plasma (ICP-MS) wurden dazu genutzt, Hinweise für die Existenz von Co-S-Clustern in IscU zu untermauern. Zusätzlich weisen erste Experimente darauf hin, dass diese Cluster sogar auf Zielproteine übertragen werden können. Dies ist ein entscheidender Schritt in Richtung effektiver biokatalytischer Gewinnung von Wasserstoff auf Co basierenden künstlichen Biokatalysatoren zur nachhaltigen Energiegewinnung.

Der dritte Artikel (Olbrich *et al.* (2021) Blue Multicopper Oxidases T1 Cu Axial Ligand Mutations) befasst sich auch mit einem nachhaltigen Biokatalysator: der Multikupfer Oxidase Ssl1. Diese Enzyme katalysieren die Ein-elektronen-oxidation von Substratmolekülen mit O_2 als Co-Substrat und H_2O als Nebenprodukt. In diesem Artikel untersuchen wir die Bedeutung des axialen Liganden von T1 Cu in Ssl1 für seine katalytische Aktivität in Bereichen des Umweltschutzes, wie z.B. der Detoxifizierung von Schadstoffen oder der Bioremediation, um die Möglichkeiten in der Anwendung zu erweitern. Fünf verschieden Mutationen des axialen Liganden wurden eingeführt und mit Elektronenspinresonanzspektroskopie, CD, EAS, sowie Kristallstrukturanalyse untersucht. Für alle fünf Varianten konnten wir die Kristallstruktur lösen, was uns detaillierte Informationen über die Abhängigkeiten der katalytischen Aktivität von strukturellen Veränderungen liefert. Die spektroskopischen Ergebnisse sowie Stopped-Flow Messungen untermauern die Wichtigkeit des axialen Liganden von T1 Cu in Ssl1 für seine katalytische Aktivität. Dieser Artikel fördert die Anwendungsmöglichkeiten dieser nachhaltigen Katalysatoren. Abschließend liefert die gesamte Arbeit interessante und wichtige Ergebnisse insbesondere auf dem Gebiet der Metalloproteine für den Einsatz als "grüne" Katalysatoren in der H_2-Produktion als nachhaltige Energiequelle oder im Umweltschutz und trägt daher dazu bei, einige der größten Herausforderungen unseres Jahrhunderts zu meistern.

Summary

Metalloproteins combine the reactivity of metals with the selectivity of the protein environment. Various transition metals, such as iron and copper, can exert similar biological roles, ranging from electron transport to redox catalysis. Evolutionary, iron-sulfur (Fe–S) proteins played a dominant role before the oxygen concentration increased. Due to a higher concentration of oxygen in the air, the oxygen-sensitive cofactors were partially replaced by other transition metals, such as copper. Nevertheless, both Fe–S proteins and copper proteins remain essential for the transfer of electrons and the catalysis of redox processes. The present work aims at understanding the structure and function of naturally occurring Fe–S and copper-containing enzymes, as well as the production and characterization of artificial cobalt-sulfur (Co–S) proteins. The focus is on unravelling the assembly of natural Fe-S clusters and apply this knowledge for the generation of artificial Co–S cofactors and their incorporation into Fe-S scaffold proteins. The goal is to understand natural redox catalysts and to produce artificial biocatalysts with improved properties for biotechnological applications.

The first article (Mielenbrink *et al.* (2020) Maturation of Fe–S Cluster Containing Proteins) describes different maturation strategies for three well-characterized [4Fe–4S] proteins *in vitro* and *in vivo*. Yet, the influence of different strategies on the maturation of Fe–S proteins has not been investigated in detail. Therefore, the completeness of cluster assembly of various *in vivo* systems was compared with *in vitro* methods applied to apo-proteins. These include expression systems with increased Fe–S cluster assembly activity and chemical and semi-enzymatic reconstitution. Our studies show that the successful synthesis of Fe–S proteins can strongly depend on the maturation strategy. This underlines how important it is not to use a general protocol for the development of Fe–S proteins in order to get an optimal result from the maturation of Fe–S proteins. Hereby, the isolation of holo radical SAM enzyme ThnB, which could only be matured *in vitro*, could be significantly improved. Our results will enable the production of Fe–S protein that are correctly maturated and, thus, will contribute to an improved understanding of this highly divers metalloprotein family.

The second article (Mielenbrink *et al.* (2021) Co–S Cluster Assembly in Fe–S Proteins) presents the first *in vitro* maturation of artificial Co–S clusters in various Fe–S protein scaffolds, as well as their cluster transfer interactions with target proteins. Cobalt has emerged as one of the most promising transition metal for the production of hydrogen gas. Thus, artificial Co–S proteins have a great potential for biocatalytic hydrogen production. The bacterial Fe–S cluster scaffold protein IscU from various organisms was used to assemble Co–S clusters *in vitro* using chemical and semi-enzymatic reconstitution. Electron absorption spectroscopy (EAS), circular dichroism spectroscopy (CD) and inductively coupled plasma mass spectrometry (ICP-MS) support the formation of Co–S species in IscU proteins from different organisms. In addition, a point mutation was introduced in *Archaeoglobus fulgidus* IscU to increase the stability of the Co-S cluster under aerobic conditions. Our data present the first evidence for a protein-bound Co–S cluster. In addition, initial experiments indicate that these clusters can even be transferred to other apo proteins implying the possibility that IscU can be used to generate a large variety

of artificial metalloproteins. This is an important step towards the generation of hydrogen on Co-based artificial biocatalysts for a sustainable energy production.

The third article (Olbrich *et al.* (2021) Blue Multicopper Oxidases T1 Cu Axial Ligand Mutations) also focuses on a sustainable biocatalyst: the multicopper oxidase Ssl1. These enzymes catalyze the one-electron oxidation of substrate molecules with O_2 as co-substrate and H_2O as by-product. In this article we investigate the importance of the axial ligand of T1 Cu in Ssl1 for its catalytic activity in environmental protection processes, such as the detoxification of pollutants or bioremediation, in order to expand their applications. Five different mutations of the axial ligand were introduced and investigated using electron paramagnetic resonance spectroscopy, CD spectroscopy, EAS, and x ray crystallography. We were able to solve the crystal structures of five variants, which provides insights on the structural changes accompanying the exchange of one ligand of the T1 Cu site in Ssl1. The spectroscopic results and stopped-flow measurements reveals how the axial ligand of T1 Cu in Ssl1 influences the catalytic activity.

Finally this thesis provides interesting and important results in the field of metalloproteins, especially for the usage as sustainable catalysts in H_2 production as energy source or in the protection of environmental pollutions and therefore contributes to tackle some of the biggest challenges of our century.

1 Introduction

1.1 Biological Role of Metalloproteins

Metalloproteins are proteins that contain one or more metal ions as cofactor (Banci & Bertini, 2013; Shriver *et al.*, 1999). Metal ions are required to serve several functions, such as electron transport, strucutral stability, or as binding sites for substrates leading to the desired catalytic function (Rees, 2002). As metalloproteins link the reactivity of metals to the selectivity of the protein environment, this cofactor can specifically be used for different functions including structural stability, the storage and transport of other proteins, charge carrier processes such as membrane potentials or signaling, as well as the catalytic redox activity of enzymes (Carver, 2013; Waldron & Robinson, 2009). Some examples for the great diversity of metals taking part in these reactions are Na and K as essential elements in charge carrier processes (e.g. membrane potentials and signaling). Metal ion cofactors that are in the focus of this thesis serve functions as key elements in electron transport and redox catalysis and include Fe, Co, and Cu. Chapter 2 (Mielenbrink *et al.* (2020) Maturation of Fe–S Cluster Containing Proteins) is focused on the *in vivo* and *in vitro* maturation of [4Fe–4S] cluster, which serve in electron transport and redox catalysis. Different approaches and their advantages and disadvantages of [4Fe–4S] proteins are presented. In Chapter 3 (Mielenbrink *et al.* (2021) Co–S Cluster Assembly in Fe–S Proteins) Co is serving as promising replacement for Fe in Fe–S cluster scaffold proteins resulting in artificial Co–S clusters to enhance Fe–S dependent processes like "green" H_2 production. Finally, enhancing effects of catalytic activity are represented by mutations of Cu monooxygenase Ssl1 in Chapter 4 (Olbrich *et al.* (2021) Blue Multicopper Oxidases T1 Cu Axial Ligand Mutations). The mutation of certain amino acids in close proxymity to the active site shows dependencies of the activity on structural properties.

1.2 Fe–S Proteins

Iron (Fe) and sulfur (S) were amongst the most prevalent elements in early geolocial history. This led to the formation of Fe–S clusters, which was the basis for Fe–S proteins to become the first biocatalysts. Today Fe is known as the fourth most abundant element on earth, most of it in the oxidation state Fe^{2+} and Fe^{3+} (Frey & Reed, 2012). S is found in several states, ranging from S^{2-} to S^{6+}. Fe–S clusters can be found in almost all living organisms, whereby the geometry and size of the clusters can significantly differ (Beinert, 2000). The story of Fe–S protein research started in 1960 with the isolation of a mitochondrial membrane Fe–S protein (Beinert & Sands, 1960). The next Fe–S proteins discovered were small soluble Fe–S proteins, including the first ferredoxins (Malkin & Rabinowitz, 1966; Mortenson *et al.*, 1962). Fe–S clusters are able to perform a wide variety of functions. This includes a great number of redox and non-redox reactions, Fe–S clusters as part of electron transport systems, and the catalysis of essential cellular processes such as gene regulation, DNA replication, or oxidative phosphory-

lation (Beinert, 2000; Fontecave, 2006; Py *et al.*, 2011; Webert *et al.*, 2014). Further functions include the structural stabilization of catalytically active forms of proteins or protection from intracellular proteases (Grandoni *et al.*, 1989; Thayer *et al.*, 1995). All these functions and properties make Fe–S cluster the prevalent cofactors in proteins. One unfavorable characteristic of Fe–S clusters is their high oxygen sensitivity (Vincent *et al.*, 2005). The protein scaffold can protect the cluster from degradation by oxygen, demonstrated in the scaffold of thermophilic proteins (Mitou *et al.*, 2003). In addition, inserted mutations can extend the lifetime of labile Fe–S clusters from hours to days or even weeks, supporting the investigation of the function of these cofactors (Kim *et al.*, 2012; Marinoni *et al.*, 2012; Shimomura *et al.*, 2008).

1.2.1 Diversity of Fe–S Clusters

Biological Fe–S clusters exist in many different sizes and nuclearities. The most common and therefore also the best studied clusters are the rhombic [2Fe–2S] and the cubic [4Fe–4S] cluster (Cambray *et al.*, 1977). In addition, the simplest form of Fe–S proteins, the tetrahedral coordinated [1Fe] cluster, is well investigated (Lovenberg & Sobel, 1965). Similar to the tetranuclear cluster, the [3Fe–4S] cluster is another interesting form of this diverse cofactor family. The function of this cluster is not yet fully understood, but interestingly it can bind metal ions such as ionic forms of Mn, Ni, Cadmium (Cd), Cu, Titanium (Ti), or Co (Beinert, 2000). Cluster of higher complexity are mostly based on combinations of the rhombic and cubic forms and can also contain other metals like Mo or V (Rees, 2002).

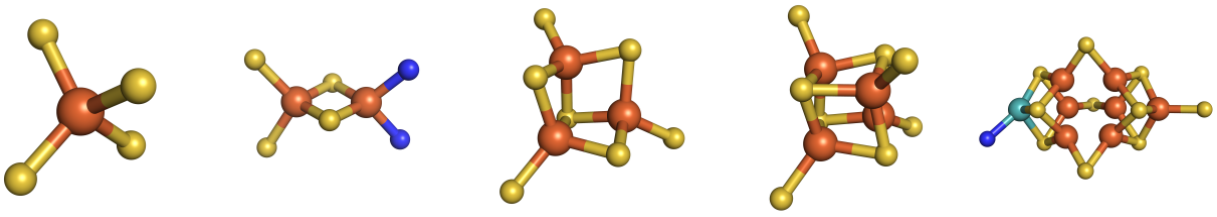

Figure 1.1: Examples of different Fe–S cluster types. From left to right: mononuclear tetrahedral [1Fe] cluster bound to four side chain sulfur, dinuclear rhombic [2Fe–2S] cluster bound to two side chain sulfur and two side chain nitrogen, trinuclear "cubic" [3Fe–4S] cluster bound to three side chain sulfur, tetranuclear cubic [4Fe–4S] cluster bound to four side chain sulfur, octonuclear cluster representing high complex clusters bound to side chain sulfur and nitrogen.

Fe–S clusters can be bound to the protein backbone by the side chains of varying amino acids. Typically, the cluster is coordinated by the sulfur atom of a cysteine residue. However, the nitrogen atom of histidines or arginines as well as the oxygen atom of serines and aspartates can also coordinate Fe–S clusters (Meyer, 2008). Further, water or enzyme substrates have been reported to be able to coordinate Fe–S clusters (Fontecave, 2006). Fe–S clusters have a

high tendency to self-assemble, however, inside the cells the assembly is performed by various Fe–S assembly machieneries, which will be described in more detail in the following Chapters.

1.2.2 Bacterial Fe–S Biosynthesis

Due to the toxicity of free Fe and S, the *in vivo* assembly of Fe–S clusters is a highly regulated process (Müller *et al.*, 2015; Munday, 1989). Although several different machineries have been identified that perform the bioassembly of Fe–S clusters in cells, the process of these machineries can be devided into two parts (i) the formation of the Fe–S cluster and (ii) the transport of the cluster to an apo target protein.

In bacteria, three different machineries for the assembly and transport of Fe–S clusters are known so far. Each of these machineries is activated under specific conditions or for special needs. While the Fe–S Cluster (ISC) machinery and the sulfur Utilization Factor (SUF) are the best studied machineries for Fe–S cluster formation in bacteria, the Nitrogen Fixation (NIF) machinery is only used for the maturation of nitrogenase in azototrophic bacteria (Frazzon & Dean, 2003; Jacobson *et al.*, 1989) and for the cluster formation in hydrogenases followed by further maturation systems (Hu *et al.*, 2008; Leach & Zamble, 2007; Rubio & Ludden, 2008). The ISC system is active under normal standard conditions, whereas the SUF pathway is activated unter stress conditions (Ayala-Castro *et al.*, 2008; Bandyopadhyay *et al.*, 2008; Fontecave & Ollagnier-de Choudens, 2008; Johnson *et al.*, 2005; Takahashi & Tokumoto, 2002; Zheng *et al.*, 1998).

The bioassembly of Fe–S clusters in these machineries follows always the same pattern: In the first step, a cysteine desulfurase (IscS, SufS or NifS) reduces a cysteine residue to alanin to provide organic S, which is then transferred to a scaffold protein (IscU, SufU, or NifU), where the actual Fe–S cluster is formed (Blanc *et al.*, 2015; Lill, 2009). In addtion to the sulfur source, Fe and electrons are needed for the formation of Fe–S clusters. Until now, the exact Fe source remains unknown, while ferredoxin and ferredoxin reductases have been identified for the electron transfer (Mühlenhoff *et al.*, 2003; Yan *et al.*, 2015). Both the desulfurase reaction as well as the assembly on the scaffold protein are assigned to the first part of Fe–S cluster protein maturation. After the assembly, the cluster has to be transferred to the desired apo target protein, where the clusters are needed to fulfill the protein's function. This transfer step requires additional proteins such as the adenosine triphosphate (ATP) dependent chaperones HscA and HscB and/or the Fe–S cluster carrier proteins IscA, SufA, and NifA (Blanc *et al.*, 2015; Lill, 2009).

Due to evolutionary processes, ISC homologues can be found in eukaryotes (Lill & Mühlenhoff, 2006, 2008), whereas SUF homologues can be found in plastids (Balk & Lobréaux, 2005; Xu & Møller, 2008). In Chapters 1.2.3 and 1.2.4, both the ISC and the SUF machinery are discussed and described in greater detail.

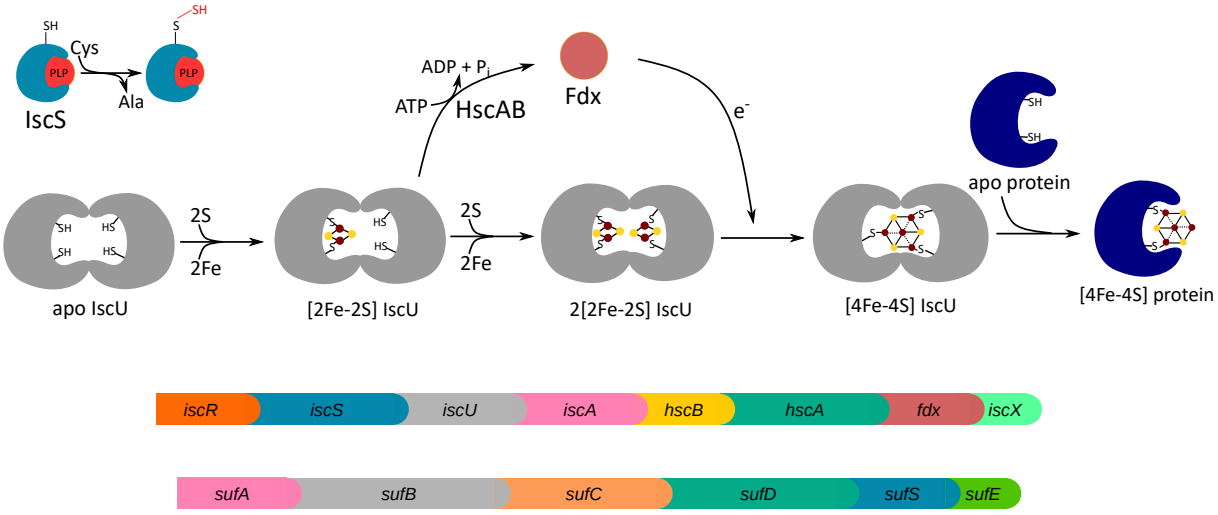

Figure 1.2: Scheme and operons of Fe–S cluster bioassembly. On the top left in blue the pyridoxal phosphate (red) dependent IscS as S supplier reducing cysteine to alanine. In grey Fe–S scaffold protein IscU in dimeric form with sequential formation of Fe–S clusters. Top centered electron providing Fdx to merge $2\times$ [2Fe–2S] to $1\times$ [4Fe4S] cluster. Right side in blue simplified transfers of the Fe–S cluster to an apo target protein. Bottom part: operon of ISC machinery (top) and SUF machinery (bottom).

1.2.3 ISC Machinery

The ISC machinery is the Fe–S cluster assembly pathway under normal conditions, e.g. in the absence of oxidative-stress or resource limitation. It was discovered with the identification of the *isc* operon in 1998 (Zheng *et al.*, 1998). Two key players could be identified in this pathway, the cysteine desulfurase IscS, and the scaffold protein IscU. The first step in cluster formation is performed by IscS. I reduces cysteine to alanine and provides the resulting sulfur to the assembly in IscU. The crystal structure of IscS shows a dimeric two-domain form. The larger domain binds the activating cofactor pyridoxal-phosphate (PLP). The smaller domain carries the active site that binds the sulfur as persulfide from a free donor cysteine residue (Cupp-Vickery *et al.*, 2003; Kaiser *et al.*, 2000).

IscU provides three coordinating cysteine residues for cluster formation (Mühlenhoff *et al.*, 2003; Raulfs *et al.*, 2008; Yuvaniyama *et al.*, 2000). The detailed mechanism of the cluster formation on the scaffold protein IscU is still not fully understood (Fontecave & Ollagnier-de Choudens, 2008; Johnson *et al.*, 2005). It has been shown that IscU can be reconstituted *in vitro* in a sequential manner: In a first step, one [2Fe–2S] cluster is incorporated per IscU dimer, followed by a second [2Fe–2S] cluster. In the next step, the two [2Fe–2S] clusters are merged to form one [4Fe–4S] (Agar *et al.*, 2000a). However, several studies support the hypothesis that IscU binds one [2Fe–2S] per dimer *in vivo* (Shakamuri *et al.*, 2012; Unciuleac *et al.*, 2007). Also, the crystal structure of a trimeric IscU from *Aquifex aeolicus* shows one [2Fe–2S] (Shimomura *et al.*, 2008). A potential candidate for providing Fe to the Fe–S cluster formation is still not identified yet(Kim *et al.*, 2014; Layer *et al.*, 2006; Wofford *et al.*, 2019; Yoon & Cowan, 2003). Candidates like iron-binding CyaY, IscA, or IscX, which are participating in iron-sulfur cluster formation (Chapter 1.2.3) are verified to fulfill other functions but not yet iron donation. In ad-

dition, Fe–S cluster assembly depend on electron transfer from the [2Fe–2S] ferredoxin (Fdx), which is a [2Fe–2S] protein, obtaining the electrons from a ferredoxin reductase (Lill, 2009). The electrons are required to reduce S^0, as present in cysteine, to S^{2-}, as present in Fe–S clusters (Lill, 2009). Another reaction, which requires electrons, is the merge of two [2Fe–2S] cluster to [4Fe–4S] cluster in the later step of reductive coupling for the formation of complex Fe–S clusters (Chandramouli *et al.*, 2007; Unciuleac *et al.*, 2007).

The final step in the maturation of Fe–S cluster proteins is the transfer of the formed cluster to an apo target protein. This step consists of the cluster release from the scaffold protein IscU to cluster transfer proteins, which might be directly involved in the maturation of target Fe–S proteins in further maturation systems (Lill, 2009). The release of the cluster from IscU is assisted by a chaperone system consisting of two proteins, HscA and HscB. HscA is performing a specific ATP-hydrolysis-dependent interaction with IscU (Dutkiewicz *et al.*, 2004), which leads to structural changes in HscA. The co-chaperone, HscB, is also involved in this step that leads to a destabilization of the binding between the Fe–S cluster and IscU and finally to the transfer of the cluster to the apo target protein. The exact mechanism and the role of HscA and HscB, however, are not yet fully understood (Andrew *et al.*, 2006; Bonomi *et al.*, 2008; Chandramouli & Johnson, 2006). Some protein candidates are identified to take the Fe–S cluster from the ISC bioassemly machinery to use them for maturation of different Fe–S proteins. One of these candidates is IscA, which is involved in the further maturation of [4Fe–4S] aconitase and hydroxy-acid dehydratase, whereas the maturation of [2Fe–2S] proteins like ferredoxins do not need extra maturation steps (Tan *et al.*, 2009). Another maturation protein is suggested to be ErpA, which is essential for the maturation of the Fe–S proteins of isoprenoid biosynthesis (Loiseau *et al.*, 2007).

Scaffold Protein IscU

IscU has a central role in the well orchestrated process of Fe–S bioassembly and it is one of the proteins that are in the focus of this thesis. Its function as a scaffold protein for [2Fe–2S] clusters could be shown in both *in vitro* and *in vivo* experiments (Agar *et al.*, 2000a; Raulfs *et al.*, 2008; Tokumoto & Takahashi, 2001). That is, it has to be able to receive Fe and S separately to build up these clusters. Although IscU is known to function as scaffold it could not be isolated in its holo form, what makes it much more difficult to characterize the nature of this protein *in vivo*. Nevertheless, studies have shown that under anaerobic conditions it is possible to reconstitute the apo form with Fe and S, which results in [2Fe–2S] holo dimeric IscU (Agar *et al.*, 2000a). The maturation of holo IscU can sequentially reach from a 1 [2Fe–2S] dimeric IscU form to a 2 $\times$ [2Fe–2S] IscU dimer or an IscU dimer hosting a [4Fe–4S] cluster, although it is still not fully understood, if the formation of [4Fe–4S] IscU is ErpaA dependent (Agar *et al.*, 2000a). Moreover, these studies could show that the [4Fe–4S] form can be reduced by oxygen exposure, revealing a dynamic equilibrium of [4Fe–4S] and [2Fe–2S] clusters in IscU (Agar *et al.*, 2000a). These studies, however, came to the conclusion that the physiologically relevant conformation is the $1\times$ [2Fe–2S] cluster form. Structural analysis of IscU from the thermophilic

organism *A. aeolicus* corroborated this hypothesis by X-ray diffraction experiments (Shimomura *et al.*, 2008). The physiological relevance of the $1\times$ [2Fe–2S] dimeric form was also supported by cluster transfer experiments. Studies with IscU from *Azotobacter vinelandii* revealed that the cluster transfer from the 1x [2Fe–2S] form to apo target proteins could be significantly enhanced by the presence of chaperone systems, whereas the higher occupied cluster forms showed a significantly slower cluster transfer activity, which could not be enhanced by chaperones (Shakamuri *et al.*, 2012; Unciuleac *et al.*, 2007). Moreover one of the two clsuters in the $2\times$ [2Fe–2S] dimeric form seems to be unstable in the presence of the Fe chelator EDTA (Agar *et al.*, 2000a).

Multiple approaches have been applied to improve the cluster stability in the scaffold IscU of different bacterial organisms. Some candidates, where the cluster stability could be improved by mutations close to a coordinating cysteine residue are the D39A (Figure 1.5) mutant of *E. coli*, the D38A mutant of *Aquifex aeolicus* (Figure 1.3), or the D35A mutant of *Archaeoglobus fulgidus* (Figure 1.4) (Kim *et al.*, 2012; Marinoni *et al.*, 2012; Shimomura *et al.*, 2008). In addition to this one coordinating cysteine, two other conserved cysteines are involved in the coordination of the [2Fe–2S] cluster in IscU. For *E. coli* it is known that also His105 can directly participate in active site coordination, although in this study a zinc binding monomer was investigated (Ramelot *et al.*, 2004). Other studies could show that during the process of Fe–S cluster maturation, IscU can change between two different interconvertible conformational states, the apo form at the beginning of this process and the holo form at the end of Fe–S cluster maturation. The apo conformational form was identified as the disordered state, and the structured state with bound Fe–S cluster (Kim *et al.*, 2009). This supports the assumption that IscU has to perform some structural changes to make the active site more accessible for Fe–S cluster maturation.

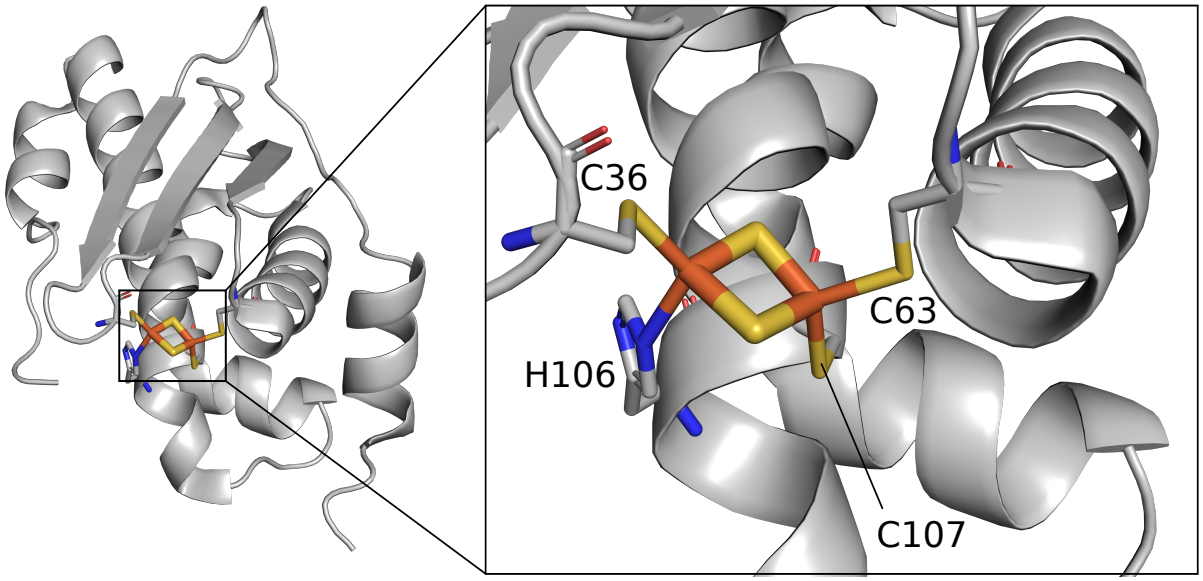

Figure 1.3: Crystall structure of holo D38A variant of *A.a.* IscU. The [2Fe–2S] cluster is coordinated by C36, C63, H106, and C107. PDB ID 2Z7E ((Shimomura *et al.*, 2008))

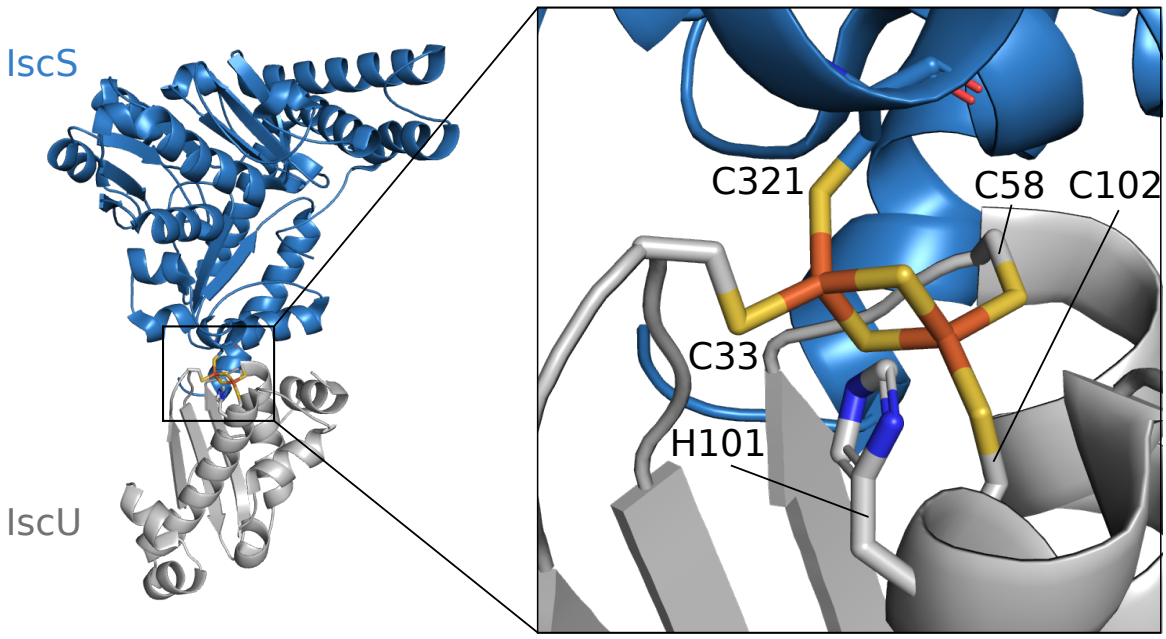

Figure 1.4: Crystal structure of hetero dimeric holo D35A IscU variant and IscS of *A. fulgidus*. The [2Fe–2S] cluster is coordinated by C321 from IscS and C33, C58, and C102 from IscU. His101 has a stabilizing effect but no coordinating function. PDB ID 4EB5 ((Marinoni *et al.*, 2012))

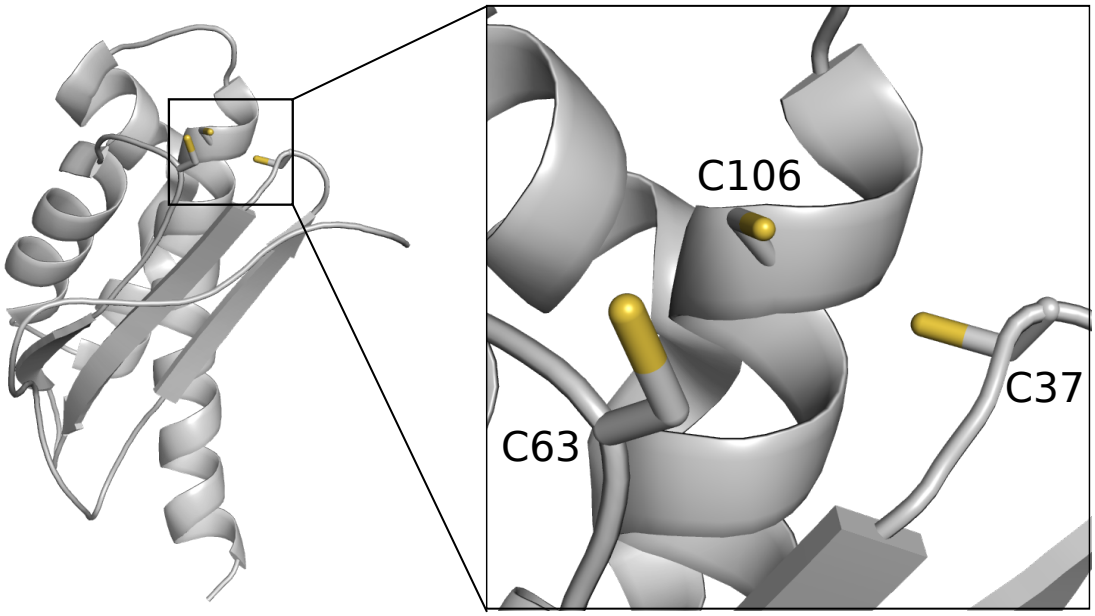

Figure 1.5: Solution NMR structure of apo IscU D39A variant of *E. coli* The cluster would be coordinated by highlighted cysteine residues C37, C63, and C107 shown as side chains. PDB ID 2KQK ((Kim *et al.*, 2012))

The Role of IscS

IscS is one of the most improtant sidekicks of IscU in bacterial Fe–S cluster assembly. The 45 kDa large and highly conserved member of the ISC machinery functions as homodimeric unit with one bound PLP per monomer (Prischi *et al.*, 2010a). As an essential element in S supply, it reduces free cysteine to alanin, which leads to temporarely stored persulfide at a conserved cysteine of the protein itself (Cys328 in *E. coli*) (Mihara *et al.*, 2000; Schwartz *et al.*, 2000). The crystal structure of IscS shows that this catalytic cysteine residue is located in a partially disordered loop apart from the active sites of PLP and the cysteine substrate (Cupp-Vickery *et al.*, 2003; Shi *et al.*, 2010). In contrast to that, the conserved cysteine of the IscS analogous in the NIF and the SUF machinery are placed on a shorter loop, what makes a big difference in the conformational properties of this structural region (Shi *et al.*, 2010). The differences in this two desulfurase types could be due to the fact that IscS is not only a S supplier for Fe–S cluster assembly, as NifS and SufS are thought to be, but also provides persulfides for several other organic sulfurated cofactors such as thiamine, tRNAs, molybdenum cofactors etc. (Shi *et al.*, 2010). Therefore, the longer Cys328-containing disordered loop of IscS might be essential for S donation to various acceptors.

Orchestras of the ISC Machinery

In addition to IscU and IscS, which are under investigation in this thesis, the functions of many other proteins participating in Fe–S cluster biogenesis are still under debate. Over the time it turned out that every step in the process of Fe–S cluster maturation might be supported by orchestrated binary and ternary complexes (Blanc *et al.*, 2015). Two of the Fe donor can-

didates could be identified to interact with IscS *in vitro*: CyaY and IscX both having a large negatively charged part at their surface and behave very similar in Fe binding (Pastore *et al.*, 2006). First characterizations of an IscS-CyaY complex have been succeeded by Isothermal Titration Calorimetry (ITC). This study revealed that IscS and CyaY bind in an 1:1 stoichiometry. The same study could show that an IscS-CyaY complex can be isolated by gel filtration chromatography from cell lysates (Prischi *et al.*, 2010b). Small-angle X-ray scattering (SAXS) measurements identified a globular structure for the IscS-CyaY complexes, as CyaY binds near the IscS dimer interface (Prischi *et al.*, 2010a). The binding amino acids in IscS from *E. coli* were identified as residues R220, R223, and R225, as these residues are positively charged, what makes them favorable for the negatively charged surface of CyaY (Prischi *et al.*, 2010a). The binding of CyaY to IscS has no significant effect on S production activity of IscS (Adinolfi *et al.*, 2009; Iannuzzi *et al.*, 2011; Kim *et al.*, 2014). For IscX, structural investigation could show that it can also bind near the dimeric interface of IscS to form a complex with it (Kim *et al.*, 2014; Shi *et al.*, 2010). This also has no effect on the S production activity (Kim *et al.*, 2014). Thus, CyaY and IscX behave very similar in interactions with IscS and are able to bind to it *in vitro*, although this has no effect on the functional activity of IscS. This makes complexes of CyaY and IscX with IscS not suitable to investigate their function.

Another binary interaction of IscS with an Fe binding protein is the 1:1 stoichiometric complex with Fdx. This complex was identified by nuclear magnetic resonance (NMR) and SAXS experiments (Kim *et al.*, 2013; Yan *et al.*, 2013). The binding interface of Fdx to IscS is close to the Fe–S cluster binding site, making Fdx be suspicious to play a role in the catalytic activity of IscS (Kim *et al.*, 2013; Yan *et al.*, 2013). This is supported by the fact that IscS and Fdx are interacting with their complementary amino acid residues concerning their charge: the positively charge residues R220, R223, and R225 of IscS and the negatively charged residues D79, D71, and D74 in Fdx (Kim *et al.*, 2013). The functional part of Fdx in this interaction is to provide and transport electrons to IscS to support its catalytic activity and the S donation to IscU (Blanc *et al.*, 2015).

Beside these interesting binary complexes also ternary complexes of ISC proteins could be observed during ISC investigation within the last years. One complex could be identified by pull-down assays, where it was shown that IscU can bind IscS and CyaY simultaneously (Shi *et al.*, 2010). This IscS-IscU-Cya complex could also be observed in chemical cross-linking experiments (Kim *et al.*, 2013). As the binary complexes, this ternary complex also forms in an equimolar 1:1:1 stoichiometry (Prischi *et al.*, 2010a). An interesting difference to the binary complexes of IscS is that the desulfurating activity of IscS is reduced, also compared to IscS alone (Bridwell-Rabb *et al.*, 2012; Iannuzzi *et al.*, 2011; Kim *et al.*, 2014). CyaY is believed to influence the assembly rate of Fe–S clusters on IscU, but not its conformation (Adinolfi *et al.*, 2009; Iannuzzi *et al.*, 2011; Prischi *et al.*, 2010a). As IscU can form a trimeric complex together with the dimeric IscS-CyaY complex, it can also form a trimeric complex together with the IscS-IscX complex (Kim *et al.*, 2014; Shi *et al.*, 2010). Here, the properties of the complex are very similar to its CyaY analogon. Some differences are a lower cysteine desulfurase activity in

this complex and a reduced ability to form Fe–S clusters on IscU. Despite these findings, the relevance of this complex is not yet fully understood.

Another ternary complex that is worth being mentioned is the IscS-IscU-Fdx complex, an extension of the binary IscS-Fdx complex. This complex was identified by the addition of IscU to a solution containing the IscS-Fdx complex. The experiment did not show any evidence for a displacement of Fdx, resulting in a ternary complex of IscS-IscU-Fdx (Yan *et al.*, 2013). The structural composition of this complex makes it capable to transfer electrons from Fdx to IscS and/or IscU (Yan *et al.*, 2013). As mentioned before, CyaY can also bind to IscS-IscU dimer to form a ternary complex. This was also shown for the ternary IscS-IscU-Fdx complex, as CyaY can be discplaced by Fdx in the competition for the same binding site (Kim *et al.*, 2014; Yan *et al.*, 2013). This can be favorable as CyaY is known to support cluster stability after cluster formation in the ternary complex with Fdx or it causes conformational changes to facilitate cluster transfer (Colin *et al.*, 2013).

1.2.4 SUF Machinery

The SUF machinery is used for the bioassembly of Fe–S clusters under Fe depletion or oxidative-stress conditions (Ayala-Castro *et al.*, 2008; Leach & Zamble, 2007). Deletion of the standard *isc* operon in organisms hosting both the SUF and the ISC machinery, did not lead to any phenotypic changes, indicating that the function of the ISC machinery can be completely compensated by the SUF machinery (Takahashi & Tokumoto, 2002; Tokumoto *et al.*, 2004). Since many of the SUF proteins are also found in plastids, it is assumed that the SUF machinery is less oxygen sensitive than the ISC machinery (Lill, 2009). The *suf* operon is regulated by *sufR*, encoding for the main regulator of the SUF pathway, SufR. Both, SufR and IscR, function as transcriptional repressors of their systems (Ayala-Castro *et al.*, 2008). In addition, the dedicated ISC regulator IscR, in its apo form, has positive regulatory effects on the SUF pathway: in case of Fe-limiting or oxidative-stress conditions the efficiency of Fe–S-protein maturation is supported by the gene expression of both systems (Lill, 2009).

As previously described, the Fe–S cluster assembly in the SUF pathway follows well studied principles. Here, the cysteine desulfurase function is performed by a complex of two proteins: SufS and SufE. SufE stimulates the cysteine reducing activity of SufS, which reduces cysteine to alanine resulting in a cysteine bound intermediate persulfide, which is then transferred to a conserved cysteine of the S transfer protein SufE. Although SufE has a very similar structure to the ISC scaffold protein IscU, it is not known to fulfill the same function (Liu *et al.*, 2005). From SufE the S is finally transferred to the scaffold protein complex $SufBC_2D$ (Layer *et al.*, 2007; Saini *et al.*, 2010; Sendra *et al.*, 2007). The cysteine desulfurase function of SufS is very similar to bacterial IscS or NifS and its mitochondrial homologues, but it has significant differences in the mechanistic reactions (Kessler, 2006; Loiseau *et al.*, 2003; Outten *et al.*, 2003). In the $SufBC_2D$ scaffold complex, SufB plays a key role in the assembly of Fe–S clusters, since it comprises several conserved cysteine residues and is capable to receive persulfide from the cysteine desulfurase SufS (Layer *et al.*, 2007). The protein SufC was reported to be an ATPase.

Binding of ATP to SufC induces the dimerization of two SufC proteins. This homodimerization finally induces a conformational change in the $SufBC_2D$ complex that allows the formation of Fe–S clusters (Hirabayashi *et al.*, 2015; Yuda *et al.*, 2017). Further the SufC ATPase function is 100-fold higher when the protein is in complex with SufB-SufD (Nachin *et al.*, 2003; Outten *et al.*, 2003). The function of the third protein of the scaffold complex, SufD, is not yet fully understood, but it is suggested to have a role in Fe acquisition during the assembly process (Saini *et al.*, 2010). This is supported by studies that identified SufB as cluster binding protein with SufC as supportive helper for cluster binding and transfer to target proteins (Ayala-Castro *et al.*, 2008; Fontecave & Ollagnier-de Choudens, 2008). SufA is presumably an IscA homologue.

Proteins of the SUF machinery are not directly under investigation in this thesis. The impact of the *suf* operon, however, has been studied for the maturation of different [4Fe–4S] proteins to improve protocols for their *in vivo* maturation and isolation for spectroscopic characterization as described in Chapter 2 (Mielenbrink *et al.* (2020) Maturation of Fe–S Cluster Containing Proteins).

1.3 Cobalt in Biological Systems

1.3.1 The Element Cobalt

Co is a transition metal, which can be found world wide as trace element down in the soil. The most common forms of Co are Co^{2+} and Co^{3+} (Gál *et al.*, 2008). Both forms are soluble in water and show a much higher resistance towards damage/oxidation by oxygen than Fe. Regarding its other chemical and physical properties it is very similar to its neighboring elements in the periodic table, Fe and Ni (Barceloux & Barceloux, 1999). In every pro- and eukaryotic organism, Co is part of essential cofactors in several proteins, e.g. in vitamin B12 dependent enzymes or conalbumines (Cvetkovic *et al.*, 2010; Kobayashi & Shimizu, 1999; Koutmos *et al.*, 2009). Interestingly, slightly higher concentrations of free Co^{2+} lead to toxic effects in both, pro- and eukayotes (Catalani *et al.*, 2012; Ranquet *et al.*, 2007).

1.3.2 Cobalt Stress in *E. coli*

As one part of this thesis focuses on Co-substituted Fe–S proteins, it is interesting to understand how Co effects bacterial growth and metabolism to investigate the utility of these systems *in vivo*. As usual, it is a question of dose and concentration: *E. coli* cells do not show any effect on Co concentrations in the growth medium under 500 µM, whereas the growth is fully inhibited at a concentration of 1 mM Co (Majtan *et al.*, 2011b). Other organisms like *Salmonella enterica* are much more sensitive to Co and stop their growth already at concentrations of 160 µM (Thorgersen & Downs, 2007). Note, when using full medium containing tryptone and yeast extract, the formation of Co chelates should be considered, as there is a difference between the amount of Co added and biologically accessible (Cheng *et al.*, 2011). To prevent the cells from damage induced by Co stress, several mechanisms have been established to bind and

remove excess Co ions. In *E. coli* the expression of certain membrane proteins is induced by Co or Ni stress to transport Co and Ni to the extracellular environment (Rodrigue *et al.*, 2005). In other systems like *Saccharomyces cerevisiae*, mechanisms are activated during Co stress, which are also activated in case of Fe deficiency. Under these conditions, Fe uptake is highly enhanced, which leads to high intracellular Fe conentrations making Co less toxic (Ranquet *et al.*, 2007; Stadler & Schweyen, 2002). It has been shown that bacterial cells can adapt to high Co concentrations and are able to bypass and replace disturbed metabolic pathways (Barras & Fontecave, 2011). The details of the mechanisms Co toxicity is based on are not yet fully understood. After all, it is known that Co is involved in the formation of reactive oxygen species (ROS), which lead to oxidative stress (Leonard *et al.*, 1998). In addition, Co is suspected to inhibit S uptake by the cells or interact with Fe–S proteins and disturb them in their function (Ranquet *et al.*, 2007; Thorgersen & Downs, 2007).

1.3.3 Interference of Cobalt with Fe–S proteins

The elements Fe and Co have very similar physicochemical properties, including the redox states they can form, 2+ and 3+, and therefore have a high affinity towards S (Barras & Fontecave, 2011). Hence, it is not surprising that they compete for the same binding sites in proteins. Studies revealed that the incorporation of [4Co–4S] clusters into the *E. coli* aconitat hydratase B (AcnB) is possible, but leads to a loss of activity of this protein. That means that high intracellular Co concentrations can but not necessarily have to lead to a reduced activity of Fe–S cluster containing proteins (Ranquet *et al.*, 2007). The same competitive behaviour is known for the binding sites of the proteins in the Fe–S assembly machineries. Here, with correspondingly high Co concentrations, Co can be incorporated into the active center of these proteins instead of Fe. A difference in sensitivity for Co can be clearly seen between the ISC, which is more sensitive, and the SUF machinery (Ranquet *et al.*, 2007). Several *in vitro* experiments on structural properties have also revealed an interaction of Co^{2+} with the active site of the scaffold proteins IscU from *E. coli* and SufU from *Streptococcus mutans* (Roy *et al.*, 2017), but only as single atom interactions and not in Co–S cluster form. The approach to incorporate Co into catalytic proteins often leads to a loss of activity of up to 80% in different Fe–S proteins like AcnB or tRNA modifying methylthiotransferase MiaB (Ranquet *et al.*, 2007).

Another approach to create artificial Co catalysts is the manipulation of existing catalysts to improve their properties. Studies revealed that the substitution of Zn by Co in carboxypeptidase A could enhance the activity of the enzyme by a factor of two (Folk & Gladner, 1960). In addition, in heme proteins Fe could be replaced by other transition metals such as Co to form artificial catalysts (Key *et al.*, 2016). All these alterations can be performed *in vitro* by reconstitution methods or by *in vivo* incorporation using Co containing, Fe free M9 minimal medium during recombinant expression to obtain functional Co substituted catalysts (Majtan *et al.*, 2011a). In addition, the simplest forms of Fe proteins, the rubredoxins have been reconstituted with Co (Galle *et al.*, 2018). In this thesis, we focus on Co-substitution in proteins that are part of the Fe–S cluster assembly machineries, as we are convinced that these proteins are perfect target

proteins. Successful incorporation of Co into these proteins is also the starting point for the establishment of a straight-forward protocol for a (semi-)enzymatic Co-reconstitution of other Fe–S cluster containing proteins.

1.3.4 Cobalt as Hydrogen Production Catalyst

Besides Co-containing cofactors in Fe–S proteins, a number of artificial, catalytically active Co complexes have been created *in vitro*. Of particular interest are Co^{2+} ions that are immobilized on a metalloorganic surface, as well as the mononuclear Co complex [Co^{3+}(DPK OH)$_2$]Cl (DPK = dimethyl(dipyridyl ketone)), both showing oxidative catalytic activity on water (Kung *et al.*, 2015; Zhao *et al.*, 2015). Approaches to adapt [4Fe–4S] clusters to form Co containing analogues were performed with [4Fe–4S-(S_{Cys})$_3$-L] (L= amino acid or water/hydroxid). These approaches led to structurally very similar Co substituted variants of the cubic metallo clusters (Deng *et al.*, 2009; Venkateswara Rao & Holm, 2004). Solubility and catalytic activity of these clusters could only be demonstrated in organic solvents, where they show a high catalytic potential, depending on the ligand (Deng *et al.*, 2009). Another interesting artificial Co-containing complex is a cubic [4Co-4O] cluster that was synthesized based on the cofactor of photosystem II. It was demonstrated that this synthetic cofactor is capable of oxidizing water which was proven by the detection of oxygen (McCool *et al.*, 2011). A promising catalyst should be convincing with a high catalytic turnover rate, a significant stability, and solubility in aqueous solutions. These are synthetic approaches on water oxidation, which are not soluble in aqueous solutions. Promising progress has been done in the last years to evolve an efficient and robust biological Co-containing catalyst for hydrogen production.

One approach is to modify or extend parts of the Photosystem I (PSI). The modification of PSI with Co(dmgH)$_2$pyCl lead to high turnoverrates of 170 mol of H_2 (mol of PSI)$^{-1}$ min^{-1} but is lacking a significant stability. A similar approach is the insertion of Co(dmgH)$_2$ and Co(dmgBF$_2$)$_2$ into apo-sperm whale myoglobin. A big issue here is the catalytic deactivation of this complex after a low number of turnovers. These approaches are quite challenging, because these molecules are not made to bind synthetic catalysts (Kandemir *et al.*, 2016). Another way to develop suitable Co-containg catalysts for hydrogen production is to take existing catalysts and engineer them to desired functions. Co-substituted protoporphyrin IX showed a 4-fold increase of H_2 production than the WT form before activity decreases quickly below a pH of 7. Amino acid mutations lead to increased activity also at pH 6.5 (Kandemir *et al.*, 2016). This indicates that in this case mutations can enhance the properties of a catalyst in a positive way. A new approach is recently succeeded in Co-substituted cytochrome C with promising turnover values. However, here again a rapid deactivation is limiting this molecule to be an efficient catalyst (Kandemir *et al.*, 2016).

As biological catalysts with high turnover rates but without significant stability exist, it is very important to develop suitable catalysts to make H_2 production more effective. One important step in this process is to find a suitable cofactor. Fe–S proteins are potential candidates to function as catalysts, because of the high electrochemical potential of Fe–S clusters. Our idea

is to adopt the great versatility of Fe–S clusters to Co–S clusters coming along with less oxygen sensitivity. Another advantage of Co as transition metal in Fe–S proteins is that Co and Fe share their common oxidation states Co^{2+}/Fe^{2+} and Co^{3+}/Fe^{3+} (Barceloux & Barceloux, 1999), what makes Co more suitable as a replacement for Fe than any other metal. In addition, Co is already known as parts of essential cofactors of pro- and eukaryotic proteins, e.g. in the metalloproteome of *P. fusiosus*, vitamin B12 coenzymes, and as cobalamin in methionine synthase (Cvetkovic *et al.*, 2010; Kobayashi & Shimizu, 1999; Koutmos *et al.*, 2009).

1.4 Multicopper Oxidase Ssl1

Laccases are known as members of the blue multicopper oxidase family. As oxidoreductases they are able to oxidize several electron-rich substrates such as phenols, aryl diamines, benzenethiols, hydroxyindoles, and inorganic metal ions (Piscitelli *et al.*, 2010). These reactions can be found in many biological processes, such as lignification of plant cell walls, heavy metal homeostasis, spore morphology, and lignin degradation (Giardina *et al.*, 2010). The main functional role in this reactions play four Cu ions that are coordinated in two binding sites. One mono-copper site coordinated by one casteine and two histidines, and one tri-copper site coordinated by eight histidine residues. The cysteine and its charge transfer interaction with Cu^{2+} are responsible for the deep blue appearance of these enzymes due to electron absorption at wavelengths in the region of approximately 600 nm (Solomon *et al.*, 1996b). The electron transport is induced by the oxidation of four substrate molecules by a one-electron abstraction at the type 1 (T1) Cu site. With the help of a cysteine-histidine bridge the electrons are then transported to the trinuclear Cu site, where molecular oxygen is finally reduced to water by a four-electron reduction (Gunne *et al.*, 2014). The redox potential of the T1 Cu of laccases varies greatly depending on the organism of origin. Organisms in which laccases have been found include fungi, plants, bacteria, archaea, and insects (Alcalde, 2007; Uthandi *et al.*, 2010). The T1 Cu redox potential of laccases in plants and bacteria is around 0.4 V, whereas the T1 Cu redox potetial of fungi laccases can be 0.8 V (Maté *et al.*, 2011). Other factors that influence the activity of laccases are the differences in the redox potentials of T1 Cu and the substrate (Saito *et al.*, 2013; Xu *et al.*, 1996), as well as changes in the substrate binding site leading to altered substrate binding (Kallio *et al.*, 2011; Toscano *et al.*, 2013). For a long time, only laccases with three domains (Piontek *et al.*, 2002) were known until a few years ago a new class of laccases with two domains has been discovered, named Ssl1 (Machczynski *et al.*, 2004). The absence of the third domain in these laccases leads to the formation of a homotrimer, which forms the functional domain of the trinuclear site (Endo *et al.*, 2003; Gunne & Urlacher, 2012; Machczynski *et al.*, 2004; Skálová *et al.*, 2009). Laccases with three domains (SLAC) have already been well investigated (Durao *et al.*, 2006, 2008; Xu *et al.*, 1999). In contrast, only little is known about the structure and function of Ssl1. With the introduction of point mutations of amino acids that are involved in Cu coordination, the knowledge about structural factors and activity should be further investigated.

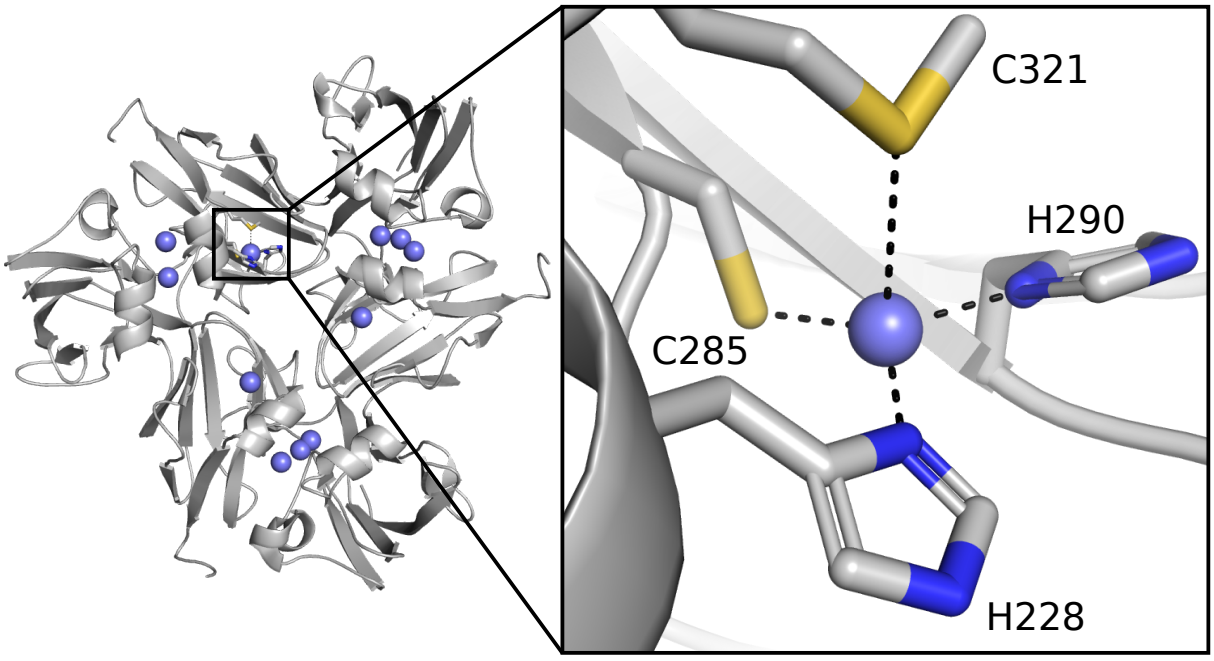

Figure 1.6: Overview and zoom into T1 Cu site of WT Ssl1 crystal structure. Protein shown in grey. Cu shown as blue spheres. Zoom into T1 Cu site where Cu is coordinated by two histidines and one cysteine as well as the axial ligand methionine shown as sticks. PDB ID 4M3H ((Gunne *et al.*, 2014))

1.5 Aim

The field of metalloenzymes is one of the most interesting research fields in biochemistry. Naturally, metalloenzymes already have a great variety of functions. Therefor it is of very high interest to understand the formation of these multifunctional molecules and use this knowhow to improve and adapt biomolecular processes for scientific and industrial purposes. In this thesis, X-ray crstallography, electron absorbtion spectroscopy, circular dichoism spectroscopy, electron paramagnetic resonance spectroscopy, *in vitro* reconstitution, and chromatographic techniques will be applied to obtain a deeper understanding of Fe–S cluster and Cu containing metalloenzymes. Usually the activity of metalloenzymes *in vitro* is much lower than *in vivo*. This makes them unsuitable to use for large scale applications in science or industry. Therefor methods and techniques have to be developed to enhance the potential of these multifnctional proteins. A promising way to reach this is to manipulate the properties or the environment in close proximity of their active site. However, it is not much known about the enhancement of the (catalytic) function of metalloenzymes *in vitro*. In this thesis, two large groups of metalloproteins are under investigation to enhance their properties and usefulness for scientific and industrial large scale applications *in vitro*: Fe–S cluster proteins and Cu monooxigenases. For this classes the knowledge of methods and techniques to improve their activity and effectiveness is still lacking with important questions waiting to be answered.

Chapter 2 (Mielenbrink *et al.* (2020) Maturation of Fe–S Cluster Containing Proteins) gives insights into the best way to assemble [4Fe–4S] cluster for different types of [4Fe–4S] proteins to get the best functionality for each class of [4Fe–4S] proteins. The first systematically investigation of protein type dependent [4Fe–4S] cluster assembly is presented in this Chapter. An artificial approach to improve the properties and functionality of Fe–S cluster containg proteins is presented in Chapter 3 (Mielenbrink *et al.* (2021) Co–S Cluster Assembly in Fe–S Proteins). The idea is to replace iron with cobalt in Fe–S proteins. In theory, the advabtages of Co in first mononuclear approaches are very promising. However, nothing is known about the assembly of multinuclear Co–S cluster in Fe–S scaffold proteins, which could eb a large step towards "green" hydrogen production using artificial biocatalysts. The approach to make the Cu monoxigenase Ssl1 useful for large scale scientific and industrial use is presented in Chapter 4 (Olbrich *et al.* (2021) Blue Multicopper Oxidases T1 Cu Axial Ligand Mutations). Here again, little is known about the enhancement of the functionality of this protein *in vitro*. The manipulation of the axial ligand of the active sight should expand the understanding of the catalytic mechanisms of this protein.

The first objective of this thesis is to provide enhanced protocols for the production of Fe–S clusters in order to improve the accessibility of these highly oxygen sensitive proteins in their holo form for structural and spectroscopic analyses (Chapter 2 "Mielenbrink *et al.* (2020) Maturation of Fe–S Cluster Containing Proteins"). Since the isolation of fully loaded Fe–S cluster proteins is a significant bottleneck in the characterization of those macromolecules, their investigation is often performed on reconstituted protein samples. The subsequent reconstitution, however, can lead to artifacts or even protein degradation. For this purpose, the development of improved protocols for the expression and protein isolation by addressing the special needs of particular proteins is of broad interest for the bioinorganic community. Here, the formation of Fe–S clusters and the impact of SUF and ISC machinery on cluster formation in the 4-hydroxy-3-methylbut-2-enyl diphosphate reductase (IspH), the Quinolinate synthase A (NadA), the Aconitase B (AcnB) from *E. coli*, and the radical S-Adenosylmethionine protein ThnB from Bacillus thuringiensis are in the focus of this work.

Based on this, the main objective of this thesis deals with one of the biggest challenges of mankind: green hydrogen production. One approach on this way is to produce robust and efficient Co–S biohybrids, which are able to perform photo catalytic water splitting. A first step is to use the scaffold proteins of Fe–S cluster biosynthesis and adapt them to Co–S cluster formation (Chapter 3 "Mielenbrink *et al.* (2021) Co–S Cluster Assembly in Fe–S Proteins"). Consequently, the successful reconstitution of Co–S clusters in the scaffold protein from the ISC machinery, IscU, is one objectiv of this thesis. This is a great step towards Co–S cluster formation in order to generate a universally functional Co–S assembly protein for the generation of artificial Co–S cluster proteins as "green" hydrogen producing biocatalysts.

A third aim of this thesis is in the field of multicopper oxidases. Here the laccase Ssl1 is also playing an interesting role as a "green" catalyst. The enzyme only requires oxygen as a co-substrate, while no expensive cofactor is needed, and the protein only produces water as

a by-product. Ssl1 laccases have a high potential for the use in the detoxification of pollutants and bioremediation of phenolic compounds and in delignification processes. The axial ligand at the active site of this molecules plays an important role for their redox potentials. The aim is to investigate mutants of the axial ligand with structural, spectroscopic and kinetic methods (Chapter 4 "Olbrich *et al.* (2021) Blue Multicopper Oxidases T1 Cu Axial Ligand Mutations"). Therefor the crystallization and structure elucidation of the five presented mutants is one objective, followed by the identification of spectroscopic characteristics in EAS, CD, and EPR spectroscopy. Together with kinetic assays of stopped flow measurements and spectrophotometric redox titrations the results should underline the importance of the axial T1 Cu ligand in the functionality of this enzyme.

The [4Fe–4S] assembly protocols should give a systematic overview of which protcol is the best for successful and correct [4Fe–4S] cluster assembly for certain protein(-classes) (Chapter 2 "Mielenbrink *et al.* (2020) Maturation of Fe–S Cluster Containing Proteins"). This is a great step towards the functional and structural investigation of correct assembled multinuclear Fe–S cluster containing proteins. The results of Chapter 3 (Mielenbrink *et al.* (2021) Co–S Cluster Assembly in Fe–S Proteins) will give deep insights into the properties of Co–S cluster assembly in Fe–S proteins. The functionality of Co–S cluster containg Fe–S proteins would be a game changer in "green" H_2 production as light driven energy source for the future. The results presented in this Chapter are a large step to reach this deep goal. The manipulation of the axial ligand of Ssl1 in Chapter 4 (Olbrich *et al.* (2021) Blue Multicopper Oxidases T1 Cu Axial Ligand Mutations) gives insights into the role of the axial ligand concerning the redox potential. This can be used to erase their effectiveness and make them also usable in large scale for applications like detoxification of pollutants and bioremediation of phenolic compounds and in delignification processes with great positive effects on environmental issues.

2 Maturation of [4Fe–4S] cluster-containing proteins *in vivo* and *in vitro*

This chapter reflects content of the following publication.

2.1 Publication information

Steffen Mielenbrink, Hannah Rosenbach, Melissa Jansing, Sabine Metzger, and Ingrid Span
Submitted to: **Metallomics**

2.2 Abstract

Fe–S clusters are ubiquitous cofactors that are essential in many biological processes. The biosynthesis of Fe–S clusters is strictly regulated in all organisms. Several strategies have been reported for the maturation of recombinantly produced proteins, however, a systematic comparison of different maturation protocols for the same target proteins has not yet been reported. In this work, we use three well-characterized [4Fe–4S] proteins, including aconitase B, 4-hydroxy-3-methylbut-2-enyl diphosphate reductase (IspH), and quinolinate synthase (NadA), to investigate the influence of different maturation strategies. These include the maturation of the apo protein using chemical or semi-enzymatic reconstitution, co-expression with two different plasmids containing the iron-sulfur cluster (*isc*) or sulfur formation (*suf*) operon, and a cell strain lacking IscR, the transcriptional regulator of the ISC machinery. Our results show that the maturation of the Fe–S proteins *in vivo* is more specific and efficient compared to reconstitution. Surprisingly, we observed that the differences between the *in vivo* maturation systems are pronounced, although ISC and SUF should be capable of maturating the same proteins. We observed that it is difficult to predict which strategy results in successful maturation, thus, the optimal cell strain has to be determined experimentally. We also provide a rationale for preferences for SUF versus ISC pathway. Furthermore, we show that the *in vivo* strategies can be extended to more complex enzymes, such the radical SAM protein ThnB, which was previously only maturated by reconstitution. Our results shed light on the differences of *in vitro* and *in vivo* Fe–S cluster maturation and points out the pitfalls of chemical reconstitution.

2.3 Introduction

Fe–S clusters are ancient and ubiquitous cofactors in proteins. They are involved in many essential biological processes, including such as oxidative respiration, photosynthesis, hydrogen production, nitrogen fixation, and DNA replication/repair. The most common species found in proteins are the rhombic [2Fe–2S] and cubic [4Fe–4S] forms and they are predominantly coordinated by cysteine residues, however, other residues can be involved as ligands as well (Freibert *et al.*, 2018). Fe–S proteins are predominantly involved in electron transfer reactions. Furthermore, they also play important roles in providing stability to protein structures, regulation of gene expression, non-redox catalysis, repair and processing of nucleic acids, regulation of cellular processes, and iron homeostasis (Beinert, 2000; Beinert *et al.*, 1997; White & Dillingham, 2012).

Fe–S cofactors have played a significant role in the metabolism of the primordial cells, which were formed in an atmosphere with an extremely low oxygen concentration. Under these conditions, oxidation of Fe^{2+} to Fe^{3+}, which is insoluble in water, by molecular oxygen leading to the degradation of the cluster was not a major issue. The versatility and stability of the cluster lead to a dominant role in primordial catalysis. With rising oxygen concentration in the atmosphere, some organisms have evolved to utilize copper proteins instead of Fe–S proteins, since both oxidation states of copper are soluble in aqueous solutions. Despite the need to protect the cofactors from oxygen, Fe–S proteins are still wildly used cofactors in nature and their key role in many biological processes makes them the focus of a large research community.

The sensitivity of Fe–S proteins towards oxygen requires special attention during gene expression, protein isolation and purification. Gene expression occurs in the cytosol with a reducing environment and virtually no free molecular oxygen, so in most cases the cells can be cultivated under aerobic conditions without an impact on the Fe–S proteins. However, cultivation of cells under shaking with low speed as well as expression under anaerobic conditions have been shown to have a beneficial effect on Fe–S protein production (Kuchenreuther *et al.*, 2010). *Escherichia coli* (*E. coli*) is a facultative anaerobic bacterium, thus, it can also be cultivated at low oxygen concentrations. After cell lysis, the Fe–S proteins are exposed to molecular oxygen and their cofactor decomposes rapidly in most cases due to the insolubility of ferric ions. Some members of the Fe–S protein family are capable of stabilizing protein-bound ferric ions, such as rubredoxins, or the clusters are protected from the environment by the protein, such as some ferredoxins, resulting in no or slow degradation of the cluster under aerobic conditions. In most cases though, isolation and purification of Fe–S proteins lead to protein in apo form or with partial cluster loading.

Another important consideration is the assembly and transfer of the cofactors to recombinantly produced proteins using the Fe–S bioassembly machinery of the host (Figure 2.1) for a schematic representation of the components of Fe–S assembly machineries in general). While the recombinant gene is expressed to an abnormally and excessively high level, the level of the Fe–S assembly proteins remains unchanged and the machinery is not capable of keeping up with the production of the cofactor. The Fe–S cluster content in partially loaded proteins

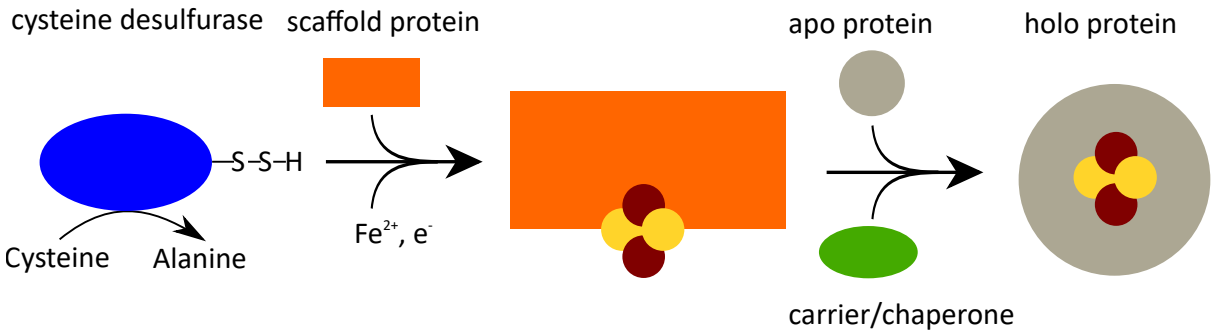

Figure 2.1: Schematic representation of iron sulfur cluster assembly machineries such as the ISC and SUF machinery. Adapted from Lill (2009).

can be enhanced by chemical reconstitution, which is performed by treating the protein with an inorganic iron and sulfide source in the presence of a reductant (Malkin & Rabinowitz, 1966). A more sophisticated variation of the reconstitution reaction is a semi-enzymatic approach that involves the protein cysteine desulfurase and L-Cysteine instead an inorganic sulfur source (Figure 2.2A) (Gao *et al.*, 2013).

In cases where the nature of the native Fe–S cluster has not been ascertained, chemical reconstitution can result in incomplete cluster formation or assembly of artifacts (Archer *et al.*, 1994; Leartsakulpanich *et al.*, 2000). Biosynthesis of the Fe–S clusters *in vivo* by co-expression of the genes encoding for the Fe–S cluster assembly machinery ensures the incorporation of biologically relevant cluster forms. While the Iron Sulfur Cluster (ISC) machinery is used for housekeeping cluster assembly under standard growth conditions in bacteria and eukaryotic mitochondria (Lill, 2009), the Sulfur Formation (SUF, also termed Sulfur Utilization Factor) machinery is used under stress conditions in bacteria and chloroplasts of eukaryotes (Bai *et al.*, 2018). SUF is the sole machinery for Fe–S cluster biogenesis in archaea, cyanobacteria, and many Gram-positive, thermophilic and pathogenic bacteria (Pérard & de Choudens, 2018). Additional machineries responsible for Fe–S cluster assembly are the Nitrogen Fixation (NIF) system that plays a specialized role in the maturation of Fe–S cluster proteins in nitrogen fixing organisms such as *Azotobacter vinelandii* (Pérard & de Choudens, 2018), the Cysteine Sulfinate Desulfinase (CSD) from *E. coli* that has components similar to the ISC or SUF system, but lacks a scaffold protein (Loiseau *et al.*, 2005), and the Cytosolic Iron-Sulfur Cluster Assembly (CIA) system, that is responsible for cytosolic and nuclear Fe–S cluster assembly in eukaryotes (Sharma *et al.*, 2010)). All Fe–S biosynthesis pathways follow the same pattern and include enzymes with similar function (Figure 2.1). The cysteine desulfurase converts the substrate L-Cysteine into L-Alanine and provides the sulfur to the scaffold protein. The requirement of an iron donor protein or the specific iron source are not clear (Iannuzzi *et al.*, 2011; Layer *et al.*, 2006; Roche *et al.*, 2015). For the bacterial pathway, it has been shown that a complex of cysteine desulfurase and scaffold protein is formed that assembles [2Fe–2S] and possibly also [4Fe–4S] clusters in the presence of an electron source (Agar *et al.*, 2000a,b; Marinoni *et al.*,

2012). Previous studies have shown that co-expression of genes encoding for Fe–S proteins with the *isc* or *suf* operon have resulted in higher protein yields and increased cofactor content (Figure 2.2B) (Gräwert *et al.*, 2004; Hänzelmann *et al.*, 2004). Furthermore, it was reported that the deletion of the gene encoding for the transcriptional regulator of the ISC machinery, iscR, in *E. coli* BL21(DE3) cells results in an enhanced expression of the *isc* operon providing as an alternative to plasmid-based overexpression (Figure 2.2B) (Schwartz *et al.*, 2001). Each method has been successfully used for one or several proteins (Akhtar & Jones, 2008; Gao *et al.*, 2013; Gräwert *et al.*, 2004; Hänzelmann *et al.*, 2004; Malkin & Rabinowitz, 1966), however, systematic studies comparing several different strategies for the same protein have not been reported. The obvious approach would be to use the biosynthesis machinery that is biological relevant, which is only possible for prokaryotic proteins. In addition, the co-expression of two plasmids may result in an additional stress for the host cells and, therefore, reduce the productivity of protein synthesis.

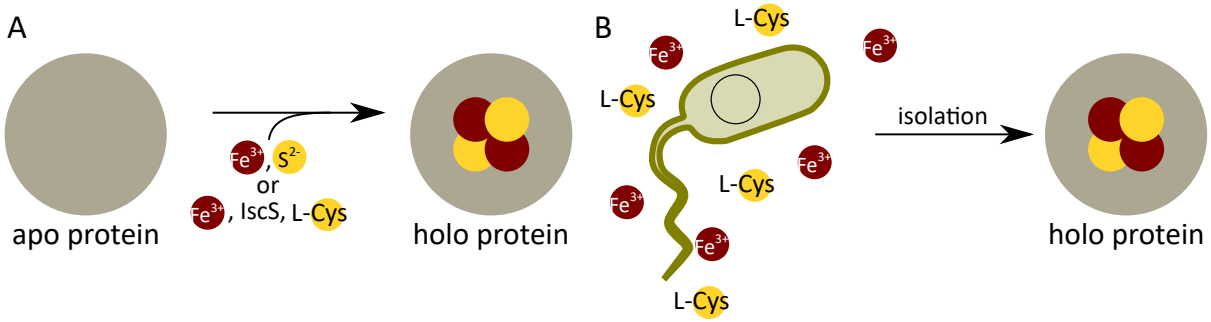

Figure 2.2: Assembly of Fe–S clusters in proteins. (A) Schematic overview on the workflow for chemical and semi-enzymatic *in vitro* reconstitution of Fe–S cluster into the apo form of a protein. While for chemical reconstitution an inorganic sulfur source is required, semi-enzymatic reconstitution requires the cysteine desulfurase IscS and L-Cysteine as an organic sulfur source. Both methods require an inorganic iron source. (B) Schematic overview of *in vivo* assembly for the isolation of Fe cluster proteins in their holo form using the co-expression of the target protein with the plasmids pSUF or pISC in BL21(DE3) as well as the expression of the target protein in BL21(DE3) Δ*iscR*. Cells are cultivated in growth media supplemented with inorganic iron and L-Cysteine as a sulfur source.

In this study, we investigate six different strategies for the production of [4Fe–4S] proteins using four different target proteins. Our study shows that selection of the appropriate strategy for cluster incorporation not only influences the cofactor content in proteins, but also significantly alters the expression levels of the recombinant genes. We use electronic absorption spectroscopy (EAS) and circular dichroism (CD) spectroscopy to assess the amount of Fe–S cluster bound to the proteins as well as the specificity of the method. In addition, we quantified the Fe–S cluster content of the samples using inductively coupled plasma mass spectroscopy (ICP-MS).

We chose *E. coli* aconitase B (AcnB), *E. coli* 4-hydroxy-3-methylbut-2-enyl diphosphate reductase (IspH), *E. coli* quinolinate synthase A (NadA) and *Bacillus thuringiensis* Thurincin B (ThnB) as target proteins, since all proteins bind [4Fe–4S] clusters that are coordinated by three cysteine residues. ThnB harbors a second [4Fe–4S] cluster that is coordinated by four cysteines. We have chosen three proteins that have previously been studied extensively and the properties of their cofactor is well established. In addition, we included a radical SAM enzyme in our study, where we have observed a dramatic impact of the expression system.

In the presence of iron, AcnB from *E. coli* functions as an enzyme in the essential citric acid cycle and the glyoxylate cycle which assembles a [4Fe–4S] cluster. Under oxidative stress conditions and iron starvation, the Fe–S cluster disassembles and the enzymatically inactive apo protein functions as a nucleic acid binding protein, that binds to its own mRNA for positive regulation (Beinert & Kennedy, 1993; Tang & Guest, 1999; Williams *et al.*, 2002). The crystal structure of an inactive porcine heart mitochondrial aconitase hosting a [3Fe–4S] cluster reveals that the cluster is ligated by three cysteine residues (Robbins & Stout, 1989). The fourth coordination partner in the active form of the aconitase with a [4Fe–4S] cluster is proposed to be the citrate substrate (Beinert & Kennedy, 1993). IspH from *E. coli* produces the universal precursors of terpenes in the methylerythritol phosphate isoprenoid biosynthesis using its $2H^+$ /$2e^-$ reductase activity (Span *et al.*, 2012). The protein hosts a [4Fe–4S] cluster (Span *et al.*, 2012), but enzymatic activity has also been discovered in the presence of a [3Fe–4S] cluster (Gräwert *et al.*, 2009). In both cases, the cluster is coordinated by three cysteine residues, as known from the aconitase. NadA from *E. coli* plays an important role in the synthesis of nicotinamide adenine dinucleotide (NAD), an essential cofactor in numerous important redox reactions (Begley *et al.*, 2001). It harbors a [4Fe–4S] cluster coordinated by 3 cysteine residues (Cicchillo *et al.*, 2005). The protein ThnB from *B. thuringiensis* is a member of the so-called radical SAM enzymes, that are reported to be involved in the maturation process of sactipeptides (Wieckowski *et al.*, 2015). Sactipeptides represent a new class of natural products featuring promising antimicrobial activities. However, the role of these peptides within the producer strain remains unknown (Flühe & Marahiel, 2013). The first step in the biosynthesis of these sactipeptides is the formation of the characteristic cysteine-sulfur to α-carbon thioether linkage in the precursor peptide (Flühe & Marahiel, 2013; Lohans & Vederas, 2014). It has been shown that this reaction is catalyzed by enzymes that incorporate two Fe–S clusters and a SAM cofactor. These enzymes share a characteristic CX3CX2C motif, which is capable of binding one catalytic [4Fe–4S] cluster that is required for the reductive cleavage of SAM into methionine and a 5'-deoxyadenosyl (5'-dA) radical (Broderick *et al.*, 2014; Roach, 2011). The function of a second [4Fe–4S] cluster, hosted by radical SAM enzymes and studied for example in the radical SAM enzyme family members subtilisin A (AlbA) and sporulation killing factor (SkfB) is supposed to be electron transfer during the process of thioether bond formation (Flühe *et al.*, 2013, 2012; Flühe & Marahiel, 2013).

The proteins AcnB, IspH and NadA studied in that work were all taken from *E. coli*, whereas the radical SAM enzyme ThnB was taken from *B. thuringiensis*. While *E. coli* hosts both the ISC and the SUF machinery (Mettert & Kiley, 2014), in for Gram-positive bacteria such as *B.*

subtilis, only the SUF machinery is thought to be the sole prevalent pathway (Selbach *et al.*, 2014). Therefore, we set special focus on how the co-expression with the ISC or SUF machinery from *E. coli* influences the expression of the radical SAM protein from *B. thuringiensis*.

Several spectroscopic techniques, including the optical absorption methods EAS and CD spectroscopy, can be used for the biophysical characterization of Fe–S cluster containing proteins. Among the broad variety of spectroscopic methods including electron paramagnetic resonance (EPR) (Jasniewski *et al.*, 2019), Mössbauer (Dunham *et al.*, 1994), X-ray absorption (Ward *et al.*, 2014) or resonance Raman spectroscopy (Spiro & Czernuszewicz, 1995), EAS and CD spectroscopy are the most widespread techniques that require only µM protein concentrations and small volumes of the samples.

Fe–S clusters usually show broad but characteristic absorption bands in the EAS These characteristic features can be used to roughly estimate the type of Fe–S cluster present in the protein. Generally spoken, proteins containing a [2Fe–2S] show more complex absorption bands between 410 nm and 430 nm, in the range of 470 nm, as well as a relatively broad maximum between 550 nm and 600 nm, while proteins containing a [4Fe–4S] cluster show a characteristic peak between 400 nm and 420 nm (Freibert *et al.*, 2018).

2.4 Material and Methods

2.4.1 Gene Expression and Protein Isolation

For gene expression in *E. coli* BL21(DE3) overnight starting cultures containing one of the plasmids hosting the genes *acnB*, *ispH*, *nadA* or *thnB* were used to inoculate 2x Yeast extract (2YT) medium at 1% (v/v). 2YT medium was supplemented with a final concentration of 100 µg/ml ampicillin and the cells were cultivated under shaking at 37 °C and 160 rpm until the optical density measured at 600 nm (OD_{600}) reached 2. Gene expression was induced by adding 0.5 mM Isopropyl-β-D-thiogalactopyranosid (IPTG). For the gene expression supported by the operons of the Fe–S cluster assembly machineries, overnight starting cultures of *E. coli* BL21(DE3) Δ*iscR* (Akhtar & Jones, 2008) containing the plasmids encoding for the target protein as well as *E. coli* BL21(DE3) containing one plasmid encoding for the target protein as well as a second plasmid pACYC*iscS-fdx* (pISC) (Gräwert *et al.*, 2004) or pACYC-Duet-1-*suf* (pSUF) (Hänzelmann *et al.*, 2004) were used to inoculate 2YT medium at 1% (v/v). TB medium was supplemented with kanamycin (50 µg/ml), ampicillin (100 µg/ml) or chloramphenicol (25 µg/ml) as needed, as well as ferric ammonium citrate (2 mM final concentration). Cells were cultivated aerobically at 37 °C and 160 rpm until the OD_{600} reached 2. Subsequently, the gene expression was induced using 0.5 mM IPTG. To facilitate Fe–S cluster assembly 2 mM L-Cysteine were added. All cultures were incubated at 25 °C and 140 rpm for 20 h following induction. Cells were harvested by centrifugation for 10 min at 6,000 x *g* and 4 °C. For cell lysis cells were resuspended in 50 mM Tris pH 8.0, 150 mM NaCl containing EDTA-free cOmplete™ Protease Inhibitor Cocktail Tablets (Roche, Basel, Switzerland) were added according to the manufacturer's instructions. After stirring at room temperature (RT) for 20 min under anaerobic

conditions, the samples were covered with argon to maintain anaerobic conditions and the cell suspension was sonicated for 20 min with an amplitude of 60% and a pulse of 1 s every 3 s using VS70/T sonotrode (Bandelin electronic, Berlin, Germany). Argon covered lysates were clarified by centrifugation at 40,000 x *g*.

2.4.2 Anaerobic Protein Purification

Protein purification and all following procedures were carried out under strictly anaerobic condition in an anaerobic chamber with < 2 ppm O_2. Isolation and purification of the protein was performed using immobilized metal affinity chromatography. Therefore, protein lysates were applied to a Protino Ni-NTA Agarose column (Macherey-Nagel, Düren, Germany) that was equilibrated in wash buffer (50 mM Tris pH 8.0, 150 mMNaCl) using an ÄKTA start system (GE Healthcare, Little Chalfont, UK). The column was then washed with wash buffer containing 50 mM imidazole to remove unspecifically bound proteins and the target protein was eluted with 250 mM imidazole. Fractions containing the target protein were pooled, dialyzed against wash buffer, and their purity was analyzed by SDS-PAGE. Protein concentrations of the protein samples were determined using the Bradford method (Bradford, 1976).

2.4.3 Chemical Reconstitution

For the first step of the chemical reconstitution reaction, the reduction of the as-isolated protein with dithiothreitol (DTT), 100 µM protein solution were incubated with 1 mM DTT for 1 h on ice and then supplemented with 600 µM ferric ammonium citrate (FAC) and 600 µM Li_2S for the proteins with one [4Fe–4S] cluster. In case of ThnB, which contains two [4Fe–4S] clusters 600 µM FAC and 900 µM Li_2S were added. After an incubation time of 1 h the protein was applied to a PD-10 Desalting Column (GE Healtthcare, Little Chalfont, UK) that was equilibrated with 50 mM HEPES, pH 7.5; 100 mM KCl to separate the protein from excess iron and sulfide. Finally, the volume of the protein solution was adjusted to 500 µl.

2.4.4 Semi-enzymatic Reconstitution

For the semi-enzymatic reconstitution reaction 100 µM protein solution were incubated on ice with 1 mM DTT for 1 h. Then 20 µM *E. coli* cysteine desulfurase IscS, 5 mM L-Cysteine, and 600 µM FAC were added to the protein followed by an incubation of 1 h at RT. Subsequently, excess reagents were removed using a PD-10 Desalting Column (GE Healtthcare, Little Chalfont, UK) equilibrated with 50 mM HEPES, pH .5; 100 mM KCl. Finally, the volume of the protein solution was adjusted to 500 µl.

2.4.5 Determination of Metal Content

To obtain the metal-to-monomer ratio of the isolated samples, we determined the protein concentration using the Bradford method (Bradford, 1976) and measured the iron content using

inductively coupled plasma mass spectroscopy. Samples were prepared by precipitating 10 µM of freshly, anaerobically isolated protein with 3% trace-metal grade nitric acid. Precipitate was removed by centrifugation for 30 min at 15,000 $\times$ *g* and the sample was then transferred to a metal-free centrifugation tube (VWR, Radnor, PA, USA). Measurements of the iron content were performed using an Agilent 7700 ICP-MS (Agilent Technologies, Waldbronn, Germany) in the Biocenter MS-Platform at the University of Cologne. The measurements were done by strictly following the manufacturer's instructions using He in the collision cell mode to minimize spectral interferences. Measurements were performed in technical triplicates and the presented data has an r^2 value of 0.999.

2.4.6 Electronic Absorption Spectroscopy (EAS)

Electronic absorption spectra were collected using a Cary-60 spectrophotometer (Agilent Technologies, Ratingen, Germany) with 1 nm bandwidth, a scanning speed of 120 nm/min and a 1-cm-path-length quartz cuvette at RT.

2.4.7 Circular Dichroism (CD) Spectroscopy

CD spectra were collected using a Jasco J-815 Circular dichroism spectrometer (Jasco Germany, Pfungstadt, Germany) with a scanning speed of 100 nm/min and a bandwidth of 5 nm in a 2 mm path length quartz cuvette. An average of 20 scans was collected at 20 °C with 1 nm resolution. The spectra were processed with the Spectra Analysis software using the Adaptive-Smoothing function with the following parameters: convolution width 15, noise deviations 1. CD spectra of HEPES and Tris buffer (Figure S2.3) were subtracted from protein spectra prior to the calculation of the molar ellipticity and plotting the data. Samples for CD spectroscopy were in a concentration range between 150 and 300 µM.

2.5 Results and Discussion

The production of correctly assembled Fe–S cluster proteins is a major challenge in the field. We have compared six different strategies for protein production in this work: (i) expression in BL21(DE3); (ii) expression in BL21(DE3) and chemical reconstitution; (iii) expression in BL21(DE3) and semi-enzymatic reconstitution; (iv) co-expression in BL21(DE3) with pISC; (v) co-expression in BL21(DE3) with pSUF; and (vi) expression in BL21(DE3) Δ*iscR*. Hereby, gene expression was always performed under aerobic conditions, cell lysis and all further steps under anaerobic conditions. The target proteins *E. coli* AcnB, *E. coli* IspH, and *E. coli* NadA contain one [4Fe–4S] cluster ligated by three cysteine residues. We also studied cluster incorporation into the radical SAM enzyme *B. thuringiensis* ThnB that contains two Fe–S clusters, one of them with an open coordination site for the SAM cofactor. We studied the impact of the protocol on expression levels, Fe–S cluster content, and specificity of cluster incorporation.

2.5.1 Expression Levels

We compared the protein levels obtained in different cell lines, including XL1-Blue, BL21(DE3), and BL21 (DE3) Δ*iscR* utilizing SDS-PAGE and Western blot analysis (Figure 2.3). Common BL21(DE3) cells harbor both, the ISC and SUF Fe–S pathways (Barras *et al.*, 2005; Johnson *et al.*, 2005). However, when expressing genes to an abnormally high level, the endogenous enzymes involved in biosynthesis are not capable of producing and transferring a sufficient amount of Fe–S clusters. BL21(DE3) cells containing an additional plasmid encoding for the Fe–S assembly machineries ISC or SUF produce an increased level of ISC or SUF proteins, respectively, which may result in increased levels of Fe–S cluster content in the target protein. XL1-Blue cells are routinely utilized for cloning, yet they have been successfully applied for co-expression of IspH with the ISC proteins (Gräwert *et al.*, 2004), therefore, we included expression tests with XL1-Blue cells harboring pISC or pSUF in our study. Another approach to increase the level of Fe–S biosynthesis proteins is to delete the regulator of the ISC pathway, IscR, which is responsible for the attenuation of the ISC proteins. The *E. coli* BL21(DE3) Δ*iscR* cell strain shows an upregulation of *isc* operon expression, leading to higher levels of the ISC proteins and the ability to maturate abnormally high levels of Fe–S proteins. Notably, recent studies indicate a more general role of IscR in the regulation of Fe–S cluster biogenesis, therefore the deletion of IscR may also influence the SUF protein levels (Giel *et al.*, 2006).

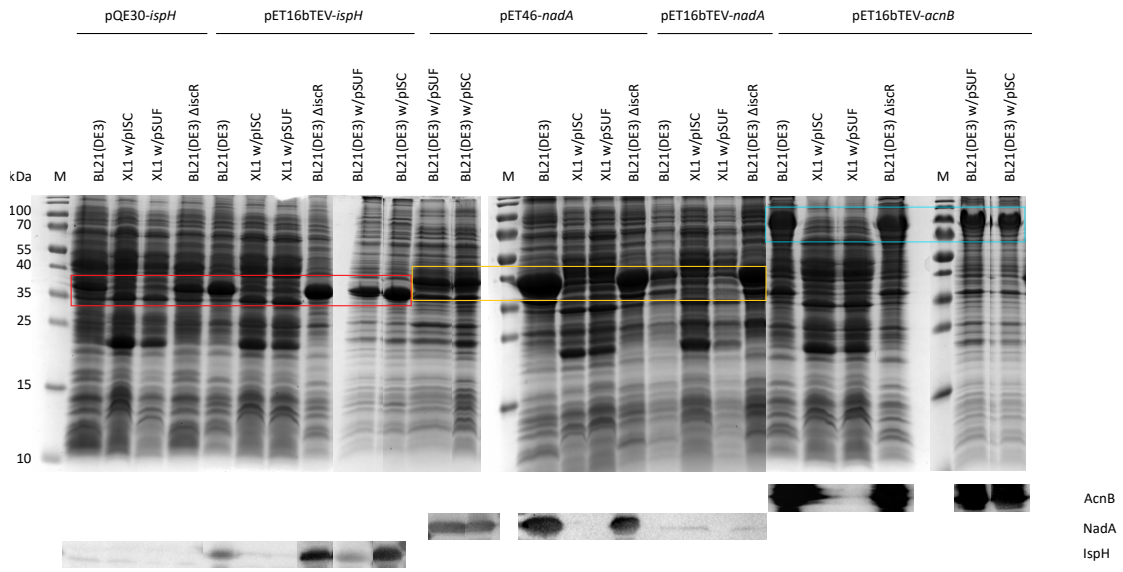

Figure 2.3: Analysis of *ispH*, *nadA* and *acnB* expression in different systems. The cell lysate was analyzed by SDS-PAGE on a 15% Tris-Glycine gel and proteins were visualized by Coomassie staining (top) and the corresponding a Western blot analysis using a conjugated anti-Histidine antibody (bottom).

The constructs for IspH, NadA, and AcnB were designed to result in proteins with an N-terminal Histidine affinity tag followed by the recognition site for the TEV protease to allow for

cleavage of the Histidine affinity tag. In addition, we have also investigated the expression of the constructs pQE30-*ispH* (Gräwert *et al.*, 2004) with a Histidine affinity tag and no protease recognition site as well as pET46-*nadA* with a Histidine affinity tag and an enterokinase cleavage site. These constructs were previously used for protein production, however, the Histidine affinity tag enhances the purity after the first purification step and is, thus, more suitable for our study. We expressed the five different constructs in six different cell lines, except pQE30-*ispH*, which did not co-transform with neither the pISC, nor the pSUF plasmid.

Western blot analysis indicated that pQE30-*ispH* does not express in either cell strain, which is surprising, as previous studies report high protein yields for pQE30-*ispH* using the XL1-Blue cells harboring the pISC plasmid (Gräwert *et al.*, 2004). The pISC plasmid used for protein biosynthesis in this study is different from the one previously used, since it was discovered that the originally used pISC plasmid contained three point mutation in the *iscS* and *iscU* genes (Span, 2012). Interestingly, correction of these mutations resulted in a dramatic reduction of *ispH* expression in *E. coli* XL1-Blue cells. SDS-PAGE analysis shows protein bands for expression in BL21(DE3) and BL21(DE3) Δ*iscR*, suggesting that IspH protein is synthesized. The Histidine affinity tag of this construct is shorter, which could influence the Western blot analysis. Another possibility is that the Histidine affinity tag is not accessible, possibly due to dimer formation, which was also observed in the crystal structure (Gräwert *et al.*, 2009).

We also observe no detectable expression of either protein in the XL1-Blue cell line independent of the co-transformed plasmid. Furthermore, we obtained high amounts of protein for all other samples and Western blot analysis confirmed that the proteins carry a Histidine affinity tag and are most certainly our target proteins. Notably, the intensity of the signal on the Western blot does not necessary correspond to the amount of protein, since there are several factors that influence staining. Thus, we base our decision of which expression system to select for protein production not fully on SDS-PAGE or Western blot analysis, but on the resulting protein yield after the initial purification step.

The protein AcnB from *E. coli* is a [4Fe–4S] cluster protein that plays a key role in the citric acid cycle under conditions in which sufficient iron is present, whereas in the absence of iron, the protein loses its enzymatic activity and functions as a nucleic acid binding protein, stabilizing its own mRNA (Beinert & Kennedy, 1993; Tang & Guest, 1999; Williams *et al.*, 2002). Western blot analysis of cell lysates after the expression of the protein in E. coli BL21(DE3) provide evidence that additional co-expression of the *acnB* gene with genes encoding for the SUF or ISC machinery do not have an influence on the protein levels of AcnB. The same is true for the expression of *acnB* in BL21(DE3) Δ*iscR* (Figure 2.3). In all cases, expression was directed from a pET16bTEV expression plasmid resulting in a target protein with an N-terminal Histidine affinity tag .

Purification of AcnB has only slightly been influenced by the choice of the expression system. Isolation of AcnB from BL21(DE3) with the additional plasmid pSUF and from BL21(DE3) Δ*iscR* resulted in 500 µl protein solution with a concentration of approximately 300 µM (75 nmol, 7 mg) obtained from 1 l expression culture using immobilized metal affinity chromatography (IMAC). Isolation of AcnB from BL21(DE3) with and without the additional plasmid pISC resulted in

500 µl protein solution with a slightly lower concentration of 250 µM (63 nmol, 6 mg) (Table 2.1, Figure S2.1).

The protein IspH from *E. coli* is an enzyme catalyzing the conversion of 1-hydroxy-2-methyl-2-(E)-butenyl diphosphate into isopentenyl diphosphate and dimethylallyldiphosphate in the nonmevalonate isoprenoid biosynthesis pathway. The protein hosts a [4Fe–4S] cluster (Span *et al.*, 2012), but enzymatic activity can also be discovered in a variant hosting a [3Fe–4S] cluster (Gräwert *et al.*, 2009). In this study, we expressed the *ispH* gene fused to an N-terminal Histidine affinity tag from a pET16bTEV expression vector in BL21(DE3) and BL21(DE3) Δ*iscR* cells in the presence and absence of the plasmids pSUF and pISC and compared our results with previously reported spectroscopic data on IspH. Previous studies on IspH used either the *E. coli* strain M15[pREP4] or XL1-Blue with the *ispH* gene hosted in a pQE30 expression vector (Gräwert *et al.*, 2004; Wolff *et al.*, 2003). In the latter study using *E. coli* XL1-Blue cells for gene expression, the pISC plasmid was co-expressed with the pQE30 expression vector hosting the target protein, however the growth medium was not supplemented with additional iron or sulfur sources. Isolation of the protein was carried out under strictly anaerobic conditions resulting in a protein fraction that shows a significant peak at 410 nm with a molar extinction coefficient of 11.9 mM^{-1} cm^{-1} for a monomeric protein structure (Gräwert *et al.*, 2004). Purification of IspH isolated from *E. coli* M15[pREP4] was performed aerobically and the Fe–S cluster was then anaerobically reconstituted using Na_2S, $FeCl_3$ and DTT. Here, a molar extinction coefficient at 410 nm with a value of 18.75 mM^{-1} cm^{-1} has been observed for a dimeric protein structure (Wolff *et al.*, 2003). In this study, we explored that the co-expression of the *ispH* gene with the plasmids pSUF and pISC had a positive effect on the protein level in BL21(DE3) (Figure 2.3). For Expression in BL21(DE3) in the absence of pSUF and pISC as well as the expression in BL21(DE3) Δ*iscR* reduced protein levels have been observed. Additionally, we tested the expression of *ispH* directed from the expression vector pET16bTEV in *E. coli* XL1-Blue with the additional plasmids pISC and pSUF respectively, but Western blot analysis revealed that the protein production using these expression systems was not successful. The same is true for the expression of *ispH* directed from the expression vector pQE30 in BL21(DE3) with and without the plasmids pSUF and pISC as well as in BL21(DE3) Δ*iscR* (Figure 2.3). The protein yields obtained after the purification process are in agreement with the observations for the expression levels of *ispH*. After the IspH isolation from BL21(DE3) with pSUF or pISC 500 µl with a concentration of 150 µM (38 nmol, 1.4 mg) were obtained, while the concentrations were higher in samples obtained from the expression in BL21(DE3) and from BL21(DE3) Δ*iscR* (500 µl with a concentration of 250 µl, i.e. 63 nmol, 2.3 mg) (Table 2.2 and Figure S2.1).

Quinolinic acid is an intermediate in the synthesis of NAD that is an important cofactor in numerous redox reactions (Begley *et al.*, 2001). *E. coli* and most other prokaryotes generate quinolinic acid via a condensation reaction between dihydroxyacetone phosphate and iminosuccinate. For this purpose, two proteins are required: the quinolinate synthetase, NadA, and the aspartate oxidase, NadB (Begley *et al.*, 2001). In this study we are focusing on the [4Fe–4S] cluster protein NadA. In a previous study, the presence and nature of the Fe–S cluster has been explored after the expression of *nadA* on the expression plasmid pET-28A in *E. coli*

with an additional arabinose-inducible plasmid pDB1282 harboring the genes encoding for the proteins of the ISC machinery (Cicchillo *et al.*, 2005). Spectroscopic analysis to verify the presence of the [4Fe–4S] cluster was carried out either on the as-isolated protein using EAS and EPR spectroscopy or with a chemically reconstituted sample using Mössbauer spectroscopy. In the present study, we tested two constructs for the expression of the gene *nadA*: In analogy to our studies on AcnB, IspH and ThnB we generated a construct in which the gene was incorporated into the expression plasmid pET16bTEV. However, using Western blot analysis, we could not detect any recombinant protein production neither in *E. coli* BL21(DE3), BL21(DE3) Δ*iscR*, nor XL1-Blue (Figure 2.3). Interestingly, the NadA protein levels could be significantly increased using a pET46-*nadA* construct that also allows for the expression of a fusion protein with an N-terminal Histidine affinity tag. Here, the highest expression levels could be detected in BL21(DE3) in the presence of pSUF in BL21 Δ*iscR*, while the expression levels were moderate when the genes encoding for the ISC machinery were co-expressed in BL21(DE3) as well as in BL21(DE3) without co-expression. Purification via IMAC resulted in highly pure protein samples. In a reduced volume of 500 µl after the isolation process a concentration of 250 µM (63 nmol, 2.5 mg) was detected for the samples obtained from BL21(DE3) Δ*iscR*, and BL21(DE3) with the additional plasmid pSUF, while a significantly lower concentration of 150 µM (38 nmol, 1.5 mg) has been detected in the sample obtained from BL21(DE3) without the co-expression of Fe–S cluster assembly machineries and with additional co-expression of pISC (Table 2.3 and Figure S2.1).

2.5.2 Analysis of Iron Content

The first protein that we investigated in terms of Fe–S cluster maturation is *E. coli* AcnB, which contains an [3Fe–4S] cluster in the inactive form that can be activated by conversion to the [4Fe–4S] form. Our spectroscopic analysis of AcnB produced using the previously mentioned strategies reveals significant differences in the cluster occupancy of the different samples. Expression in BL21(DE3) cells in the absence or presence of an additional plasmid encoding for the genes for the ISC or SUF machinery led to the isolation of the apo protein without significant amounts of iron as indicated by an electronic spectra (Figure 2.4A). The absorption bands at 325 nm and in the range of 400–420 nm with low intensities and molar extinction coefficients below 3 $mM^{-1}cm^{-1}$ (Table 2.1) are a strong indicators for low Fe–S cluster content. Protein obtained from *E. coli* BL21(DE3) Δ*iscR* cells shows a molar extinction coefficient of 7.6 $mM^{-1}cm^{-1}$ at 420 nm, suggesting an improved incorporation of Fe–S clusters into the protein. According to the literature, values of 10 $mM^{-1}cm^{-1}$ are common for fully loaded Fe–S proteins (Jacquot, 2017), leading to the conclusion that the majority of AcnB protein obtained from *E. coli* BL21(DE3) Δ*iscR* cells contains an Fe–S cluster. We were able to increase the amount of Fe–S cluster in protein isolated in the apo form from *E. coli* BL21(DE3) cells using chemical or semi-enzymatic reconstitution. Both protocols led to samples with a molar extinction coefficient of > 18 $mM^{-1}cm^{-1}$ for the major absorption band. Surprisingly, the molar extinction coefficients of the major signal are significantly higher than previously reported for *E. coli*

AcnB obtained by expression in the *E. coli* strain W3110 and reconstituted with $(NH_4)_2Fe(SO_4)$, Na_2S, and DTT after (8 $mM^{-1}cm^{-1}$ to 10 mM^{-1} cm^{-1}) (JORDAN *et al.*, 1999). Interestingly, we also observe a shift of the most prominent signal from 420 nm to 400 nm in the protein sample obtained by chemical reconstitution. Furthermore, we observe a large absorption feature at wavelengths higher than 650 nm, indicating impurities that are not bound to the protein but cannot be separated using a desalting column.

To investigate the sample in more detail, we measured CD spectra in the visible region (Stephens *et al.*, 1978). The ciral nature of Fe–S clusters inside proteins makes Fe–S proteins amenable for CD spectroscopy. While all Fe–S proteins exhibit characteristic CD signals, the CD spectra of [4Fe–4S] cluster containing proteins are less defined compared to [2Fe–2S] proteins and often of low intensity (Freibert *et al.*, 2018). Low intensity of absence of a signal in the CD spectrum is an indicator of either low concentration of a species or a highly symmetric environment. The advantage of CD spectroscopy over EAS is that the absorption bands split up to maxima and minima, therefore, facilitating the detection of subtle changes, and bands deriving from absorbing impurities do not contribute to the spectrum. The latter includes metal ions in solution, as well as metal complexes formed with buffer substances or other reagents, such as reducing substances.

The electronic spectra of the AcnB samples show bands at 325 nm and in the region of 400–420 nm, which are characteristic for protein-bound [4Fe–4S] clusters, however, all absorption features are quite broad with a high background. The bands in the CD spectra show minima at 325 nm and 400 nm as well as maxima at 310 nm, 360 nm, 450 nm, 590 nm, and 640 nm. When taking a closer look at the 400–450 nm range of the CD spectrum it becomes evident that the absorption bands for both reconstituted samples are at 410 nm, whereas the predominant band of the samples from the BL21(DE3) Δ*iscR* cells is located at 450 nm. This shift most likely indicates differences in the oxidation states of the [4Fe–4S] cluster, similar to the observations for the [4Fe–4S] ferredoxin from *Bacillus stearothermophilus* (Mullinger *et al.*, 1975). The electronic spectrum of the oxidized cluster in ferredoxin resembles the spectrum of AcnB protein. The maximum at 410 nm in the ferredoxin spectrum was assigned to the oxidized form of the [4Fe–4S] cluster, whereas the maximum at 450 nm corresponds to the reduced form. These findings suggest that the [4Fe–4S] cluster is in a different oxidation state when matured *in vitro*, which has a dramatic impact on the characterization of proteins by spectroscopy.

Absorption features in CD spectra can be more easily distinguished from each other than in electronic spectra, especially the features beyond 550 nm. The baseline was corrected for the buffer used for the samples, however, the baseline of some of the AcnB samples is unexpectedly high above 600 nm. In addition, the noise levels increase significantly beyond 600 nm. Therefore, it is difficult to compare the molar ellipticity values analogous to molar extinction coefficients. Despite the shifted baselines, the CD spectra indicate that the samples obtained by chemical and semi-enzymatic reconstitution do not contain significantly more Fe–S clusters than the *in vivo* maturated samples isolated from *E. coli* BL21(DE3) Δ*iscR* cells. In addition, the broad features at 590 nm and 640 nm support the presence of impurities consisting most likely of Fe–S aggregates.

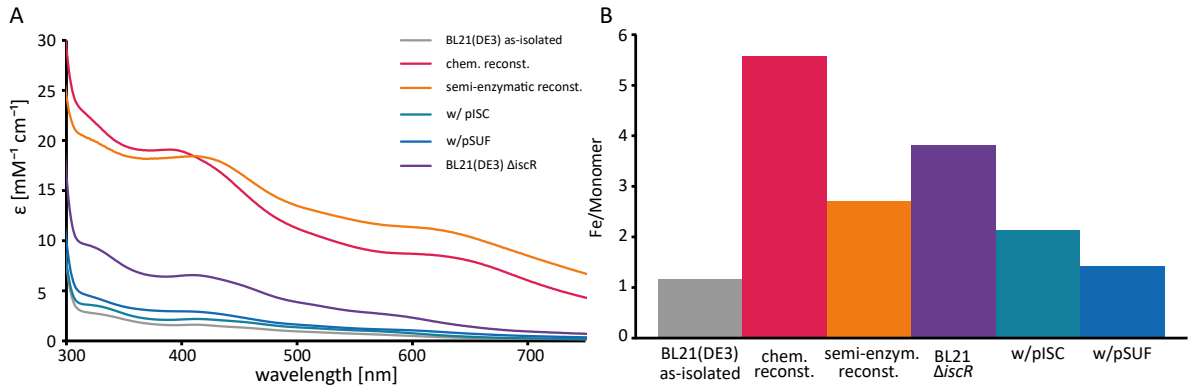

Figure 2.4: Analysis of Fe–S content of AcnB protein obtained by different strategies. (A) Electronic absorption spectra reveal the Fe–S content of the AcnB protein. Corresponding CD spectra are shown in Figure S2.2A. (B) Iron content per monomer of the samples in (A) determined by ICP-MS measurements. AcnB protein as-isolated from *E. coli* BL21(DE3) is shown in grey, samples obtained by subsequent chemical or semi-enzymatic reconstitution are displayed in pink or orange, respectively. Samples co-expressed with either pISC or pSUF are shown in green or blue, respectively, and protein isolated from BL21(DE3) Δ*iscR* is presented in purple.

To determine the amount of iron bound to the AcnB protein, we adjusted the protein concentration of all samples and measured the iron content utilizing ICP-MS. Hence, we were able to determine the iron per monomer ratio for AcnB obtained by different protocols. Our results show that the samples isolated form *E. coli* BL21(DE3) contain approximately one iron per monomer, while the samples isolated from *E. coli* BL21(DE3) co-expressed with either the pISC or pSUF plasmid contain up to two iron per monomer (Figure 2.4B). AcnB as isolated from *E. coli* BL21(DE3) Δ*iscR* binds close to four iron per monomer, pointing to a fully loaded Fe–S protein. In line with the spectroscopic results, the protein obtained by chemical reconstitution binds more than five irons per monomer, suggesting adventitious metal binding. Surprisingly, the samples obtained by semi-enzymatic reconstitution show an iron content lower than 3, which is significantly lower than expected based on the high absorption at 420 nm in the EAS. We speculate that the discrepancy between this ICP-MS result and the EAS may be caused by inaccuracy during determining the protein concentration, which has previously been reported to be the most error-prone step (Galle *et al.*, 2018). In summary, our results show that reconstitution of Fe–S cluster using the chemical or semi-enzymatic approach lead to high amount of Fe–S cluster content, however, these samples contain also a larger amount of impurities, presumably consisting of Fe–S aggregates. Assembly of Fe–S clusters *in vivo* is more specific and efficient, as the reconstitution step as well as subsequent purification steps are not required. The best result for AcnB protein was achieved by isolating the protein from BL21(DE3) Δ*iscR*.

The ISC machinery is responsible for the housekeeping Fe–S cluster production in *E. coli*. In contrast, the SUF machinery is responsible for the production of Fe–S clusters under stress conditions. Under oxidative stress or iron depletion condition, AcnB enhances its own production by binding to its own mRNA and inducing a positive regulation mechanism (Tang & Guest, 1999). AcnB plays a key role in the citric acid cycle as well as the glyoxylate cycle. Neverthe-

Table 2.1: Overview on different expression strategies and reconstitution methods for the Fe–S cluster protein AcnB.

Expression strategy	Significant band [nm]	Extinction coefficient [$mM^{-1}cm^{-1}$]	Fe/monomer	Yield [nmol] per liter cell culture	Purity [%]
BL21(DE3)	420	1.6	1.1	60	>90
BL21(DE3) chemic. reconst.	400	18.9	5.5	53	–
BL21(DE3) semi-enzym. reconst.	420	18.3	2.8	55	–
BL21 Δ*iscR*	420	7.6	3.9	76	>90
BL21(DE3) w/pISC	420	2.0	2.1	63	>90
BL21(DE3) w/pSUF	420	2.9	1.2	75	>90

less, deletion of this important protein in *E. coli* can be compensated by a second aconitase, AcnA (Gruer *et al.*, 1997), although the sequence identity between both proteins is only 17% (Bradbury *et al.*, 1996). Whereas AcnB is adapted for the major catabolic function (JORDAN *et al.*, 1999), AcnA is responsible for maintenance of the citric acid cycle activity during oxidative stress (Cunningham *et al.*, 1997). A previous study has shown that the $SufBC_2D$ complex is capable of inserting an Fe–S cluster into AcnB, however, we speculate that the interaction of AcnB with the SUF machinery is not biological relevant, since the function of AcnB is compensated by AcnA during oxidative stress conditions. Therefore, the ISC machinery is most likely responsible for the maturation of AcnB inside the cell, which is in line with our observation that the *E. coli* BL21(DE3) Δ*iscR* cells lead to the highest yield of Fe–S containing AcnB protein.

Surprisingly, the co-expression of the *acnB* gene with the additional plasmid pISC in *E. coli* BL21(DE3) cells leads to incomplete cluster assembly in the as-isolated protein. This effect may be a result of additional stress for the host cell caused by the expression of a second plasmid.

The second protein that we investigated is the [4Fe–4S] cluster containing protein IspH. The EAS of the protein samples obtained by different methods are dominated by an absorption band at 415 nm (Figure 2.5A), which is in agreement with previous studies (Gräwert *et al.*, 2004; Wolff *et al.*, 2003). In general, we observe similar trends as for AcnB, even though the differences between as-isolated a reconstituted samples are not as pronounced as for AcnB. IspH protein isolated from *E. coli* BL21(DE3) cells that was then maturated using the semi-enzymatic method shows a lower Fe–S content compared to AcnB, while the co-expression in presence of the pSUF plasmid yields a larger portion of Fe–S containing protein. As for AcnB, we observe a shift of the band at 410 nm to 400 nm for the chemically reconstituted

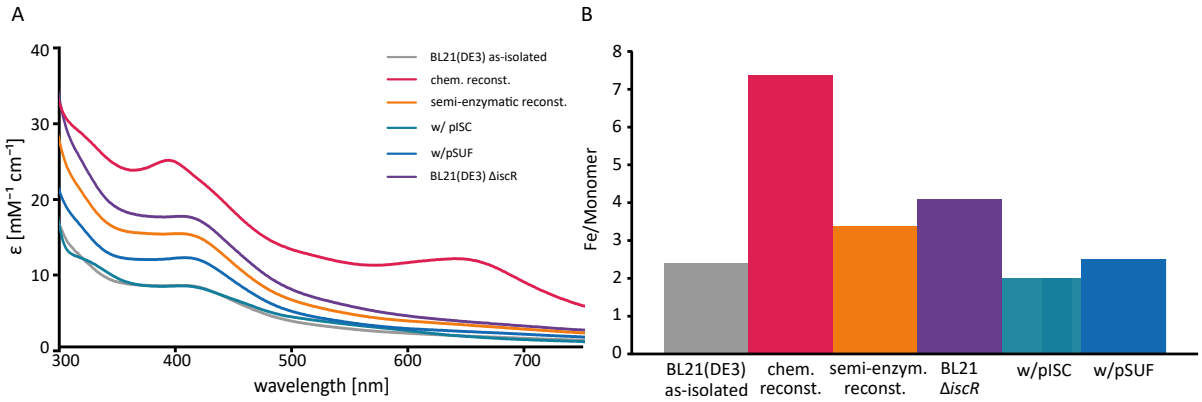

Figure 2.5: Analysis of Fe–S content of IspH protein obtained by different strategies. (A) EAS of IspH protein from different cell strains and after Fe–S reconstitution reactions. Corresponding CD spectra are shown in Figure S2.2B. (B) Iron content per monomer of the samples in (A) determined by ICP-MS measurements. IspH protein as-isolated from *E. coli* BL21(DE3) is shown in grey, samples obtained by subsequent chemical or semi-enzymatic reconstitution are displayed in pink or orange, respectively. Samples co-expressed with either pISC or pSUF are shown in green or blue, respectively, and protein isolated from BL21(DE3) Δ*iscR* is presented in purple.

IspH sample in addition to a broad feature at 650 nm. The large feature beyond 600 nm in the electronic spectrum of chemically reconstituted IspH indicates again the presence of large amount of Fe–S aggregates, which is also supported by the CD spectra (Figure S2.2B). In line with these observations, ICP-MS measurements show that this protein sample contains an average of seven iron per monomer (Figure 2.5B). Overall, the molar extinction coefficients of all IspH samples are higher compared to AcnB (Table 2.2), but the iron per monomer ratios follow the same trend as for AcnB (Figure 2.5B). The absorption feature at 415 nm in the CD spectrum shown for the protein samples obtained by chemical reconstitution and as-isolated from *E. coli* BL21(DE3) Δ*iscR* cells (Figure S2.2B) indicates that the majority of the protein is in the oxidized form.

The amount of iron per monomer is similar for the protein isolated from *E. coli* BL21(DE3) in absence or presence of an additional plasmid encoding for the ISC or SUF machinery. While the yield of IspH protein obtained in BL21(DE3) cells is similar to AcnB, 61 nmol/l and 60 nmol/l cell culture, respectively, the yields of IspH protein obtained from co-expression with the plasmids encoding for the biosynthesis pipelines is reduced by approximately 50% (Tables 2.1 and 2.2). Semi-enzymatic reconstitution results in an iron/monomer ratio of 3, which is consistent with the molar extinction coefficient. The highest Fe–S cluster content of as-isolated protein was again achieved in *E. coli* BL21(DE3) Δ*iscR* cells, with a molar extinction coefficient of 15 $mM^{-1}cm^{-1}$ at 415 nm and 4 Fe/monomer.

Several expression strategies have been reported previously for IspH from *E. coli* as well as *Aquifex aeolicus*. For this purpose, expression was performed in *E. coli* M15, *E. coli* TOP10, and *E. coli* BL21(DE3) cells (Rekittke *et al.*, 2008; Wang *et al.*, 2010; Wolff *et al.*, 2003). These studies reported by three different groups all reported very low Fe–S content, with very low A_{280}/A_{410} ratios, which they increased by chemical reconstitution. A different study reported the

Table 2.2: Overview on different expression strategies and reconstitution methods for the Fe–S cluster protein IspH.

Expression strategy	Significant band [nm]	Extinction coefficient [$mM^{-1}cm^{-1}$]	Fe/monomer	Yield [nmol] per liter cell culture	Purity [%]
BL21(DE3)	415	8.1	2.4	31	>95
BL21(DE3) chemic. reconst.	400	24.6	7.2	23	–
BL21(DE3) semi-enzym. reconst.	415	15.2	3.2	30	–
BL21 Δ*iscR*	415	17.2	4.0	63	>90
BL21(DE3) w/pISC	415	8.0	2.0	63	>95
BL21(DE3) w/pSUF	415	11.5	2.2	38	>95

co-expression of *E. coli* IspH protein with the pISC plasmid in *E. coli* XL1-Blue cells (Gräwert *et al.*, 2004). As mentioned previously, these experiments were carried out using a pISC plasmid with three point mutation that were only discovered afterwards (Span, 2012). We have tried to reproduce these results using a pISC plasmid that was corrected using site-directed mutagenesis, however, no expression was detectable by Western Blot analysis. IspH protein obtained by chemical reconstitution results in a molar extinction coefficient of 2 $mM^{-1}cm^{-1}$ at 410 nm and 7 Fe/monomer. The broad absorption feature at 650 nm and the high iron content suggest that significant amounts of impurities have been formed during the chemical reconstitution reaction. To investigate if the excess iron is specifically bound to the protein or if the impurities consist of Fe–S aggregates, we performed size exclusion chromatography (SEC) on this sample (Figure S2.4). The electronic spectrum of the IspH protein after the SEC reveals that the absorption feature at 650 nm is completely removed by this additional purification step. The A_{650}/A_{410} ratio is reduced from 0.50 to 0.16 by SEC, showing that these impurities consist of Fe–S aggregates, which can be separated from the protein. The additional purification step improves the purity and homogeneiety of the protein sample significantly, however, it requires a fast protein liquid chromatography (FPLC) system in an anaerobic chamber. If this instrumental setup is available, then isolation of the mature Fe–S protein under anaerobic conditions is the more efficient method to obtain active protein, since chemical reconstitution followed by SEC are more time-consuming. Taken together, our results show that expression and maturation in *E. coli* BL21(DE3) Δ*iscR* cells is the most efficient strategy to obtain [4Fe–4S] IspH, as previously observed for AcnB.

The third [4Fe–4S] protein that was studied here is the quinolinate synthetase NadA. Our spectroscopic analysis of the proteins reveals that the trends observed for AcnB and IspH are not reproduced in these experiments. As previously observed for AcnB and IspH, protein maturated by chemical reconstitution using FAC and Li_2S in the presence of DTT yields a high absorption band at 415 nm and a broad feature beyond 600 nm (Figure 2.6A). In combination with the high iron content determined by ICP-MS (Figure 2.6B), the data indicate the formation of unspecific Fe–S aggregates, which is consistent with our previous observations. Unlike AcnB and IspH, the expression of *nadA* (vector pET22b+) in *E. coli BL21(DE3)* Δ*iscR* resulted in the isolation of protein with insufficient cluster loading as shown by the EAS and low Fe/monomer ratio. Expression in *E. coli* BL21(DE3) as well as *E. coli* BL21(DE3) Δ*iscR* result in molar extinction coefficients of 4–6 $mM^{-1}cm^{-1}$ for the band at 415 nm, which indicate that the majority of the protein is in the apo form (Figure 2.6A). NadA protein obtained by semi-enzymatic reconstitution or by co-expression with the *isc* operon yield slightly better results, but overall a low amount of Fe–S cluster containing protein (Table 2.3). The most promising result for NadA protein was obtained by co-expression with the pSUF plasmid in *E. coli* BL21(DE3) cells. The CD spectra of chemically reconstituted NadA and protein obtained by co-expression with the SUF plasmid (Figure S2.2C) show a maximum at 415 nm, supporting an [4Fe–4S] cluster in the oxidized form. The spectroscopic results are in good agreement with the Fe/monomer ration obtained by ICP-MS (Figure 2.6B). The Fe/monomer rations for proteins isolated from *E. coli* BL21(DE3) as well as *E. coli* BL21(DE3) Δ*iscR* are below 1, proteins obtained by semi-enzymatic reconstitution and co-expression with pISC yield a value of approximately 2, and co-expression with pSUF results in 4 Fe/monomer. As previously mentioned, chemical reconstitution leads to excess iron binding to NadA. These results are in good agreement with the presence of an [4Fe–4S] cluster in NadA protein and show that specific and efficient maturation of NadA was achieved using the co-expression strategy with the pSUF plasmid (Rousset *et al.*, 2008).

Our results on the biosynthesis and maturation of AcnB and IspH show that expression in the BL21(DE3) Δ*iscR* cells yields the highest Fe–S cluster content, as observed by EAS, without the binding of excess iron or formation of Fe–S aggregates, as deducted from the ICP-MS analysis. This lead to the initial conclusion that the deletion of the IscR regulator is a superior approach compared to introducing an additional plasmid into the cells, which may result in additional stress for the host cell. The maturation of NadA demonstrates that the co-expression with the SUF plasmid leads to increased Fe–S cluster incorporation. This raises the question whether NadA interacts specifically with the SUF machinery inside the cell. To our knowledge, the interaction of NadA with the SUF proteins have not yet been investigated in detail. Previous studies of *E. coli* NadA with an *E. coli* strains lacking the *iscS* gene have shown that NAD biosynthesis is impaired, leading to the conclusion that *iscS* is essential for the maturation of NadA (Ollagnier-de Choudens *et al.*, 2005). Apparently, *sufS* was not able to replace *iscS* in these experiments and maturate NadA protein. This hypothesis has not been further investigated on a molecular level. Controversially, another study reports a specific connection between NadA and a potential new system for Fe–S assembly in *E.coli* referred to as CSD

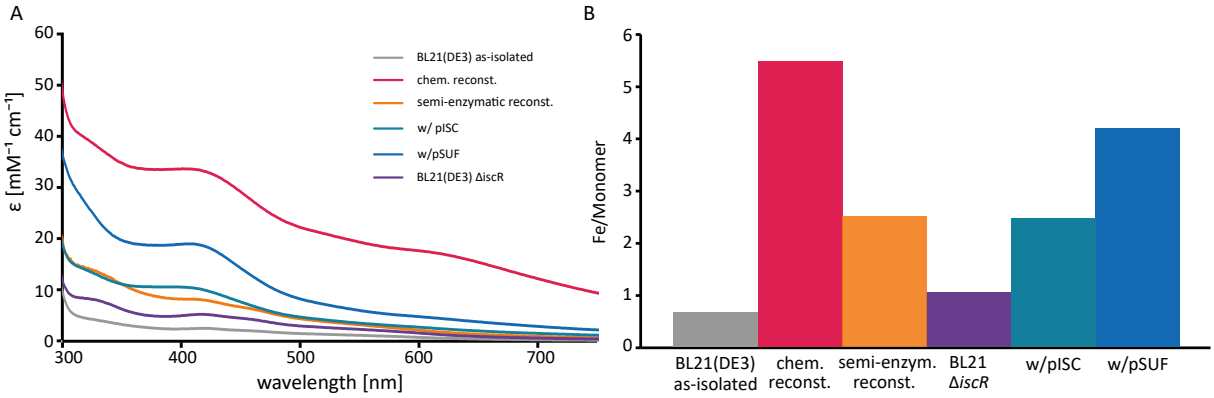

Figure 2.6: Analysis of Fe–S content of NadA protein obtained by different strategies. (A) EAS of NadA samples as-isolated from different cell strains or obtained by different reconstitution methods. Corresponding CD spectra are shown in Figure S2.2C. (B) Iron content per monomer of the samples in (A) determined by ICP-MS measurements. NadA protein as-isolated from *E. coli* BL21(DE3) is shown in grey, samples obtained by subsequent chemical or semi-enzymatic reconstitution are displayed in pink or orange, respectively. Samples co-expressed with either pISC or pSUF are shown in green or blue, respectively, and protein isolated from BL21(DE3) Δ*iscR* is presented in purple.

(Bolstad *et al.*, 2010; Kurihara *et al.*, 2003; Loiseau *et al.*, 2005). The role of this system in Fe–S cluster biosynthesis has not been established yet and recent review articles on this topic only mention two Fe–S biosynthesis pathways in *E. coli* (Lill, 2009). The only evidence for the interaction of NadA and a member of the SUF machinery was provided in *Arabidopsis thaliana* (UM *et al.*, 2007). Hereby, a characterization of two novel chloroplast SufE-like proteins from *A. thaliana* was reported and the results revealed that the mature SufE3 contains two domains, one SufE-like and one with similarity to the bacterial quinolinate synthase, NadA. They showed that SufE3 displayed both SufE activity and quinolinate synthase activity, thus, they concluded that SufE3 is the NadA enzyme of *A. thaliana*. Our results on the maturation of *E. coli* NadA protein corroborate a close relation of NadA and the SUF machinery. These findings are particularly interesting, since in *E. coli* both systems are co-existing and supposedly responsible for the maturation of the same set of proteins under different conditions. While the ISC pathway is predominantly used for Fe–S biosynthesis under standard growth conditions, the SUF pathway is essential under stress conditions. As a consequence, both systems should be able to maturate the same proteins with a high efficiency. The different preferences of the proteins for one system versus the other may be related to the role of the protein in the cell, or possibly relevance of the protein for the survival of the organism.

Taken together our results from the systematic analysis of six different strategies for the maturation of three different [4Fe–4S] proteins, we observe that *in vivo* maturation results in more specific and effective maturation of [4Fe–4S] proteins. For each protein one of the *in vivo* maturation strategies yielded fully assembled Fe–S clusters without excess iron species. However, the suitable biosynthesis method has to be determined for each protein. In all three cases, chemical reconstitution leads to high Fe–S cluster contents in the protein, but also to the formation of high amounts of Fe–S aggregates, which require an additional SEC purification step

Table 2.3: Overview on different expression strategies and reconstitution methods for the Fe–S cluster protein NadA.

Expression strategy	Significant band [nm]	Extinction coefficient [$mM^{-1}cm^{-1}$]	Fe/monomer	Yield [nmol] per liter cell culture	Purity [%]
BL21(DE3)	415	3.5	0.7	19	>95
BL21(DE3) chemic. reconst.	415	36.4	5.6	17	–
BL21(DE3) semi-enzym. reconst.	415	10.1	2.7	18	–
BL21 Δ*iscR*	415	5.5	1.0	63	>95
BL21(DE3) w/pISC	415	12.2	2.4	38	>95
BL21(DE3) w/pSUF	415	20.2	4.2	63	>95

to separate them from the protein sample. In one case, we have also observed that maturation by reconstitution results in a different oxidation state of the [4Fe–4S] cluster compared to *in vivo* maturation. CD spectroscopy has been a very useful tool to obtain more detailed information about the Fe–S cluster and provided insights on the oxidation states of the cluster. So far, we have investigated three proteins, AcnB, IspH, and NadA, which contain only one [4Fe–4S] cluster and have previously been characterized. Next, we aimed at transferring the new insights on Fe–S cluster maturation on the radical SAM enzyme ThnB, which has not yet been maturated *in vivo*.

2.5.3 Maturation of the radical SAM enzyme ThnB

The radical SAM enzyme ThnB from *B. thuringiensis* has been reported to host two [4Fe–4S] clusters and is required for thioether bond formation during the maturation of the sactipeptide ThnH (Wieckowski *et al.*, 2015). Previous spectroscopic analyses of the enzyme were performed on samples obtained from recombinant production in *E. coli* BL21(DE3) directed from the expression plasmid pET28a(+) resulting in a fusion protein with an N-terminal Histidine affinity tag. Using this construct, ThnB could be isolated with high purity by IMAC. EAS and EPR spectroscopy on the chemically reconstituted sample provide evidence for the presence of at least one [4Fe–4S] cluster. Characteristic signals have been detected at 413 nm with a molar extinction coefficient of approximately 30 $mM^{-1}cm^{-1}$ and at 325 nm with a molar extinction coefficient of approximately 40 $mM^{-1}cm^{-1}$. However, determination of the iron and metal content indicate the presence of more than one [4Fe–4S] cluster (Wieckowski *et al.*, 2015). In

the present study, we directed the expression of the *thnB* gene from the expression plasmid pET16bTEV in *E. coli* BL21(DE3) in the presence and absence of the plasmid pISC or pSUF as well as in BL21(DE3) Δ*iscR*. Analysis of the protein levels using Western blot show that the co-expression of *thnB* with the pSUF plasmid results in the highest amount of protein (Figure S2.5). A slightly lower expression level has been detected for the co-expression with pISC and the expression in BL21(DE3) Δ*iscR*. The lowest expression level has been detected for the expression in BL21(DE3) in the absence of pISC or pSUF. These results show that specific expression systems tailored for Fe–S proteins not only increase the fraction of holo protein, but also lead to higher protein levels. In some cases where expression has not resulted in detectable protein levels in common BL21(DE3), using BL21(DE3) Δ*iscR* cells improved the expression levels dramatically and large amounts of Fe–S proteins could be isolated (unpublished data).

The electronic spectra show that co-expression with pISC, expression in BL21(DE3) Δ*iscR* cells and BL21(DE3) cells leads to a large fraction of apo ThnB. This is in line with a low metal content of < 1.0 Fe/monomer (Figure 2.7B, Table 2.4). Maturation of ThnB by chemical reconstitution was previously reported to result in considerable amounts protein containing two correctly assembled [4Fe–4S] clusters (Wieckowski *et al.*, 2015). Unfortunately, we were not able to reproduce the high Fe–S content in ThnB. The absorption band at 413 nm in the electronic spectrum of the ThnB protein has a molar extinction coefficient of 12 $mM^{-1}cm^{-1}$, which is considerably lower than in the earlier study. Controversially, these samples contain 13.6 Fe/monomer, which is much higher than expected for a protein binding two [4Fe–4S] clusters. The additional iron most likely corresponds to excess reagent that was not removed by the desalting column or Fe–S aggregates that are often observed for this method.

When using IscS and L-Cysteine as sulfur source, the reconstituted ThnB protein reveals a higher Fe–S content compared to the chemical reaction with a molar extinction coefficient of 24 $mM^{-1}cm^{-1}$ at 413 nm. ICP-MS measurements shows that the protein binds 2.5 Fe/monomer. The most efficient Fe–S cluster assembly was achieved by co-expression of the *thnB* gene with the pSUF. The electronic spectra show a high absorption feature at 413 nm with a molar extinction coefficient of 32 $mM^{-1}cm^{-1}$ (Figure 2.7A, Table 2.4), which is similar to the previously reported values for chemically reconstituted ThnB protein. The metal content was determined by ICP-MS and reveals that the protein binds 5.3 Fe/monomer (Figure 2.7B, Table 2.4). The lower metal content could derive from incomplete cluster assembly or an inaccurate protein concentration determination, as reported previously (Galle *et al.*, 2018). The protein concentration was performed using the Bradford method, which so far has resulted in reliable values, however, the purity of the ThnB samples was lower compared to AcnB, IspH, and NadA. Based on SDS-PAGE analysis we estimate the purity of the samples to be between 60% and 80% (Figure S2.1). While the impurities do not seem to interfere with the spectroscopic analysis, the values for the concentration of ThnB are overestimated, resulting in a lower Fe/monomer ratio.

Another possible explanation would be that the protein contains one [2Fe–2S] cluster in addition to a [4Fe–4S] cluster. The electronic spectrum of the sample obtained from co-expression contains additional absorption bands at 515 nm and 615 nm. A previous study of the antivi-

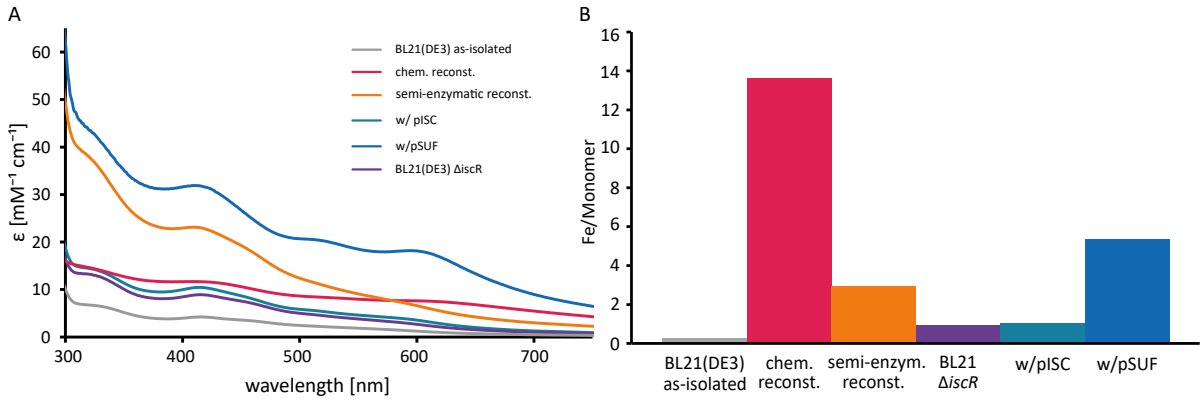

Figure 2.7: Characterization of Fe–S cluster bound to ThnB in different samples. (A) EAS of ThnB samples as-isolated from different cell strains or obtained by different reconstitution methods. Corresponding CD spectra are shown in Figure S2.2D. (B) Iron content per monomer of ThnB proteins shown in (A) determined by ICP-MS measurements. Protein as-isolated from *E. coli* BL21(DE3) is shown in grey, samples obtained by subsequent chemical or semi-enzymatic reconstitution are displayed in pink or orange, respectively. Samples co-expressed with either pISC or pSUF are shown in green or blue, respectively, and protein isolated from BL21(DE3) Δ*iscR* is presented in purple.

ral radical SAM enzyme viperin has assigned the feature at 615 nm to a $[2Fe–2S]^{2+}$ cluster (Duschene & Broderick, 2010). Similar bands have been observed in the electronic spectrum of the active spore photoproduct lyase, a member of the radical SAM superfamily from *Bacillus* (Buis *et al.*, 2006). However, these features have not been analyzed in detail. The Fe content (Figure 2.7B) would be consistent with one [4Fe–4S] and one [2Fe–2S] cluster in ThnB. The CD spectra of ThnB protein obtained by co-expression of the *thnB* gene with the pSUF plasmid and semi-enzymatic reconstitution show a maximum at 450 nm, which indicates that the two [4Fe–4S] clusters are isolated in the reduced form (Figure S2.2D). However, since a CD signal at 450 nm is also characteristic for an oxidized [2Fe–2S] cluster, we cannot exclude the presence of a [2Fe–2S] cluster in ThnB.

Our results show that the presence of the SUF machinery is required for efficient maturation of the radical SAM protein ThnB. This raises the question whether the SUF pathway is the biologically relevant biosynthesis machinery? To our knowledge the Fe–S biosynthesis in *B. thuringiensis* has not yet been investigated. However, *B. subtilis* does not harbor any protein of the ISC machinery (Albrecht *et al.*, 2010; Yokoyama *et al.*, 2018). We used BLAST (Altschul *et al.*, 1990) to perform sequence alignments in order to determine whether *B. thuringiensis* contains the *isc* operon and we were not able to find any member of the ISC pathway, suggesting that *B. thuringiensis* relies on the SUF pathway for Fe–S cluster biosynthesis.

Table 2.4: Overview on different expression strategies and reconstitution methods for the Fe–S cluster protein ThnB.

Expression strategy	Significant band [nm]	Extinction coefficient [$mM^{-1}cm^{-1}$]	Fe/monomer	Yield [nmol] per liter cell culture*	Purity [%]
BL21(DE3)	413	4.2	0.2	31	60
BL21(DE3) chemic. reconst.	413	11.7	13.6	27	–
BL21(DE3) semi-enzym. reconst.	413	24.1	2.5	29	–
BL21 Δ*iscR*	413	9.9	0.9	63	70
BL21(DE3) w/pISC	413	10.5	1.0	61	60
BL21(DE3) w/pSUF	413	31.9	5.3	63	80

* The yield refers to the total amount of protein within the sample not to the exclusive amount of target protein.

2.6 Conclusion

In this study we investigate the maturation of recombinantly produced Fe–S proteins in great detail. We compare six different strategies for protein biosynthesis, including the common expression strain BL21(DE3), three specific cell strains tailored for the maturation of high levels of Fe–S proteins, and two *in vitro* reconstitution methods. The biosynthesis of Fe–S proteins in nature has been studied extensively, however, the maturation of recombinantly produced Fe–S proteins has only been investigated for highly complex systems, such as hydrogenases or nitrogenases. We have, for the first time, systematically evaluated the most common maturation protocols for three well-characterized [4Fe–4S] proteins. The pitfalls of chemical reconstitution pointed out here, such as the formation of Fe–S aggregates, unspecifically bound iron, and different oxidation states of the cluster, have previously led to conflicting results in different studies. These strategies are not limited to proteins containing one [4Fe–4S] cluster. We have previously shown that the same strategies can be applied for the maturation of a [2Fe–2S] protein. In addition, we have demonstrated that this approach can be also used for a radical SAM enzyme. Therefore, we consider the presented methods to be applicable for a large variety of Fe–S cluster-containing proteins. As a consequence, our results will contribute to improve the maturation of Fe–S proteins and obtain samples with correctly assembled cofactors, allowing for understanding the function of the proteins. Maturation of the proteins *in vivo* also leads to more homogeneous samples, which are more amenable for structure determination.

SUPPORTING DATA

Supplementary Tables

Table S2.1: Plasmids used in this study.

Plasmid	Reference
pACYC*iscS-fdx* (pISC)	Gräwert *et al.*
pACYC-Duet-1-*suf* (pSUF)	Hänzelmann *et al.*
pET16bTEV-*acnB*	This work
pET16bTEV-*ispH*	This work
pQE30-*ispH*	Gräwert *et al.*
pET46-*nadA*	This work
pET16bTEV-*nadA*	This work
pET16bTEV-*thnB*	This work

Supplementary Figures

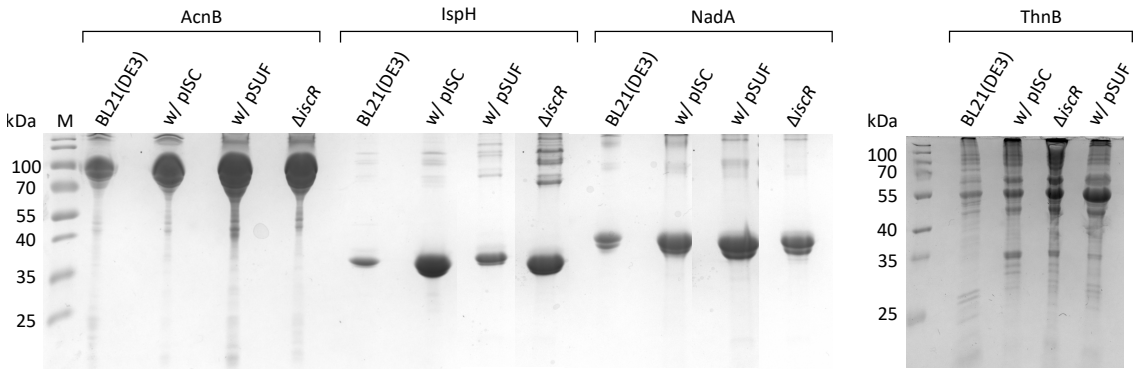

Figure S2.1: SDS PAGE (15%) to analyze the purity of the different proteins after Ni-NTA-column. The fractions containing the target protein were pooled and the volume was reduced to 500 µl, before 5 µl were applied to the gel.

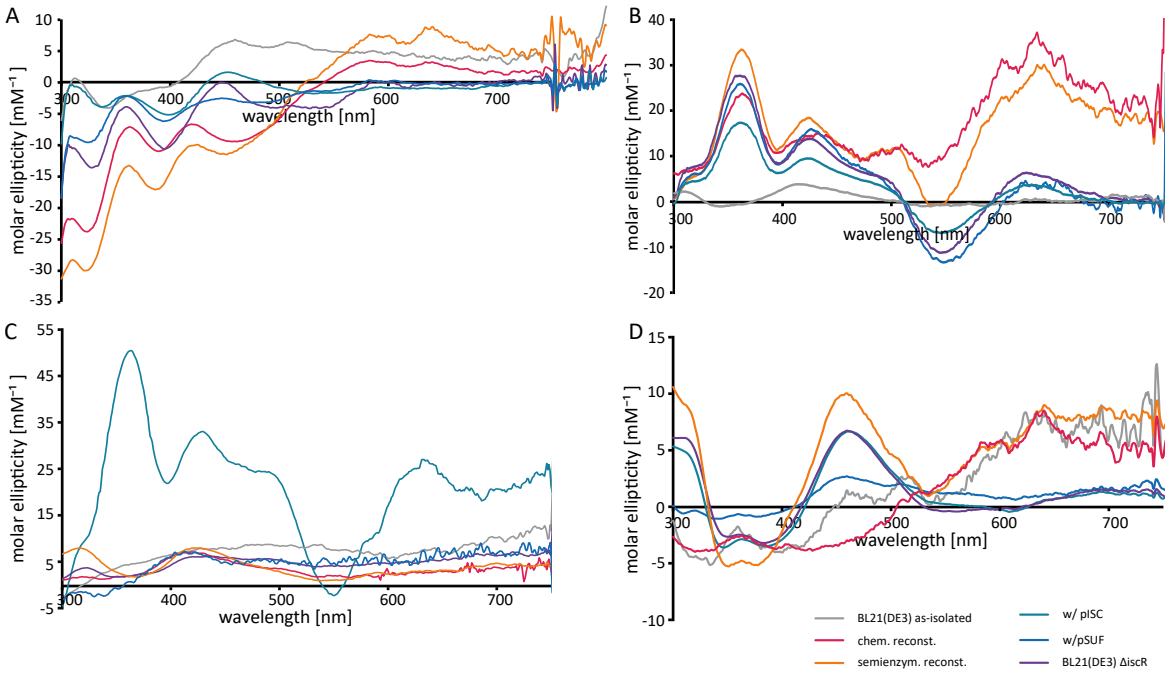

Figure S2.2: CD spectra of the Fe–S cluster containing proteins AcnB (A), IspH (B), NadA (C), and ThnB (D). The concentrations of the protein samples were in the range of 150 µM and 300 µM.

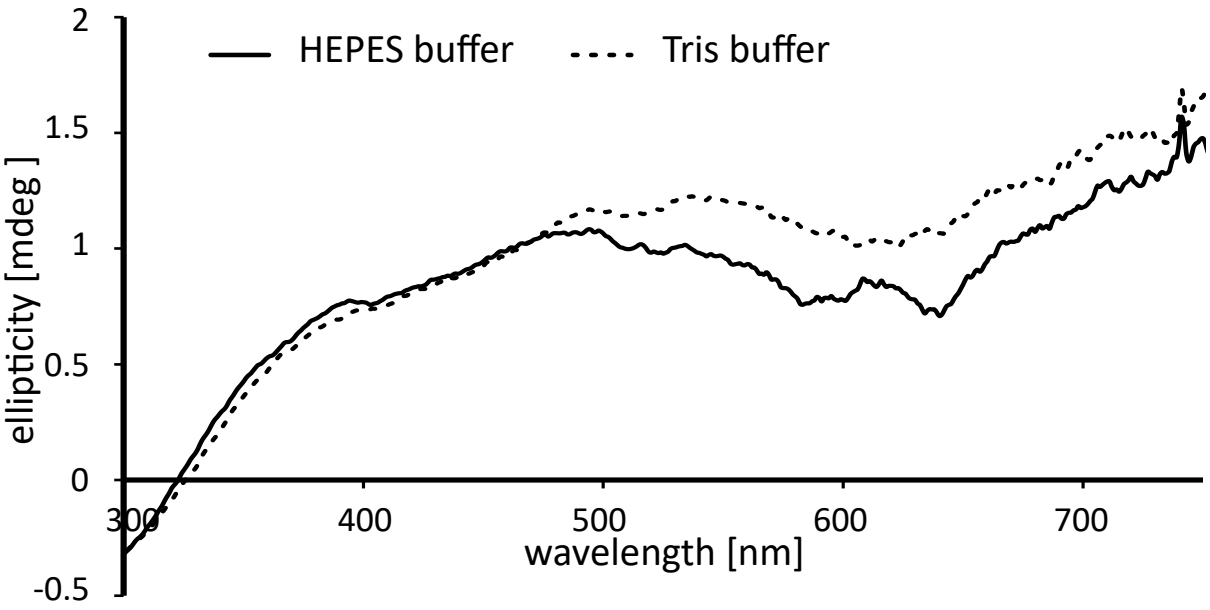

Figure S2.3: CD spectra of HEPES and Tris buffer that have been subtracted from the protein spectra prior to the calculation of the molar ellipticity and plotting the data.

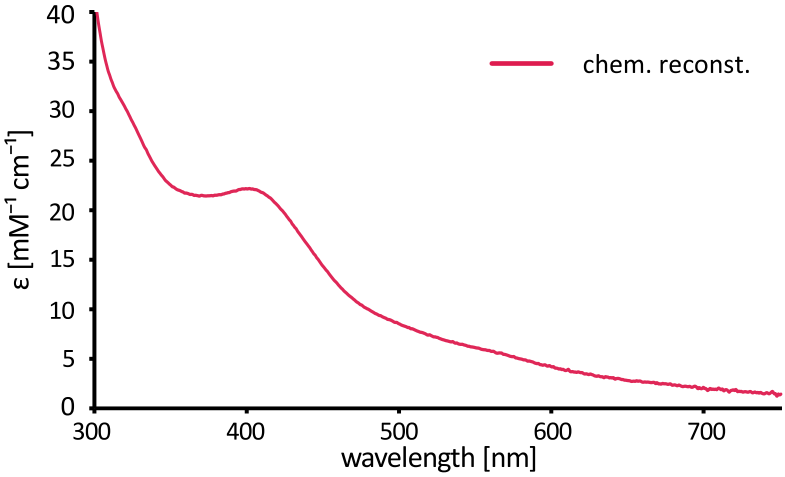

Figure S2.4: EAS of chemically reconstituted IspH after SEC.

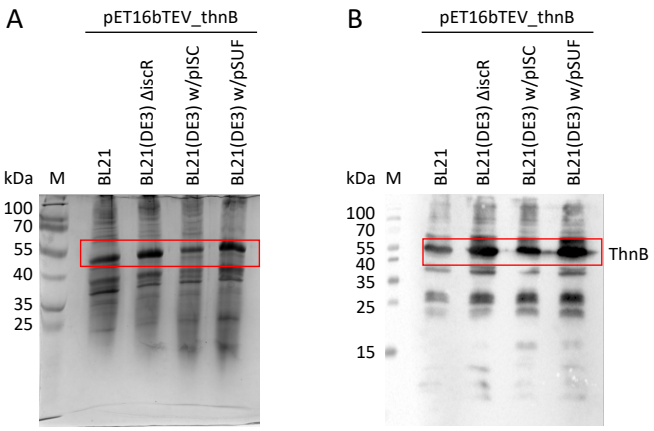

Figure S2.5: Analyzation of the expression of *thnB* and the production of the corresponding protein. (A) Sodium dodecyl sulfate (SDS) polyacrylamide gel (PAGE) (15%) and (B) Western blot using a conjugated anti-His antibody of cell lysates after gene expression.

3 Evidence for the formation of artificial cobalt-sulfur clusters in proteins

This chapter reflects content of the following publication.

3.1 Publication information

Steffen Mielenbrink, Sabine Metzger, and Ingrid Span
To be submitted to: **Journal of American Chemical Society**

3.2 Abstract

Hydrogen can be used as energy source to protect the environment from pollution and manifest sustainability in energy generation. Therefor green biocatalysts can be used to functionalize the process of water splitting. One important factor in this process is the development of suitable cofactors fulfilling essential requirements. Several approaches of Co-containing cofactors in biocatalysts could show that Co is suitable to be used for this purpose. However, the effectiveness of these catalysts is still lacking. In this study our approach is to use Fe–S scaffold proteins for the assembly of robust Co–S cluster. We used IscU from three different bacterial organisms and applied different strategies to reconstitute the Co–S cluster. Our results were analyzed by several techniques and compared to characteristics of Fe–S clusters. The combination of our spectroscopic data, quantitative determination of cobalt content, and chromatographic experiments provide evidence for the presence of the first ever reported Co–S cluster in a protein environment. This marks a great step towards the development of effective water splitting biocatalysts and sustainability in energy supply.

3.3 Introduction

Hydrogen gas (H_2) can be used as green fuel source in the future to improve sustainability in energy generation. Microorganisms are capable of producting H_2 from light (Lubitz & Tumas, 2007). This process can be devided into two separate half-reactions: (1) the oxidation of water to generate molecular oxygen, electrons, and protons and (2) proton reduction to molecular hydrogen. Both half-reactions require metal-containing proteins that enable the transfer of electrons. In nature, the first half-reaction, water oxidation, is catalyzed by a manganese complex consisting of 4 Mn, 4 O, and 1 Ca ion (Sozer *et al.*, 2011). Nature has evolved a set of enzymes for the reduction of protons to H_2, which are called hydrogenases. Based on the composition of the cofactors of hydrogenases, these can be divided into three different classes: [Fe], [NiFe], and [FeFe] hydrogenases (Lubitz *et al.*, 2014). In addition to a carbonyl (CO) ligands, the [Fe] hydrogenases contains an iron atom in an unusual coordination. The [NiFe] and [FeFe] hydrogenases are containing a cubic [4Fe–4S] cluster next to a dinuclear metal center. The [FeFe] hydrogenases are the most active H_2-producing biocatalysts; however they are highly oxygen-sensitive. These biocatalysts enable the production of H_2 with high efficiency, are stable in their native environment, and perform catalysis in water. However, their lack of stability and sensitivity towards oxygen hinders their biotechnological application.

Recently, artificial synthetic or semi-synthetic catalysts containing Co have attracted the interest of many researchers focusing on artificial photosynthesis and biological hydrogen production. Examples of synthetic and semi-synthetic catalysts for both half-reactions are shown in Figure 3.1. One approach was the generation of an artificial Co-containing metalloenzyme based on the biotin-streptavidin technology (Figure 3.1A). In this study electro- and photochemical water reduction to hydrogen could be enhanced by the incorporation of Co leading to a lower overpotential and higher production and turnover rates (Call *et al.*, 2019). In another study Co is part of a synthetic cubane [4Co-4O] cluster (Figure 3.1B), which shows catalytic activity on water oxidation, the first half-reaction of water splitting (McCool *et al.*, 2011). Similar to the first approach, a third study combined biological and synthetic approaches, which ended in the incorporation of synthetic cobaloxime derivates into the heme pocket of myoglobin (Figure 3.1C). This construct was able to show H_2 production with low overpotential but with a low turnover number of ten (Kandemir *et al.*, 2016). Each of these studies shows that Co is suitable to function as transition metal in each half-reaction of artificial photosynthesis, although we are focusing on proton reduction. The major drawback of synthetic catalysts is that they are not soluble in water, which would be highly beneficial for sustainable catalysts. The disadvantage of the protein-based systems is their lack of stability and efficiency. Therefore, they strategies are required for the generation of biocatalysts catalyzing the production of H_2 and paving the way to a society relying on green energy.

We aim at generating artificial Co–S cluster-containing metalloenzymes that function as H_2-producing catalysts. Co is already known as parts of essential cofactors of pro- and eukaryotic proteins, e.g. in the metalloproteome of *P. fusiosus*, vitamin B12 coenzymes, and as cobalamin

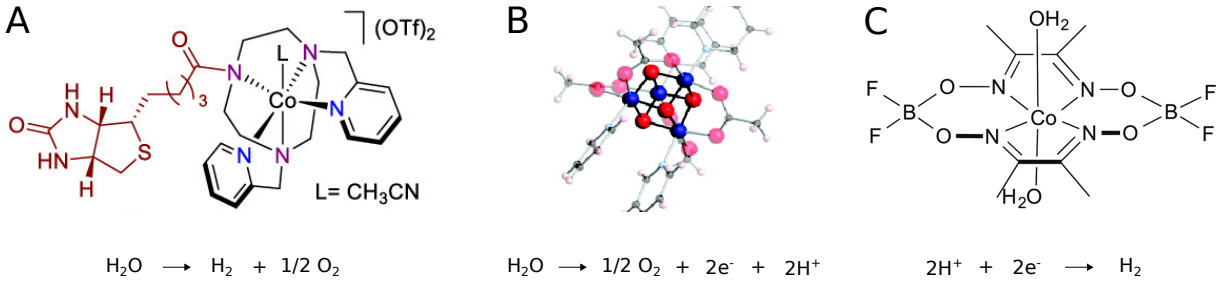

Figure 3.1: Co in catalysts performing reactions of water splitting. (A) Co loaded biotin-streptavidin molecule catalyzing water splitting in metalloenzymes (B) tetranuclear synthetic Co–oxo cluster performing water oxidation (C) cobaloxime derivate catalyzing proton reduction in the heme pocket of myoglobin.

in methionine synthase (Cvetkovic *et al.*, 2010; Kobayashi & Shimizu, 1999; Koutmos *et al.*, 2009). Our idea is to adopt the great versatility of iron-sulfur (Fe–S) clusters to Co–S clusters coming along with less oxygen sensitivity. Another advantage of Co as transition metal in Fe–S proteins is that Co and Fe share their common oxidation states Co^{2+}/Fe^{2+} and Co^{3+}/Fe^{3+} (Barceloux & Barceloux, 1999), what makes Co more suitable as a replacement for Fe than any other metal. First successful incorporation of Co into the iron site of a protein has been done with the rubredoxin like protein AlkG (Galle *et al.*, 2018). There is evidence, that Co–S cluster can be assembled in the specific microenvironment of iron sulfur proteins, as they are perfectly made to bind and use Fe–S clusters, which is e.g. not the case for the biotin-streptavidin technology. Another open question, if Co–S cluster can be assembled was already answered with a [4Co–4S] cluster, at least on a synthetic level (Deng *et al.*, 2009). Further reasons to use Fe–S proteins are, that the incorporation of Co into Fe–S scaffold proteins was shown to be possible *in vivo* and *in vitro* resulting in hybrid Co–Fe–S clusters of varying stoichiometry in IscU from *E. coli*, what shows that Co is competing for the iron binding site in Fe–S clusters. All these previous studies encourage us that we can assemble [2Co–2S] and [4Co–4S] clusters on Fe–S scaffold proteins, which are transferable to apo target proteins.

In this study, we focus on the assembly of a Co–S cluster using the bacterial Fe–S cluster scaffold protein IscU. IscU is a well-studied scaffold protein for Fe–S cluster biosynthesis in the ISC machinery (Agar *et al.*, 2000a; Raulfs *et al.*, 2008; Tokumoto & Takahashi, 2001). The initial step of bacterial Fe–S biosynthesis the apo form of IscU servs as scaffold protein in dimeric form (Figure 3.2). The iron source in bacterial Fe–S cluster biosynthesis is still under discussion. In contrast, the pyridoxal phosphate (PLP) dependent cysteine desulfurase IscS has been identified as sulfur source. It reduces cysteine to alanine and carries sulfur to the cluster site of IscU for incorporation into the Fe–S cluster, which is coordinated by four cysteines. After the assembly of the first [2Fe–2S] cluster on one of the two monomers a second [2Fe–2S] cluster can be assembled the same way the first was. Subsequently the two [2Fe–2S] cluster can then be fused to one [4Fe–4S] in a dimeric IscU. The exact mechanism is still under investigation, but the chaperone system HascAB is known to be involved in [4Fe–4S] cluster formation. The electrons required for this reaction are provided by ferredoxin. The final step of this process is the transfer of the cluster to the target protein in its apo form leading to the maturation of the

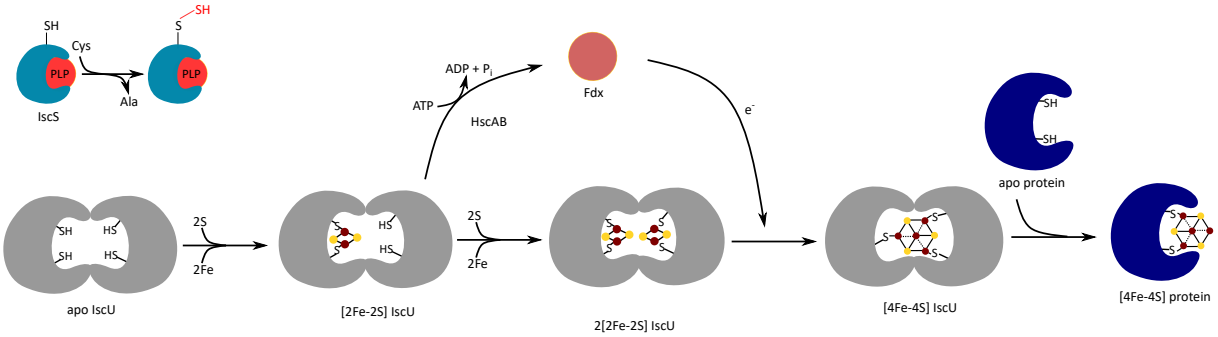

Figure 3.2: The assembly of Fe–S cluster in IscU. The scaffold protein of the Iron-Sulfur Cluster assembly machinery, is shown in dimeric form (grey). The desulfurase step is done by PLP-dependent (red) IscS (light blue). Fdx (salmon) provides electrons for the cluster fusion from dinuclear to tetranuclear Fe–S clusters. In the last step cluster transfer is done to an apo target protein (blue). Iron (dark red) and sulfur (yellow) are shown as small circles.

protein (Agar *et al.*, 2000a; Lill, 2009). Although IscU in most cases cannot be isolated as holo protein, the [2Fe–2S] cluster can be reconstituted under anaerobic conditions *in vitro* (Agar *et al.*, 2000a). As scaffold protein the role of IscU is to bind and transfer the clusters, which implies that the cluster is not bound very strongly to the protein. While this property is desirable for its biological function, it is hindering the assembly and characterization of the artificial Co–S clusters. To overcome this challenge, point mutations in the proximity of the cluster binding site have been studied to identify IscU variants with increased cluster stability. Therefor the D35A variant of *Archaeoglobus fulgidus* IscU is under investigation concerning Co–S cluster assembly *in vitro*. The mutation was introduced in close proximity to the coordination site, which stabilizes the cluster environment and enhances the longevity of [2Fe–2S] cluster from minutes up to several days (Marinoni *et al.*, 2012). In addition, the crystallization conditions of this variant are well known, what could help to solve the structure of a Co–S reconstituted species. This mutated scaffold protein will help us to assemble and investigate Co–S cluster extensively.

In this study, we present an approach for the assembly of Co–S clusters using the protein IscU as a scaffold, as well as the spectroscopic characterization of these unprecedented artificial metalloproteins. Metal binding titration studies, chemical and semi-enzymatic reconstitution could show, that Co can bind to coordinating cysteines of the Fe–S scaffold protein IscU. In addition, the results of semi-enzymatic reconstitution indicate the presence of polynuclear Co–S. These clusters are very O_2 stable and are transferable to apo *E. coli* [2Fe–2S] ferredoxin. This outcome expands the understanding of the assembly of Co–S clusters and their transfer to target proteins, which extends the knowledge about artificial cofactors and pushes the exploration and creation of powerful catalysts for "green" H_2 production.

3.4 Material and methods

All experiments are performed with *Af*IscU D35A if not stated otherwise.

3.4.1 Gene Expression and Protein Isolation

For gene expression 2× Yeast extract (2YT) medium was inoculated with *E. coli* BL21 (DE3) overnight culture (1% v/v) containing plasmids hosting the *iscU* gene from three different source organisms: *Escherichia coli*, *Aquifex aeolicus*, and *Archaeoglobus fulgidus* and a D35A mutant of *iscU* from *A. fulgidus*. For selectivity of the cells, ampicillin was added to the medium at a final concentration of 100 µg/ml. Cells were cultivated at 37°C until they reached exponential cell growth, measured by optical density at 600 nm (OD_{600}), and then the gene expression was induced by adding 0.5 mM Isopropyl-β-D-thiogalactopyranosid (IPTG). After inducing gene expression, the cells were cultivated at 30°C and 120 rpm for 20 h. Subsequently, the cells were harvested by centrifugation for 15 min at 6,000× *g* and 4°C. For protein isolation, cells were resuspended in 50 mM Tris pH 7.6, 150 mM NaCl containing EDTA-free cOmplete™Protease Inhibitor Cocktail Tablets (Roche, Basel, Switzerland). Then the resuspension was stirred at 4°C until it reaches a homogenous appearance. Cell lysis was performed by sonication for 20 min with an amplitude of 60% and a pulse of 1 s every 3 s using a VS70/T sonotrode (Bandelin electronic, Berlin, Germany). Lysate was clarified by centrifugation at 40,000× *g* and 4°C for 40 min.

Lysate containing wildtype IscU was then isolated by immobilized metal affinity chromatography (IMAC). For this purpose, protein lysates were applied to a "HiTrap Excel" column (Macherey-Nagel, Düren, Germany) which was equilibrated with wash buffer (50 mM Tris pH 7.6, 150 mM NaCl) using Äkta prime chromatography system (GE Healthcare, Little Chalfont, UK). After application of the lysate, the column was washed with 25 mM imidazole containing wash buffer to remove loosely and unspecifically bound protein before eluting IscU with 250 mM imidazole containing wash buffer. IscU containing fractions were pooled and dialyzed against wash buffer to remove imidazole. Prior to a second IMAC the poly-histidine tag was removed by cleaving it from the protein with very specific tomato etch virus (TEV) protease. Therefore 1 mM EDTA and 1 mM DTT together with TEV protease (1:100 ratio) were added and incubated for 24 h at 4°C. To remove small components of the reaction the mixture was dialyzed against 2 l wash buffer. The second IMAC was then performed to remove both the histidine tag and the protease from the target protein. Protein purity was determined by SDS-PAGE. Protein concentration was determined using electron absorption spectroscopy (EAS).

As the D35A mutant of IscU from *A. fulgidus* was cloned without an affinity tag, the isolation has to follow another protocol. Because *A. fulgidus* is a hyperthermophilic organism its proteins are very thermostable. To isolate IscU D35A, after cell harvest and sonication, the lysate was heated to 90°C for 20 min. To remove the target protein from denaturated *E. coli* proteins the mixture was centrifuged for 45 min at 15,000× *g*. Protein purity of the supernatant was determined by SDS-PAGE. Protein concentration was determined using EAS.

3.4.2 Metal Binding Studies

For titration experiments the coordinating cysteine residues of 100 µM apo protein were reduced with 1 mM DTT. Then $CoCl_2$ was added stepwise until up to 10 eq compared to the apo protein. The binding of cobalt to cysteines was monitored by recording EAS in the range of 300—800 nm.

3.4.3 Chemical Reconstitution

For chemical reconstitution 100 µM apo IscU were transferred to an anaerobic chamber and incubated overnight (o/n) to get rid of oxygen. Then 1 mM DTT was added to reduce the coordinating cysteine residues and the mixture was incubated for 1 h on ice. Subsequently, 400 µM $CoCl_2$ and 400 µM Li_2S were added to start reconstitution of [2Co–2S] cluster. After 3 h of incubation the protein was desalted using a PD-10 Desalting Column (GE Healthcare, Little Chalfont, UK). The column was equilibrated beforehand with 50 mM Tris pH 7.6 and 150 mM NaCl. The desalted protein was then analyzed via EAS.

3.4.4 Semi-enzymatic Reconstitution

For semi-enzymatic reconstitution 100 µM apo IscU were transferred to an anaerobic chamber and incubated o/n. Then 1 mM DTT was added and incubated for 1 h on ice to reduce the coordinating cysteine residues. As cobalt source 400 µM $CoCl_2$ were added. In contrast to the chemical reconstitution, the sulfur source is different: To make sulfur accessible in the semi-enzymatic reconstitution 2.5 µM pyridoxal phosphate (PLP) loaded IscS was added together with 5 mM L-Cysteine. IscS is a PLP dependent cysteine desulfurase which reduces cysteine to alanine and provides the resulting sulfur to the reconstitution. The reaction mixture was incubated at room temperature (RT) for at least 3 h. Then excess reagents were removed either using a PD-10 Desalting Column (GE Healthcare, Little Chalfont, UK) or size exclusion chromatography (Chapter 3.4.5). Both columns were equilibrated with 50 mM Tris pH 7.6 and 150 mM NaCl. After desalting the volume of the protein solution was reduced to ensure high quality of further measurements.

3.4.5 Determination of Oligomerization State

To get more information about the oligomerization state in the reconstitution mixture in solution, a size exclusion chromatography was performed with a HiLoad Superdex Prepgrade 75PG (GE Healthcare, Chicago, Il, USA) column. This column was pre calibrated with a mixture of proteins (Aprotinin 6500 M_r, Ribonuclease A 13700 M_r, Carbonic Anhydratase 29000 M_r, Ovalbumin 44000 M_r, and Canalbumin 75000 M_r), of which the retention volume is known for this column. The retention volumes of the proteins of the calibration mixture were used to determine the M_r of the protein containing fractions of the reconstitution mixture SEC run.

3.4.6 Quantification of Metal Content

To determine the metal-to-monomer ratio of the reconstituted protein samples, the total metal content of the protein solution was detected using inductively coupled plasma mass spectroscopy (ICP-MS). Therefore, the samples were adjusted to a protein concentration of 10 µM, which were then precipitated in a 1:1 ratio with 6% trace-metal grade nitric acid. Precipitate was removed by centrifugation for 30 min at 15,000$\times$ *g* and the supernatant was transferred to a metal-free reaction tube (VWR, Radnor, PA, USA). The measurements of the metal content were performed using an Agilent 7700 ICP-MS (Agilent Technologies, Waldbronn, Germany) in the Biocenter MS-Platform at the University of Cologne. The measurements were done by strictly following the manufacturer's instructions using He in the collision cell mode to minimize spectral interferences. Measurements were performed in technical triplicates and the presented data has an r^2 value of 0.999.

3.4.7 Electronic Absorption Spectroscopy

The electronic absorption spectra were collected using a Cary-60 spectrophotometer (Agilent Technologies, Ratingen, Germany) with 1 nm bandwidth, a scanning speed of 600 nm/min and a 1-cm-path-length quartz cuvette at room temperature.

3.4.8 Circular Dichroism (CD) Spectroscopy

The CD spectra were collected using a Jasco J-815 Circular dichroism spectrometer (Jasco Germany, Pfungstadt, Germany) with a scanning speed of 100 nm/min and a band width of 5 nm in a 2-mm-path-length quartz cuvette. An average of 20 cans was collected at 20°C with 1 nm resolution.

3.4.9 Cluster Transfer Experiments

The cluster transfer experiments were performed anaerobically o/n at 4°C in a 3:1 ratio of holo Co–S IscU D35A from *A. fulgidus* and apo Fdx-6His from *E. coli* in buffer containing 50 mM Tris, 150 mM NaCl and 1 mM DTT. Holo IscU was reconstituted using semi-enzymatic reconstitution and PD-10 desalting column. Apo Fdx was formed using TCA precipitation after isolation in holo form. Therefor 1.5% TCA were added to the protein solution to precipitate the protein. After centrifugation the supernatant was discarded and the protein was resolubilized in buffer containing 50 mM Tris, 150 mM NaCl and 1mM DTT. After cluster transfer an IMAC was performed and EAS spectra were taken from the separated fractions.

3.5 Results

3.5.1 Selection and Generation of the Scaffold Proteins

To investigate the formation of [2Co–2S] clusters we selected the scaffold protein IscU from three different organisms. The organisms were selected according to the availability of crystal structures to increase the chances of obtaining crystals for structural characterization. Crystal structures of IscU from *E. coli*, *Aquifex aeolicus*, and *Archaeoglobus fulgidus* have been reported (Kim *et al.*, 2012; Marinoni *et al.*, 2012; Shimomura *et al.*, 2008) (Figure 3.3). *A. aeolicus* and *A. fulgidus* are extremophilic organisms living at high temperatures of up to 95°C. The structures of *A. aeolicus* and *A. fulgidus* harbor reconstituted Fe–S clusters while the *E. coli* structure shows apo protein. The scaffold protein IscU binds the cluster transiently, however, it was selected for the assembly of the artificial cofactor for three reasons: (i) it has previously been shown to bind Co at the Fe-binding site; (ii) single point mutations have been reported that stabilize the cluster; and (iii) IscU has the ability to transfer the cluster subsequently to target proteins, thus, enabling the maturation of a variety of proteins. The wild type constructs we used were linked to a histidine tag for purification using immobilized metal affinity chromatography (IMAC), which could be cleaved to get the native protein. Heterologous expression of the *iscU* gene from the thermophilic organisms *A. fulgidus* and *A. aeolicus* in *E. coli* could be performed very specific using a fast and easy heat shock protocol (Chapter 3.4.1). The protein solution has purity of approximately 98% without any chromatographic step in the isolation process (Figure S3.1). The electronic absorbtion spectrum (EAS) of the isolated protein only shows a minor band at around 410 nm, indicative of small amounts of remaining Fe–S cluster (Agar, Zheng, et al., 2000). The majority of the protein, however, was isolated in its apo form and can be used without further purification steps. The presence of mainly apo protein is not surprising, as the life time of Fe–S cluster is highly oxygen sensitive and the isolation was performed under aerobic conditions. Further, the function of IscU as a scaffold protein (Agar *et al.*, 2000a) makes it very likely that the cluster is only weakly bound to the protein, which most likely contributes to the isolation of the protein in the apo form. All wild type IscU consist of at least 3 coordinating cysteines. In addition to the wild-type proteins, we have generated the *Af*IscU D35A variant. It has previously been shown, that replacing aspartic acid at position 35, which is located two amino acids away from one of the coordinating cysteines, by alanine stabilizes the cluster and increases its lifetime from hours to days. Concerning the mutations we focused on the variant of the most promising wild type. *A. fulgidus* IscU D35A, what is the fourth construct we investigated in this work. The wild type constructs were made before this work. IscU D35A was generated via site directed mutagenesis using the quik change protocol from Takara Bio Inc. and the wild type construct as source plasmid.

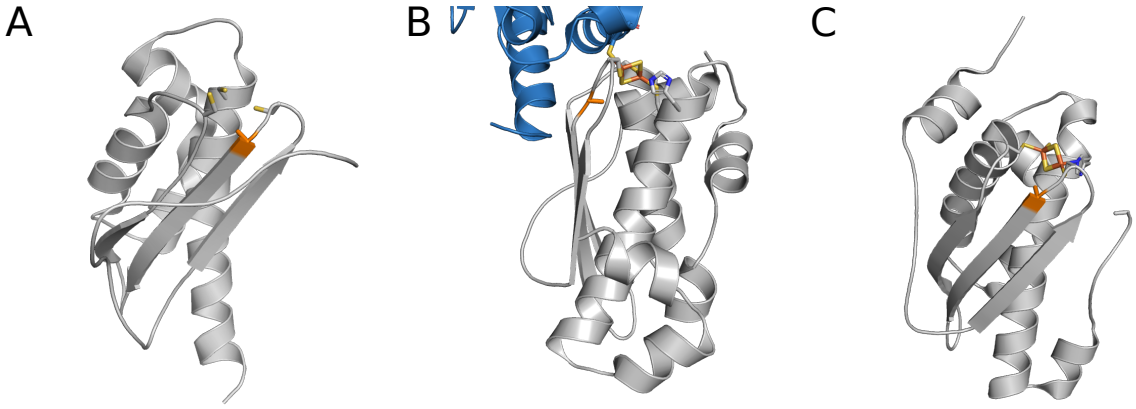

Figure 3.3: Structural view of cluster stabilizing IscU mutations (orange sidechain) close to the cluster binding site and its coordinating residues: (A) apo *E. coli* IscU D39A, PDB ID 2KQK ((Kim *et al.*, 2012)) (B) holo *A. fulgidus* IscU D35A (grey), PDB ID 4EB5 ((Marinoni *et al.*, 2012)) and parts of IscS (blue), which provides a histidine for cluster coordination (C) holo *A. aeolicus* IscU D38A, PDB ID 2Z7E ((Shimomura *et al.*, 2008)).

3.5.2 Co replaces Fe in *E. coli*, *A. aeolicus*, and *A. fulgidus* wt IscU

To evaluate the ability of IscU to bind Co, titration experiments were carried out and monitored using EAS. The titrations were performed using wild type IscU from *E. coli*, *A. aeolicus*, and *A. fulgidus* (Figure 3.4). The addition of a Co solution to IscU from all organisms give rise to new absorption bands between 460 nm and 700 nm, as it was previously shown for *E. coli* IscU by Ranquet *et al.* (2007).

The electronic spectra of *E. coli* IscU after the addition of 10 eq. Co shows bands at 460 nm, 575 nm, and a shoulder between 675 nm and 700 nm. Also for *A. fulgidus* IscU new occurring bands at 460 nm and 575 nm, as well as a shoulder between 675 nm and 700 nm could be obtained. *A. aeolicus* IscU shows bands at 550 nm and 675 nm upon the addition of 2—10 eq of $CoCl_2$. While the bands at 575 nm and 675 nm are in the range of what has been described to be characteristic for Cys coordinated Co^{2+} species (Petros *et al.*, 2006). Our observations are in line with previous Co-binding studies to *E. coli* apo IscU (Ranquet *et al.*, 2007). This indicates, that Cys can bind Co in wt IscU from all three different organisms. The differences in the shape of the three spectra could be due to the slightly different structural properties of the IscU scaffold proteins and varying amino acid composition. The coordinating cysteines of these organisms are not all at the same position. Analogue cysteines can be shifted several positions between IscU from these organisms. Furthermore *A.a.* and *A.f.* IscU is from thermophilic organisms surviving temperatures of up to 95°C. This indicates a strong difference in biochemical properties which might also have an effect on the spectra. Yet, no data about bi-nuclear Co-Cys bindings are known. In comparison to Co-substituted rubredoxin with absorption bands at 623 nm, 662 nm, 690 nm, and 753 nm (Galle *et al.*, 2018), which are indicative of d-d ligand field (LF) transitions of the distorted tetrahedral symmetry of high-spin Co^{2+} (Sugiura, 1978) and have also been similarly observed for Co-binding to an unfolded tetrathiolate peptide (Petros *et al.*, 2006), the bands of Co-substituted IscU are partially shifted to higher energies. The

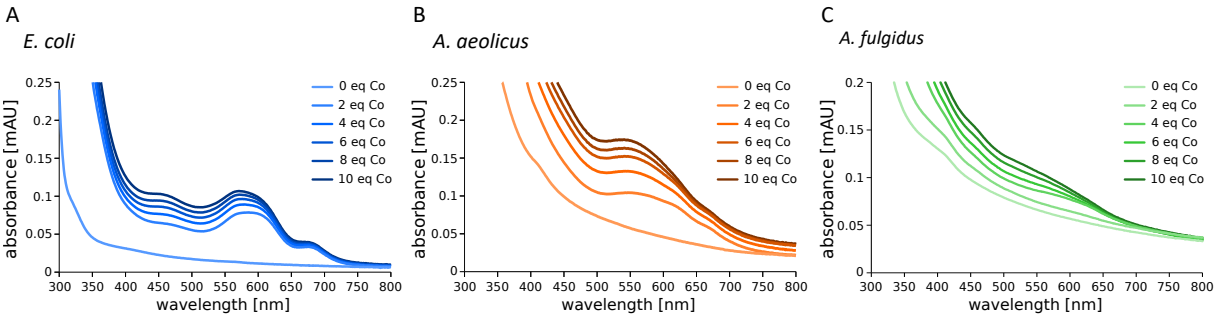

Figure 3.4: Metal-binding studies of IscU from (A) *E. coli*, (B) *A. aeolicus*, and (C) *A. fulgidus* with different amounts of $CoCl_2$ (0—10 eq.) in the presence of DTT as a reducing agent.

absorption band at 460 nm, which was observed during Co-titration to IscU suggest a different binding than in rubredoxin-type sites. This could indicate a bi-nuclear Co-Cys species but needs further validation experiments.

3.5.3 Reconstitution of [2Co–2S] Clusters in wild-type IscU

After the Cys-Co interaction was verified, the formation of Co–S cluster in the active site was investigated. Therefore, a Co–S cluster should be assembled in the active site. To reach this goal we focused on chemical and semi-enzymatic reconstitution protocols for Fe–S cluster. To incorporate [2Co–2S] cluster into the scaffold protein IscU we established a new protocol for the *in vitro* assembly of metal-sulfur clusters based on reconstitution protocols for the incorporation of [2Fe–2S] clusters (Freibert *et al.*, 2018). The results of reconstitution experiments can be monitored by using EAS and circular dichroism (CD) spectroscopy. The chemical reconstitution involves the apo protein, dithiothreitol (DTT) as a reducing agent, Li_2S as an inorganic sulfur source, and $CoCl_2$ as a cobalt source (Freibert *et al.*, 2018). We first tested chemical reconstitution for wt IscU from three different organisms: *Escherichia coli* (*E.c.*), *Archaeoglobus fulgidus* (*A.f.*), and *Aquifex aeolicus* (*A.a.*) (Figure S3.2). The results for this approach show no clearly detectable absorption bands in the range of 300-800 nm (Figure S3.2), where signals of poly-nuclear, cysteine-coordinated metal-sulfur cluster should be observed (Petros *et al.*, 2006; Ranquet *et al.*, 2007). For IscU from *E.c.* and *A.f.* a higher background can be observed than for IscU from *A.a.*, however, no well-founded statement can be given for the incorporation of [2Co–2S] cluster into IscU using chemical reconstitution. For the semi-enzymatic reconstitution we used apo protein, DTT, $CoCl_2$, L-Cysteine and the cysteine desulfurase IscS from *E. coli*. In Figure S3.4 the results show better signals in EAS spectroscopy than for chemical reconstitution. A lower background can be detected coming along with higher resolved bands for each of the three wild-type IscU. However, the spectrum of *A. aeolicus* IscU shows very high background covering the signals, which cannot clearly be distinguished in the polynuclear metal-sulfur cluster range. In contrast to that, the spectrum of *E. coli* IscU shows distinct signals around 350 nm and 450 nm. The band at 350 nm is characteristic for polythiolate Co^{2+} species (Petros *et al.*, 2006), which is not in agreement with correctly assembled Co–S clusters. The most interesting

results are represented by the spectrum of wild type IscU from *A. fulgidus*. Here we see better resolved signals around 400 nm and 480 nm, which is indicating a polynuclear metal-sulfur cluster. That means that we see signals of a Co–S cluster as there is no significant amount of any other metal than Co in this solution. In addition to that, we tried the semi-enzymatic reconstitution on the wild type apo form of [2Fe–2S] ferredoxin from *E. coli*, to see, if we can assemble a Co–S cluster directly in a protein, which is not a scaffold protein for Fe–S clusters. In Figure S3.5 the electronic absorption spectrum after semi-enzymatic reconstitution and desalting using PD-10 columns is presented. Interestingly the outcome is most similar to IscU from *A. fulgidus*. Two less distinct signals can be observed around 400 nm and 480 nm. This is a hint for Co–S cluster formation, but again the signals here a too diffuse to determine, whether this is clearly a Co–S cluster or not. Next, we investigated the suitability of the IscU variant D35A from *A. fulgidus*, whose *E. coli* analogue has been previously reported to show an increased stability of its [2Fe–2S] cluster when exposed to oxygen (Adrover *et al.*, 2015), to be semi-enzymatically reconstituted with a [2Co–2S] cluster, although metal-binding studies with wt IscU from *A. fulgidus* revealed less pronounced bands compared to wt IscU from *E. coli* (Figure 3.4). However the semi-enzymatic reconstitution for the wild type IscU shows more distinct bands in the right range for Co–S cluster. The electronic absorption spectrum in Figure 3.5 shows absorption bands at 404 nm and 479 nm and a broad shoulder at 600 nm (extinction coefficients in Table S3.1), which is in the range of polynuclear, cysteine-coordinated metal-sulfur cluster between 300 nm and 600 nm (Petros *et al.*, 2006; Ranquet *et al.*, 2007). This observation is supported by a high-resolution CD spectrum. CD spectroscopy can be used to detect chiral molecule environments. In the range of 300 nm to 800 nm the metal to protein bindings are the only detectable features of our construct. In this energy range, CD spectroscopy can be used to characterize the metals of clusters in proteins and provides information that are similar to those obtained by EAS spectroscopy, with peak minima and maxima correlating to those of the EAS spectra. In contrast to EAS spectra, shape and intensity of CD spectra of metalloproteins in the range between 300 nm and 800 nm cannot be easily predicted. The lack of a signal in a CD spectrum does not necessarily indicate the lack of the cofactor, but can also be indicative for a cluster that is bound to the protein in a highly symmetric arrangement (Freibert *et al.*, 2018). The molar extinction coefficients for the bands at 404 nm and 479 nm in the EAS are in the lower range of what is usually reported for [2Fe–2S] proteins (Freibert *et al.*, 2018; Jacquot, 2017), suggesting that either only a minor fraction of the semi-enzymatic reconstituted protein was successfully reconstituted with a [2Co–2S] cluster or that IscU binds its cluster in an oligomeric state. The presence of different IscU oligomers has previously been suggested (Agar *et al.*, 2000a; Shimomura *et al.*, 2008). The CD spectra obtained from semi-enzymatic reconstituted IscU D35A from *A. fulgidus* shows maxima around 350 nm, 420 nm, and 500 nm, as well as minima at 400 nm, 450 nm, and 550 nm, which correspond to the observed bands in the EAS spectrum (Figure 3.5A). To determine the amount of incorporated Co, we performed inductively coupled plasma mass spectrometry (ICP-MS) measurements. These measurements revealed the presence of 1.34 cobalt atoms per IscU monomer after desalting of the reconstitution mixture, which is in good agreement with what we propose for the presence

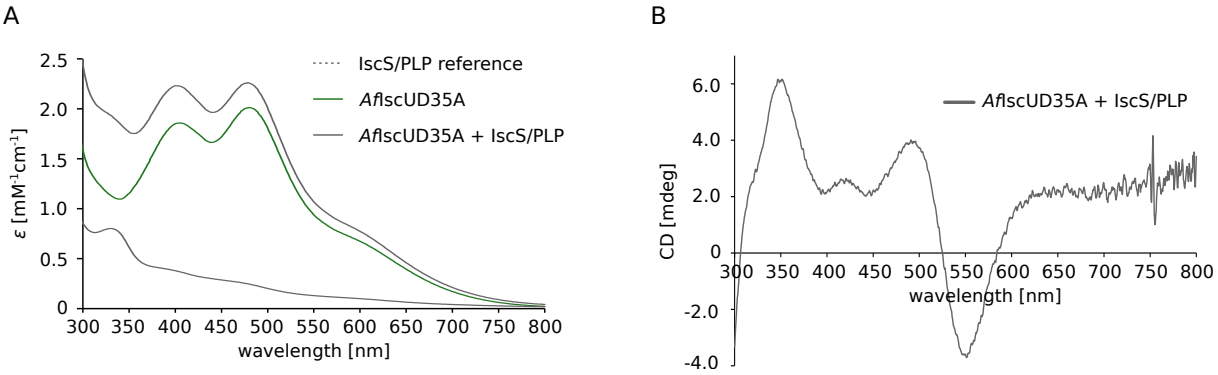

Figure 3.5: Co-content of IscU D35A from *A. fulgidus* after semi-enzymatic reconstitution prior to SEC: (A) EAS of the proteins sample and (B) CD spectrum.

of a [2Co–2S] cluster. Nevertheless, the obtained results do not allow for a detailed prediction of the oligomerization state of the protein as well as the amount of holo protein.

3.5.4 IscU can be Reconstituted in Different Oligomerization States

Although the properties and functions of IscU as a scaffold protein have been investigated for several decades, the oligomerization state of the functional protein *in vivo* is still under debate and can vary under different conditions (Galeano *et al.*, 2017).

In order to obtain more detailed information about the properties of the semi-enzymatically reconstituted IscU sample, we analyzed the reaction mixture using size exclusion chromatography (SEC) followed by SDS-PAGE (Figure 3.6). The SEC chromatogram (Figure 3.6A) shows the retention volumes of the semi-enzymatic reaction mixture. Three different species of IscU can be observed between a retention volume of 50 ml to 80 ml, which corresponds to sizes between 75 kDa and 13,7 kDa. The positions of the first green peaks correspond to the size of an IscU trimer, dimer, and monomer respectively. The large green peak between 110 ml and 120ml corresponds to very small molecules like excess DTT, PLP or $CoCl_2$. This observation of oligomeric states of Co-reconstituted IscU from *A. fulgidus* is contradictive to results found for different apo IscU variants from *E. coli* (Kim *et al.*, 2012), allowing for the assumption that cluster binding to IscU may trigger oligomerization. SDS-PAGE analysis (Figure 3.6B) indicates that all fractions between 55 ml and 75 ml elution volume contain IscU of high purity. Oligomerization cannot be observed as the molecules were denaturated during SDS-PAGE analysis. Furthermore, no protein containment for the fractions between 100 ml and 120 ml can be observed.

To go more into detail of the analysis of semi-enzymatic reconstitution, the protein-containing fractions were—in addition to SDS-PAGE—analyzed using EAS (Figure 3.7A) and ICP-MS (Figure 3.7B). The electronic absorption spectra show that the largest molar extinction coefficients (Figure 4A and Table S3.1) in the range of 300 nm to 800 nm can be observed for the dimeric fraction, followed by the trimeric and monomeric fraction. However, it has to be mentioned, that the bands of the samples after SEC are slightly shifted and significantly broader compared to

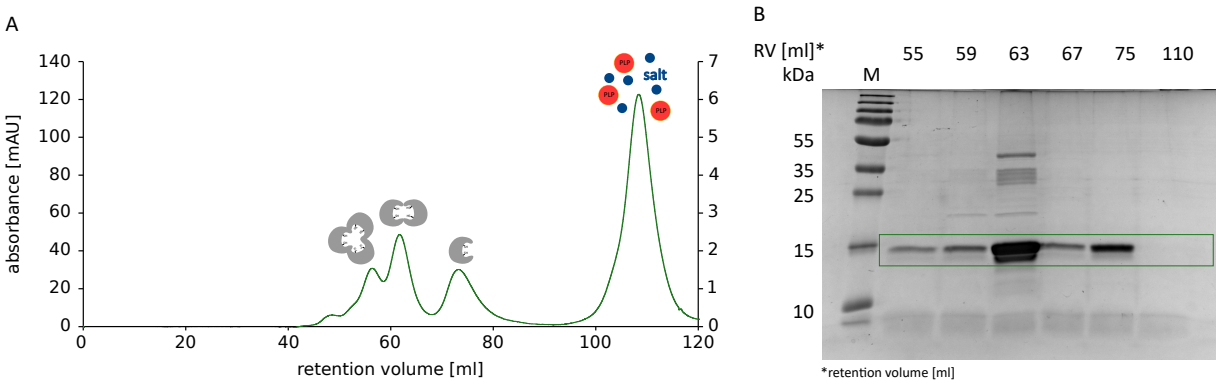

Figure 3.6: Analysis of the oligomerization state of *Af*IscUD35A (A) SEC chromatogram of the semi-enzymatically reconstituted protein and (B) SDS-PAGE analysis of the collected SEC fractions.

the protein sample prior to SEC (Table S3.1). This might be due to the removal of excess DTT and remaining IscS during SEC or due to the fact, that mixtures of IscU monomers, dimers, and trimers with different cluster geometries (distorted geometry in oligomeric fractions) may lead to overlapping spectra within the EAS of the semi-enzymatically reconstituted sample prior to SEC. ICP-MS data of the different fractions revealed that the dimeric form is the most likely form to assemble [2Co–2S] cluster. The trimeric fraction shows almost 1 Co/monomer, which results in 3 Co/trimer. This is not in agreement with successful formation of [2Co–2S] cluster, which is also supported by a lower extinction coefficient than for the dimeric fraction. In this fraction the Co–S cluster might not be formed correctly or incomplete. The monomeric fraction shows 0.27 Co/monomer in the ICP-MS results. As no part of an atom can be coordinated, just 1/3rd of the IscU monomers is occupied with just one Co atom, which means that the formation of [2Co–2S] might have failed in monomeric IscU. Another option is that just 1/6th of the IscU is loaded with complete formed [2Co–2S] cluster. The low extinction coefficient is supporting the low occupancy, whereas the shape of the spectrum suggests correct cluster formation. The best results are observable for the dimeric fraction, where 0.6 Co atoms are corresponding to one monomer of IscU. Assuming again, that no parts of an atom can be coordinated, 60% of IscU is occupied with one Co atom. As this is the dimeric fraction, 60% of the dimeric molecules are occupied with 2 Co atoms. This is in total agreement with the formation of [2Co–2S] clusters. As the [2Fe–2S] dimeric IscU is proposed to me most likely the physiological form of holo IscU (Agar *et al.*, 2000a), we are convinced that also [2Co–2S] dimeric IscU is the most likely form in [2Co–2S] cluster formation.

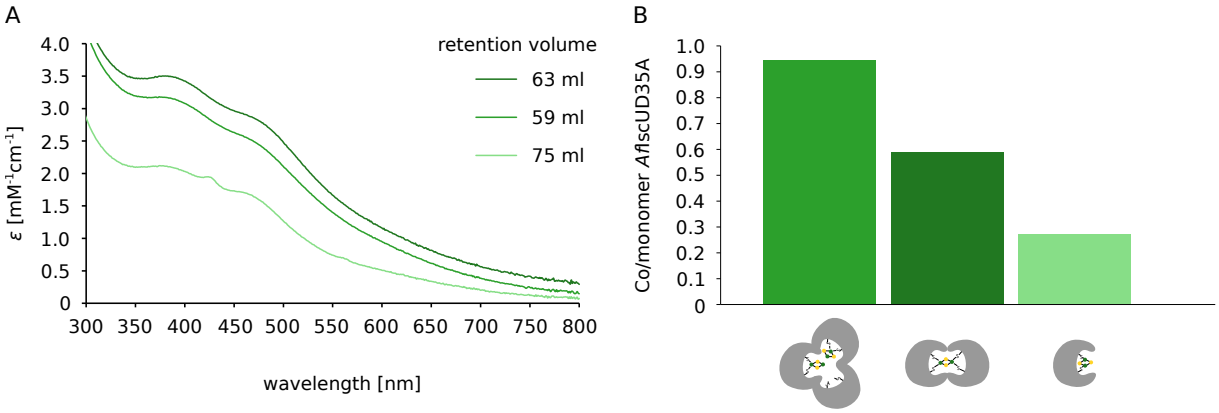

Figure 3.7: Analysis of different *Af*IscUD35A fractions after SEC (A) Electronic absorption spectra of each peak, (B) ICP-MS of each fraction.

3.5.5 Oxygen Stability and Redox Activity

Co–S clusters are believed to be less oxygen sensitive than Fe–S clusters, which has not been clearly proven yet. Therefor we analyzed the oxygen sensitivity using EAS (Figure 3.8). For this purpose, we actively purged the protein solution in a quartz cuvette with oxygen at room temperature and observed the shape of the electronic absorption spectra over time. One spectrum was recorded before exposition to oxygen (0 h), followed by spectra recorded after 0.5 h, 1 h, 2 h, 24 h, and 72 h. Compared to the spectrum prior to oxygen exposition, no significant changes in the spectra can be observed after each time point. The signals in the range of 370-480 nm are very stable over time under active oxygen addition to the protein solution. For the [2Fe–2S] IscU variant D39A from *E. coli*, which has been reported to be more oxygen stable, the cluster remains stable for 20 hours, while the [2Fe–2S] cluster in wt IscU from *E. coli* degrades after 20 min (Adrover *et al.*, 2015).

A prerequisite for metal-sulfur clusters to participate in redox reactions is the capability of the cluster to switch between different oxidation states. For this purpose, we analyzed whether semi-enzymatically reconstituted [2Co–2S] IscU can be reduced using sodium dithionite as a reducing agent. Electronic absorption spectra after the addition of 1, 2, 4, and 10 equivalents reveal that the cluster is not stable upon the addition of reducing agents and therefore, it is not possible to reduce this cluster without degrading it (Figure S3.3).

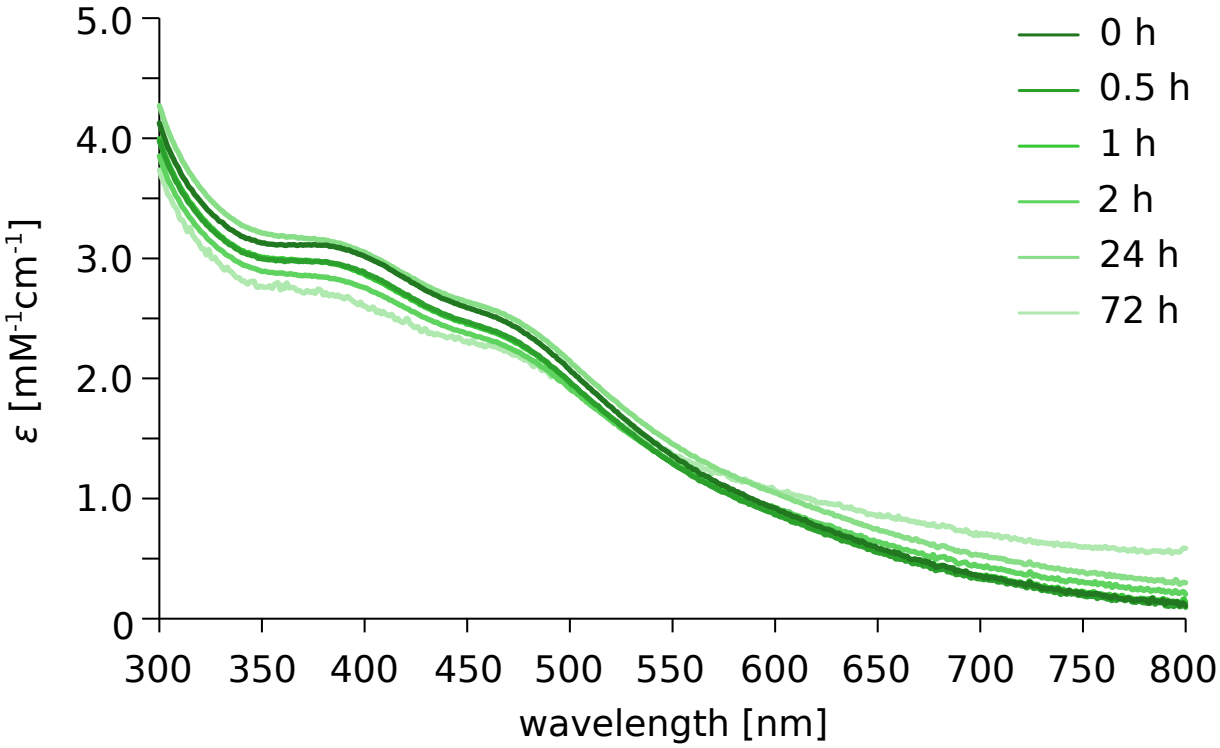

Figure 3.8: O_2-Sensitivity of IscU in EAS (sample: 63 ml retention time)

3.5.6 Cluster Transfer and Interaction between IscU and Fdx

After the characterization experiments of reconstituted Co–S IscU, the interaction with potential apo protein candidates was investigated. Therefor the apo form of [2Fe–2S] ferredoxin was isolated and incubated o/n at 4°C together with Co–S IscU. Then the proteins were separated using IMAC and EAS spectra were measured. Figure 3.9 displays the EAS spectrum of semi-enzymatically reconstituted Co–S IscU, apo Fdx as well as IscU and Fdx after a tranfer time of 12 h. Prior to the transfer process, the Fe–S cluster was removed from Fdx by treating the protein with Trichloroacetic acid (TCA).

After an incubation of the different components for 12 h, Fdx shows pronounced bands at 350 nm and approximately 475 nm that were not present in apo Fdx. Absorption bands at 350 nm have previously been reported to be indicative of ligand-to-metal-charge-transfer (LMCT) between Cys-S^- and Co^{2+} (Curdel & Iwatsubo, 1968; Drum & Vallee, 1970; McMillin *et al.*, 1974). This observation highly indicates the transfer of Co to apo ferredoxin by the semi-enzymatically reconstituted [2Co–2S] IscU variant *Af*IscU D35A.

Surprisingly, also the spectrum of IscU changes during the transfer process. Here, the broad and overlapping bands between 350 and 600 m, transform to a significant band at 475 nm and a shoulder in the range of 350 nm. This can be due to a shift of Co during the transfer process. As for Fdx at 350 nm a polythiolate Co^{2+} species is likely, also the IscU could change its conformation to mononuclear Co^{2+} species. This would indicate that in this case the cluster

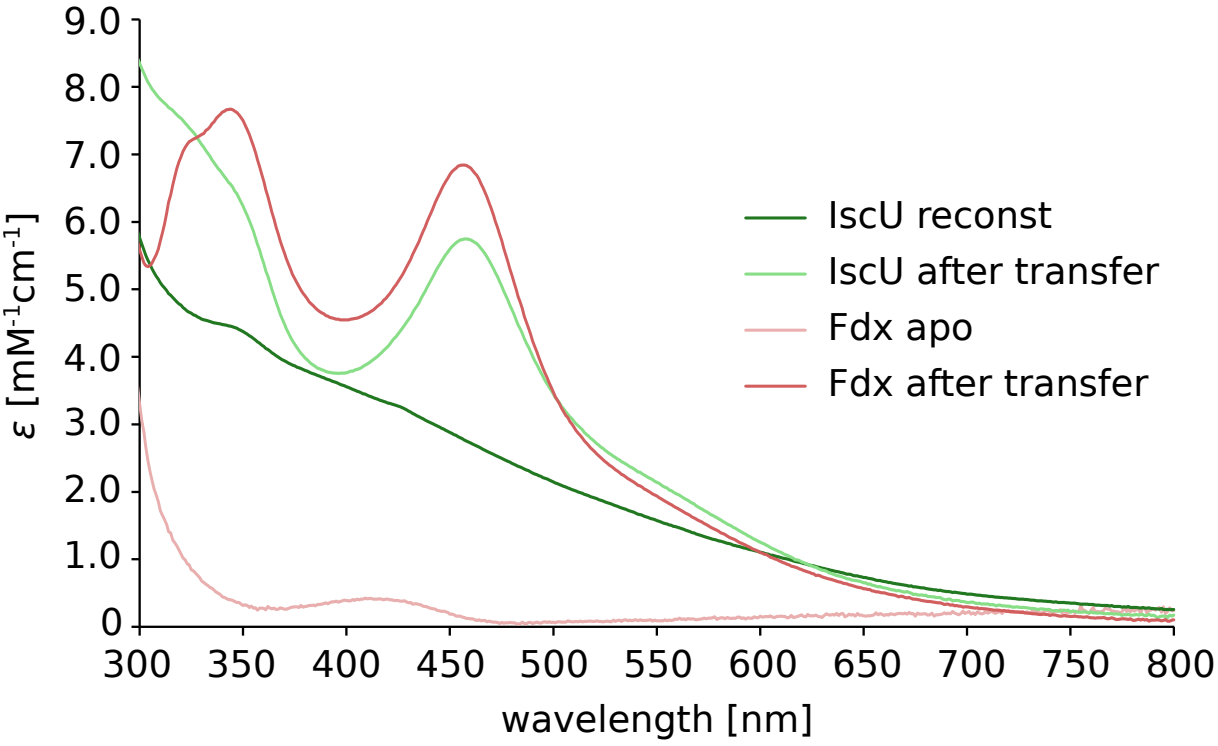

Figure 3.9: EAS of Cluster transfer (proteins were separated using affinity chromatography).

transfer does not happen in one step without degrading the cluster. The spectra reveal that there is an equilibrium-like state of IscU and Fdx harboring polythiolate bound Co^{2+} species.

3.5.7 Aconitase as [4Fe–4S] Cluster Protein in Co–S Cluster Assembly

At the end of these approaches to assemble [2Co–2S] cluster in [2Fe2S] proteins we were convinced to try the same semi-enzymatic assembly in a [4Fe–4S] protein. Therefor we chose *E. coli* aconitase B (AcnB), which is a [4Fe–4S] cluster protein in its active form. In the presence of iron, AcnB functions as an enzyme in the essential citric acid cycle and the glyoxylate cycle that assembles a [4Fe–4S] cluster. Under oxidative stress conditions and iron starvation, the Fe–S cluster disassembles and the enzymatically inactive apo protein functions as a nucleic acid binding protein, that binds to its own mRNA for positive regulation (Beinert & Kennedy, 1993).

The results in Figure 3.10 show clear detectable absorption bands in the electronic absorption spectrum at around 400 nm and 470 nm and a broad shoulder at 600 nm, which is again in the range of poly-nuclear, cysteine-coordinated metal-sulfur cluster between 300 nm and 600 nm (Petros *et al.*, 2006). This is in agreement with the results for IscU D35A from *A. fulgidus*. The characteristics of this bands at around 400 nm and 470 nm in the EAS are still usually reported for [2Fe–2S] proteins (Freibert *et al.*, 2018; Jacquot, 2017), suggesting that either only [2Co–2S] clusters could be assembled in AcnB or that [4Co–4S] clusters bound to cysteines have very similar EAS characteristics to [2Co–2S] clusters in IscU. However, it is

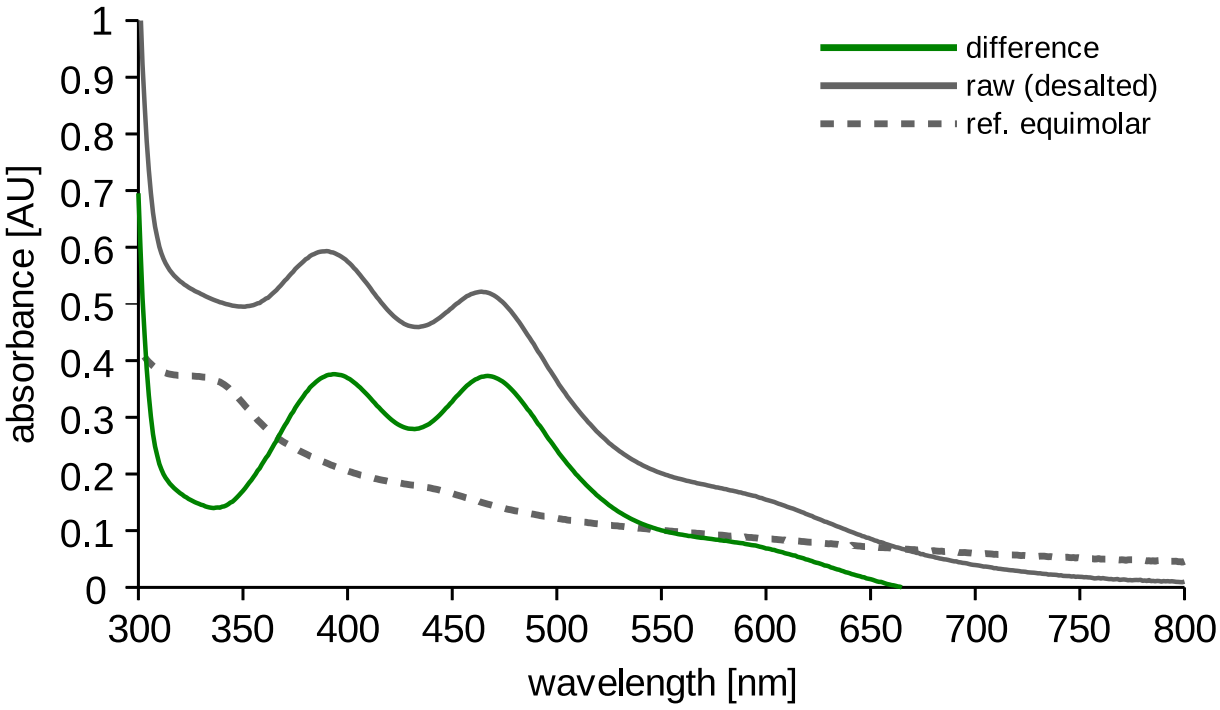

Figure 3.10: Co-content of AcnB from *E. coli* after semi-enzymatic reconstitution shown in EAS.

of high interest that signal of polynuclear Co–S cluster can be detected in a Co reconstituted [4Fe–4S] protein.

3.6 Discussion

The assembly of Co–S cluster in Fe–S proteins made great progress in this study, although it is still quite challenging to identify the nuclearity and geometry of the assembled clusters. The idea to choose different Fe–S scaffold proteins for the assembly of Co–S cluster turned out to be a suitable strategy for successful cluster formation. IscU from different organisms revealed that different properties of the scaffold protein lead to different results in cluster formation. The most likely Co–S cluster formation could be done in the scaffold protein of *A.fulgidus*. Both, the wild type and the D35A mutant show two distinct bands in the EAS in a range, where also characteristic bands of Fe–S clusters are located (Ranquet *et al.*, 2007). This is an almost undefeatable hint for Co–S cluster formation, because there is not any other significant amount of metal in this solution than Co. The two other IscU candidates show either two diffuse bands in the right range or distinct bands in the wrong range. In case of IscU from *A.aeolicus* we observed diffuse bands in the right range. From literature we know that the holo protein exists in trimeric form, partially loaded with [2Fe–2S] cluster, what makes it hard to identify characteristic spectroscopic properties (Shimomura *et al.*, 2008). Without crystallographic data IscU from *A. aeolicus* is an unsuitable candidate for spectroscopic analysis of Co–S cluster formation. In the case of *E. coli* IscU we saw distinct bands in EAS at 350 nm and 450 nm. The 450 nm

band is in the range of what we expect but no characteristic properties are known about it in this context. The 350 nm band is also still in the range of what we expected but from this band we know that it is a typical band for polythiolate mononuclear Co^{2+} species (Petros *et al.*, 2006). This leads to the conclusion that in this case the assembly of Co–S clusters was not successful. Coming back to the most likely Co–S assembly scaffold IscU from *A. fulgidus*. Here we observed the most distinct bands for Co–S cluster in the same area, where also Fe–S cluster can be detected in EAS. Because of this we focused our further analysis only on this D35A mutant from *A. fulgidus* IscU. In addition to the EAS analysis a CD spectrum of the EAS sample was recorded in the range of 300 nm to 800 nm, which supports the presence of Co–S clusters. Further analysis of these samples concerning homogenicity and oligomerization revealed that the reconstituted sample contains monomeric, dimeric, and trimeric IscU D35A. Subsequently, ICP-MS measurements show that the dimeric form is the most likely species, in which Co–S cluster can be assembled. One important property, which has to be checked concerning hydrogen production, is oxygen sensitivity. Here we observed no significant oxygen sensitivity for at least 72 hours. That shows that reconstituted Co–S cluster are stable for longer time in IscU, what makes extensive investigations possible without any time limiting factors. Building on that we did first cluster transfer approaches to apo Fdx from *E. coli*. Here we observe changes in the EAS before and after cluster transfer experiments leading to the conclusion that holo Co–S IscU can interact whith apo Fdx. The results need deeper investigation, although Fdx seems to take Co from IscU, because of occurring absorption bands at 350 nm and 450 nm, what we observed also for semi-enzymatic reconstitution of wild type IscU from *E. coli*. The semi-enzymatic Co–S cluster reconstitution approaches on proteins, which have other functions than being a scaffold protein, gave different results. On the one hand the Fdx from *E. coli* shows same diffuse signals as IscU from *A. aeolicus*, which makes it hard to determine the existence of a Co–S cluster. On the other hand the [4Fe–4S] protein AcnB shows very similar signals like both IscU types from A. fulgidus, which is a strong hint for the existence of Co–S clusters.

Compared to the previous studies, where only mononuclear Co was present in catalysts taking part at water splitting reactions, we present multinuclear Co–S clusters. Only one previous study is known yet, where multinuclear Co–S cluster could be generated and investigated (Deng *et al.*, 2009). However, this study generated a synthetic Co–S cluster to investigate redox series and magnetic ground states. In our work, we present the first ever assembled Co–S cluster in a protein. This marks a great step in the development of artificial biocatalysts, which can be used in water splitting reactions to produce “green” hydrogen.

SUPPORTING DATA

Supplementary Tables

Table S3.1: Molar extinction coefficients and metal ion content of Co–S IscU

sample	ε_1 [mM^{-1}cm^{-1}]	ε_2 [mM^{-1}cm^{-1}]	Co/monomer IscU
Prior to SEC, after desalting	1.85 (404 nm)	2.01 (479 nm)	1.34
Monomer, after SEC	2.86 (390 nm)	2.13 (477 nm)	0.27
Dimer, after SEC	3.50 (377 nm)	2.79 (477 nm)	0.58
Trimer, after SEC	2.12 (378 nm)	1.58 (477 nm)	0.94
After transfer	6.55 (344 nm)	5.75 (458 nm)	-
After transfer (Fdx)	7.67 (344 nm)	6.84 (457 nm)	-

Supplementary Figures

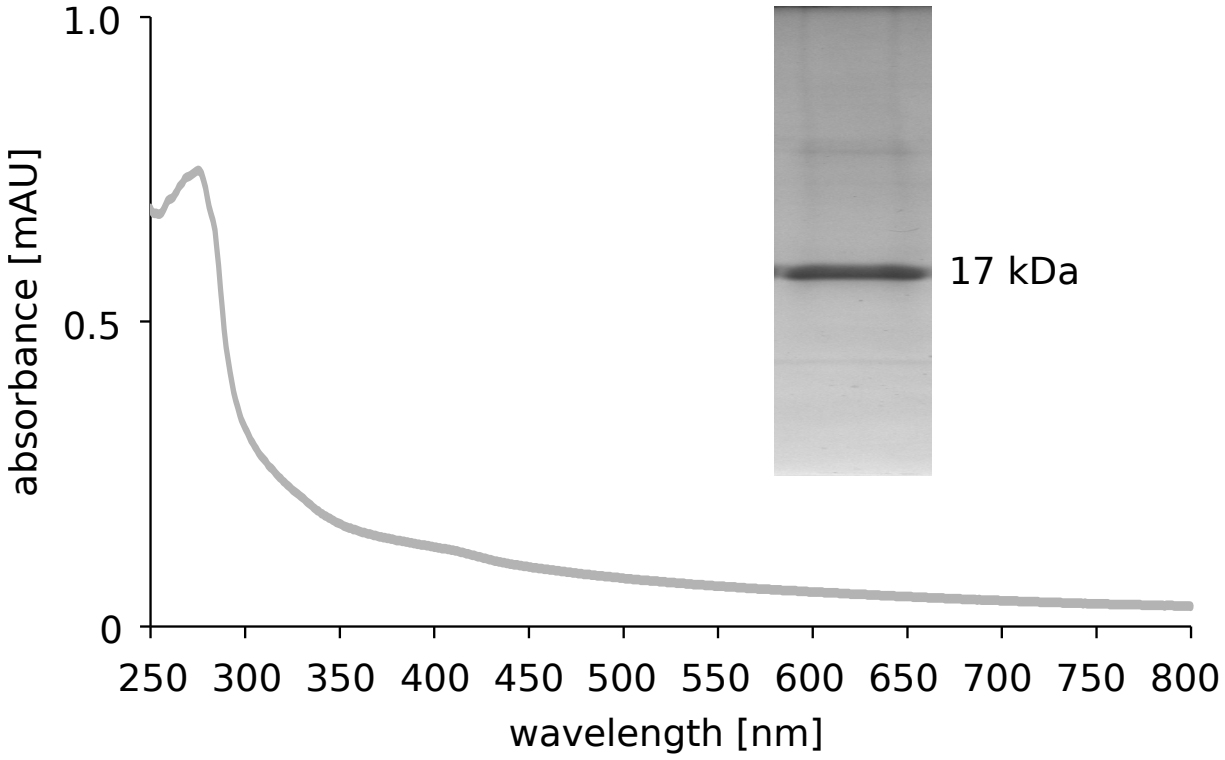

Figure S3.1: Purification of *Af*IscU D35A EAS after isolation/prior to reconstitution and gel prior to reconstitution.

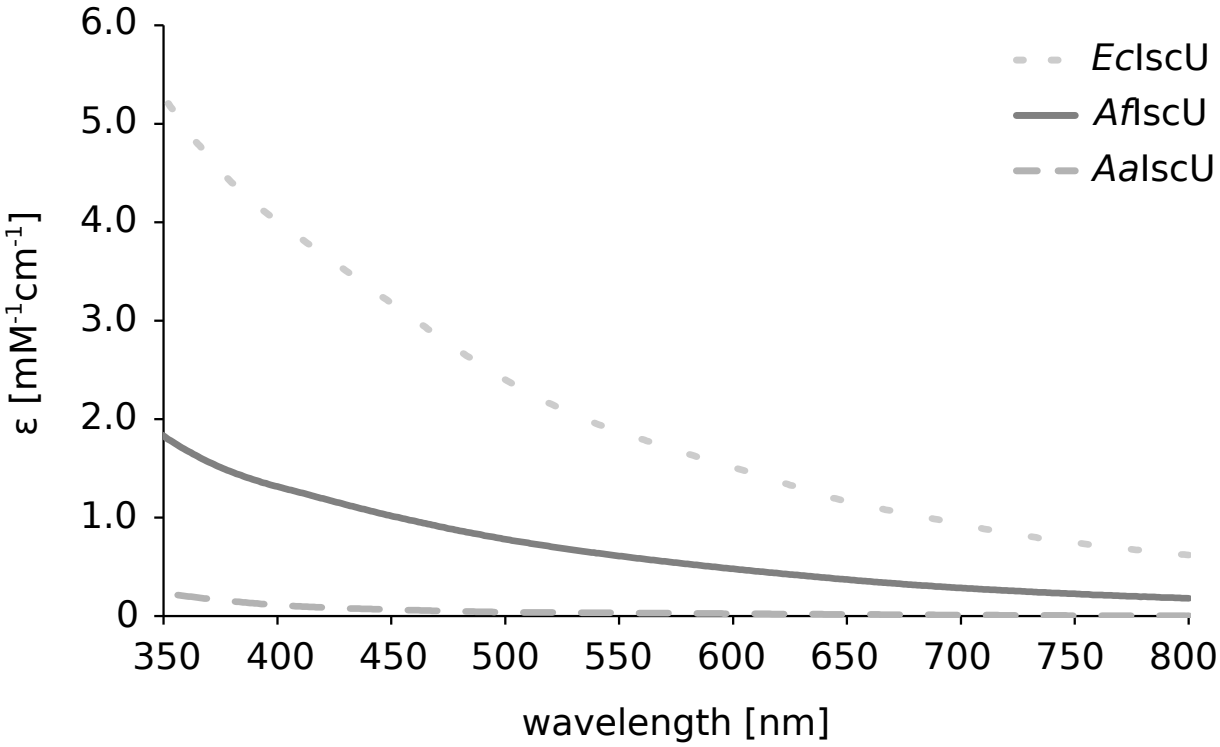

Figure S3.2: Electronic absorption spectra of chemically reconstituted wt IscU from *E. coli*, *A. fulgidus*, and *A. aeolicus*.

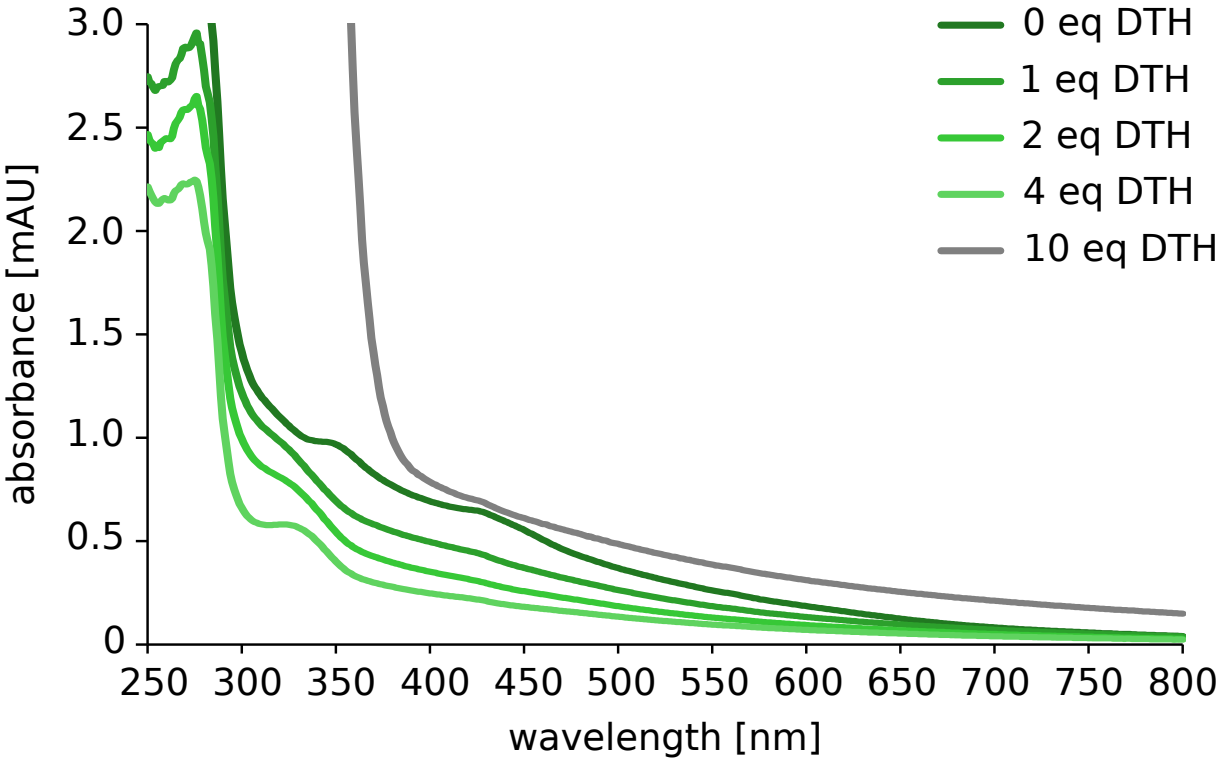

Figure S3.3: Electronic absorption spectra of *Af*IscU D35A after treatment with 0-10 eq. DTH.

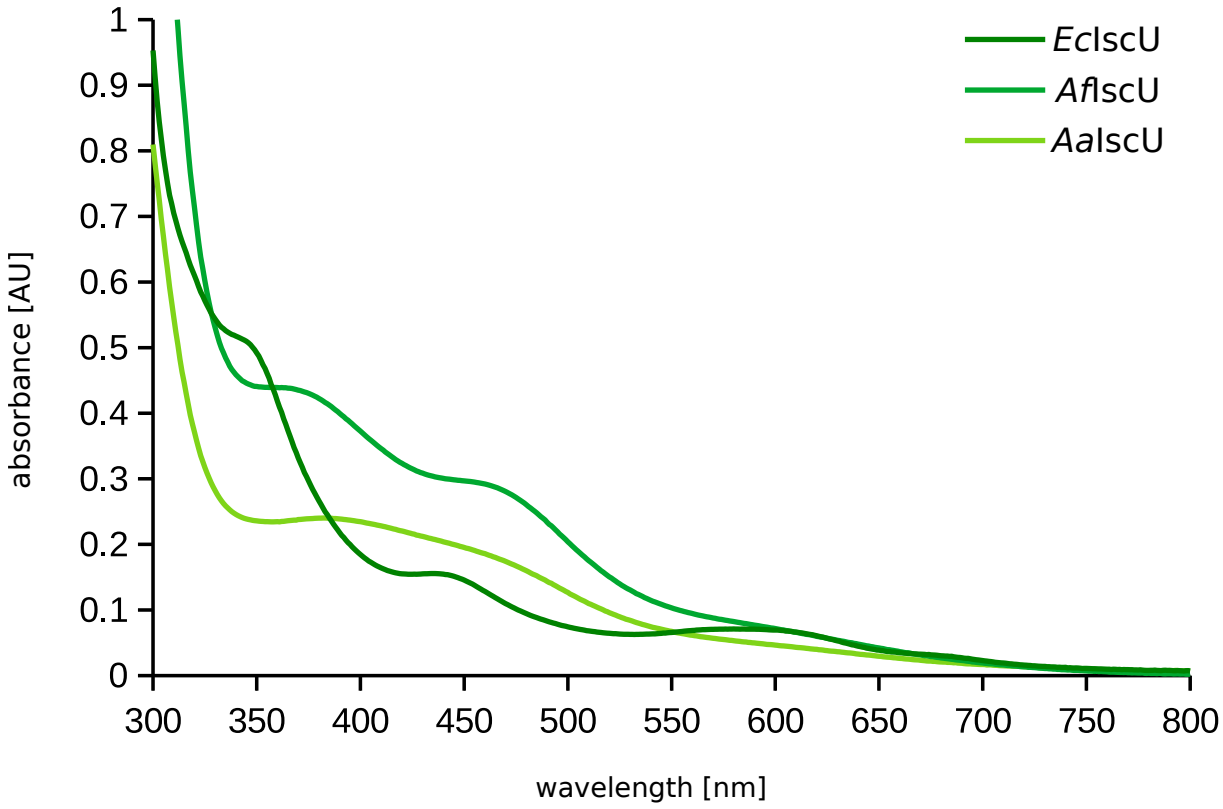

Figure S3.4: Semienzymatic reconstitutions of IscU from *E. coli*, *A. aeolicus*, and *A. fulgidus* after desalting via PD-10 columns.

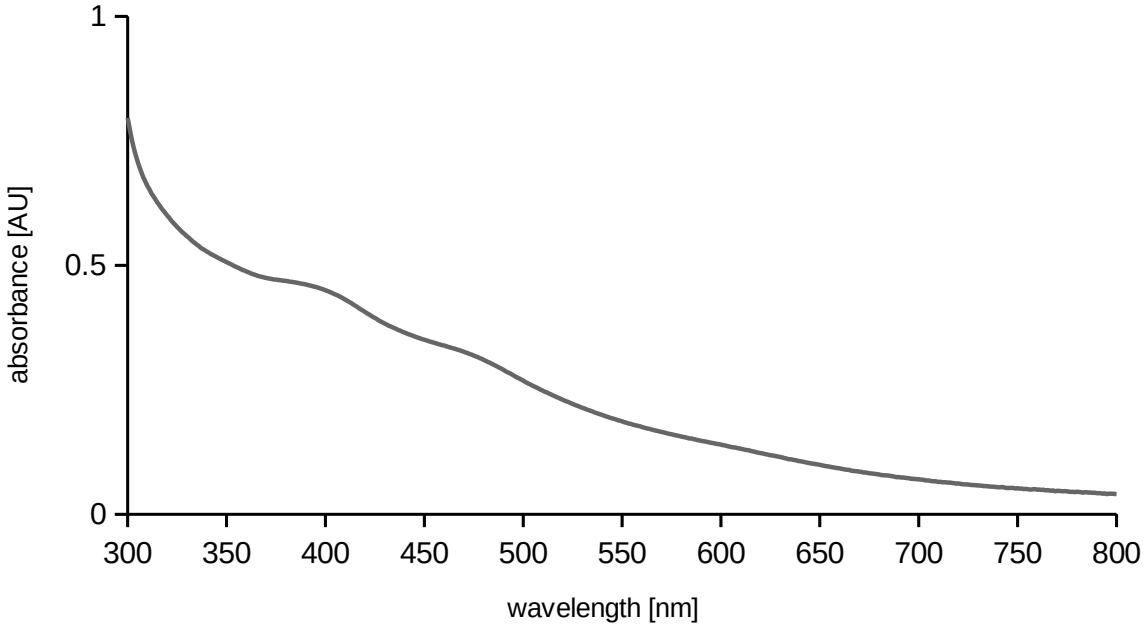

Figure S3.5: Electronic absorption spectrum of semi-enzymatic Co reconstituted Fe–S protein Fdx from *E. coli*.

4 Influence of the T1 Cu axial ligand on kinetic, spectral, and structural properties of the laccase Ssl1 from *Streptomyces sviceus*

This chapter reflects content of the following publication.

4.1 Publication information

Anna Olbrich, Steffen Mielenbrink, Vivian P. Willers, George E. Cutsail III, James A. Birrel, Ingrid Span and Vlada Urlacher

To be submitted to: **International Journal of Biological Macromolecules**

4.2 Abstract

Laccases are multicopper oxidases which couple the oxidation of substrates at a type 1 (T1) copper site to the reduction of O_2 to H_2O. The T1 Cu in bacterial two-domain laccases has four ligands, a cysteine, two histidines and a methionine as the axial ligand. The axial ligand of the T1 Cu has a major influence on the reduction potential which affects the substrate scope and catalytic activity of laccases. To explore the impact of the ligand on the T1 Cu of the two-domain laccase Ssl1 from *Streptomyces sviceus* we analyzed spectral and structural characterizatics of Ssl1 variants in which the axial methionine was replaced by valine, isoleucine, alanine, phenylalanine, threonine, and tyrosine. All these variants displayed perturbed spectral features with an increased absorption of the N(His) $\rightarrow$ Cu charge transfer at 430 nm and a more rhombic signal in EPR spectroscopy. These are typical for T1 Cu sites with an axial oxygen ligand. Indeed, the crystal structures of the Ssl1 variants M295A/V/I/Y/F revealed a water molecule coordinating the T1 Cu. The influence of the mutations on reorganization energy and/or substrate-T1 Cu electronic coupling became apparent from kinetic measurements of the T1 Cu reduction.

4.3 Introduction

Laccases (EC 1.10.3.2) are multi-copper oxidases that catalyze the one-electron oxidation of various aromatic compounds (Thurston, 1994; Xu, 1996; Xu *et al.*, 1996) coupled to the reduction of molecular oxygen to water. Laccases are widely distributed in nature and were found in fungi (Baldrian, 2006), higher plants (Mayer & Staples, 2002), insects (Dittmer & Kanost, 2010), and bacteria (Claus, 2003). Their physiological functions include lignification in plants (Schuetz *et al.*, 2014) and delignification in white-rot fungi (Thurston, 1994), cuticle sclerotization in insects (Arakane *et al.*, 2005; Dittmer & Kanost, 2010), and spore pigmentation (Hullo *et al.*, 2001) and copper homeostasis (Outten *et al.*, 2001) in bacteria. Laccases are considered attractive "green" catalysts (Riva, 2006) since they do not rely on expensive cofactors, only need oxygen as co-substrate, and only produce water as a by-product. Due to their broad substrate scope they are potential candidates for various biotechnological applications like the detoxification of pollutants and bioremediation of phenolic compounds (Singh *et al.*, 2011; Zerva *et al.*, 2019), the delignification of lignocellulose in biorefineries (Osma *et al.*, 2010) and pulp bio-bleaching (Mate & Alcalde, 2017).

Typically, laccases consist of three cupredoxin-like domains (Figure 4.1). Each domain contains two beta-sheets with seven β-strands arranged in a Greek-key-β-barrel. This architecture is closely related to that of small copper proteins like azurin or plastocyanin and typical for all multi-copper oxidases (Giardina *et al.*, 2010). Laccases contain a total of four copper ions, organized in one mononuclear type 1 copper site in domain 3 and an interdomain trinuclear cluster (TNC) with one type 2 (T2) and two type 3 (T3) copper ions which is located at the interface between domain 1 and 3. Domain 2 assists in the positioning of the two other domains and is involved in formation of the substrate pocket (Hakulinen & Rouvinen, 2015). In addition, bacterial two-domain laccases where identified (Endo *et al.*, 2002; Lawton *et al.*, 2009; Machczynski *et al.*, 2004) which lack domain 2. To compensate for the lack of domain 2, two-domain laccases require trimerization to form a functional TNC between two neighboring monomers. These two-domain laccases contain the required characteristics of a common ancestor in the evolution of multicopper oxidases with three and six domains (Komori *et al.*, 2009; Nakamura *et al.*, 2003). The type 1 (T1) Cu is strongly coordinated by at least three ligands, one cysteine and two histidine residues in a pseudo-trigonal manner (Warren *et al.*, 2012). The variations in T1 Cu sites that are observed in different proteins arise from different axial interactions. Methionine is a common axial ligand, e.g. in azurin and bacterial laccases, while fungal laccases have non-coordinating leucine or phenylalanine in the axial position instead. Stellacyanin has a glutamine axial ligand and azurin has an additional ligand beneath the S(Cys)-N(His)-N(His) plane, a backbone carbonyl oxygen. Valine (Dennison *et al.*, 2003; Yanagisawa & Dennison, 2005) and arginine (Hosseinzadeh *et al.*, 2016) were also found in the position of the axial ligand. The arginine residue was found to rotate away from the Cu so that a water is bound in the axial position of the T1 Cu (Hosseinzadeh *et al.*, 2016). The T1 Cu is responsible for electron shuttling between the reducing substrate and the TNC where oxygen is reduced to water. Thus, it participates in two electron transfer (ET) steps, the intermolecular ET from the substrate to the

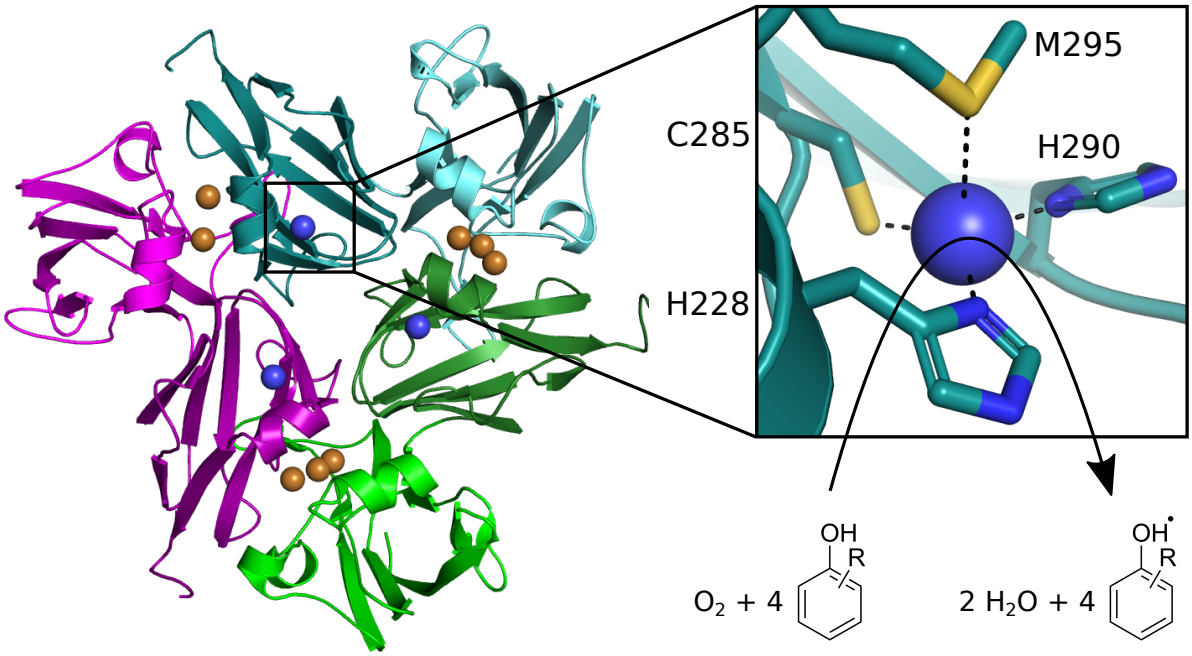

Figure 4.1: Overview of homotrimeric structure of Ssl1. The cartoon of the three different monomers is shown in three different colors. Each of the two domains in one monomer is shown in a different shade.The T1 Cu is shown as blue spheres, all other Cu are shown in brown spheres. The black box presents a zoom on the T1 Cu, which is the substrate binding site. The Cu-coordinating residues are shown as sticks. Black dashed lines show the bond between the Cu and the coordinating atoms. At the bottom right a reaction scheme of the phenolic substrate is presented via a curved arrow connected to the T1 Cu zoom box. PDB ID 4M3H ((Gunne *et al.*, 2014))

T1 Cu and the intramolecular ET from the T1 Cu to the TNC. It has an intense charge transfer (CT) transition at 600 nm in the ultraviolet-visible (UV/Vis) spectrum and a small parallel hyperfine coupling constant in electron paramagnetic resonance (EPR) ($A_{||}$ = 40-90 x 10-4 cm-1) (Solomon, 2006). These spectroscopic characteristics are a result of the high covalency of the Cu^{II}-S(Cys) bond (Solomon *et al.*, 2004) which provides strong electronic coupling into the superexchange pathway to the TNC (Lowery *et al.*, 1993).

The three copper ions of the TNC are coordinated by eight histidine residues from two different domains. The T2 Cu has a square planar coordination by two histidine residues and one water molecule (Enguita *et al.*, 2003). It has no absorption feature and a parallel hyperfine coupling constant which is characteristic for tetragonal copper centers ($A_{||}$ = 140-200 $\times$ 10^{-4} cm^{-1}) (Solomon, 2006). The T3 Cu pair is coordinated by six N_{ε} atoms of histidine side chains in two-domain laccases. The T3 Cu's are antiferromagnetically coupled through a bridging hydroxide ligand, thus not observable in EPR spectroscopy. They contribute to the absorption spectrum with charge transfer (CT) transition from the bridging OH^- ligand at $\sim$300 nm. Each of the copper ions in the TNC has an open coordination position oriented into the cluster resulting in an unsaturated coordination that is necessary for the bridged intermediates in the reduction of O_2 to H_2O (Solomon *et al.*, 2008). Fungal laccases exhibit high activities and a broad substrate spectrum attributed to the high reduction potentials of up to 800 mV of the electron accepting T1 Cu. However, their activity is restricted to acidic conditions and they are inhibited by a very

wide range of compounds, which has prevented its applications in biotechnological applications (Baldrian, 2006). Due to their higher stabilities, bacterial laccases including two-domain laccases like "small laccase" (SLAC) from *Streptomyces coelicolor* and Ssl1 from *Streptomyces sviceus* have gained research interest. Ssl1 displays phenol oxidation activity at alkaline pH and tolerance towards detergents, organic co-solvents, and elevated temperatures (Gunne & Urlacher, 2012). The reduction potential of Ssl1 (375 mV) (Gunne *et al.*, 2014) is comparable to other bacterial laccases but low compared to fungal laccases. In our previous studies axial ligand was mutated to increase the T1 Cu reduction potential for increasing oxidation rates and extending substrate spectra (Gunne *et al.*, 2014; Olbrich *et al.*, 2019). To this end, the axial ligand of the T1 Cu in Ssl1 was mutated to leucine, phenylalanine, alanine, threonine, valine, isoleucine, and tyrosine. The mutation of an axial methionine to phenylalanine, leucine, and alanine were previously reported to increase the reduction potential (Durao *et al.*, 2006; Ellis *et al.*, 2002; Farver *et al.*, 2004; Marshall *et al.*, 2009). Due to their structural similarity to leucine and phenylalanine the amino acids valine, isoleucine, and tyrosine were identified as additional promising candidates to increase the reduction potential. On the other hand, threonine was chosen because it was expected to decrease the reduction potential and the methionine to threonine mutation in nitrite reductase led to great changes in the electronic structure of the T1 Cu site (Basumallick *et al.*, 2003). Our previous results demonstrated that the hydrophobicity of the axial ligand was determining the reduction potential changes in axial ligand mutants(Olbrich *et al.*, 2019). To gain a deeper understanding of how these various axial ligands influence the T1 Cu reduction rate (k_{ET}) as well as the spectral and structural properties of a two-domain laccase, herein we systematically investigated a series of Ssl1 mutants. To the best of our knowledge a systematic spectroscopic and structural investigation of a two-domain laccase where different axial ligands were introduced at the T1 Cu site is still missing. For this purpose, we used electronic absorption, circular dichroism (CD) and electron paramagnetic resonance (EPR) spectroscopy and X-ray crystallography. The kinetics of the T1 Cu reduction were measured using a stopped-flow method.

4.4 Material and Methods

4.4.1 Mutagenesis

T2 copper depleted (T2D) Ssl1 variants were created by introducing the H99Y mutation using the QuikChange mutagenesis protocol (Stratagene, San Diego, CA, USA). The primer sequences were 5'-GG GCG AGC CTG TAC GTC CAC GGC CTG-3' and 5'-CC GTG GAC GTA CAG GCT CGC CCG GAC-3'. Mutated *ssl1* sequences were confirmed by Sanger sequencing.

4.4.2 Expression and Purification of Ssl1 and Spectrophotometric Redox Titrations

Expression and purification of Ssl1 and variants thereof as well as the spectrophotometric redox titrations were performed as described previously (Olbrich *et al.*, 2019). Briefly, Ssl1 laccase from *S. sviceus* (UniProtKB B5HSR1) and Ssl1 variants carrying a N-terminal hexahistidine tag were expressed in E. coli BL21-CodonPlus(DE3)-RP. The soluble fraction obtained after sonication of the cells was incubated with $CuSO_4$ at room temperature for 2 h or until no further increase in activity was observed to increase copper loading. Purification was carried out using heat precipitation at 65°C and immobilized metal ion affinity chromatography (IMAC). Finally, the buffer was exchanged to 50 mM potassium phosphate buffer (pH 7.5) and the protein concentrations were determined using the Bradford method (Bradford, 1976). The reduction potentials were determined by spectrophotometric redox titrations using the redox couple potassium hexacyanoferrate(III)/potassium hexacyanidoferrate(II) as mediator. The oxidation of the T1 Cu was followed spectrophotometrically using the increase in absorption at $\sim$600 nm and plotted against the reduction potential established by the mediator. The midpoint potential of the laccase was obtained from fitting the data to the Nernst equation.

4.4.3 Stopped-Flow Measurements

The reduction of the T1 Cu by hydroquinone (Benzene-1,4-diol, HQ) under anaerobic conditions was measured using a SX20 Stopped-Flow System (Applied Photophysics Limited, Leatherhead, United Kingdom) equipped with a photodiode array detector. To ensure an anaerobic environment a constant flow of nitrogen was maintained at the sample handling unit and through the thermostat water. Additionally, 1 g of sodium dithionite were added to the thermostat water to eliminate any adsorbed or dissolved oxygen. All samples and buffers were prepared in a Glovebox under nitrogen *atmosphere* and contained 180 mU glucose oxidase and 100 mM glucose to maintain oxygen free conditions. Equal volumes of 20 µM laccase in 50 mM potassium phosphate buffer (pH 7.5) and 20 mM HQ in water (both solutions also containing glucose and glucose oxidase) were rapidly mixed. The exponential decay rates were obtained by fitting the absorbance decrease at the $\sim$592 nm to a first order exponential decay using Origin pro 9.0G (OriginLab Corporation, Northampton, MA, USA).

4.4.4 Electronic Absorption Spectroscopy

Electronic absorption spectra of Ssl1 were recorded on a Lambda35 spectrophotometer (Perkin Elmer, Rodgau, Germany) in 1 nm intervals in the range of 300-1000 nm with a slit width of 1 nm and a scan speed of 480 nm/min. For each variant three cycles were accumulated. The solution contained purified Ssl1 variants in 50 mM potassium phosphate buffer (pH 7.5). Molar extinction coefficients for Ssl1 variants were calculated using the Lambert-Beer law and protein concentrations determined by the Bradford method (Bradford, 1976).

4.4.5 Circular Dichroism Spectroscopy

Circular dichroism (CD) spectroscopy was performed on a Jasco J-815 CD Spectrometer (Jasco Germany, Pfungstadt, Germany). An average of 20 scans was collected at 20°C with a scanning speed of 100 nm/min and a bandwidth of 5 nm in a quartz glass high precision cell with a 1 mm path length. Samples contained 500 µM Ssl1 WT or M295I/V/F, 1148 µM Ssl1 M295A, ,1189 µM Ssl1 M295T, or 287 µM Ssl1 M295Y in 50 mM potassium phosphate buffer (pH 7.5).

4.4.6 Electron Paramagnetic Resonance

Continuous-wave (CW) X-band (∼9.63 GHz) EPR spectra were collected on a Bruker E500 spectrometer equipped with an Oxford liquid helium flow cryostat operated at 30 K. The spectra were collected with 100 kHz field modulation at 6 G amplitude, a 163.84 ms time constant, and a 40.96 ms conversion time for the 4096 point spectrum. Data were simulated in Matlab 2017a using the EasySpin software package (v 5.2) (Stoll & Schweiger, 2006).

4.4.7 Crystallization

Crystals were obtained using sitting drop vapor diffusion method with a 1:1 mixture of the protein solution at a concentration of 10 mg/ml in 50 mM potassium phosphate buffer (pH 7.5) and a reservoir solution at room temperature. M295A crystals were obtained with a reservoir solution consisting of 50 mM HEPES at pH 7.0, 1.1 M $(NH_4)_2SO_4$, and 5 mM $[Co(NH_3)_6]Cl_3$. M295F crystals were obtained with a reservoir solution consisting of 50 mM HEPES at pH 7.0, 1.1 M $(NH_4)_2SO_4$, and 20 mM $[Co(NH_3)_6]Cl_3$. M295I crystals were obtained with a reservoir solution consisting of 50 mM HEPES at pH 7.0, 1.4 M $(NH_4)_2SO_4$, and 10 mM $[Co(NH_3)_6]Cl_3$. M295V crystals were obtained with a reservoir solution consisting of 50 mM HEPES at pH 7.0, 1.3 M $(NH_4)_2SO_4$, and 20 mM $[Co(NH_3)_6]Cl_3$. M295Y crystals were obtained with a reservoir solution consisting of 50 mM HEPES at pH 7.0, 1.2 M $(NH_4)_2SO_4$, and 15 mM $[Co(NH_3)_6]Cl_3$. Blue-colored and rod-shaped crystals were observed within 14 days, flash frozen immediately after soaking for 60 s in cryo-protecting solution (saturated $LiSO_4$), mounted into MiTeGen MicroMounts/MicroLoops, and stored in liquid nitrogen.

4.4.8 Data Collection and Structure Determination

Data sets were collected at 100 K using synchrotron radiation at P11 beamline, PETRA III, Hamburg, Germany. High-resolution native data sets for structure refinement were collected at 12.4 keV. For the anomalous scattering contribution of copper atoms, a second, high-multiplicity data set was collected at 9 keV for each Ssl1 variant. The data was processed using the program package XDS (Kabsch, 2010). Molecular replacement and structure refinement were performed using the software package ccp4 (Winn *et al.*, 2011) starting from *Streptomyces sviceus* Ssl1 (PDB ID 4M3H) as the starting model. More detailed, data reduction was performed with AIMLESS (Evans & Murshudov, 2013), phasing was done by PHASER (McCoy *et al.*, 2007). Coot (Emsley & Cowtan, 2004) was used for model building and validation, and REFMAC5 (Murshudov *et al.*, 2011) was employed for structure refinement. Maps were calculated using FFT (Immirzi, 1966). PyMOL (Schrödinger, 2017) was used to prepare the figures and to calculate the root-mean-square deviation (RMSD) of the Cα atoms using the align command with the number of cycles set to 0, thus, not including outlier rejection. The structures were visualized using PyMol and the atomic coordinates have been deposited with the Protein Data Bank, Research Collaboratory for Structural Bioinformatics at Rutgers University (PDB ID: 6YZD, 6YZY, 6YZF, 6Y4A, 6YO5). The final models of M295A, M295F, M295I, and M295Y contained 98.00% in the favored region and 0.00% in outlier regions of the Ramachandran plot as defined by MolProbity (Chen *et al.*, 2010). The final model of M295V has 94.00% in the favored and 0.00% in the outlier regions of the Ramachandran plot.

4.5 Results and Discussion

4.5.1 Reduction Potentials of Ssl1 Variants

To disrupt the intramolecular electron flow from the T1 Cu to the TNC we constructed the corresponding T2 Cu depleted Ssl1 variants. The T2 Cu coordinating His99 was mutated to glutamine to prevent T2 Cu coordination as previously described in the production of T2 copper depleted Fet3 (Blackburn *et al.*, 2000). Further, the T2 copper depleted variants (T2D) bearing various axial residues at the T1 Cu site were analyzed regarding their reduction potentials (Figure 4.2). In our previous work, we have shown that the axial ligand influences the T1 Cu reduction potential (Olbrich *et al.*, 2019). In this work, we first investigated the relation between k_{ET} and E^0 in Ssl1 variants differing in their axial ligands and reduction potentials. Exchange of the axial ligand Met295 with the less hydrophobic amino acids alanine and threonine led to a decrease of the reduction potential, M295Y shows no significant effects, while the variants M295V, M295I, and M295F possess increased reduction potentials (Figure 4.2).

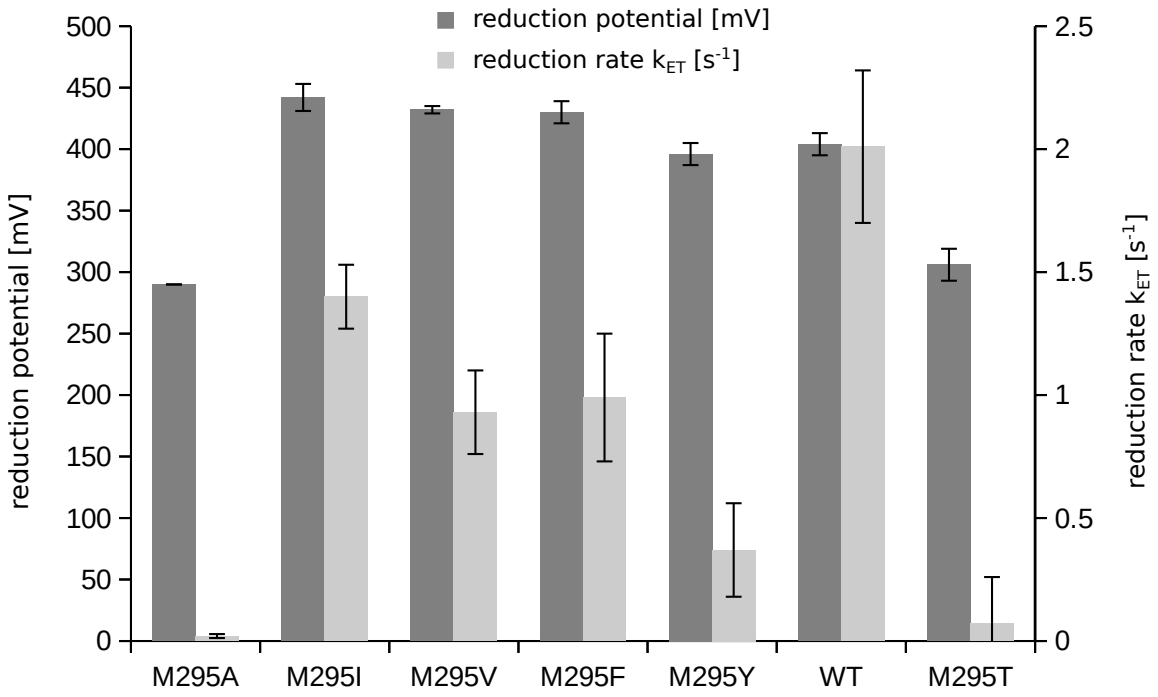

Figure 4.2: Reduction potentials of T2D Ssl1 variants (dark grey) and reduction rates k_{ET} for the reduction of the T1 Cu by HQ (light grey). Values are given as mean $\pm$ standard deviation of at least triplicates.

The first reaction step in Ssl1, the transfer of one electron from the common low potential laccase substrate hydroquinone (HQ) (Steenken & Neta, 1982) to the T1 Cu was analyzed using a stopped-flow approach (Figures S4.2-S4.8). The k_{ET} values varied over two orders of magnitude between the fastest reduction in the T2D variant with the wild-type axial methionine

with k_{ET} = 2.01 s^{-1} and the slowest measured with Ssl1 T2D M295A (0.02 s^{-1}) (Figure 4.2). While decreased T1 Cu reduction potentials indeed resulted in smaller k_{ET}, increased T1 Cu reduction potentials did not necessarily lead to increased values for k_{ET}. This underlines the importance of further contributions, i.e. from changes in the reorganization energy λ. To assess those contributions, the spectroscopic and structural properties of the Ssl1 variants were investigated.

4.5.2 X-ray Crystallography

To obtain high-resolution structural information of the T1 Cu site in Ssl1, we set up crystallization trials for several Ssl1 variants and were able to obtain crystals for the five Ssl1 variants M295A, M295F, M295I, M295V, and M295Y. The structure of the wild-type and the variant Ssl1 M295L were previously reported (PDB ID 4M3H and PDB ID 4WTO, respectively). All crystals showed an intense blue color, indicating the presence of copper at the T1 Cu site (M295V and M295F as representatives in Figure S4.1). The Ssl1 variants crystallized in the orthorhombic space group $P2_12_12_1$, and the asymmetric unit contains one biological assembly consisting of a protein trimer. The poor diffraction of the Ssl1 M295T variant did not lead to high quality data suitable for structure solution. Native and anomalous data for all Ssl1 variants were collected and their crystal structures were solved using molecular replacement with the structure as a starting model published by Gunne *et al.* (2014) (PDB ID 4M3H). A summary of the data collection and refinement statistics can be found in the crystallographic table (Table S4.2).

The overall architecture of all Ssl1 variants is very similar to the wild-type structure (Gunne *et al.*, 2014) with root mean square deviations (RMSD) in the range of 0.330–0.599 Å (calculated for all Cα atoms of residues 43–311 without outlier rejection). The electron density at the T1 Cu site reveals that none of the amino acids introduced as axial ligand at position 295 is directly interacting with the copper (Figure 4.3). However, we observe an effect of the amino acid exchange on the residues in the vicinity of position 295 and the residues 203–205. The side chains of alanine, isoleucine, and valine in their respective variants (M295A, M295I, M295V) are well-defined, which is probably due to the short side chain of this residues. The electron density of the larger residues Phe295 and Tyr295 is not well defined. This indicates that these Ssl1 variants have a higher degree of flexibility in the vicinity of the larger residues at position 295. Notably, the residues 203–205 that are located close to residue 295 could also be affected in their flexibility. The disorder in the region 203–205 may be caused by the disorder of large residues at position 295. Both the phenylalanine and tyrosine residues are flipped away from the Cu coordination site towards the region of residues 203–205 while the alanine, isoleucine, and valine residues point towards the Cu coordination site. Met295 in the wild-type protein reaches far into the metal-binding site of Ssl1 and coordinates to the T1 Cu, while all introduced mutations are not capable of filling this space and interacting with the copper. We assume that the side chains of phenylalanine and tyrosine are too large to reach into the pocket, while isoleucine, valine, and alanine are smaller than methionine and do not occupy the entire space in the pocket. As a result, water molecules can occupy the open coordination

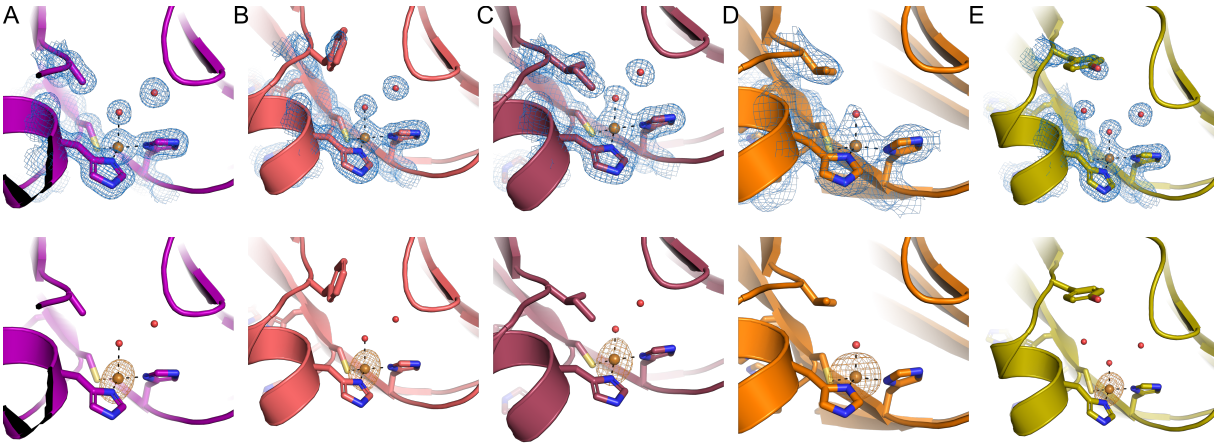

Figure 4.3: Structure of the T1 Cu sites of the Ssl1 variants (A) M295A (purple), (B) M295F (red), (C) M295I (dark red), (D) M295V (orange), and (E) M295Y (green). T1 Cu is shown in brown spheres. Red spheres show oxygen atoms representing water molecules. Dashed black lines show bonds between atoms of Cu-coordinating molecules. The coordinating amino acid residues and the side chain of the axial ligand of T1 Cu are shown as sticks. The blue mesh in the top row shows the native electron density map measured at 12 keV (contoured at 1.0 σ). The brown mesh in the bottom row shows the Cu electron density map measured at 9 keV (contoured at 1.0 σ).

site in the variants. The number of well-defined water molecules in the first and second coordination sphere of the T1 Cu varies in each variant. Additionally, the number of water molecules can vary in the different protomers of the protein, which may correlate with the observation that not all amino acid chains of Ssl1 are equally well defined. The T1 Cu site from the protomer that is best defined is shown in Figure 4.3. We observe two well-defined water molecules in the structures of the variants M295A, M295I, and M295F. The active site of the variant M295Y harbors three water molecules in close proximity to the T1 Cu. The variant M295V shows one water molecule directly coordinated to the T1 Cu. The absence of additional water molecules in this variant may also be a result of the low resolution of this structure as compared to the other structure.

4.5.3 Electronic Absorption Spectroscopy and Circular Dichrosim

Wild-type Ssl1 is characterized by a deep blue color and its absorption spectrum in the UV/Vis region is characteristic for laccases (Figure 4.4) (Gunne *et al.*, 2014). During isolation of the mutants we recognized that the colors of Ssl1 in solution can differ from the so far known color of the wild type (Figure S4.1). In order to investigate the effects of the mutations on the spectroscopic characteristics, we captured electronic absorption spectra as well as circular dichroism spectra between wavelength of 300 - 800 nm (Figure 4.4) and compared them with the spectra of the wild type. Due to the high Cu-S(Cys) bond covalency there is an intense S(Cys)$\pi \rightarrow Cu^{II}$ $3d_{x2-y2}$ CT transition at 592 nm. The shoulder at 330 nm corresponds to the T3 Cu site and originates from an $OH^{-} \rightarrow Cu^{II}$ CT. The d-d transitions form a shoulder to the 592 nm maximum and are centered around 730 nm in the wild-type's spectrum. The T2 Cu does not contribute to the absorption spectrum.

The most intriguing effect of the mutation of Met295 on the absorption spectrum (Figure 4.4) is the presence of an additional band at ∼430 nm assigned to the His(N) → Cu^{II} charge transfer based on its negative feature in the CD spectrum. This band is usually weak for multicopper oxidases (Sakurai & Kataoka, 2007) and also not recognized from the absorption spectrum of wild-type Ssl1. The increase in absorption indicates an increased overlap of the N(His)π-orbitals with the Cu d_{x2-y2} orbital and is indicative of a tetrahedral distortion. The intensity of the 430 nm transition varies between mutants (Figure 4.4 and Table S4.3) and is always less intense than the ∼590 nm feature in the absorption spectra. The strongest absorption at ∼430 nm was observed in the M295F mutant ($_{\varepsilon 427}$ = 1.454 $mM^{-1}cm^{-1}$). The S(Cys)π → Cu^{II} CT transition at ∼590 nm is the most prominent feature in the absorption spectrum whereas the S(Cys)σ → Cu^{II} CT (500–530 nm) is only resolved in CD spectroscopy. The intensity of the 600 nm absorption decreased in all mutants except for M295A ($_{\varepsilon 590}$ = 3.158 mM^{-1} cm^{-1}). The S(Cys)σ → Cu^{II} CT forms a pronounced shoulder to the ∼600 nm transition in CD spectra of M295Y, M295V, M295F, M295A, and M295T. In spectra of M295I and wild-type Ssl1 the S(Cys)σ → Cu^{II} CT is more intense and there is one broad intense feature between 500 and 600 nm.

The transition at 330 nm that is observed both in the absorption and CD spectrum is a OH → Cu^{II} CT from the T3 Cu site. Compared to the wild-type (1.835 $mM^{-1}cm^{-1}$) the intensity of the absorption at 330 nm increased in the M295A variant (2.245 $mM^{-1}cm^{-1}$) (Table S4.3). In spectra of M295V, M295Y and M295I a transition at 330 nm is not resolved, but it is present in the CD spectra of the respective mutants.

Mutation of the T1 Cu axial ligand impacted the d-d transitions (mostly d_{xz}/d_{yz} → d_{x2-y2} from the T1) between 700 and 800 nm. They are shifted to higher wavelength/lower energy and are less intense in the M295F, M295V, M295Y, M295A, and M295T mutants as compared to the wild-type (Table S4.4) reflecting a weaker ligand field and indicating tetrahedral distortion of the T1 Cu site. For the M295I mutant the d-d transition feature shifted to lower wavelength/higher energies compared to Ssl1 wild-type. This would indicate a larger ligand field splitting, increasing the energy of the d_{x2-y2}, possibly reflecting a tetragonal distortion relative to the T1 site with an axial methionine.

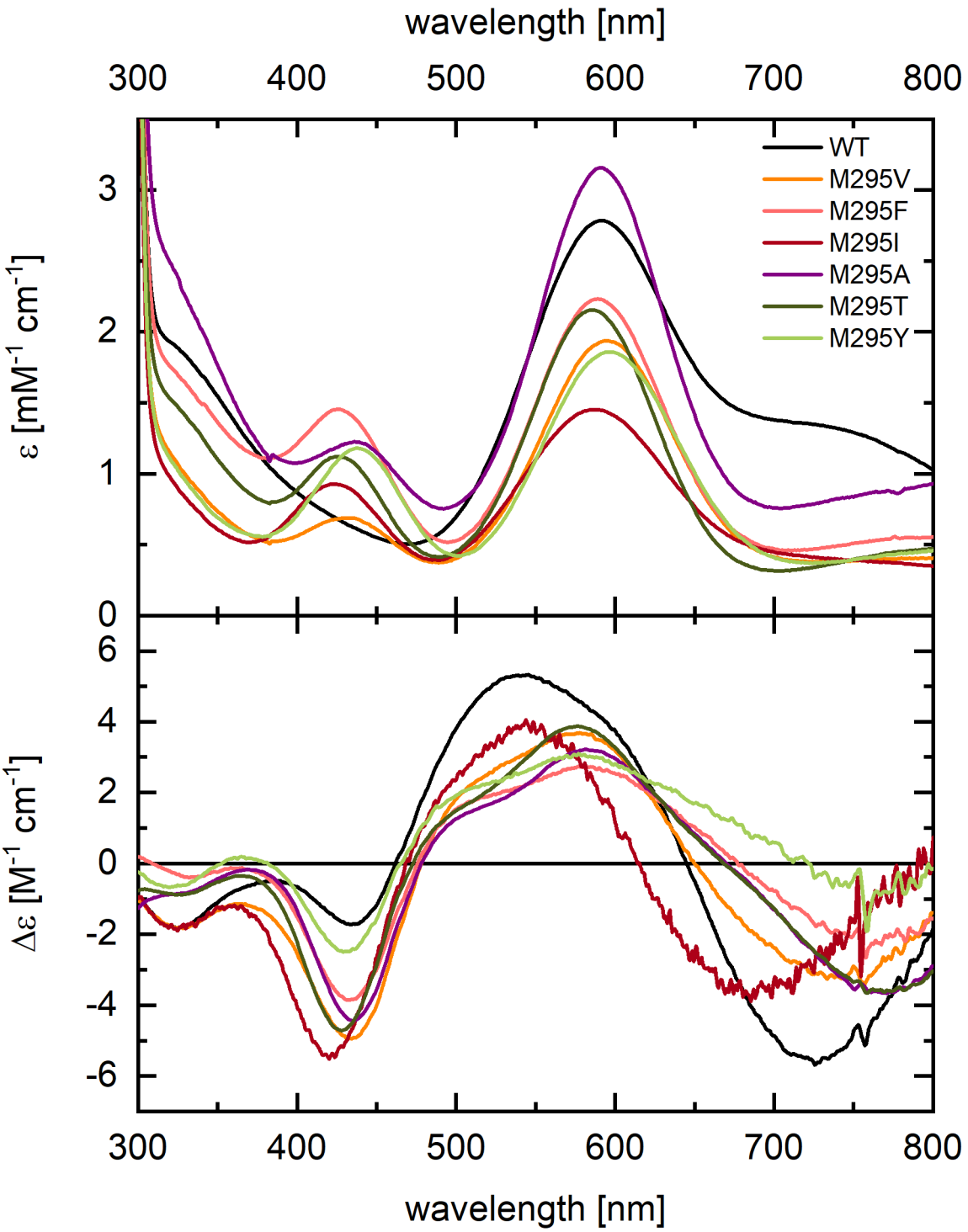

Figure 4.4: Electronic absorption & Circular dichroism spectra (top & bottom) of wild-type Ssl1 (black curves) and the variants M295V (orange), M295F (salmon), M295I (red), M295A (puple), M295T (dark green), and M295Y (lime).

4.5.4 EPR

Continuous wave (cw) X-band (9.64 GHz) EPR spectra were measured for wild-type and all mutants. Experimental spectra along with spectral simulations are shown in Figure 4.5 and the simulation parameters are shown in Table S4.5. The EPR spectrum of the wild-type protein is reminiscent of typical laccases with two components. The first is an axial spectrum ($g_1 = g_\parallel =$ 2.230 and $g_2 = g_3 = g_\perp =$ 2.046) with a small anisotropic Cu hyperfine coupling ($A_\parallel$ = 221.8 MHz and $A_\perp$ = 35 MHz) that splits the $g_\parallel$ into four lines. This is typical for distorted tetrahedral T1 copper sites where the singly occupied molecular orbital (SOMO) has d_{x2-y2} character, where a large amount of covalency lowers the hyperfine coupling relative to that observed for the square planar $CuCl_4^{2-}$ complex. The second component is also axial ($g_\parallel$ = 2.215 and $g_\perp$ = 2.05) but with a much larger anisotropic Cu hyperfine ($A_\parallel$ = 599.6 MHz and $A_\perp$ = 3 MHz). This is typical of tetragonal T2 copper sites with a highly ionic Cu center (low covalency).

Interestingly, the methionine variants all show drastically different EPR spectra where the characteristic T1 copper site is significantly altered with higher $g_\parallel$-values (ca. 2.3), much smaller $A_\parallel$ values (ca. 100 MHz), and a slightly rhombic line shape (i.e. g2 $\neq$ g3). The hyperfine coupling has three components: 1) The Fermi contact interaction relates to the s-electron density at the nucleus, which is indirectly affected by the d-electrons (through spin polarization of 3s and 2s electrons) and contributes to the isotropic part ($A_{iso} = (A_\parallel + 2A_\perp)/2$) of the hyperfine coupling tensor, 2) spin dipolar coupling between the electron spin and the nuclear spin, which contributes to the anisotropic part. This $A_\parallel$ is usually large and negative. Lastly, the orbital dipolar coupling, between the magnetic field experienced by the electron as it orbits the nucleus and its intrinsic spin, is also anisotropic, and is proportional to the g-values. Components 1 and 2 are reduced by covalency – electron delocalization from the d_{x2-y2} onto the ligands. The small values of $A_\parallel$ and A_{iso} are both due to the high covalency of the T1 site with Cu-S/N bonding. Interestingly, removing the axial Met ligand generally gives even smaller $A_\parallel$ indicating increased covalency (stronger Cu-S/N bonding). In general, the rhombicity of the EPR spectrum is increased in the mutants, indicative of some d_{z2} mixing into the d_{x2-y2} ground state, in agreement with the lower energy ligand field transitions observed in UV/Vis. Also, the g_1 value increases, indicating larger spin-orbit coupling through mixing of excited states into the d_{x2-y2} ground state.

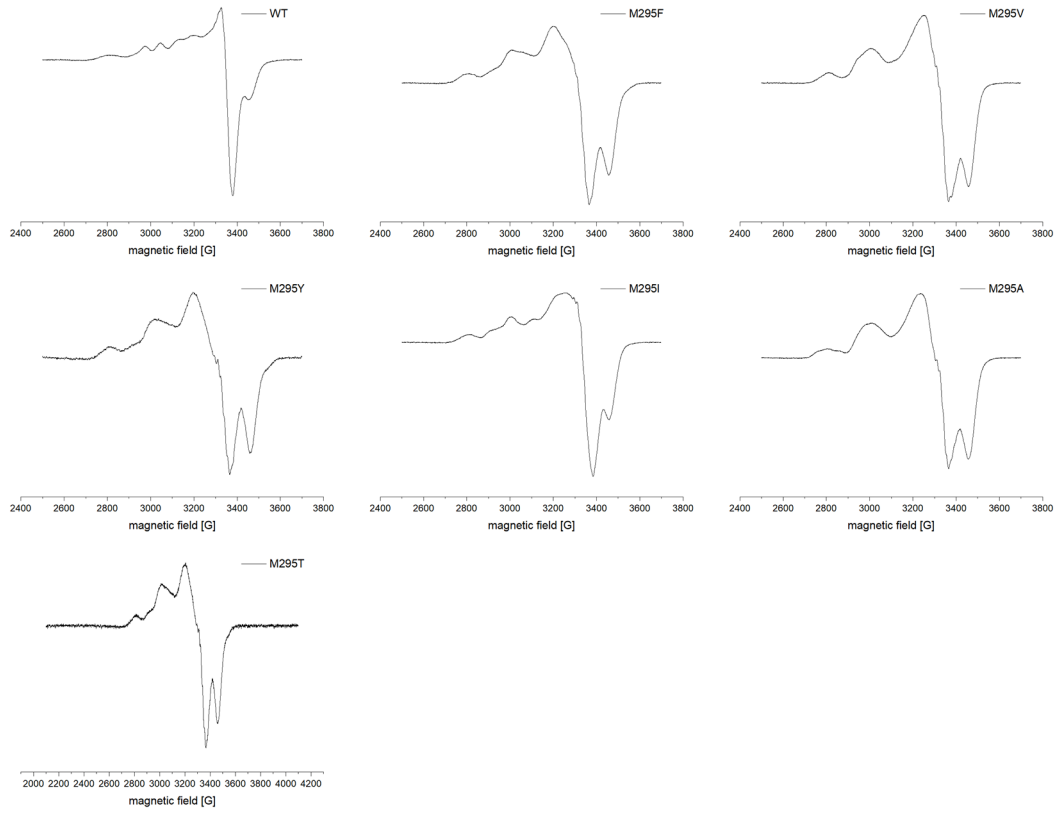

Figure 4.5: Experimental EPR spectra of Ssl1 variants.

4.6 Discussion

The T1 or blue copper sites in numerous proteins have been extensively studied including mutants of the axial ligands due to the major influence of the axial ligand on the reduction potential and electronic structure. One of the best studied proteins in this regard is azurin. The axial methionine of azurin has been mutated to every other natural amino acid (Clark *et al.*, 2010; Karlsson *et al.*, 1989, 1991; Kroes *et al.*, 1996; Pascher *et al.*, 1993) as well as non-natural amino acids (Berry *et al.*, 2003; Clark *et al.*, 2010; Garner *et al.*, 2006). Axial ligand mutations have also been studied in other cupredoxins (Carrell *et al.*, 2007; DeBeer George *et al.*, 2003; Hall *et al.*, 1999; Kataoka *et al.*, 2000) and multicopper oxidases, including nitrite reductase (Basumallick *et al.*, 2003; Ellis *et al.*, 2002; Kataoka *et al.*, 2003) bilirubin oxidase (Kamitaka *et al.*, 2007; Kataoka *et al.*, 2008) and laccases (Durao *et al.*, 2006; Gunne *et al.*, 2014; Kurose *et al.*, 2009; Olbrich *et al.*, 2019; Osipov *et al.*, 2014; Palmer *et al.*, 2003; Prins *et al.*, 2015; Xu *et al.*, 1998, 1999). Thus, there are already detailed descriptions of the electronic structures available for many T1 Cu containing proteins and variants thereof with different axial ligands of the T1 Cu. Herein we provide structural and spectroscopic data for axial ligand variants of a two-domain laccase, Ssl1 from *S. sviceus*. Ssl1 WT has spectral characteristics of a classic blue Cu/T1 Cu site like plastocyanin with two N(His), a highly covalent S(Cys), and an axial S(Met) ligand (Gewirth & Solomon, 1988; Solomon *et al.*, 1996a). There is an intense S(Cys)$\pi \rightarrow Cu^{II}$ CT at 591 nm and only little absorption at $\sim$450 nm in the absorption spectrum. Additionally, there is the contribution of a $OH^{-} \rightarrow Cu^{II}$ CT from the T3 Cu pair in the TNC. A contribution from the S(Met) $\rightarrow Cu^{II}$ CT transition at 390 nm that is observed e.g. in nitrite reductase (Basumallick *et al.*, 2003) and is sometimes noticeable when performing curve analysis (Sakurai & Kataoka, 2007) was not recognized from the UV/Vis and CD spectra of wild-type Ssl1.

The overall architecture of all Ssl1 variants is very similar to the wild-type structure and there were no significant effects on the TNC observed in the crystal structures. Removing the axial methionine in Ssl1 resulted in a water molecule occupying the open axial coordination site of the T1 Cu and perturbed spectroscopic features. Both the increased covalency of the N(His) $\rightarrow Cu^{II}$ bond and the decreased ligand field strength indicate a tetrahedral distortion of the T1 Cu site (LaCroix *et al.*, 1998). The weak S(Cys) pseudo-σ CT in all Ssl1 variants investigated in this study also indicates that there is no tetragonal distortion of the T1 Cu site but instead a tetrahedral geometry (DeBeer George *et al.*, 2003). This distorted tetrahedral geometry is characteristic for T1 Cu sites with an oxygen bound to the T1 Cu in the axial position such as stellacyanin (LaCroix *et al.*, 1998) and the M121Q mutant of azurin (Romero *et al.*, 1993). Analogous to the Ssl1 wild-type, the Q99M mutant of stellacyanin has no tetragonal distortion and a more trigonal site (DeBeer George *et al.*, 2003). Even though the origin of the coordinating oxygen differs the effects on the T1 Cu site are similar. Spectroscopic perturbations consistent with oxygen coordinating the axial position of the T1 Cu (increased absorption of the His(N) $\rightarrow Cu^{II}$ CT at 450 nm, red-shifted d-d transitions) were also observed in the *E. coli* CueO mutants Met510Gln/Ala/Thr (Kurose *et al.*, 2009). This led the authors to the conclusion that the axial position in these three mutants is occupied by an oxygen ligand, presumably originating from

the respective side chains in the Met510Gln and Met510Thr mutants and a water molecule in Met510Ala (Kurose *et al.*, 2009). In bilirubin oxidase from *Myrothecium verrucaria* the open coordination site in the axial ligand mutants Met467Phe and Met467Leu became occupied by the amide oxygen of an adjacent asparagine (Kataoka *et al.*, 2008). This resulted in spectral features similar to the Met467Gln mutant of bilirubin oxidase (Kataoka *et al.*, 2005a,b; Shimizu *et al.*, 1999).

EPR data supports the crystallographic results and gives further insights into effects of the mutations on the geometry of the T1 Cu site. Unsurprisingly, the mutations have an effect on the covalency in the active site, as the loss of the axial donor might be compensated by interactions to His(N) and Cys(S), which is supported by the presence of a 430 nm band in the UV/Vis spectrum. Also the strength of the axial ligand interaction influences the Cu-S(Cys) covalency (DeBeer George *et al.*, 2003) and is thereby also influencing the electronic coupling into the superexchange pathway to the TNC (Yanagisawa & Dennison, 2005). On the other hand, values for the electronic coupling matrix element (H_{DA}) for the superexchange pathway in different MCOs are not significantly different (Hadt *et al.*, 2014; Sekretaryova *et al.*, 2019; Solomon *et al.*, 2004). Interestingly this is underlined by our results for Cu-N(His) interactions. The His(N) $\rightarrow$ Cu^{II} band is considerably stronger for blue copper proteins showing the rhombic EPR signal (Sakurai & Kataoka, 2007) which we also observed in the M295Y, M295F, M295T (w/o structure), M295V, and M295A mutants of Ssl1 inferring an increased rhombicity for this mutants. An interesting feature of the axial position of the T1 Cu in the mutants is that water is occupying this space and takes the role of the axial ligand, which also influences the geometry, supported by the EPR spectra, considering a small parallel hyperfine coupling constant ($A_{||}$ = 40-90 $\times$ $10^{-4}cm^{-1}$) of the T1 Cu. Due to more space at the axial position of the T1 Cu the coordination site can form a more tetrahedral geometry. This is also reported for a Cu-containing nitrite reductase. In this Cu-containing nitrite reductase from *Achromobacter cycloclastes* the mutation Met150, the axial ligand, to Gln changed the type of Cu coordination geometry and led to CD and UV/Vis spectral features like stellacyanin, but still axial symmetry in EPR instead of the rhombic signal observed for stellacyanin, which is in agreement with a symmetrical tetrahedron (Kataoka *et al.*, 2003). Considering a parallel hyperfine coupling constant characteristic for tetragonal copper centers ($A_{||}$ = 200 $\times$ $10^{-4}cm^{-1}$) for the T2 Cu ion, no absorption features or alterations can be detected for the T2 Cu site.

The side chains of phenylalanine and tyrosine as axial ligands at position 295 flipped away from the T1 Cu and increased the exposure of the T1 Cu to the solvent. The analogous M502F mutation of the axial ligand in CotA from *B. subtilis* only led to a slight movement of the mutated residue towards the protein surface and the phenylalanine residue was still oriented towards the Cu ion (Durao *et al.*, 2006). In a purple cupredoxin from *Nitrosopumilus maritimus* arginine in axial position rotates away from the T1 Cu and there is a water bound to the Cu (Hosseinzadeh *et al.*, 2016). Since spectroscopy supports the presence of oxygen bound as the axial ligand to the T1 Cu in Ssl1 M295Y and M295F, we assume that this movement is not a crystallographic artifact. Unfortunately, we were unable to solve a structure for M295T, but based on spectroscopy we can assume an oxygen coordinating the T1 Cu in this mutant but cannot

state if this originates from the threonine hydroxyl group or a water molecule. The spectral perturbations observed in Ssl1 mutants need to be distinguished from another type of distorted T1 Cu sites (green Cu sites), which are present e.g. in *Rhodobacter sphaeroides* nitrite reductase with an axial methionine (LaCroix *et al.*, 1998). Relative to the classical blue copper site in plastocyanin the Cu-S(Cys) bond is longer and weaker, the geometry is tetragonally distorted, and the Cu $3d_{x2-y2}$ rotates (Basumallick *et al.*, 2003). This results in intense σ and weak π S(Cys) $\rightarrow$ Cu^{II} charge-transfer transitions at $\sim$450 nm and $\sim$600nm, respectively (Basumallick *et al.*, 2003). These kinds of perturbations are also associated with mutation of the axial ligand of the T1 Cu. Exchanging the axial Leu513 with His in *Myceliophthora thermophila* laccase changed the T1 Cu site to a green Cu site (Palmer *et al.*, 2003). The absorption intensity of the OH^{-} $\rightarrow$ Cu^{II} CT at 330 nm displayed a two-fold decrease in Ssl1 M295V, M295Y, and M295I. Possible explanations for this are a depletion of T3 Cu, absence of the bridging hydroxide, or (partly) reduced T3 Cu ions. The M502L and M502F mutants of CotA have a dioxygen and a peroxide moiety, respectively, bound at the TNC and therefore no absorption shoulder at 330 nm (Durao *et al.*, 2006). The lower absorption intensities of the OH^{-} $\rightarrow$ Cu^{II} CT in both Met467Phe and Met467Leu mutants of bilirubin oxidase were due to the TNC being in a partly reduced state and an unbridged form (Kataoka *et al.*, 2008). Depletion of the T2 Cu as observed in the Ssl1 crystal structures can result in partly reduced T3 Cu sites as it was shown for T2D *Rhus vernicifera* laccase, that the T2D variant contains a reduced type 3 site and does not show significant absorption at 330 nm (Kau *et al.*, 1987; LuBien *et al.*, 1981).

Our previous study revealed that the increase of the T1 Cu reduction potential in Ssl1 was not necessarily accompanied with an increase in activity towards syringaldazine, indigo carmine, and alizarin red S (Olbrich *et al.*, 2019). This observation was also confirmed in this study when T2 Cu depleted Ssl1 variants with various axial ligands to the T1 Cu were investigated in the stopped-flow experiments with HQ as reducing substrate. Herein we observed no direct correlation between the T1 Cu reduction potential and the rate of reduction of the T1 Cu. Decreasing the reduction potential led to lower values for k_{ET} as expected and increasing the reduction potential from the M295V/F to M295I also increased k_{ET}. However, in all three variants k_{ET} was lower than k_{ET} measured for the T2 depleted wild-type with a lower reduction potential (Figure 4.2). According to the Marcus theory (Marcus & Sutin, 1985) for electron transfer, the electron transfer rate k is determined by three contributions: the free energy difference ΔG° which is directly related to the reduction potential difference ΔE, the reorganization energy (λ), and the electronic coupling matrix element H_{DA} (Hadt *et al.*, 2014). The absence of a direct correlation between k_{ET} and ΔE implies changes in the reorganization energy and/or electronic coupling accompanying the mutation of the axial ligand.

An increase in reorganization energy for the Cu^{2+} to Cu^{+} reduction is supported by the spectroscopic data which indicate a tetrahedral distortion of the T1 Cu site in Ssl1 variants with axial ligands other than methionine. Removal of the axial methionine allows the Cu center to relax into a state with locally lower energy but with a larger reorganization energy. Following the Rack/entatic state (Guckert *et al.*, 1995; LaCroix *et al.*, 1996; Vallee & Williams, 1968) theory, the protein environment, specifically, the axial ligand enforces a slightly unfavorable

conformation of the Cu ion, but one that is close to the transition state structure during reduction/oxidation. The impact of the axial ligand on the reorganization energy was previously demonstrated for several T1 Cu sites (Harrison & Dennison, 2004; Wijma *et al.*, 2007; Yanagisawa & Dennison, 2005). The reorganization energy of the T1 Cu was 0.3 eV (30 kJ mol^{-1}) higher in the Met150Gly, Met150His, and Met150Thr mutants of nitrite reductase (Met150 is the axial ligand in the wild-type protein) (Wijma *et al.*, 2007). In umecyanin the introduction of an axial methionine instead of the wild-type glutamine was also preferable for fast electron transfer which was attributed to a smaller inner sphere reorganization energy in the Gln95Met variant (Harrison & Dennison, 2004; Yanagisawa & Dennison, 2005). While this seems indeed to be an important factor, because it leads to the two-fold lower reduction rates in the case of the Ssl1 M295V and F variants, it is not the dominant factor in the Ssl1 M295A and M295T variants, which appear to have much lower redox potentials, and consequently up to 100-fold decreases in reduction rates (Figure 4.2). Structurally, M295A and V are very similar, yet they have huge differences in both their T1 Cu center redox potentials as well as their reduction rates. It seems likely that this would be due to electrostatic effects, i.e., differences in the hydrophobicity of the local T1 Cu environment. Similar observations have been made previously with azurin (Garner *et al.*, 2006). However, it is noteworthy to mention that the M295A variant shows a much larger decrease in energy for the ligand-field transition (absorption at 767 nm) than the M295V variant (absorption at 738 nm), indicating a larger tetrahedral distortion for the former. The crystal structures also support higher solvent access to the T1 Cu site in M295A compared to M295V (Figure 4.3). This can be due to more accessible space around the axial position of the T1 Cu site. Alanine offers more space for the solvent as it is the amino acid with the smallest side chain pointing towards the T1 Cu. Due to the orientation of the isoleucine side chain there is space for two water molecules, while valine seems to occupy more space than isoleucine. Solvent accessibility also influences the reorganization energy as was recently demonstrated by the correlation between the solvent accessible surface area and the reorganization energy using a series of engineered T1 Cu sites (Szuster *et al.*, 2020).

For the Ssl1 variant M295A we have previously hypothesized that water might occupy the axial position of the T1 Cu as its reduction potential is considerably lower (<290 mV) than anticipated from the correlation between reduction potential and axial ligand hydrophobicity (Olbrich *et al.*, 2019). Usually, the T1 Cu reduction potential decreases when oxygen binds at the axial position due to stabilization of the Cu^{II} state (Lowery & Solomon, 1992). Consequently, the reduction potential of the T1 Cu sites decreases in going from an axial Met to Gln, e.g. from 240 mV to 113 mV in nitrite reductase (Kataoka *et al.*, 2003) or from 470 to 270 mV in bilirubin oxidase (Kataoka *et al.*, 2005a). The mutation that led to a water molecule bound to the T1 Cu in CotA also decreased the reduction potential (Durao *et al.*, 2008). Thus, the presence of a water molecule and the increased reduction potentials of the M295Y/V/F/L/I (Olbrich *et al.*, 2019) mutants seem to contradict each other. On the other hand, only Met295 was found to be able to exclude water from the axial T1 Cu position so far in Ssl1 and a more polar environment of the T1 Cu makes it even more sensitive to the hydrophobicity of the axial ligand. For both stellacyanin (Nersissian *et al.*, 1998) which has a greater active site solvent exposure and azurin

with an additional axial carbonyl ligand display a higher sensitivity for the hydrophobicity of the axial ligand compared to other T1 Cu sites was observed (Garner *et al.*, 2006).

4.7 Conclusion

In this study we provided he structural and spectroscopic description of the T1 Cu site of a two-domain laccase with various axial ligands. Replacement of the axial ligand methionine by valine, isoleucine, alanine, phenylalanine, threonine, and tyrosine in Ssl1 influences the T1 Cu reduction potential and results in perturbed spectral features which are often found in four-coordinate T1 Cu sites with an axial oxygen ligand, i.e., the carbonyl oxygen of the glutamine side chain or a water molecule. Indeed, the crystal structures of the Ssl1 variants M295A/V/I/Y/F contain a water molecule bound to the T1 Cu instead of the methionine thioether in wildtype Ssl1. Stopped-flow experiments on the T1 Cu reduction kinetics revealed that mutation of the axial ligand not only influences the T1 Cu reduction potential but also the reorganization energy and/or the electronic coupling between substrate and the T1 Cu. Changes in reorganization energy upon mutation of the axial ligand were supported by the observed tetrahedral distortion of the T1 Cu site which increases the reorganization energy for the Cu^{II}/Cu^{I} reduction. Additionally, the changes in solvent accessibility of the T1 Cu site in axial ligand mutants might increase the contribution of the solvent to the reorganization energy. Overall, this work underlines the importance of the axial ligand for the T1 Cu site in two-domain laccases and the complex interactions between the factors determining electron transfer rates, namely reduction potential, reorganization energy, and donor-acceptor electronic coupling.

SUPPORTING DATA

Supplementary Tables

Table S4.1: Structural parameters of T1 Cu site.

		Cu-Ligand distances in Å		
	chain	Cu-Cys285 (S_γ) d1	Cu-His228 (N_δ) d2	Cu-His290 (N_δ) d3
WT	A	2.30	1.98	1.94
M295A	A	2.06	1.95	1.87
M295F	A	2.13	1.99	1.92
M295I	A	2.17	1.99	1.98
M295V	A	2.08	1.93	1.96
M295Y	A	2.20	1.93	1.91

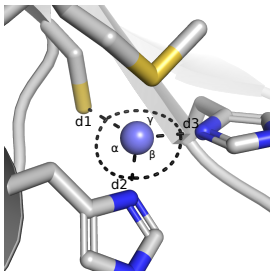

		Cu-Ligand angles in °		
		His228(N_δ)-Cu-Cys285(S_γ) α	His290(N_δ)-Cu-His228(N_δ) β	Cys285(S_γ)-Cu-His290(N_δ) γ
WT	A	129.35	103.17	123.15
M295A	A	135.90	103.15	110.53
M295F	A	132.39	102.65	118.02
M295I	A	138.66	99.55	107.16
M295V	A	138.85	96.1	110.44
M295Y	A	134.17	103.44	113.57

Table S4.2: Data collection and refinement statistics.

	M295A	M295F	M295I	M295V	M295Y
Data collection					
Space group	$P2_12_12_1$	$P2_12_12_1$	$P2_12_12_1$	$P2_12_12_1$	$P2_12_12_1$
Cell dimensions					
a, b, c (Å)	51.440, 104.100, 163.130	51.41, 104.46, 162.21	51.38, 104.32, 162.33	51.35, 103.96, 161.67	51.40, 104.24, 162.06
α, β, γ (°)	90, 90, 90	90, 90, 90	90, 90, 90	90, 90, 90	90, 90, 90
Resolution (Å)	30.36-1.41 (1.43-1.41)	50.00-1.5 (1.59-1.5)	50.00-1.79 (1.89-1.79)	50.00-2.28 (2.42-2.28)	50.00-1.68 (1.79-1.68)
R_{merge}	0.093 (1.852)	0.082 (1.160)	0.185 (1.910)	0.344 (1.686)	0.1395 (1.913)
$I/\sigma I$	13.0 (1.2)	13.05 (1.34)	7.64 (0.88)	4.96 (0.96)	8.87 (0.90)
Completeness (%)	99.9 (99.9)	99.9 (70.4)	99.8 (99.0)	98.7 (96.8)	99.3 (97.3)
Redundancy	12.9 (11.8)	-	-	-	-
Refinement					
Resolution (Å)	30.36-1.41	48.06-1.5	48.08-1.79	48.99-2.28	49.00-1.68
No. reflections	168969	138706	83649	39762	98712
R_{work}/R_{free}	0.200/0.225	0.176/0.199	0.186/0.228	0.227/0.285	0.191/0.232
No. atoms					
Protein	12295	12309	12230	12256	12212
Ligand/ion	24	34	9	30	25
Water	225	516	641	60	675
B-factors					
Protein	21	21	26	36	24
Ligand/ion	32,375	28,444	27.556	46.214	31.462
Water	-	-	-	-	
Rms deviations					
Bond lengths (Å)	0.012	0.013	0.009	0.006	0.012
Bond angles (°)	1.657	1.750	1.559	1.411	1.625

Table S4.3: Electronic absorption transitions and their molar extinction coefficients.

	$OH^- \rightarrow Cu^{II}$ CT	S(Cys) $\pi \rightarrow Cu^{II}$ CT		N(His) $\rightarrow Cu^{II}$ CT	
Ssl1 variant	$\varepsilon 330$ [$mM^{-1}cm^{-1}$]	wavelength [nm]	ε [$mM^{-1}cm^{-1}$]	wavelength [nm]	ε[$mM^{-1}cm^{-1}$]
WT	1.835	591	2.785	-	-
M295F	1.636	589	2.232	427	1.454
M295V	0.990	594	1.938	428	0.687
M295Y	0.950	597	1.859	438	1.182
M295I	0.830	587	1.451	423	0.927
M295A	2.245	590	3.158	436	1.225
M295T	1.409	585	2.154	425	0.120

Table S4.4: Circular dichroism transitions of Ssl1 mutants. Wavelengths in nm were obtained from Gaussian fits using MagicPlot. Details and plots for Gaussian fits are given in the supplementary information.

	$OH^- \rightarrow Cu^{II}$ CT	N(His) $\rightarrow Cu^{II}$ CT	S(Cys)$\sigma \rightarrow Cu^{II}$ CT	S(Cys)$\pi \rightarrow Cu^{II}$ CT	d-d (-) centered at
Ssl1 variant	(-)[nm]	(-)[nm]	(+)[nm]	(+)[nm]	[nm]
WT	326	441	535	615	725
M295F	335	434	498	582	761
M295V	328	437	507	589	738
M295Y	321	432	492	577	760
M295I	326	422	523	570	687
M295A	322	435	498	583	767
M295T	322	428	492	576	770

Table S4.5: EPR parameters of Ssl1 variant.

	T1								T2					
Ssl1 variant	g1	g2	g3	g-perp	rhomb.	A1	A2	A3	g1	g2	g3	A1	A2	A3
WT	2.23	2.059	2.033	2.046	2.6	221.8	40	30	2.215	2.05	2.05	599.6	3	3
M295F	2.298	2.108	2.04	2.074	6.8	180	100	60	2.216	2.05	2.05	599.6	40	40
M295V	2.298	2.075	2.05	2.0625	2.5	130	120	60	2.214	2.05	2.05	595	40	40
M295Y	2.3	2.12	2.05	2.085	7	200	40	40	2.215	2.05	2.05	599.6	40	40
M295I	2.255	2.075	2.045	2.06	3	280	90	40	2.215	2.05	2.05	599.6	40	40
M295A	2.298	2.075	2.05	2.0625	2.5	130	100	40	2.215	2.05	2.05	599.6	3	3
M295T	2.298	2.12	2.05	2.085	7	180	85	40	2.215	2.05	2.05	599.6	40	40

Supplementary Figures

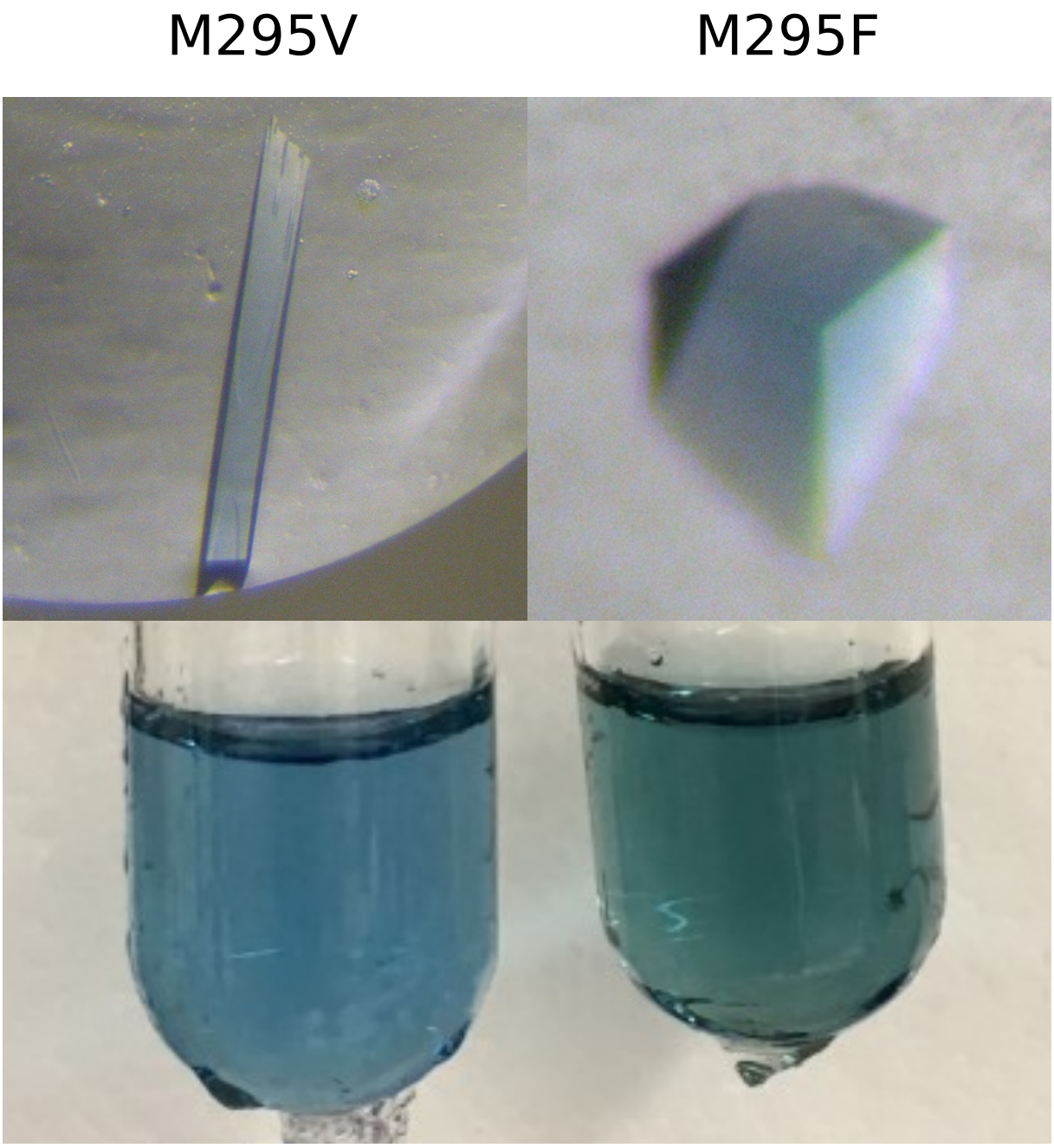

Figure S4.1: Pictures of M295V and M295F variants of Ssl1 in crystalline form (top) and in solution (bottom).

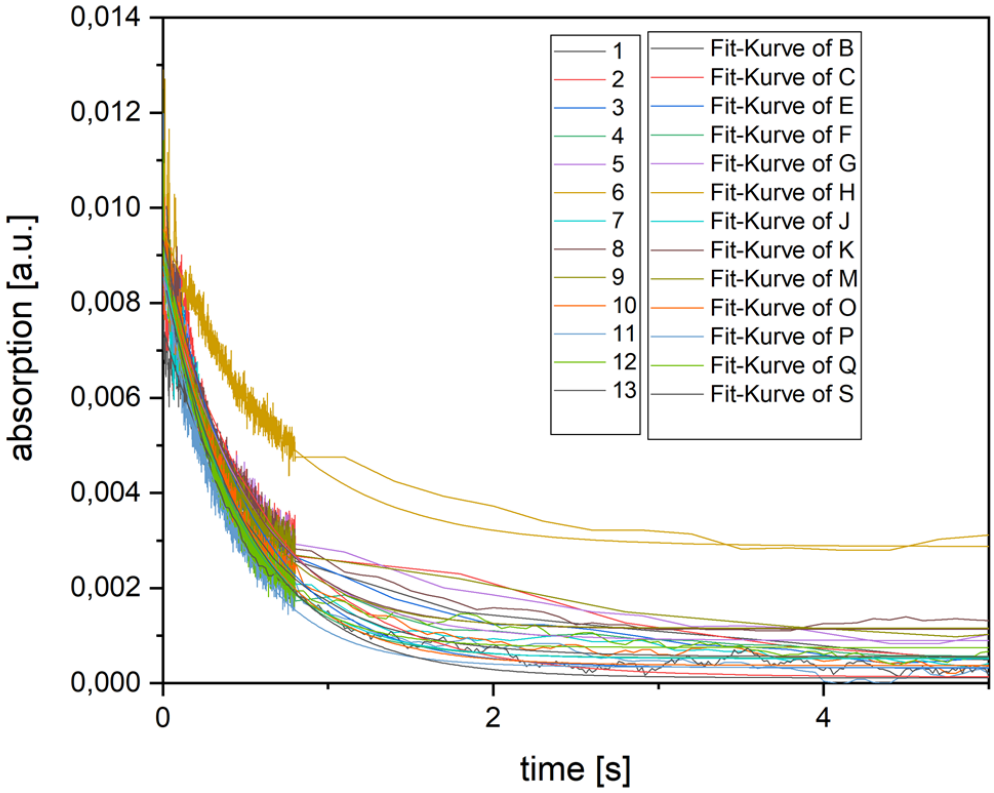

Figure S4.2: Absorption traces for the reduction of the T1 Cu in SsI1 H99Y by hydroquinone followed at 592 nm. The data was fitted to a first order exponential decay using Origin pro 9.0G.

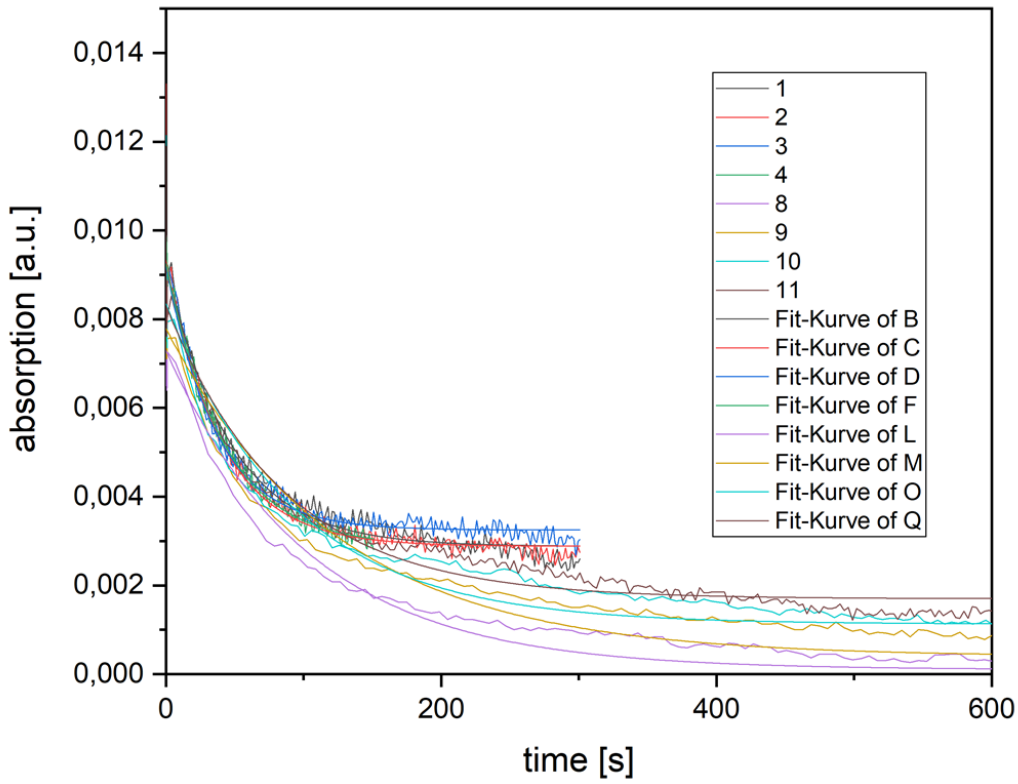

Figure S4.3: Absorption traces for the reduction of the T1 Cu in Ssl1 H99Y/M295A by hydroquinone followed at 592 nm. The data was fitted to a first order exponential decay using Origin pro 9.0G.

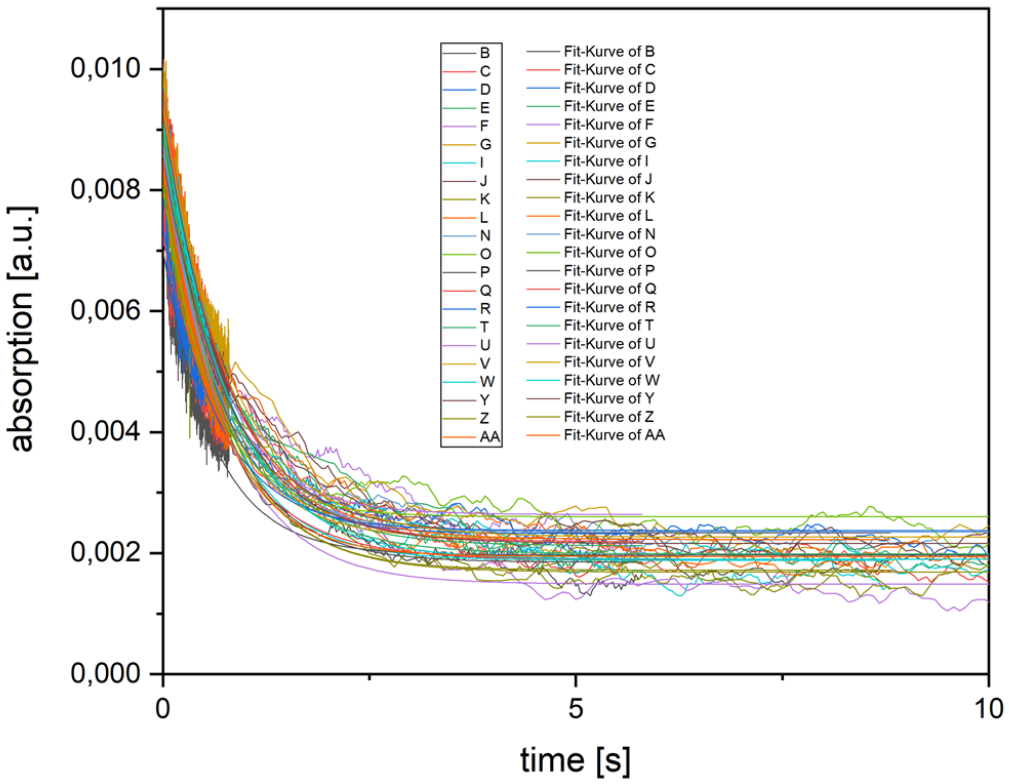

Figure S4.4: Absorption traces for the reduction of the T1 Cu in SsI1 H99Y/M295I by hydroquinone followed at 592 nm. The data was fitted to a first order exponential decay using Origin pro 9.0G.

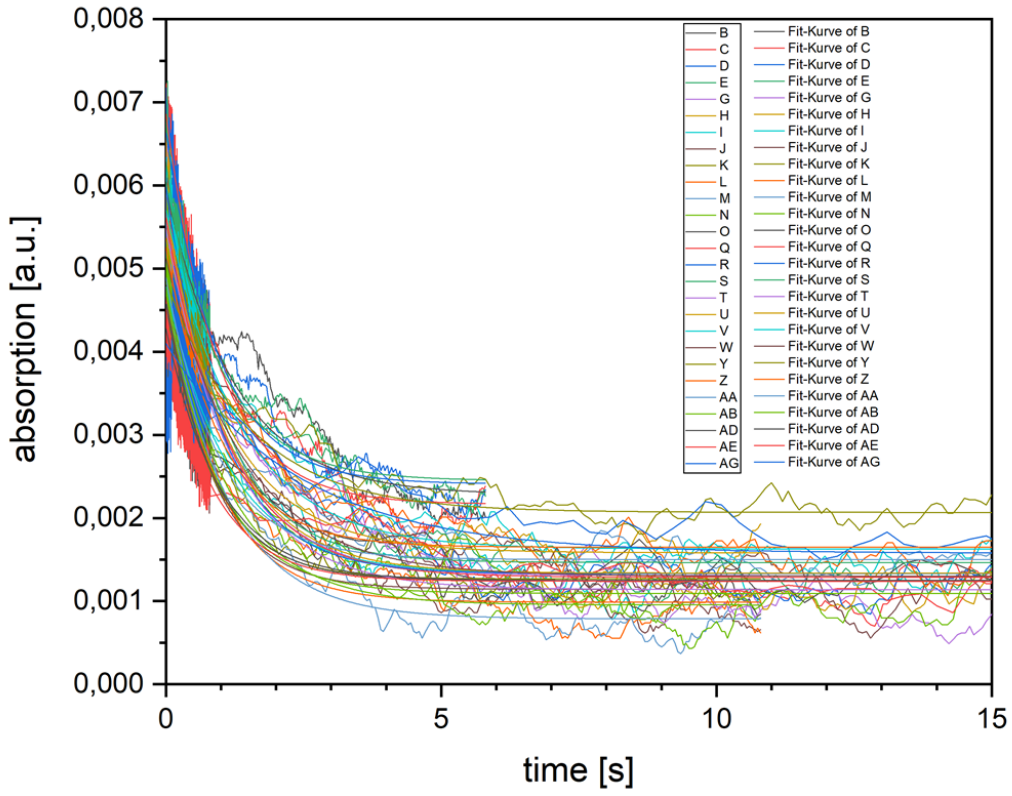

Figure S4.5: Absorption traces for the reduction of the T1 Cu in SsI1 H99Y/M295V by hydroquinone followed at 592 nm. The data was fitted to a first order exponential decay using Origin pro 9.0G.

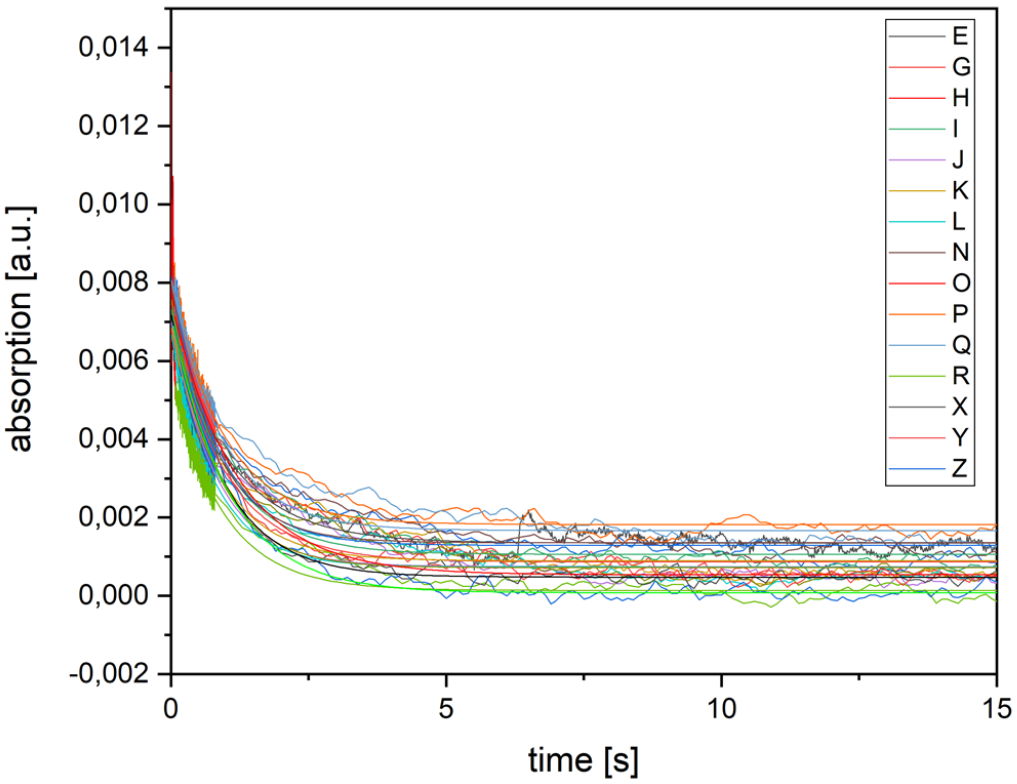

Figure S4.6: Absorption traces for the reduction of the T1 Cu in SsI1 H99Y/M295F by hydroquinone followed at 592 nm. The data was fitted to a first order exponential decay using Origin pro 9.0G.

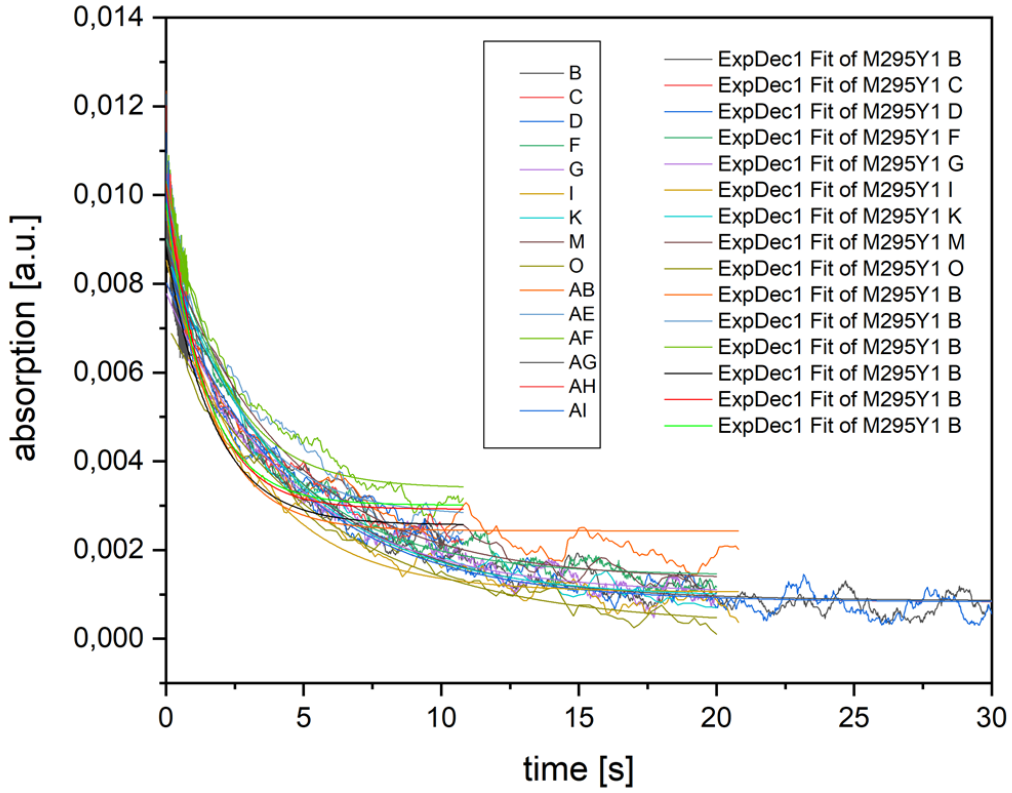

Figure S4.7: Absorption traces for the reduction of the T1 Cu in Ssl1 H99Y/M295Y by hydroquinone followed at 592 nm. The data was fitted to a first order exponential decay using Origin pro 9.0G.

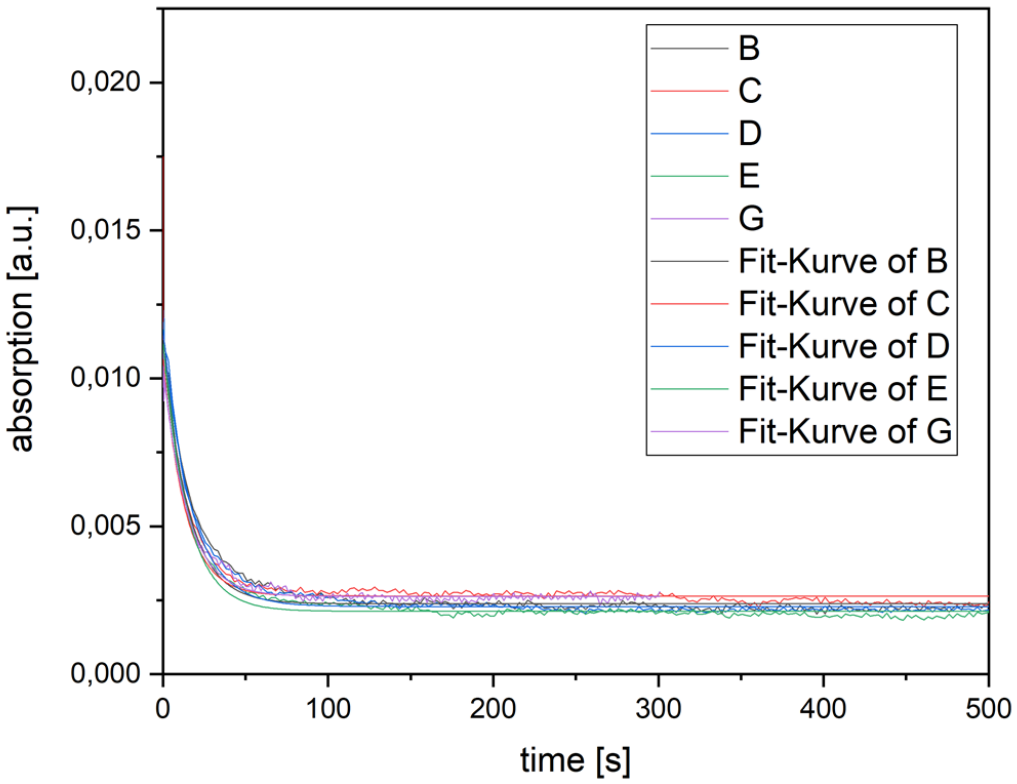

Figure S4.8: Absorption traces for the reduction of the T1 Cu in SsI1 H99Y/M295T by hydroquinone followed at 592 nm. The data was fitted to a first order exponential decay using Origin pro 9.0G.

5 Discussion

Metal-ion cofactors can be found in a broad variety of different proteins in all areas of life and they are catalyzing numerous different reactions. In this thesis, we investigated proteins with different cofactors harboring iron, cobalt, and copper as metal ions. We addressed questions dealing with the correct incorporation of recombinantly produced Fe–S cluster proteins (Chapter 2 "Mielenbrink *et al.* (2020) Maturation of Fe–S Cluster Containing Proteins"), the impact of point mutations of Cu-containing proteins on their redoxactiviy (Chapter 4 "Olbrich *et al.* (2021) Blue Multicopper Oxidases T1 Cu Axial Ligand Mutations"), and the generation of artificial Co–S proteins with an enhanced suitability for "green" H_2 production (Chapter 3 "Mielenbrink *et al.* (2021) Co–S Cluster Assembly in Fe–S Proteins").

In the first part of this thesis (Mielenbrink *et al.* (2021) Co–S Cluster Assembly in Fe–S Proteins) the objective was to provide enhanced protocols for the correct assembly of Fe–S clusters for structural and spectroscopic characterization. Yet, the investigation of these oxygen sensitive proteins was quite challenging, because they are either isolated in apo form or their reconstitution lead to artifacts affecting scientific research. That is why enhanced protocols with respect to the special needs of different proteins are of broad interest for a reliable analysis and characterization. The proteins under investigation were AcnB, IspH, NadA, and ThnB. While the proteins AcnB, IspH, and NadA have already been studied in great detail (Bradbury *et al.*, 1996; Gräwert *et al.*, 2004; JORDAN *et al.*, 1999; Rousset *et al.*, 2008), only little is known about the radical SAM enzyme ThnB, which consists of two [4Fe–4S] clusters (Wieckowski *et al.*, 2015). The second part of this thesis (Mielenbrink *et al.* (2020) Maturation of Fe–S Cluster Containing Proteins) deals with the production of artificial Co–S proteins. For this purpose, we used Fe–S cluster proteins in their apo form and reconstituted those proteins with Co–S clusters. The aim here was to use the bacterial Fe–S cluster scaffold protein IscU to assemble the Co–S cluster. In the past, promising progress has been made in the development of a water splitting biocatalyst using Co in its cofactor (Kandemir *et al.*, 2016). The assembly of an artificial [2Co–2S] cofactor in Fe–S proteins marks the next big step in the research of artificial Co containing cofactors after the successful incorporation of Co in the rubredoxin protein AlkG (Galle *et al.*, 2018). In this thesis, we used the Fe–S cluster scaffold protein IscU from *E. coli*, *A. aeolicus*, and *A. fulgidus* for reconstitution experiments with cobalt and sulfur sources. Since the Co–S cluster in IscU was not stable enough to investigate the protein properly due to the lose binding of clusters in scaffold proteins for a later transfer to their target proteins, we introduced the cluster stabilizing mutation D35A in the most promising IscU candidate from *A. fulgidus*. This helped to assemble [2Co–2S] in IscU D35A from *A. fulgidus*. The results presented in this part raise the versatile use of metal-sulfur cluster to an even higher level. Here we present the first ever [2Co–2S] cluster assembled in Fe–S proteins, which is another decisive step to "green" hydrogen production. The third part of this thesis (Olbrich *et al.* (2021) Blue Multicopper Oxidases T1 Cu Axial Ligand Mutations) deals with the enhancement of multi-copper Oxidase Ssl1 by altering the axial ligand of the T1 Cu site. This enzyme catalyzes one-electron oxidation of aromatic compounds (Thurston, 1994; Xu, 1996; Xu *et al.*, 1996). They can be used as "green"

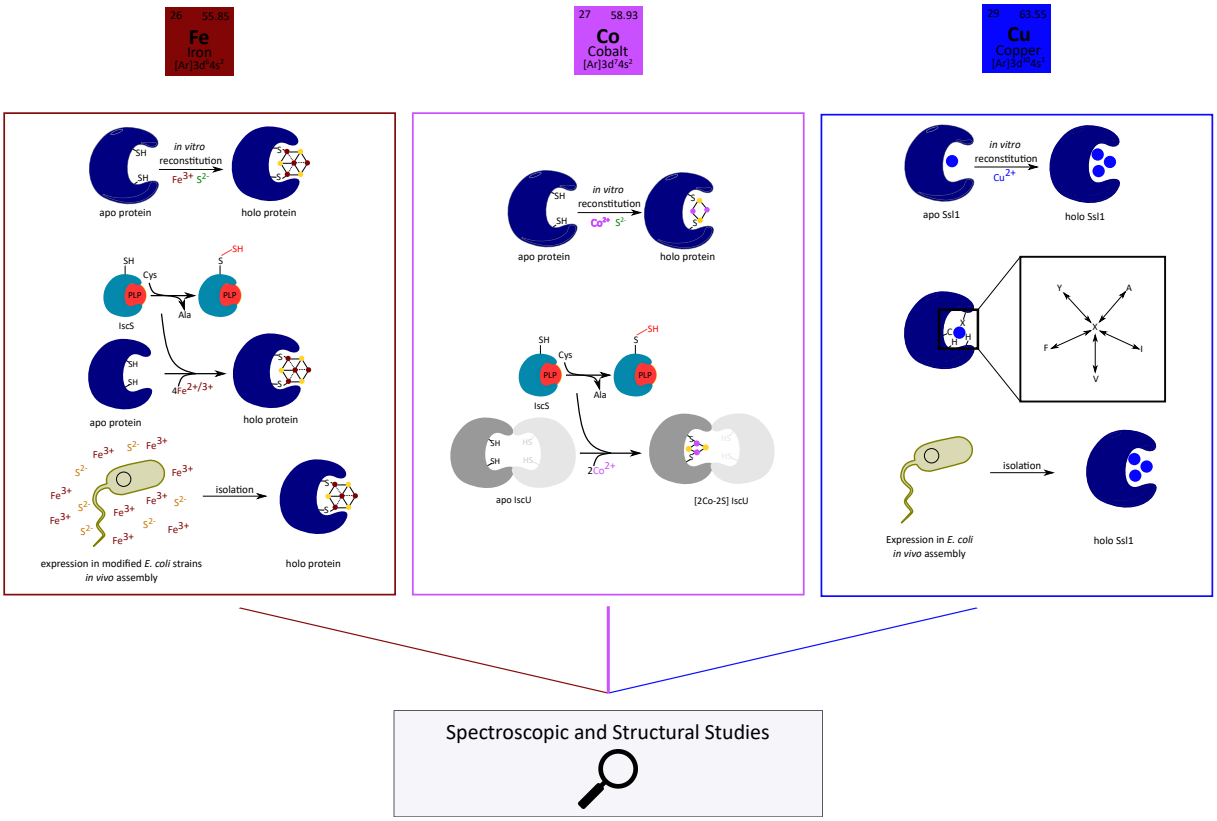

Figure S5.1: Summarized graphical abstract of the articles presented in this thesis. The graphical abstract shows the scheme of the scientific process of each chapter presenting one of the articles. From left to right: maturation of Fe–S cluster containing proteins, Co–S cluster assembly in Fe–S proteins, blue multicopper Oxidases T1 Cu axial ligand mutations.

catalysts, e. g. in detoxification of pollutants and biomediation of phenolic substances (Singh *et al.*, 2011; Zerva *et al.*, 2019). Methionine as the axial ligand of the wt T1 Cu site was mutated to different amino acids, which had different effects on the structural environment of the T1 Cu site and the catalytic activity of the whole enzyme. The outcome of this part helps to understand and functionalize the high potential of laccases as undemanding "green" catalysts in environmental protection. Although different proteins with different cofactors have been investigated in this thesis, all experiments aim on a better understanding of bioinorganic catalysts and to improve those catalysts for applications. We used different combinations of isolationd and reconstitution procedures to obtain the proteins under investigation in a native form and we applied different spectroscopic methods and structural studies for a reliable characterization of those proteins. Figure S5.1 summarizes the workflows used in this thesis.

5.1 Special Needs for the Maturation of Different Fe–S Proteins

As mentioned, one of goal of this thesis was to investigate the effects of differnt expression systems on the Fe–S cluster incorporation in different target proteins that are known to harbor

[4Fe–4S] clusters. Our strategy to investigate the incorporation of [4Fe–4S] clusters was to use well established protocols for the recombinant production of holo Fe–S proteins. These strategies include (i) the co-expression of the protein together with a plasmid coding for the proteins of the ISC machinery, (ii) co-expression of the target proteins together with a plasmid coding for the proteins of the SUF machinery, and (iii) the expression of the target protein in an *E. coli* cell strain, in which the transcriptional regulator for the ISC machinery has been removed (Chapter 2 "Mielenbrink *et al.* (2020) Maturation of Fe–S Cluster Containing Proteins"). Many studies have been performed to investigate the biosynthesis of Fe–S proteins. However, these investigations have not been done in that great detail as we can show in our study. We present in depth maturation of holo Fe–S proteins *in vivo*, as we focus on the intracellular expression conditions using well established expression constructs. These constructs consist of genes linked to a His6 or His10 affinity tag. We could show that the expression levels highly depend on the construct, which is used. Intracellular conditions concerning additional plasmids, the absence of the ISC repressor or the conditions of native BL21(DE3) cells do not show significant effect on the expression levels, except for IspH. Here we could see a lower expression level in *E. coli* BL21 (DE3) with and without pSUF as additional plasmid during expression (Figure 2.3). In case of correct cluster assembly we could obtain dramatic differences between the different expression systems. In case of AcnB and IspH only the isolation of the proteins expressed in *E. coli* BL21 (DE3) ΔiscR resulted in high yield and high purity and a correct cluster assembly indicated by spectroscopic features that are in very good agreement with previous reported data for their holo forms (Gräwert *et al.*, 2004; JORDAN *et al.*, 1999). In addition, ICP-MS data support this observation with four Fe atoms per monomer on a quantified level (Figure 2.4B and 2.5B). These results can be explained by the lack of additional stress, which could be caused by an additional plasmid and the fact that without the ISC repressor enough Fe–S assembly proteins were present to serve the high amount of target protein.

Different results could be obtained for NadA. Here the best results for cluster assembly have been found for the proteins, which were isolated from expression in *E. coli* BL21 (DE3) together with the SUF machinery from the pSUF plasmid (Figure 2.6). Yet, the interaction of NadA with pSUF has poorly been investigated. Interestingly, previous studies show controversional results to our study: The expression of NadA in an *E. coli* cell strain lacking the *iscS* gene had negative effects on the cluster assembly leading to the conclusion that SufS seems not to be able to replace IscS in that study (Ollagnier-de Choudens *et al.*, 2005). Other studies recognized specific interactions between NadA and a further Fe–S cluster maturation system: Cysteine Sulfinate Desulfinase (CSD) (Bolstad *et al.*, 2010; Kurihara *et al.*, 2003; Loiseau *et al.*, 2005). A trace, where NadA could be interacting with proteins from the SUF machinery, can be found in a study about NadA from *Arabidopsis thaliana* (UM *et al.*, 2007). In this study SufE3, a SufE like protein, was characterized with two domains: one SufE like domain and one, which is very similar to bacterial NadA, also hosting a [4Fe–4S] cluster. This cluster resulted from reconstitution with a Cysteine desulfurase, L-Cysteine, and Fe^{2+}, which suggests that NadA might also interact with proteins from the SUF machinery during recombinant expression in *E. coli*.

Very new and interesting results have been observed for the expression of the radical SAM enzyme ThnB. Previously, this protein could only be isolated in its apo form and therefor all studies on its active holo form were based on less favorable chemically reconstituted protein (Wieckowski *et al.*, 2015). Comparing the yields after expression and isolation from BL21 (DE3) and all other expression systems, less protein was obtained from BL21 (DE3), whereas all modified expression systems lead to similar high amounts (Figure S2.1). Completely new and of high interest are the results concerning the cluster content of isolated ThnB. The co-expression of *thnB* together with the pSUF plasmid is the most successful strategy. Here, we obtained data by EAS and ICP-MS measurements providing evidence for the presence of a [4Fe–4S] cluster (Figure 2.7). Also the molar extinction coefficients are in agreement with what was reported in previous studies for radical SAM enzymes (Flühe *et al.*, 2012). Previously, successful co-expression of radical SAM enzymes with pSUF has been reported for CteB (Grove *et al.*, 2017), CofH, and CofG (Decamps *et al.*, 2012). We are convinced that the SUF machinery is the biological relevant machinery in *B. thuringiensis*, where the Fe–S biosynthesis is poorly investigated yet. The SUF machinery as the relevant assembly machinery in *Bacillus* is supported by the absence of an ISC machinery in *B. subtilis* (Albrecht *et al.*, 2010; Yokoyama *et al.*, 2018). During sequence alignments we wanted to check, if *B. thuringiensis* is harboring any genes of the ISC machinery but we could not find any hit for an ISC protein, what confirms the importance of the SUF machinery for the maturation of radical SAM enzymes (data not shown).

As already mentioned in the beginning, chemical reconstitution led to artifacts like precipitate, which as to be removed before any measurements, because it strongly affects EAS or ICP-MS results. The removal of these artifacts leads to a loss of protein what makes reconstitution an unfavorable method for the maturation of Fe–S cluster proteins. Therefor we investigated several strategies to maturate Fe–S proteins *in vivo*. The general outcome of our work is that there is no general protocol for *in vivo* assembly of Fe–S proteins. Once a suitable construct is found for a specific protein, the expression system has to be adjusted to the specific needs of the target protein. Supporting CD measurements reveal that the expression system also has an impact on the oxidation state of the cluster in the isolated protein (Figure S2.2). This makes it even more important to find the optimal expression strategy which fulfills the needs of the desired holo Fe–S target protein. Overall, our studies led to the conclusion that the expression and maturation system should be as close as possible to the native system.

5.2 Co Replacement in Fe–S Scaffolds

Artificial biocatalysts can be used to produce H_2 as favorable energy source of the future. One important factor of the maturation of these catalysts is the development of suitable cofactors fulfilling essential requirements. Several approaches of Co-containing cofactors in biocatalysts could show that Co is suitable to use for this purpose (Call *et al.*, 2019; Kandemir *et al.*, 2016). However, the effectiveness of these catalysts is still lacking. In order to find a suitable cofactor

of artificial biocatalysts for industrial scale "green" H_2 production, we modified well characterized Fe–S cluster proteins. Fe–S clusters can fulfill a large variety of functions but are useless for industrial H_2 production due to their high oxygen sensitivity. Cobalt has previously been reported as a cofactor in water splitting catalysts in some systems, however, some disadvantages such as unsolubility in water, low turnover numbers, and short longevity have been described (Kandemir *et al.*, 2016; McCool *et al.*, 2011). These biocatalysts are just holding one Co in their cofactor, what could limit their potential. The tetranuclear Co–oxo cluster described by McCool *et al.* (2011) is lacking a certain solubility. Another interesting cluster is the [4Co–4S] cluster described by Deng *et al.* (2009), that is not incorporated in any protein or another organic environment. For our studies, we adapted the idea of using a [4Co–4S] cluster, but in addition using the biological environment of Fe–S cluster proteins for the assembly of Co–S clusters. Co and Fe are sharing important chemical and physical properties such as oxidation states and similar radii. We chose the bacterial Fe–S scaffold protein IscU for our attempts to artificially reconstitute a protein with a Co–S cluster, as – in case the attempt is successful – the protein could be used to transfer its cluster on other target apo proteins. That reconstitution of proteins with cobalt can be achieved has previously been reported. The rubredoxin-like protein AlkG was already reconstituted with cobalt resulting in a polythiolate Co rubredoxin-like protein (Galle *et al.*, 2018).

In this part of the thesis (Mielenbrink *et al.* (2021) Co–S Cluster Assembly in Fe–S Proteins), we present several important steps towards Co–S cluster assembly in Fe–S proteins. The first important step is the design and generation of suitable constructs. For our studies we tested IscU from *E. coli*, *A. aeolicus*, and *A. fulgidus*. While *E. coli* is a model organism for bacterial protein studies, the other two organisms belong to the family of extremophiles, resulting in an increased cluster stability of the corresponding IscU proteins. In addition, the crystallization conditions for the IscU proteins from these two proteins have known (Adrover *et al.*, 2015; Marinoni *et al.*, 2012; Shimomura *et al.*, 2008), what could potentially help to study the Co–S cluster formation more extensively. Unfortunately, we were not able to crystallize the proteins after the reconstitution with Co–S clusters. However, we demonstrated that the different IscU proteins from different organisms differ in their capability for a successful reconstitution with Co–S clusters using two different approaches: chemical and semi-enzymatic reconstitution. In all cases, chemical reconstitution led to poor results as revealed by electronic absorption spectroscopy, including high background signals due to large amounts of precipitate (Figure S3.2). For semi-enzymatic reconstitution methods with IscS, L-Cystein, and $CoCl_2$ analysis by electronic absorption spectrosocpy revealed that IscU from *A. aeolicus* and *E. coli* are less suitable than IscU from *A. fulgidus*. We expect, that the spectroscopic features of Co–S cluster are similar to the features of the spectra obtained from Fe–S cluster proteins. For binuclear cluster we would expect two bands between 300 nm and 600 nm (Freibert *et al.*, 2018; Jacquot, 2017). In case of *E. coli* IscU we detected two bands and 350 nm and 450 nm (Figure S3.4). The band at 450 nm is in agreement with what would be expected for a Co–S cluster, but the band at 350 nm is a characteristic signal for polythiolate Co^{2+} species (Petros *et al.*, 2006). This is not in agreement with a correct assembled Co–S cluster. In case of *A. aeolicus* we could obtain a

broad shoulder-like band between 370 nm and 500 nm, which might present two overlapping bands (Figure S3.4). However, this spectrum is too diffuse to determine correct cluster formation, but this could also be an artifact of the asymmetric trimeric architecture of *Aa*IscU reported in the crystal structure (Shimomura *et al.*, 2008). The spectroscopic analysis of IscU from *A. fulgidus* shows results, which are more in agreement with what we would expect from a correct assembled Co–S cluster (Figure S3.4). We could obtain two distinct bands at 380 nm and 470 nm, which is in agreement with what is known about Fe–S clusters (Freibert *et al.*, 2018; Jacquot, 2017). This supports the hypothesis, that Co–S cluster can be assembled in bacterial Fe–S scaffold proteins. This also can enhance the possibilities to find suitable cofactors for the biocatalytical production of H_2.

5.3 Active Site Mutations in Metalloproteins

Point mutations close to the active site of a protein can strongly affect the properties of a protein. This offers the opportunity to alter the properties of a protein in a desired way. For example, such point mutations can have a structure-stabilizing or destabilizing effect of certain regions within the protein or they can alter the catalytic activity of a protein (Adrover *et al.*, 2015; Olbrich *et al.*, 2019).

While investigating the Co–S assembly in IscU, we found variants of the IscU proteins which are structurally stabilized. These variants are *Ec*IscU D39A, *Aa*IscU D38A, and *Af*IscU D35A (Marinoni *et al.*, 2012; Ranquet *et al.*, 2007; Shimomura *et al.*, 2008). All three mutations are two amino acids apart from a cluster coordinatig Cysteine, what is in close proximity to the active site (Figure 3.3). Unfortunately we could just clone the D35A variant of *A. fulgidus*. Luckily, investigation of the wild-type IscU from this organism previously showed the most promising results compared to the proteins from *E. coli* and *A. Aeolicus* (Figure S3.4). Spectroscopic analysis of this variant shows even more distinct and intense bands at 400 nm and 480 nm (Figure 3.5A), which is also supported by CD spectroscopy (Figure 3.5B). This is in total agreement with characteristic bands of what we would expect for Co–S cluster based on the characteristics for Fe–S cluster (Freibert *et al.*, 2018; Jacquot, 2017).To get more information about the composition of these interesting spectra we performed SEC analysis (Figure 3.6). The SEC chromatogram reveals that the reconstitution mixture consits of monomeric, dimeric, and trimeric species of IscU D35A. Together with ICP-MS measurements and further spectroscopic analysis we came to the conclusion, that the dimeric species is the most likely form to assemble Co–S cluster (Figure 3.7). Based on these results, we performed further experiments to test the oxygen sensitivity of the sample in order to evaluate whether artificial Co–S proteins are stable under O_2 exposure for a long time, as this would be a prerequisite for their application in industrial H_2 production. Figure 3.8 shows that no significant oxygen sensitivity for up to 72 h. Overall, we were able to show that mutations in close proximity to the active site can have positive effects on the investigation of metalloproteins and their cofactor. Further, we are convinced that our results give strong evidence that we were able to artificially produce the first [2Co–2S]

cluster protein, which is an important step towards the development of suitable biocatalysts for "green" hydrogen production.

We also did first experiments on the last step of a typical cluster formation: the transfer to a target protein. Here we could show that holo Co–S IscU D35A interacts with apo Fdx from *E. coli*. Electronic absorption spectra before and after the transfer assays showed new bands for both IscU and Fdx at 350 nm and 475 nm (Figure 3.9). The band at 350 nm again indicates the formation of polythiolate Co^{2+} species (Petros *et al.*, 2006). That is why further investigation needs to be performed to fully understand the above mentioned results. Another interesting side kick experiment was the semi-enzymatic reconstitution of a [4Fe–4S] apo protein AcnB. Spectral analysis shows similar shaped spectra as for IscU D35A, although AcnB is a [4Fe–4S] protein (Figure 3.10). This is an interesting clue for further investigations of Co–S cluster formation of [4Fe–4S] proteins.

In another chapter of this thesis (Chapter 4 "Olbrich *et al.* (2021) Blue Multicopper Oxidases T1 Cu Axial Ligand Mutations"), we investigated the impact of the active site axial ligand of T1 Cu in laccase Ssl1 of *S. sviceus*. Here, I set special focus on the structure elucidation and the effect of the mutations on the structural properties and their meaning for redox potentials and catalytic activity compared to the wild type. The wild type crystal structure was already solved and also the spectroscopic characteristics and redox properties were known (Gunne *et al.*, 2014). Ssl1 is a Cu monooxygenase and can be used as a "green" catalyst, e.g. in the the detoxification of pollutants and bioremediation of phenolic compounds (Singh *et al.*, 2011; Zerva *et al.*, 2019), the delignification of lignocellulose in biorefineries (Osma *et al.*, 2010) and pulp bio-bleaching (Mate & Alcalde, 2017). "Green", because they only need oxygen as co-substrate, and solely produce water as a by-product. The structural investigations presented in this thesis include the effect of the mutated axial ligand from methinine to allanine, isoleucine, valine, phenylalanin, and tyrosine. All mutated variants show a water molecule at the axial coordination site of the T1 Cu coming along with the perturbation of spectroscopic features. These spectroscopic features indicate a tetrahedral geometry as in stellacyanin and azurin, where oxygen is bound to the axial position of T1 Cu (DeBeer George *et al.*, 2003; LaCroix *et al.*, 1998; Romero *et al.*, 1993). This tetrahedral geometry can also be observed in our crystal structures (Figure 4.3).The occupation of water at the axial position of T1 Cu can be explained by more space available, where a methionine fitted perfectly (Figure 4.3). Alanine, Isoleucine, and Valine are smaller amino acids offering space for the occupying water molecule. In case of alanine and isoleucine even a second water molecule is occupying open space around the axial position. This is also the case for the M295F variant, although phenylalanine is larger than methionine. However, structure elucidation shows that the side chain of phenylalanine is pointing away from the axial position of T1 Cu (Figure 4.3). Same could be observed for the M295Y variant, where even two additional water molecules can occupy the space around axial position. Both variants consist side chains, which are largeer than the methionine of the wild type indicating, that they could be too large to fit into the axial position of T1 Cu. For the three smaller variants the electron density is of high resolution indicating a very stable position of these variants. Electron density of tyrosine and phenylalanine show a very low density showing,

that these residues are adaptable in their orientation (Figure 4.3). These geometric results can be supported by EPR data, which gives even more information about the chemical properties of the T1 Cu site (Figure 4.5). The loss of the axial donor affects the covalency of the other ligands and thereby also influencing the electronic superexchange pathway to the trinuclear Cu site of all mutants, supported by strong rhombic EPR signals. Together with further investigations like stopped-flow measurements and redox titrations this study reveals the importance of the axial ligand of the T1 Cu site in Ssl1 and the complex electron transfer interactions behind that concerning redox potential, reorganization energy, and donor-acceptor coupling. This shows that active site mutations can offer many ways to investigate the active site of your protein of interest.

List of Figures

List of Tables

Bibliography

Adinolfi, Salvatore, Iannuzzi, Clara, Prischi, Filippo, Pastore, Chiara, Iametti, Stefania, Martin, Stephen R, Bonomi, Franco & Pastore, Annalisa (2009). Bacterial frataxin CyaY is the gatekeeper of iron-sulfur cluster formation catalyzed by IscS. *Nature structural & molecular biology*, 16(4), 390.

Adrover, Miquel, Howes, Barry D, Iannuzzi, Clara, Smulevich, Giulietta & Pastore, Annalisa (2015). Anatomy of an iron-sulfur cluster scaffold protein: Understanding the determinants of [2Fe–2S] cluster stability on IscU. *Biochimica et Biophysica Acta (BBA)-Molecular Cell Research*, 1853(6), 1448–1456.

Agar, Jeffrey N, Krebs, Carsten, Frazzon, Jeverson, Huynh, Boi Hanh, Dean, Dennis R & Johnson, Michael K (2000). IscU as a scaffold for iron-sulfur cluster biosynthesis: sequential assembly of [2Fe–2S] and [4Fe–4S] clusters in IscU. *Biochemistry*, 39(27), 7856–7862.

Agar, Jeffrey N, Zheng, Limin, Cash, Valerie L, Dean, Dennis R & Johnson, Michael K (2000). Role of the IscU Protein in Iron-Sulfur Cluster Biosynthesis: IscS-mediated Assembly of a $[Fe_2S_2]$ Cluster in IscU. *Journal of the american chemical society*, 122(9), 2136–2137.

Akhtar, M Kalim & Jones, Patrik R (2008). Deletion of iscR stimulates recombinant clostridial Fe–Fe hydrogenase activity and H_2-accumulation in *Escherichia coli* BL21 (DE3). *Applied microbiology and biotechnology*, 78(5), 853–862.

Albrecht, Alexander G, Netz, Daili JA, Miethke, Marcus, Pierik, Antonio J, Burghaus, Olaf, Peuckert, Florian, Lill, Roland & Marahiel, Mohamed A (2010). SufU is an essential iron-sulfur cluster scaffold protein in *Bacillus subtilis*. *Journal of bacteriology*, 192(6), 1643–1651.

Alcalde, Miguel (2007). Laccases: biological functions, molecular structure and industrial applications. In *Industrial enzymes*, S. 461–476. Springer.

Altschul, Stephen F, Gish, Warren, Miller, Webb, Myers, Eugene W & Lipman, David J (1990). Basic local alignment search tool. *Journal of molecular biology*, 215(3), 403–410.

Andrew, Amy J, Dutkiewicz, Rafal, Knieszner, Helena, Craig, Elizabeth A & Marszalek, Jaroslaw (2006). Characterization of the interaction between the J-protein Jac1p and the scaffold for Fe–S cluster biogenesis, Isu1p. *Journal of Biological Chemistry*, 281(21), 14580–14587.

Arakane, Yasuyuki, Muthukrishnan, Subbaratnam, Beeman, Richard W, Kanost, Michael R & Kramer, Karl J (2005). Laccase 2 is the phenoloxidase gene required for beetle cuticle tanning. *Proceedings of the National Academy of Sciences*, 102(32), 11337–11342.

Archer, E Victor, Breton, Jacques, Sanchez-Garcia, Isidro, Osada, Hiroyuki, Forster, Alan, Thomson, J Andrew & Rabbitts, H Terence (1994). Cysteine-rich LIM domains of LIM-homeodomain and LIM-only proteins contain zinc but not iron. *Proceedings of the National Academy of Sciences*, 91(1), 316–320.

Ayala-Castro, Carla, Saini, Avneesh & Outten, F Wayne (2008). Fe–S cluster assembly pathways in bacteria. *Microbiology and Molecular Biology Reviews*, 72(1), 110–125.

Bai, Yu, Chen, T Rodney, Happe, Thomas, Lu, Ying-Hua & Sawyer, Anne (2018). Iron–sulphur cluster biogenesis via the SUF pathway. *Metallomics*, 10(8), 1038–1052.

Baldrian, Petr (2006). Fungal laccases–occurrence and properties. *FEMS microbiology reviews*, 30(2), 215–242.

Balk, Janneke & Lobréaux, Stéphane (2005). Biogenesis of iron–sulfur proteins in plants. *Trends in plant science*, 10(7), 324–331.

Banci, Lucia & Bertini, Ivano (2013). Metallomics and the cell: some definitions and general comments. In *Metallomics and the Cell*, S. 1–13. Springer.

Bandyopadhyay, Sibali, Chandramouli, Kala & Johnson, Michael K (2008). Iron–sulfur cluster biosynthesis. *Biochemical Society Transactions*, 36(6), 1112–1119.

Barceloux, Donald G & Barceloux, Donald (1999). Cobalt. *Journal of Toxicology: Clinical Toxicology*, 37(2), 201–216.

Barras, F & Fontecave, Marc (2011). Cobalt stress in *Escherichia coli* and *Salmonella enterica*: molecular bases for toxicity and resistance. *Metallomics*, 3(11), 1130–1134.

Barras, Frédéric, Loiseau, Laurent & Py, Béatrice (2005). How *Escherichia coli* and *Saccharomyces cerevisiae* build Fe/S proteins. *Advances in microbial physiology*, 50, 41–101.

Basumallick, Lipika, Szilagyi, Robert K, Zhao, Yiwei, Shapleigh, James P, Scholes, Charles P & Solomon, Edward I (2003). Spectroscopic studies of the Met182Thr mutant of nitrite reductase: Role of the axial ligand in the geometric and electronic structure of blue and green copper sites. *Journal of the American Chemical Society*, 125(48), 14784–14792.

Begley, Tadhg P, Kinsland, Cynthia & Strauss, Erick (2001). The biosynthesis of coenzyme A in bacteria. *Vitamins & Hormones*, 61, 157–171.

Beinert, Helmut (2000). Iron-sulfur proteins: ancient structures, still full of surprises. *Journal of Biological Inorganic Chemistry*, 5(1), 0002–0015.

Beinert, Helmut, Holm, Richard H & Münck, Eckard (1997). Iron-sulfur clusters: nature's modular, multipurpose structures. *Science*, 277(5326), 653–659.

Beinert, Helmut & Kennedy, Mary Claire (1993). Aconitase, a two-faced protein: enzyme and iron regulatory factor 1 2. *The FASEB journal*, 7(15), 1442–1449.

Beinert, Helmut & Sands, Richard H (1960). Studies on succinic and DPNH dehydrogenase preparations by paramagnetic resonance (EPR) spectroscopy.

Berry, Steven M, Ralle, Martina, Low, Donald W, Blackburn, Ninian J & Lu, Yi (2003). Probing the role of axial methionine in the blue copper center of azurin with unnatural amino acids. *Journal of the American Chemical Society*, 125(29), 8760–8768.

Blackburn, Ninian J, Ralle, Martina, Hassett, Richard & Kosman, Daniel J (2000). Spectroscopic analysis of the trinuclear cluster in the Fet3 protein from yeast, a multinuclear copper oxidase. *Biochemistry*, 39(9), 2316–2324.

Blanc, B, Gerez, C & de Choudens, S Ollagnier (2015). Assembly of Fe/S proteins in bacterial systems: biochemistry of the bacterial ISC system. *Biochimica et Biophysica Acta (BBA)-Molecular Cell Research*, 1853(6), 1436–1447.

Bolstad, Heather M, Botelho, Danielle J & Wood, Matthew J (2010). Proteomic Analysis of Protein- Protein Interactions within the Cysteine Sulfinate Desulfinase Fe- S Cluster Biogenesis System. *Journal of proteome research*, 9(10), 5358–5369.

Bonomi, Francesco, Iametti, Stefania, Morleo, Anna, Ta, Dennis & Vickery, Larry E (2008). Studies on the mechanism of catalysis of iron-sulfur cluster transfer from IscU [2Fe2S] by HscA/HscB chaperones. *Biochemistry*, 47(48), 12795–12801.

Bradbury, Alan J, Gruer, Megan J, Rudd, Kenneth E & Guest, John R (1996). The second aconitase (AcnB) of *Escherichia coli*. *Microbiology*, 142(2), 389–400.

Bradford, M Marion (1976). A rapid and sensitive method for the quantitation microgram quantities of a protein isolated from red cell membranes. *Anal. Biochem*, 72(248), e254.

Bridwell-Rabb, Jennifer, Iannuzzi, Clara, Pastore, Annalisa & Barondeau, David P (2012). Effector role reversal during evolution: the case of frataxin in Fe–S cluster biosynthesis. *Biochemistry*, 51(12), 2506–2514.

Broderick, Joan B, Duffus, Benjamin R, Duschene, Kaitlin S & Shepard, Eric M (2014). Radical S-adenosylmethionine enzymes. *Chemical reviews*, 114(8), 4229–4317.

Buis, Jeffrey M, Cheek, Jennifer, Kalliri, Efthalia & Broderick, Joan B (2006). Characterization of an active spore photoproduct lyase, a DNA repair enzyme in the radical S-adenosylmethionine superfamily. *Journal of Biological Chemistry*, 281(36), 25994–26003.

Call, Arnau, Casadevall, Carla, Romero-Rivera, Adrian, Martin-Diaconescu, Vlad, Sommer, Dayn J, Osuna, Sílvia, Ghirlanda, Giovanna & Lloret-Fillol, Julio (2019). Improved electro-and photocatalytic water reduction by confined cobalt catalysts in streptavidin. *ACS Catalysis*, 9(7), 5837–5846.

Cambray, J, Lane, RW, Wedd, AG, Johnson, Richard W & Holm, RH (1977). Chemical and electrochemical interrelationships of the 1-Fe, 2-Fe, and 4-Fe analogs of the active sites of iron-sulfur proteins. *Inorganic Chemistry*, 16(10), 2565–2571.

Carrell, Christopher J, Ma, John K, Antholine, William E, Hosler, Jonathan P, Mathews, F Scott & Davidson, Victor L (2007). Generation of novel copper sites by mutation of the axial ligand of amicyanin. Atomic resolution structures and spectroscopic properties. *Biochemistry*, 46(7), 1900–1912.

Carver, Peggy L (2013). Metal ions and infectious diseases. An overview from the clinic. In *Interrelations between Essential Metal Ions and Human Diseases*, S. 1–28. Springer.

Catalani, S, Rizzetti, MC, Padovani, A & Apostoli, P (2012). Neurotoxicity of cobalt. *Human & experimental toxicology*, 31(5), 421–437.

Chandramouli, Kala & Johnson, Michael K (2006). HscA and HscB stimulate [2Fe–2S] cluster transfer from IscU to apoferredoxin in an ATP-dependent reaction. *Biochemistry*, 45(37), 11087–11095.

Chandramouli, Kala, Unciuleac, Mihaela-Carmen, Naik, Sunil, Dean, Dennis R, Huynh, Boi Hanh & Johnson, Michael K (2007). Formation and properties of [4Fe–4S] clusters on the IscU scaffold protein. *Biochemistry*, 46(23), 6804–6811.

Chen, Vincent B, Arendall, W Bryan, Headd, Jeffrey J, Keedy, Daniel A, Immormino, Robert M, Kapral, Gary J, Murray, Laura W, Richardson, Jane S & Richardson, David C (2010). MolProbity: all-atom structure validation for macromolecular crystallography. *Acta Crystallographica Section D: Biological Crystallography*, 66(1), 12–21.

Cheng, Jiujun, Poduska, Branislava, Morton, Richard A & Finan, Turlough M (2011). An ABC-type cobalt transport system is essential for growth of Sinorhizobium melilotiat trace metal concentrations. *Journal of bacteriology*, 193(17), 4405–4416.

Cicchillo, Robert M, Tu, Loretta, Stromberg, Jeffrey A, Hoffart, Lee M, Krebs, Carsten & Booker, Squire J (2005). *Escherichia coli* quinolinate synthetase does indeed harbor a [4Fe–4S] cluster. *Journal of the American Chemical Society*, 127(20), 7310–7311.

Clark, Kevin M, Yu, Yang, Marshall, Nicholas M, Sieracki, Nathan A, Nilges, Mark J, Blackburn, Ninian J, Van Der Donk, Wilfred A & Lu, Yi (2010). Transforming a blue copper into a red copper protein: engineering cysteine and homocysteine into the axial position of azurin using site-directed mutagenesis and expressed protein ligation. *Journal of the American Chemical Society*, 132(29), 10093–10101.

Claus, Harald (2003). Laccases and their occurrence in prokaryotes. *Archives of microbiology*, 179(3), 145–150.

Colin, Florent, Martelli, Alain, Clémancey, Martin, Latour, Jean-Marc, Gambarelli, Serge, Zeppieri, Laura, Birck, Catherine, Page, Adeline, Puccio, Hélène & Ollagnier de Choudens, Sandrine (2013). Mammalian frataxin controls sulfur production and iron entry during de novo Fe4S4 cluster assembly. *Journal of the American Chemical Society*, 135(2), 733–740.

Cunningham, Louise, Gruer, Megan J & Guest, John R (1997). Transcriptional regulation of the aconitase genes (acnA and acnB) of *Escherichia coli*. *Microbiology*, 143(12), 3795–3805.

Cupp-Vickery, Jill R, Urbina, Hugo & Vickery, Larry E (2003). Crystal structure of IscS, a cysteine desulfurase from *Escherichia coli*. *Journal of molecular biology*, 330(5), 1049–1059.

Curdel, Andrée & Iwatsubo, Motohiro (1968). Biosynthetic incorporation of cobalt into yeast alcohol dehydrogenase. *FEBS letters*, 1(3), 133–136.

Cvetkovic, Aleksandar, Menon, Angeli Lal, Thorgersen, Michael P, Scott, Joseph W, Poole II, Farris L, Jenney Jr, Francis E, Lancaster, W Andrew, Praissman, Jeremy L, Shanmukh, Saratchandra, Vaccaro, Brian J *et al.* (2010). Microbial metalloproteomes are largely uncharacterized. *Nature*, 466(7307), 779–782.

DeBeer George, Serena, Basumallick, Lipika, Szilagyi, Robert K, Randall, David W, Hill, Michael G, Nersissian, Aram M, Valentine, Joan S, Hedman, Britt, Hodgson, Keith O & Solomon, Edward I (2003). Spectroscopic investigation of stellacyanin mutants: Axial ligand interactions at the blue copper site. *Journal of the American Chemical Society*, 125(37), 11314–11328.

Decamps, Laure, Philmus, Benjamin, Benjdia, Alhosna, White, Robert, Begley, Tadhg P & Berteau, Olivier (2012). Biosynthesis of F0, precursor of the F420 cofactor, requires a unique two radical-SAM domain enzyme and tyrosine as substrate. *Journal of the American Chemical Society*, 134(44), 18173–18176.

Deng, Liang, Bill, Eckhard, Wieghardt, Karl & Holm, RH (2009). Cubane-type Co4S4 clusters: synthesis, redox series, and magnetic ground states. *Journal of the American Chemical Society*, 131(31), 11213–11221.

Dennison, Christopher, Harrison, Mark D & Lawler, Anne T (2003). Alkaline transition of phytocyanins: a comparison of stellacyanin and umecyanin. *Biochemical Journal*, 371(2), 377–383.

Dittmer, Neal T & Kanost, Michael R (2010). Insect multicopper oxidases: diversity, properties, and physiological roles. *Insect biochemistry and molecular biology*, 40(3), 179–188.

Drum, David E & Vallee, Bert L (1970). Optical properties of catalytically active cobalt and cadmium liver alcohol dehydrogenases. *Biochemical and biophysical research communications*, 41(1), 33–39.

Dunham, W Richard, Harding, L J & Sands, H Richard (1994). Mössbauer spectroscopy of metalloproteins and the use of Fourier transforms. *EJB Reviews 1993*, S. 77–84.

Durao, Paulo, Bento, Isabel, Fernandes, Andre T, Melo, Eduardo P, Lindley, Peter F & Martins, Lígia O (2006). Perturbations of the T1 copper site in the CotA laccase from *Bacillus subtilis*: structural, biochemical, enzymatic and stability studies. *JBIC Journal of Biological Inorganic Chemistry*, 11(4), 514–526.

Durao, Paulo, Chen, Zhenjia, Silva, Catarina S, Soares, Cláudio M, Pereira, Manuela M, Todorovic, Smilja, Hildebrandt, Peter, Bento, Isabel, Lindley, Peter F & Martins, Lígia O (2008). Proximal mutations at the type 1 copper site of CotA laccase: spectroscopic, redox, kinetic and structural characterization of I494A and L386A mutants. *Biochemical Journal*, 412(2), 339–346.

Duschene, Kaitlin S & Broderick, Joan B (2010). The antiviral protein viperin is a radical SAM enzyme. *FEBS letters*, 584(6), 1263–1267.

Dutkiewicz, Rafal, Schilke, Brenda, Cheng, Sara, Knieszner, Helena, Craig, Elizabeth A & Marszalek, Jaroslaw (2004). Sequence-specific interaction between mitochondrial Fe–S scaffold protein Isu and Hsp70 Ssq1 is essential for their *in vivo* function. *Journal of Biological Chemistry*, 279(28), 29167–29174.

Ellis, Mark J, Prudêncio, Miguel, Dodd, Fraser E, Strange, Richard W, Sawers, Gary, Eady, Robert R & Hasnain, S Samar (2002). Biochemical and crystallographic studies of the Met144Ala, Asp92Asn and His254Phe mutants of the nitrite reductase from Alcaligenes xylosoxidans provide insight into the enzyme mechanism. *Journal of molecular biology*, 316(1), 51–64.

Emsley, Paul & Cowtan, Kevin (2004). Coot: model-building tools for molecular graphics. *Acta crystallographica section D: biological crystallography*, 60(12), 2126–2132.

Endo, Kohki, Hayashi, Yutaka, Hibi, Takahiro, Hosono, Kuniaki, Beppu, Teruhiko & Ueda, Kenji (2003). Enzymological characterization of EpoA, a laccase-like phenol oxidase produced by Streptomyces griseus. *Journal of Biochemistry*, 133(5), 671–677.

Endo, Kohki, Hosono, Kuniaki, Beppu, Teruhiko & Ueda, Kenji (2002). A novel extracytoplasmic phenol oxidase of Streptomyces: its possible involvement in the onset of morphogenesisThe DDBJ accession number for the sequence reported in this paper is AB056583. *Microbiology*, 148(6), 1767–1776.

Enguita, Francisco J, Martins, Lígia O, Henriques, Adriano O & Carrondo, Maria Arménia (2003). Crystal structure of a bacterial endospore coat component: a laccase with enhanced thermostability properties. *Journal of Biological Chemistry*, 278(21), 19416–19425.

Evans, Philip R & Murshudov, Garib N (2013). How good are my data and what is the resolution? *Acta Crystallographica Section D: Biological Crystallography*, 69(7), 1204–1214.

Farver, Ole, Eady, Robert R, Sawers, Gary, Prudêncio, Miguel & Pecht, Israel (2004). Met144Ala mutation of the copper-containing nitrite reductase from Alcaligenes xylosoxidans reverses the intramolecular electron transfer. *FEBS letters*, 561(1-3), 173–176.

Flühe, Leif, Burghaus, Olaf, Wieckowski, Beata M, Giessen, Tobias W, Linne, Uwe & Marahiel, Mohamed A (2013). Two [4Fe–4S] clusters containing radical SAM enzyme SkfB catalyze thioether bond formation during the maturation of the sporulation killing factor. *Journal of the American Chemical Society*, 135(3), 959–962.

Flühe, Leif, Knappe, Thomas A, Gattner, Michael J, Schäfer, Antje, Burghaus, Olaf, Linne, Uwe & Marahiel, Mohamed A (2012). The radical SAM enzyme AlbA catalyzes thioether bond formation in subtilosin A. *Nature chemical biology*, 8(4), 350–357.

Flühe, Leif & Marahiel, Mohamed A (2013). Radical S-adenosylmethionine enzyme catalyzed thioether bond formation in sactipeptide biosynthesis. *Current opinion in chemical biology*, 17(4), 605–612.

Folk, JE & Gladner, Jules A (1960). Cobalt activation of carboxypeptidase A. *Journal of Biological Chemistry*, 235(1), 60–63.

Fontecave, Marc (2006). Iron-sulfur clusters: ever-expanding roles. *Nature chemical biology*, 2(4), 171–174.

Fontecave, Marc & Ollagnier-de Choudens, Sandrine (2008). Iron–sulfur cluster biosynthesis in bacteria: mechanisms of cluster assembly and transfer. *Archives of biochemistry and biophysics*, 474(2), 226–237.

Frazzon, Jeverson & Dean, Dennis R (2003). Formation of iron–sulfur clusters in bacteria: an emerging field in bioinorganic chemistry. *Current opinion in chemical biology*, 7(2), 166–173.

Freibert, Sven-Andreas, Weiler, Benjamin D, Bill, Eckhard, Pierik, Antonio J, Mühlenhoff, Ulrich & Lill, Roland (2018). Biochemical Reconstitution and Spectroscopic Analysis of Iron–Sulfur Proteins. *Methods in enzymology*, 599, 197–226.

Frey, Perry A & Reed, George H (2012). The ubiquity of iron.

Gál, Judit, Hursthouse, Andrew, Tatner, Paul, Stewart, Fran & Welton, Ryan (2008). Cobalt and secondary poisoning in the terrestrial food chain: data review and research gaps to support risk assessment. *Environment International*, 34(6), 821–838.

Galeano, BK, Ranatunga, W, Gakh, O, Smith IV, DY, Thompson, JR & Isaya, G (2017). Zinc and the iron donor frataxin regulate oligomerization of the scaffold protein to form new Fe–S cluster assembly centers. *Metallomics*, 9(6), 773–801.

Galle, Lisa M, Cutsail III, George E, Nischwitz, Volker, DeBeer, Serena & Span, Ingrid (2018). Spectroscopic characterization of the Co-substituted C-terminal domain of rubredoxin-2. *Biological chemistry*, 399(7), 787–798.

Gao, Huanyao, Subramanian, Sowmya, Couturier, Jérémy, Naik, Sunil G, Kim, Sung-Kun, Leustek, Thomas, Knaff, David B, Wu, Hui-Chen, Vignols, Florence, Huynh, Boi Hanh *et al.* (2013). Arabidopsis thaliana Nfu2 accommodates [2Fe–2S] or [4Fe–4S] clusters and is competent for *in vitro* maturation of chloroplast [2Fe–2S] and [4Fe–4S] cluster-containing proteins. *Biochemistry*, 52(38), 6633–6645.

Garner, Dewain K, Vaughan, Mark D, Hwang, Hee Jung, Savelieff, Masha G, Berry, Steven M, Honek, John F & Lu, Yi (2006). Reduction potential tuning of the blue copper center in Pseudomonas aeruginosa azurin by the axial methionine as probed by unnatural amino acids. *Journal of the American Chemical Society*, 128(49), 15608–15617.

Gewirth, Andrew A & Solomon, Edward I (1988). Electronic structure of plastocyanin: excited state spectral features. *Journal of the American Chemical Society*, 110(12), 3811–3819.

Giardina, Paola, Faraco, Vincenza, Pezzella, Cinzia, Piscitelli, Alessandra, Vanhulle, Sophie & Sannia, Giovanni (2010). Laccases: a never-ending story. *Cellular and Molecular Life Sciences*, 67(3), 369–385.

Giel, Jennifer L, Rodionov, Dmitry, Liu, Mingzhu, Blattner, Frederick R & Kiley, Patricia J (2006). IscR-dependent gene expression links iron-sulphur cluster assembly to the control of O_2-regulated genes in *Escherichia coli*. *Molecular microbiology*, 60(4), 1058–1075.

Grandoni, Jerry A, Switzer, RL, Makaroff, CA & Zalkin, H (1989). Evidence that the iron-sulfur cluster of *Bacillus subtilis* glutamine phosphoribosylpyrophosphate amidotransferase determines stability of the enzyme to degradation *in vivo*. *Journal of Biological Chemistry*, 264(11), 6058–6064.

Gräwert, Tobias, Kaiser, Johannes, Zepeck, Ferdinand, Laupitz, Ralf, Hecht, Stefan, Amslinger, Sabine, Schramek, Nicholas, Schleicher, Erik, Weber, Stefan, Haslbeck, Martin *et al.* (2004). IspH protein of Escherichia c oli: studies on Iron-Sulfur cluster implementation and catalysis. *Journal of the American Chemical Society*, 126(40), 12847–12855.

Gräwert, Tobias, Rohdich, Felix, Span, Ingrid, Bacher, Adelbert, Eisenreich, Wolfgang, Eppinger, Jörg & Groll, Michael (2009). Structure of active IspH enzyme from *Escherichia coli* provides mechanistic insights into substrate reduction. *Angewandte Chemie International Edition*, 48(31), 5756–5759.

Gräwert, Tobias, Span, Ingrid, Eisenreich, Wolfgang, Rohdich, Felix, Eppinger, Jörg, Bacher, Adelbert & Groll, Michael (2010). Probing the reaction mechanism of IspH protein by x-ray structure analysis. *Proceedings of the National Academy of Sciences*, 107(3), 1077–1081.

Grove, Tyler L, Himes, Paul M, Hwang, Sungwon, Yumerefendi, Hayretin, Bonanno, Jeffrey B, Kuhlman, Brian, Almo, Steven C & Bowers, Albert A (2017). Structural insights into thioether bond formation in the biosynthesis of sactipeptides. *Journal of the American Chemical Society*, 139(34), 11734–11744.

Gruer, Megan J, Bradbury, Alan J & Guest, John R (1997). Construction and properties of aconitase mutants of *Escherichia coli*. *Microbiology*, 143(6), 1837–1846.

Guckert, Jeffrey A, Lowery, Michael D & Solomon, Edward I (1995). Electronic structure of the reduced blue copper active site: contributions to reduction potentials and geometry. *Journal of the American Chemical Society*, 117(10), 2817–2844.

Gunne, Matthias, Höppner, Astrid, Hagedoorn, Peter-Leon & Urlacher, Vlada B (2014). Structural and redox properties of the small laccase S sl1 from S treptomyces sviceus. *The FEBS journal*, 281(18), 4307–4318.

Gunne, Matthias & Urlacher, Vlada B (2012). Characterization of the alkaline laccase Ssl1 from Streptomyces sviceus with unusual properties discovered by genome mining. *PLoS One*, 7(12), e52360.

Hadt, Ryan G, Gorelsky, Serge I & Solomon, Edward I (2014). Anisotropic covalency contributions to superexchange pathways in type one copper active sites. *Journal of the American Chemical Society*, 136(42), 15034–15045.

Hakulinen, Nina & Rouvinen, Juha (2015). Three-dimensional structures of laccases. *Cellular and molecular life sciences*, 72(5), 857–868.

Hall, John F, Kanbi, Lalji D, Strange, Richard W & Hasnain, S Samar (1999). Role of the axial ligand in type 1 Cu centers studied by point mutations of Met148 in rusticyanin. *Biochemistry*, 38(39), 12675–12680.

Hänzelmann, Petra, Hernández, Heather L, Menzel, Christian, García-Serres, Ricardo, Huynh, Boi Hanh, Johnson, Michael K, Mendel, Ralf R & Schindelin, Hermann (2004). Characterization of MOCS1A, an oxygen-sensitive iron-sulfur protein involved in human molybdenum cofactor biosynthesis. *Journal of Biological Chemistry*, 279(33), 34721–34732.

Harrison, Mark D & Dennison, Christopher (2004). An axial met ligand at a type 1 copper site is preferable for fast electron transfer. *ChemBioChem*, 5(11), 1579–1581.

Hirabayashi, Kei, Yuda, Eiki, Tanaka, Naoyuki, Katayama, Sumie, Iwasaki, Kenji, Matsumoto, Takashi, Kurisu, Genji, Outten, F Wayne, Fukuyama, Keiichi, Takahashi, Yasuhiro *et al.* (2015). Functional dynamics revealed by the structure of the SufBCD complex, a novel ATP-binding cassette (ABC) protein that serves as a scaffold for iron-sulfur cluster biogenesis. *Journal of Biological Chemistry*, 290(50), 29717–29731.

Hosseinzadeh, Parisa, Tian, Shiliang, Marshall, Nicholas M, Hemp, James, Mullen, Timothy, Nilges, Mark J, Gao, Yi-Gui, Robinson, Howard, Stahl, David A, Gennis, Robert B *et al.* (2016). A purple cupredoxin from Nitrosopumilus maritimus containing a mononuclear type 1 copper center with an open binding site. *Journal of the American Chemical Society*, 138(20), 6324–6327.

Hu, Yilin, Fay, Aaron W, Lee, Chi Chung, Yoshizawa, Janice & Ribbe, Markus W (2008). Assembly of nitrogenase MoFe protein. *Biochemistry*, 47(13), 3973–3981.

Hullo, Marie-Françoise, Moszer, Ivan, Danchin, Antoine & Martin-Verstraete, Isabelle (2001). CotA of *Bacillus subtilis* is a copper-dependent laccase. *Journal of bacteriology*, 183(18), 5426.

Iannuzzi, Clara, Adinolfi, Salvatore, Howes, Barry D, Garcia-Serres, Ricardo, Clémancey, Martin, Latour, Jean-Marc, Smulevich, Giulietta & Pastore, Annalisa (2011). The role of CyaY in iron sulfur cluster assembly on the *E. coli* IscU scaffold protein. *PloS one*, 6(7), e21992.

Immirzi, Attilio (1966). Crystallographic Computing Techniques (Ahmed FR, editor., ed) p. 399. *Munksgaard, Copenhagen*.

Jacobson, Marty R, Cash, Valerie L, Weiss, Mary C, Laird, Nancy F, Newton, William E & Dean, Dennis R (1989). Biochemical and genetic analysis of the nifUSVWZM cluster from Azotobacter vinelandii. *Molecular and General Genetics MGG*, 219(1-2), 49–57.

Jacquot, Jean-Pierre (2017). Iron–Sulfur Clusters in Chemistry and Biology. Volume 1: Characterization, Properties and Applications. Edited by Tracey Rouault. De Gruyter, 2017. Pp. xv+ 447. Price EUR 99.95, GBP 90.99, USD 114.99 hardcover, ISBN 978-3-11-047850-1. *Acta Crystallographica Section D*, 73(12), 1030–1030.

Jasniewski, Andrew, Hu, Yilin & Ribbe, Markus W (2019). Electron Paramagnetic Resonance Spectroscopy of Metalloproteins. In *Metalloproteins*, S. 197–211. Springer.

Johnson, Deborah C, Dean, Dennis R, Smith, Archer D & Johnson, Michael K (2005). Structure, function, and formation of biological iron-sulfur clusters. *Annu. Rev. Biochem.*, 74, 247–281.

JORDAN, Peter A, TANG, Yue, BRADBURY, Alan J, THOMSON, Andrew J & GUEST, John R (1999). Biochemical and spectroscopic characterization of *Escherichia coli* aconitases (AcnA and AcnB). *Biochemical Journal*, 344(3), 739–746.

Kabsch, Wolfgang (2010). Xds. *Acta Crystallographica Section D: Biological Crystallography*, 66(2), 125–132.

Kaiser, Jens T, Clausen, Tim, Bourenkow, Gleb P, Bartunik, Hans-D, Steinbacher, Stefan & Huber, Robert (2000). Crystal structure of a NifS-like protein from Thermotoga maritima: implications for iron sulphur cluster assembly. *Journal of molecular biology*, 297(2), 451–464.

Kallio, Juha P, Gasparetti, Chiara, Andberg, Martina, Boer, Harry, Koivula, Anu, Kruus, Kristiina, Rouvinen, Juha & Hakulinen, Nina (2011). Crystal structure of an ascomycete fungal laccase from Thielavia arenaria–common structural features of asco-laccases. *The FEBS journal*, 278(13), 2283–2295.

Kamitaka, Yuji, Tsujimura, Seiya, Kataoka, Kunishige, Sakurai, Takeshi, Ikeda, Tokuji & Kano, Kenji (2007). Effects of axial ligand mutation of the type I copper site in bilirubin oxidase on direct electron transfer-type bioelectrocatalytic reduction of dioxygen. *Journal of Electroanalytical Chemistry*, 601(1-2), 119–124.

Kandemir, Banu, Chakraborty, Saikat, Guo, Yixing & Bren, Kara L (2016). Semisynthetic and biomolecular hydrogen evolution catalysts. *Inorganic chemistry*, 55(2), 467–477.

Karlsson, B Göran, Aasa, Roland, Malmström, Bo G & Lundberg, Lennart G (1989). Rack-induced bonding in blue copper proteins: Spectroscopic properties and reduction potential of the azurin mutant Met-121→ Leu. *FEBS letters*, 253(1-2), 99–102.

Karlsson, B Göran, Nordling, Margareta, Pascher, Torbjörn, Tsai, Li-Chu, Sjölin, Lennart & Lundberg, Lennart G (1991). Cassette mutagenesis of Met121 in azurin from Pseudomonas aeruginosa. *Protein Engineering, Design and Selection*, 4(3), 343–349.

Kataoka, Kunishige, Kitagawa, Rieko, Inoue, Megumi, Naruse, Daisaku, Sakurai, Takeshi & Huang, Hong-wei (2005). Point mutations at the type I Cu ligands, Cys457 and Met467, and at the putative proton donor, Asp105, in Myrothecium verrucaria bilirubin oxidase and reactions with dioxygen. *Biochemistry*, 44(18), 7004–7012.

Kataoka, Kunishige, Kondo, Akihisa, Yamaguchi, Kazuya & Suzuki, Shinnichiro (2000). Spectroscopic and electrochemical properties of the Met86Gln mutant of Achromobacter cycloclastes pseudoazurin. *Journal of inorganic biochemistry*, 82(1-4), 79–84.

Kataoka, Kunishige, Tanaka, Kazuhiro, Sakai, Yoko & Sakurai, Takeshi (2005). High-level expression of Myrothecium verrucaria bilirubin oxidase in Pichia pastoris, and its facile purification and characterization. *Protein expression and purification*, 41(1), 77–83.

Kataoka, Kunishige, Tsukamoto, Keishi, Kitagawa, Rieko, Ito, Takahiro & Sakurai, Takeshi (2008). Compensatory binding of an asparagine residue to the coordination-unsaturated type I Cu center in bilirubin oxidase mutants. *Biochemical and biophysical research communications*, 371(3), 416–419.

Kataoka, Kunishige, Yamaguchi, Kazuya, Sakai, Shinobu, Takagi, Kohichi & Suzuki, Shinnichiro (2003). Characterization and function of Met150Gln mutant of copper-containing nitrite reductase from Achromobacter cycloclastes IAM1013. *Biochemical and biophysical research communications*, 303(2), 519–524.

Kau, Lung Shan, Spira-Solomon, Darlene J, Penner-Hahn, James E, Hodgson, Keith O & Solomon, Edward I (1987). X-ray absorption edge determination of the oxidation state and coordination number of copper. Application to the type 3 site in Rhus vernicifera laccase and its reaction with oxygen. *Journal of the American Chemical Society*, 109(21), 6433–6442.

Kessler, Dorothea (2006). Enzymatic activation of sulfur for incorporation into biomolecules in prokaryotes. *FEMS microbiology reviews*, 30(6), 825–840.

Key, Hanna M, Dydio, Paweł, Clark, Douglas S & Hartwig, John F (2016). Abiological catalysis by artificial haem proteins containing noble metals in place of iron. *Nature*, 534(7608), 534–537.

Kim, Jin Hae, Bothe, Jameson R, Frederick, Ronnie O, Holder, Johneisa C & Markley, John L (2014). Role of IscX in iron–sulfur cluster biogenesis in *Escherichia coli*. *Journal of the American Chemical Society*, 136(22), 7933–7942.

Kim, Jin Hae, Frederick, Ronnie O, Reinen, Nichole M, Troupis, Andrew T & Markley, John L (2013). [2Fe–2S]-Ferredoxin Binds Directly to Cysteine Desulfurase and Supplies an Electron for Iron–Sulfur Cluster Assembly but Is Displaced by the Scaffold Protein or Bacterial Frataxin. *Journal of the American Chemical Society*, 135(22), 8117–8120.

Kim, Jin Hae, Füzéry, Anna K, Tonelli, Marco, Ta, Dennis T, Westler, William M, Vickery, Larry E & Markley, John L (2009). Structure and Dynamics of the Iron-Sulfur Cluster Assembly Scaffold Protein IscU and Its Interaction with the Cochaperone HscB. *Biochemistry*, 48(26), 6062–6071.

Kim, Jin Hae, Tonelli, Marco, Kim, Taewook & Markley, John L (2012). Three-dimensional structure and determinants of stability of the iron–sulfur cluster scaffold protein IscU from *Escherichia coli*. *Biochemistry*, 51(28), 5557–5563.

Kobayashi, Michihiko & Shimizu, Sakayu (1999). Cobalt proteins. *European Journal of Biochemistry*, 261(1), 1–9.

Komori, Hirofumi, Miyazaki, Kentaro & Higuchi, Yoshiki (2009). X-ray structure of a two-domain type laccase: a missing link in the evolution of multi-copper proteins. *FEBS letters*, 583(7), 1189–1195.

Koutmos, Markos, Datta, Supratim, Pattridge, Katherine A, Smith, Janet L & Matthews, Rowena G (2009). Insights into the reactivation of cobalamin-dependent methionine synthase. *Proceedings of the National Academy of Sciences*, 106(44), 18527–18532.

Kroes, Sandra J, Hoitink, Carla WG, Andrew, Colin R, Ai, Jingyuan, Sanders-Loehr, Joann, Messerschmidt, Albrecht, Hagen, Wilfred R & Canters, Gerard W (1996). The mutation Met121→ His creates a type-1.5 copper site in Alcaligenes denitrificans azurin. *European journal of biochemistry*, 240(2), 342–351.

Kuchenreuther, Jon M, Grady-Smith, Celestine S, Bingham, Alyssa S, George, Simon J, Cramer, Stephen P & Swartz, James R (2010). High-yield expression of heterologous [FeFe] hydrogenases in *Escherichia coli*. *PloS one*, 5(11), e15491.

Kung, Chung-Wei, Mondloch, Joseph E, Wang, Timothy C, Bury, Wojciech, Hoffeditz, William, Klahr, Benjamin M, Klet, Rachel C, Pellin, Michael J, Farha, Omar K & Hupp, Joseph T (2015). Metal–organic framework thin films as platforms for atomic layer deposition of cobalt ions to enable electrocatalytic water oxidation. *ACS applied materials & interfaces*, 7(51), 28223–28230.

Kurihara, Tatsuo, Mihara, Hisaaki, Kato, Shin-ichiro, Yoshimura, Tohru & Esaki, Nobuyoshi (2003). Assembly of iron–sulfur clusters mediated by cysteine desulfurases, IscS, CsdB and CSD, from *Escherichia coli*. *Biochimica et Biophysica Acta (BBA)-Proteins and Proteomics*, 1647(1-2), 303–309.

Kurose, Shinji, Kataoka, Kunishige, Shinohara, Naoya, Miura, Yuko, Tsutsumi, Maiko, Tsujimura, Seiya, Kano, Kenji & Sakurai, Takeshi (2009). Modification of spectroscopic properties and catalytic activity of *Escherichia coli* CueO by mutations of methionine 510, the axial ligand to the type I Cu. *Bulletin of the Chemical Society of Japan*, 82(4), 504–508.

LaCroix, Louis B, Randall, David W, Nersissian, Aram M, Hoitink, Carla WG, Canters, Gerard W, Valentine, Joan S & Solomon, Edward I (1998). Spectroscopic and geometric variations in perturbed blue copper centers: electronic structures of stellacyanin and cucumber basic protein. *Journal of the American Chemical Society*, 120(37), 9621–9631.

LaCroix, Louis B, Shadle, Susan E, Wang, Yaning, Averill, Bruce A, Hedman, Britt, Hodgson, Keith O & Solomon, Edward I (1996). Electronic structure of the perturbed blue copper site in nitrite reductase: spectroscopic properties, bonding, and implications for the entatic/rack state. *Journal of the American Chemical Society*, 118(33), 7755–7768.

Lawton, Thomas J, Sayavedra-Soto, Luis A, Arp, Daniel J & Rosenzweig, Amy C (2009). Crystal structure of a two-domain multicopper oxidase. *Journal of Biological Chemistry*, 284(15), 10174–10180.

Layer, Gunhild, Gaddam, S Aparna, Ayala-Castro, Carla N, Ollagnier-de Choudens, Sandrine, Lascoux, David, Fontecave, Marc & Outten, F Wayne (2007). SufE transfers sulfur from SufS to SufB for iron-sulfur cluster assembly. *Journal of biological chemistry*, 282(18), 13342–13350.

Layer, Gunhild, Ollagnier-de Choudens, Sandrine, Sanakis, Yiannis & Fontecave, Marc (2006). Iron-sulfur cluster biosynthesis: characterization of *Escherichia coli* CYaY as an iron donor for the assembly of [2Fe–2S] clusters in the scaffold IscU. *Journal of Biological Chemistry*, 281(24), 16256–16263.

Leach, Michael R & Zamble, Deborah B (2007). Metallocenter assembly of the hydrogenase enzymes. *Current opinion in chemical biology*, 11(2), 159–165.

Leartsakulpanich, Ubolsree, Antonkine, Mikhail L & Ferry, James G (2000). Site-Specific Mutational Analysis of a Novel Cysteine Motif Proposed To Ligate the 4Fe–4S Cluster in the Iron-Sulfur Flavoprotein of the Thermophilic MethanoarchaeonMethanosarcina thermophila. *Journal of bacteriology*, 182(19), 5309–5316.

Leonard, Stephen, Gannett, Peter M, Rojanasakul, Yon, Schwegler-Berry, Diane, Castranova, Vince, Vallyathan, Val & Shi, Xianglin (1998). Cobalt-mediated generation of reactive oxygen species and its possible mechanism. *Journal of inorganic biochemistry*, 70(3-4), 239–244.

Lill, Roland (2009). Function and biogenesis of iron–sulphur proteins. *Nature*, 460(7257), 831–838.

Lill, Roland & Mühlenhoff, Ulrich (2006). Iron-sulfur protein biogenesis in eukaryotes: components and mechanisms. *Annu. Rev. Cell Dev. Biol.*, 22, 457–486.

Lill, Roland & Mühlenhoff, Ulrich (2008). Maturation of iron-sulfur proteins in eukaryotes: mechanisms, connected processes, and diseases. *Annu. Rev. Biochem.*, 77, 669–700.

Liu, Gaohua, Li, Zhaohui, Chiang, Yiwen, Acton, Thomas, Montelione, Gaetano T, Murray, Diana & Szyperski, Thomas (2005). High-quality homology models derived from NMR and X-ray structures of *E. coli* proteins YgdK and Suf E suggest that all members of the YgdK/Suf E protein family are enhancers of cysteine desulfurases. *Protein science*, 14(6), 1597–1608.

Lohans, Christopher T & Vederas, John C (2014). Structural characterization of thioether-bridged bacteriocins. *The Journal of antibiotics*, 67(1), 23–30.

Loiseau, Laurent, Gerez, Catherine, Bekker, Martijn, Ollagnier-de Choudens, Sandrine, Py, Béatrice, Sanakis, Yannis, de Mattos, Joost Teixeira, Fontecave, Marc & Barras, Frédéric (2007). ErpA, an iron–sulfur (Fe–S) protein of the A-type essential for respiratory metabolism in *Escherichia coli*. *Proceedings of the National Academy of Sciences*, 104(34), 13626–13631.

Loiseau, Laurent, Ollagnier-de Choudens, Sandrine, Lascoux, David, Forest, Eric, Fontecave, Marc & Barras, Frédéric (2005). Analysis of the heteromeric CsdA-CsdE cysteine desulfurase, assisting Fe–S cluster biogenesis in *Escherichia coli*. *Journal of Biological Chemistry*, 280(29), 26760–26769.

Loiseau, Laurent, Ollagnier-de Choudens, Sandrine, Nachin, Laurence, Fontecave, Marc & Barras, Frédéric (2003). Biogenesis of Fe–S cluster by the bacterial suf system sufs and sufe form a new type of cysteine desulfurase. *Journal of Biological Chemistry*, 278(40), 38352–38359.

Lovenberg, Walter & Sobel, Burton E (1965). Rubredoxin: a new electron transfer protein from Clostridium pasteurianum. *Proceedings of the National Academy of Sciences of the United States of America*, 54(1), 193.

Lowery, Michael D, Guckert, Jeffrey A, Gebhard, Matthew S & Solomon, Edward I (1993). Active-site electronic structure contributions to electron-transfer pathways in rubredoxin and plastocyanin: direct versus superexchange. *Journal of the American Chemical Society*, 115(7), 3012–3013.

Lowery, Michael D & Solomon, Edward I (1992). Axial ligand bonding in blue copper proteins. *Inorganica chimica acta*, 198, 233–243.

LuBien, CD, Winkler, ME, Thamann, TJ, Scott, RA, Co, MS, Hodgson, KO & Solomon, EI (1981). Chemical and spectroscopic properties of the binuclear copper active site in Rhus laccase: direct confirmation of a reduced binuclear type 3 copper site in type 2 depleted laccase and intramolecular coupling of the type 3 to the type 1 and type 2 copper sites. *Journal of the American Chemical Society*, 103(23), 7014–7016.

Lubitz, Wolfgang, Ogata, Hideaki, Rüdiger, Olaf & Reijerse, Edward (2014). Hydrogenases. *Chemical reviews*, 114(8), 4081–4148.

Lubitz, Wolfgang & Tumas, William (2007). Hydrogen: an overview. *Chemical reviews*, 107(10), 3900–3903.

Machczynski, Michael C, Vijgenboom, Erik, Samyn, Bart & Canters, Gerard W (2004). Characterization of SLAC: a small laccase from Streptomyces coelicolor with unprecedented activity. *Protein science*, 13(9), 2388–2397.

Majtan, Tomas, Freeman, Katherine M, Smith, Aaron T, Burstyn, Judith N & Kraus, Jan P (2011). Purification and characterization of cystathionine β-synthase bearing a cobalt protoporphyrin. *Archives of biochemistry and biophysics*, 508(1), 25–30.

Majtan, Tomas, Frerman, Frank E & Kraus, Jan P (2011). Effect of cobalt on *Escherichia coli* metabolism and metalloporphyrin formation. *Biometals*, 24(2), 335–347.

Malkin, Richard & Rabinowitz, Jesse C (1966). The reconstitution of clostridial ferredoxin. *Biochemical and biophysical research communications*, 23(6), 822–827.

Marcus, Rudolph A & Sutin, Norman (1985). Electron transfers in chemistry and biology. *Biochimica et Biophysica Acta (BBA)-Reviews on Bioenergetics*, 811(3), 265–322.

Marinoni, Elodie N, de Oliveira, Jaim S, Nicolet, Yvain, Raulfs, Estella C, Amara, Patricia, Dean, Dennis R & Fontecilla-Camps, Juan C (2012). (IscS-IscU) 2 complex structures provide insights into Fe2S2 biogenesis and transfer. *Angewandte Chemie*, 124(22), 5535–5538.

Marshall, Nicholas M, Garner, Dewain K, Wilson, Tiffany D, Gao, Yi-Gui, Robinson, Howard, Nilges, Mark J & Lu, Yi (2009). Rationally tuning the reduction potential of a single cupredoxin beyond the natural range. *Nature*, 462(7269), 113–116.

Maté, Diana, García-Ruiz, Eva, Camarero, Susana & Alcalde, Miguel (2011). Directed evolution of fungal laccases. *Current Genomics*, 12(2), 113–122.

Mate, Diana M & Alcalde, Miguel (2017). Laccase: a multi-purpose biocatalyst at the forefront of biotechnology. *Microbial biotechnology*, 10(6), 1457–1467.

Mayer, Alfred M & Staples, Richard C (2002). Laccase: new functions for an old enzyme. *Phytochemistry*, 60(6), 551–565.

McCool, Nicholas S, Robinson, David M, Sheats, John E & Dismukes, G Charles (2011). A Co4O4 “cubane” water oxidation catalyst inspired by photosynthesis. *Journal of the American Chemical Society*, 133(30), 11446–11449.

McCoy, Airlie J, Grosse-Kunstleve, Ralf W, Adams, Paul D, Winn, Martyn D, Storoni, Laurent C & Read, Randy J (2007). Phaser crystallographic software. *Journal of applied crystallography*, 40(4), 658–674.

McMillin, David R, Holwerda, Robert A & Gray, Harry B (1974). Preparation and spectroscopic studies of cobalt (II)-stellacyanin. *Proceedings of the National Academy of Sciences*, 71(4), 1339–1341.

Mettert, Erin L & Kiley, Patricia J (2014). Coordinate regulation of the Suf and Isc Fe–S cluster biogenesis pathways by IscR is essential for viability of *Escherichia coli*. *Journal of bacteriology*, 196(24), 4315–4323.

Meyer, Jacques (2008). Iron–sulfur protein folds, iron–sulfur chemistry, and evolution. *JBIC Journal of Biological Inorganic Chemistry*, 13(2), 157–170.

Mihara, Hisaaki, Kurihara, Tatsuo, Yoshimura, Tohru & Esaki, Nobuyoshi (2000). Kinetic and mutational studies of three NifS homologs from *Escherichia coli*: mechanistic difference between L-cysteine desulfurase and L-selenocysteine lyase reactions. *The Journal of Biochemistry*, 127(4), 559–567.

Mitou, Géraldine, Higgins, Catherine, Wittung-Stafshede, Pernilla, Conover, Richard C, Smith, Archer D, Johnson, Michael K, Gaillard, Jacques, Stubna, Audria, Münck, Eckard & Meyer, Jacques (2003). An Isc-Type Extremely Thermostable [2Fe- 2S] Ferredoxin from *Aquifex aeolicus*. Biochemical, Spectroscopic, and Unfolding Studies. *Biochemistry*, 42(5), 1354–1364.

Mortenson, Leonard E, Valentine, Raymond C & Carnahan, James E (1962). An electron transport factor from Clostridiumpasteurianum. *Biochemical and biophysical research communications*, 7(6), 448–452.

Mühlenhoff, Ulrich, Gerber, Jana, Richhardt, Nadine & Lill, Roland (2003). Components involved in assembly and dislocation of iron–sulfur clusters on the scaffold protein Isu1p. *The EMBO journal*, 22(18), 4815–4825.

Müller, Caroline, Kuki, Kacilda Naomi, Pinheiro, Daniel Teixeira, de Souza, Laíse Rosado, Silva, Advânio Inácio Siqueira, Loureiro, Marcelo Ehlers, Oliva, Marco Antonio & Almeida, Andréa Miyasaka (2015). Differential physiological responses in rice upon exposure to excess distinct iron forms. *Plant and Soil*, 391(1), 123–138.

Mullinger, Roger N, Cammack, Richard, Rao, K Krishna, Hall, D O, Dickson, D P, Johnson, C E, Rush, J D & Simopoulos, A (1975). Physicochemical characterization of the four-iron-four-sulphide ferredoxin from *Bacillus stearothermophilus*. *Biochemical Journal*, 151(1), 75–83.

Munday, Rex (1989). Toxicity of thiols and disulphides: involvement of free-radical species. *Free Radical Biology and Medicine*, 7(6), 659–673.

Murshudov, Garib N, Skubák, Pavol, Lebedev, Andrey A, Pannu, Navraj S, Steiner, Roberto A, Nicholls, Robert A, Winn, Martyn D, Long, Fei & Vagin, Alexei A (2011). REFMAC5 for the refinement of macromolecular crystal structures. *Acta Crystallographica Section D: Biological Crystallography*, 67(4), 355–367.

Nachin, Laurence, Loiseau, Laurent, Expert, Dominique & Barras, Frédéric (2003). SufC: an unorthodox cytoplasmic ABC/ATPase required for [Fe—S] biogenesis under oxidative stress. *The EMBO journal*, 22(3), 427–437.

Nakamura, Kensuke, Kawabata, Takeshi, Yura, Kei & Go, Nobuhiro (2003). Novel types of two-domain multi-copper oxidases: possible missing links in the evolution. *Febs Letters*, 553(3), 239–244.

Nersissian, Aram M, Valentine, Joan Selverstone, Immoos, Chad, Hill, Michael G, Hart, P John, Williams, Gregory & Herrmann, Reinhold G (1998). Uclacyanins, stellacyanins, and plantacyanins are distinct subfamilies of phytocyanins: Plant-specific mononuclear blue copper proteins. *Protein Science*, 7(9), 1915–1929.

Olbrich, Anna C, Schild, Jan N & Urlacher, Vlada B (2019). Correlation between the T1 copper reduction potential and catalytic activity of a small laccase. *Journal of inorganic biochemistry*, 201, 110843.

Ollagnier-de Choudens, Sandrine, Loiseau, Laurent, Sanakis, Yiannis, Barras, Frédéric & Fontecave, Marc (2005). Quinolinate synthetase, an iron–sulfur enzyme in NAD biosynthesis. *FEBS letters*, 579(17), 3737–3743.

Osipov, Evgeny, Polyakov, Konstantin, Kittl, Roman, Shleev, Sergey, Dorovatovsky, Pavel, Tikhonova, Tamara, Hann, Stephan, Ludwig, Roland & Popov, Vladimir (2014). Effect of the L499M mutation of the ascomycetous Botrytis aclada laccase on redox potential and catalytic properties. *Acta Crystallographica Section D: Biological Crystallography*, 70(11), 2913–2923.

Osma, Johann F, Toca-Herrera, José L & Rodríguez-Couto, Susana (2010). Uses of laccases in the food industry. *Enzyme research*, 2010.

Outten, F Wayne, Huffman, David L, Hale, Jeremy A & O'Halloran, Thomas V (2001). The independent cue and cusSystems confer copper tolerance during aerobic and anaerobic growth in *Escherichia coli*. *Journal of Biological Chemistry*, 276(33), 30670–30677.

Outten, F Wayne, Wood, Matthew J, Muñoz, F Michael & Storz, Gisela (2003). The SufE protein and the SufBCD complex enhance SufS cysteine desulfurase activity as part of a sulfur transfer pathway for Fe–S cluster assembly in *Escherichia coli*. *Journal of Biological Chemistry*, 278(46), 45713–45719.

Palmer, Amy E, Szilagyi, Robert K, Cherry, Joel R, Jones, Aubrey, Xu, Feng & Solomon, Edward I (2003). Spectroscopic characterization of the Leu513His variant of fungal laccase: effect of increased axial ligand interaction on the geometric and electronic structure of the type 1 Cu site. *Inorganic chemistry*, 42(13), 4006–4017.

Pascher, Torbjörn, Karlsson, B Göran, Nordling, Margareta, Malmström, Bo G & Vänngård, Tore (1993). Reduction potentials and their pH dependence in site-directed-mutant forms of azurin from Pseudomonas aeruginosa. *European journal of biochemistry*, 212(2), 289–296.

Pastore, Chiara, Adinolfi, Salvatore, Huynen, Martjin A, Rybin, Vladimir, Martin, Stephen, Mayer, Mathias, Bukau, Bernd & Pastore, Annalisa (2006). YfhJ, a molecular adaptor in iron-sulfur cluster formation or a frataxin-like protein? *Structure*, 14(5), 857–867.

Pérard, J & de Choudens, Sandrine Ollagnier (2018). Iron–sulfur clusters biogenesis by the SUF machinery: close to the molecular mechanism understanding. *JBIC Journal of Biological Inorganic Chemistry*, 23(4), 581–596.

Petros, Amy K, Reddi, Amit R, Kennedy, Michelle L, Hyslop, Alison G & Gibney, Brian R (2006). Femtomolar Zn (II) affinity in a peptide-based ligand designed to model thiolate-rich metalloprotein active sites. *Inorganic chemistry*, 45(25), 9941–9958.

Piontek, Klaus, Antorini, Matteo & Choinowski, Thomas (2002). Crystal structure of a laccase from the fungusTrametes versicolor at 1.90-Å resolution containing a full complement of coppers. *Journal of Biological Chemistry*, 277(40), 37663–37669.

Piscitelli, Alessandra, Pezzella, Cinzia, Giardina, Paola, Faraco, Vincenza & Sannia, Giovanni (2010). Heterologous laccase production and its role in industrial applications. *Bioengineered bugs*, 1(4), 254–264.

Prins, Alaric, Kleinsmidt, L, Khan, Nuraan, Kirby, Bronwyn, Kudanga, Tukayi, Vollmer, Jannik, Pleiss, Juergen, Burton, Stephanie & Le Roes-Hill, M (2015). The effect of mutations near the T1 copper site on the biochemical characteristics of the small laccase from Streptomyces coelicolor A3 (2). *Enzyme and microbial technology*, 68, 23–32.

Prischi, Filippo, Konarev, Petr V, Iannuzzi, Clara, Pastore, Chiara, Adinolfi, Salvatore, Martin, Stephen R, Svergun, Dmitri I & Pastore, Annalisa (2010). Structural bases for the interaction of frataxin with the central components of iron–sulphur cluster assembly. *Nature communications*, 1(1), 1–10.

Prischi, Filippo, Pastore, Chiara, Carroni, Marta, Iannuzzi, Clara, Adinolfi, Salvatore, Temussi, Pierandrea & Pastore, Annalisa (2010). Of the vulnerability of orphan complex proteins: the case study of the *E. coli* IscU and IscS proteins. *Protein expression and purification*, 73(2), 161–166.

Py, Béatrice, Moreau, Patrice L & Barras, Frédéric (2011). Fe–S clusters, fragile sentinels of the cell. *Current opinion in microbiology*, 14(2), 218–223.

Ramelot, Theresa A, Cort, John R, Goldsmith-Fischman, Sharon, Kornhaber, Gregory J, Xiao, Rong, Shastry, Ritu, Acton, Thomas B, Honig, Barry, Montelione, Gaetano T & Kennedy, Michael A (2004). Solution NMR structure of the iron–sulfur cluster assembly protein U (IscU) with zinc bound at the active site. *Journal of molecular biology*, 344(2), 567–583.

Ranquet, Caroline, Ollagnier-de Choudens, Sandrine, Loiseau, Laurent, Barras, Frédéric & Fontecave, Marc (2007). Cobalt stress in *Escherichia coli*: the effect on the iron-sulfur proteins. *Journal of Biological Chemistry*, 282(42), 30442–30451.

Raulfs, Estella C, O'Carroll, Ina P, Dos Santos, Patricia C, Unciuleac, Mihaela-Carmen & Dean, Dennis R (2008). *In vivo* iron–sulfur cluster formation. *Proceedings of the National Academy of Sciences*, 105(25), 8591–8596.

Rees, Douglas C (2002). Great metalloclusters in enzymology. *Annual review of biochemistry*, 71(1), 221–246.

Rekittke, Ingo, Wiesner, Jochen, Röhrich, Rene, Demmer, Ulrike, Warkentin, Eberhard, Xu, Weiya, Troschke, Kathrin, Hintz, Martin, No, Joo Hwan, Duin, Evert C *et al.* (2008). Structure of (E)-4-hydroxy-3-methyl-but-2-enyl diphosphate reductase, the terminal enzyme of the non-mevalonate pathway. *Journal of the American Chemical Society*, 130(51), 17206–17207.

Riva, Sergio (2006). Laccases: blue enzymes for green chemistry. *TRENDS in Biotechnology*, 24(5), 219–226.

Roach, Peter L (2011). Radicals from S-adenosylmethionine and their application to biosynthesis. *Current opinion in chemical biology*, 15(2), 267–275.

Robbins, A Hv & Stout, CD (1989). The structure of aconitase. *Proteins: Structure, Function, and Bioinformatics*, 5(4), 289–312.

Roche, Béatrice, Huguenot, Allison, Barras, Frédéric & Py, Béatrice (2015). The iron-binding CyaY and IscX proteins assist the ISC-catalyzed F e-S biogenesis in *Escherichia coli*. *Molecular microbiology*, 95(4), 605–623.

Rodrigue, Agnes, Effantin, Géraldine & Mandrand-Berthelot, Marie-Andrée (2005). Identification of rcnA (yohM), a nickel and cobalt resistance gene in *Escherichia coli*. *Journal of bacteriology*, 187(8), 2912–2916.

Romero, Antonio, Hoitink, Carla WG, Nar, Herbert, Huber, Robert, Messerschmidt, Albrecht & Canters, Gerard W (1993). X-ray analysis and spectroscopic characterization of M121Q azurin: A copper site model for stellacyanin. *Journal of molecular biology*, 229(4), 1007–1021.

Rousset, Carine, Fontecave, Marc & de Choudens, Sandrine Ollagnier (2008). The [4Fe–4S] cluster of quinolinate synthase from *Escherichia coli*: Investigation of cluster ligands. *FEBS letters*, 582(19), 2937–2944.

Roy, Poorna, Bauman, Mariia A, Almutairi, Hayfa Habes, Jayawardhana, Walimuni Geethamala, Johnson, Nathan M & Torelli, Andrew T (2017). Comparison of the response of bacterial IscU and SufU to Zn^{2+} and select transition-metal ions. *ACS chemical biology*, 13(3), 591–599.

Rubio, Luis M & Ludden, Paul W (2008). Biosynthesis of the iron-molybdenum cofactor of nitrogenase. *Annual review of microbiology*, 62.

Saini, Avneesh, Mapolelo, Daphne T, Chahal, Harsimranjit K, Johnson, Michael K & Outten, F Wayne (2010). SufD and SufC ATPase activity are required for iron acquisition during *in vivo* Fe–S cluster formation on SufB. *Biochemistry*, 49(43), 9402–9412.

Saito, Kaori Otsuka, Kurose, Shinji, Tsujino, Yoshio, Osakai, Toshiyuki, Kataoka, Kunishige, Sakurai, Takeshi & Tamiya, Eiichi (2013). Electrochemical characterization of a unique,“neutral” laccase from Flammulina velutipes. *Journal of bioscience and bioengineering*, 115(2), 159–167.

Sakurai, Takeshi & Kataoka, Kunishige (2007). Structure and function of type I copper in multicopper oxidases. *Cellular and Molecular Life Sciences*, 64(19), 2642–2656.

Schrödinger, LLC (2017). The PyMOL Molecular Graphics System, Version 2.0 Schrödinger, LLC (2017). *n.a.*

Schuetz, Mathias, Benske, Anika, Smith, Rebecca A, Watanabe, Yoichiro, Tobimatsu, Yuki, Ralph, John, Demura, Taku, Ellis, Brian & Samuels, A Lacey (2014). Laccases direct lignification in the discrete secondary cell wall domains of protoxylem. *Plant Physiology*, 166(2), 798–807.

Schwartz, Christopher J, Djaman, Ouliana, Imlay, James A & Kiley, Patricia J (2000). The cysteine desulfurase, IscS, has a major role in *in vivo* Fe–S cluster formation in *Escherichia coli*. *Proceedings of the National Academy of Sciences*, 97(16), 9009–9014.

Schwartz, Christopher J, Giel, Jennifer L, Patschkowski, Thomas, Luther, Christopher, Ruzicka, Frank J, Beinert, Helmut & Kiley, Patricia J (2001). IscR, an Fe–S cluster-containing transcription factor, represses expression of *Escherichia coli* genes encoding Fe–S cluster assembly proteins. *Proceedings of the National Academy of Sciences*, 98(26), 14895–14900.

Sekretaryova, Alina, Jones, Stephen M & Solomon, Edward I (2019). O_2 Reduction to water by high potential Multicopper Oxidases: Contributions of the T1 Copper Site Potential and the Local Environment of the trinuclear copper cluster. *Journal of the American Chemical Society*, 141(28), 11304–11314.

Selbach, Bruna P, Chung, Alexander H, Scott, Aubrey D, George, Simon J, Cramer, Stephen P & Dos Santos, Patricia C (2014). Fe–S cluster biogenesis in Gram-positive bacteria: SufU is a zinc-dependent sulfur transfer protein. *Biochemistry*, 53(1), 152–160.

Sendra, Maïté, de Choudens, Sandrine Ollagnier, Lascoux, David, Sanakis, Yiannis & Fontecave, Marc (2007). The SUF iron–sulfur cluster biosynthetic machinery: sulfur transfer from the SUFS–SUFE complex to SUFA. *FEBS letters*, 581(7), 1362–1368.

Shakamuri, Priyanka, Zhang, Bo & Johnson, Michael K (2012). Monothiol glutaredoxins function in storing and transporting [Fe2S2] clusters assembled on IscU scaffold proteins. *Journal of the American Chemical Society*, 134(37), 15213–15216.

Sharma, Anil K, Pallesen, Leif J, Spang, Robert J & Walden, William E (2010). Cytosolic iron-sulfur cluster assembly (CIA) system: factors, mechanism, and relevance to cellular iron regulation. *Journal of Biological Chemistry*, 285(35), 26745–26751.

Shi, Rong, Proteau, Ariane, Villarroya, Magda, Moukadiri, Ismaïl, Zhang, Linhua, Trempe, Jean-François, Matte, Allan, Armengod, M Eugenia & Cygler, Miroslaw (2010). Structural basis for Fe–S cluster assembly and tRNA thiolation mediated by IscS protein–protein interactions. *PLoS Biol*, 8(4), e1000354.

Shimizu, Atsushi, Kwon, Jung-Hee, Sasaki, Takashi, Satoh, Takanori, Sakurai, Nobuhiko, Sakurai, Takeshi, Yamaguchi, Shotaro & Samejima, Tatsuya (1999). Myrothecium verrucaria bilirubin oxidase and its mutants for potential copper ligands. *Biochemistry*, 38(10), 3034–3042.

Shimomura, Yoshimitsu, Wada, Kei, Fukuyama, Keiichi & Takahashi, Yasuhiro (2008). The asymmetric trimeric architecture of [2Fe–2S] IscU: implications for its scaffolding during iron–sulfur cluster biosynthesis. *Journal of molecular biology*, 383(1), 133–143.

Shriver, Duward F, Atkins, Peter W & Langford, Cooper H (1999). Inorganic chemistry.

Singh, Gursharan, Bhalla, Aditya, Kaur, Paramjit, Capalash, Neena & Sharma, Prince (2011). Laccase from prokaryotes: a new source for an old enzyme. *Reviews in Environmental Science and Bio/Technology*, 10(4), 309–326.

Skálová, Tereza, Dohnálek, Jan, Østergaard, Lars Henrik, Østergaard, Peter Rahbek, Kolenko, Petr, Dušková, Jarmila, Štěpánková, Andrea & Hašek, Jindřich (2009). The structure of the small laccase from Streptomyces coelicolor reveals a link between laccases and nitrite reductases. *Journal of molecular biology*, 385(4), 1165–1178.

Solomon, Edward I (2006). Spectroscopic methods in bioinorganic chemistry: blue to green to red copper sites. *Inorganic chemistry*, 45(20), 8012–8025.

Solomon, Edward I, Augustine, Anthony J & Yoon, Jungjoo (2008). O_2 Reduction to H_2O by the multicopper oxidases. *Dalton Transactions*, (30), 3921–3932.

Solomon, Edward I, Penfield, Kevin W, Gewirth, Andrew A, Lowery, Michael D, Shadle, Susan E, Guckert, Jeffrey A & LaCroix, Louis B (1996). Electronic structure of the oxidized and reduced blue copper sites: Contributions to the electron transfer pathway, reduction potential, and geometry. *Inorganica chimica acta*, 243(1-2), 67–78.

Solomon, Edward I, Sundaram, Uma M & Machonkin, Timothy E (1996). Multicopper oxidases and oxygenases. *Chemical reviews*, 96(7), 2563–2606.

Solomon, Edward I, Szilagyi, Robert K, DeBeer George, Serena & Basumallick, Lipika (2004). Electronic structures of metal sites in proteins and models: contributions to function in blue copper proteins. *Chemical reviews*, 104(2), 419–458.

Sozer, Ozge, Kis, Mihaly, Gombos, Zoltan & Ughy, Bettina (2011). Proteins, glycerolipids and carotenoids in the functional photosystem II architecture. *Front. Biosci*, 16, 619–643.

Span, Ingrid (2012). *Strukturelle und funktionelle Charakterisierung des Eisen-Schwefel-Proteins IspH in Komplex mit Liganden*. PhD thesis, Technische Universität München.

Span, Ingrid, Wang, Ke, Wang, Weixue, Zhang, Yonghui, Bacher, Adelbert, Eisenreich, Wolfgang, Li, Kai, Schulz, Charles, Oldfield, Eric & Groll, Michael (2012). Discovery of acetylene hydratase activity of the iron–sulphur protein IspH. *Nature communications*, 3(1), 1–8.

Spiro, Thomas G & Czernuszewicz, Roman S (1995). [18] Resonance Raman spectroscopy of metalloproteins. *Methods in enzymology*, 246, 416–460.

Stadler, Jochen A & Schweyen, Rudolf J (2002). The yeast iron regulon is induced upon cobalt stress and crucial for cobalt tolerance. *Journal of Biological Chemistry*, 277(42), 39649–39654.

Steenken, S & Neta, P (1982). One-electron redox potentials of phenols. Hydroxy-and aminophenols and related compounds of biological interest. *The Journal of Physical Chemistry*, 86(18), 3661–3667.

Stephens, PJ, Thomson, AJ, Dunn, JBR, Keiderling, TA, Rawlings, J, Rao, KK & Hall, DO (1978). Circular dichroism and magnetic circular dichroism of iron-sulfur proteins. *Biochemistry*, 17(22), 4770–4778.

Stoll, Stefan & Schweiger, Arthur (2006). EasySpin, a comprehensive software package for spectral simulation and analysis in EPR. *Journal of magnetic resonance*, 178(1), 42–55.

Sugiura, Yukio (1978). Electronic properties of sulfhydryl-and imidazole-containing peptide-cobalt (II) complexes: their relationship to cobalt (II)-substituted “blue” copper proteins. *Bioinorganic chemistry*, 8(5), 453–460.

Szuster, Jonathan, Zitare, Ulises A, Castro, María A, Leguto, Alcides J, Morgada, Marcos N, Vila, Alejandro J & Murgida, Daniel H (2020). Cu A-based chimeric T1 copper sites allow for independent modulation of reorganization energy and reduction potential. *Chemical science*, 11(24), 6193–6201.

Takahashi, Yasuhiro & Tokumoto, Umechiyo (2002). A third bacterial system for the assembly of iron-sulfur clusters with homologs in archaea and plastids. *Journal of Biological Chemistry*, 277(32), 28380–28383.

Tan, Guoqiang, Lu, Jianxin, Bitoun, Jacob P, Huang, Hao & Ding, Huangen (2009). IscA/SufA paralogues are required for the [4Fe–4S] cluster assembly in enzymes of multiple physiological pathways in *Escherichia coli* under aerobic growth conditions. *Biochemical Journal*, 420(3), 463–472.

Tang, Yue & Guest, John R (1999). Direct evidence for mRNA binding and post-transcriptional regulation by *Escherichia coli* aconitases. *Microbiology*, 145(11), 3069–3079.

Thayer, Maria M, Ahern, Holly, Xing, Dongxia, Cunningham, Richard P & Tainer, John A (1995). Novel DNA binding motifs in the DNA repair enzyme endonuclease III crystal structure. *The EMBO journal*, 14(16), 4108–4120.

Thorgersen, Michael P & Downs, Diana M (2007). Cobalt targets multiple metabolic processes in *Salmonella enterica*. *Journal of bacteriology*, 189(21), 7774–7781.

Thurston, Christopher F (1994). The structure and function of fungal laccases. *Microbiology*, 140(1), 19–26.

Tokumoto, Umechiyo, Kitamura, Seiichi, Fukuyama, Keiichi & Takahashi, Yasuhiro (2004). Interchangeability and distinct properties of bacterial Fe–S cluster assembly systems: functional replacement of the isc and suf operons in *Escherichia coli* with the nifSU-like operon from Helicobacter pylori. *Journal of biochemistry*, 136(2), 199–209.

Tokumoto, Umechiyo & Takahashi, Yasuhiro (2001). Genetic analysis of the isc operon in *Escherichia coli* involved in the biogenesis of cellular iron-sulfur proteins. *The Journal of biochemistry*, 130(1), 63–71.

Toscano, Miguel D, De Maria, Leonardo, Lobedanz, Sune & Østergaard, Lars H (2013). Optimization of a Small Laccase by Active-Site Redesign. *ChemBioChem*, 14(10), 1209–1211.

UM, Narayana Murthy, Ollagnier-de Choudens, Sandrine, Sanakis, Yiannis, Abdel-Ghany, Salah E, Rousset, Carine, Ye, Hong, Fontecave, Marc, Pilon-Smits, Elizabeth AH & Pilon, Marinus (2007). Characterization of Arabidopsis thaliana SufE2 and SufE3: functions in chloroplast iron-sulfur cluster assembly and Nad synthesis. *Journal of Biological Chemistry*, 282(25), 18254–18264.

Unciuleac, Mihaela-Carmen, Chandramouli, Kala, Naik, Sunil, Mayer, Suzanne, Huynh, Boi Hanh, Johnson, Michael K & Dean, Dennis R (2007). *In Vitro* Activation of Apo-Aconitase Using a [4Fe–4S] Cluster-Loaded Form of the IscU [Fe- S] Cluster Scaffolding Protein. *Biochemistry*, 46(23), 6812–6821.

Uthandi, Sivakumar, Saad, Boutaiba, Humbard, Matthew A & Maupin-Furlow, Julie A (2010). LccA, an archaeal laccase secreted as a highly stable glycoprotein into the extracellular medium by Haloferax volcanii. *Applied and environmental microbiology*, 76(3), 733–743.

Vallee, Bert L & Williams, RtJ (1968). Metalloenzymes: the entatic nature of their active sites. *Proceedings of the National Academy of Sciences of the United States of America*, 59(2), 498.

Venkateswara Rao, P & Holm, RH (2004). Synthetic analogues of the active sites of iron-sulfur proteins. *Chemical reviews*, 104(2), 527–560.

Vincent, Kylie A, Parkin, Alison, Lenz, Oliver, Albracht, Simon PJ, Fontecilla-Camps, Juan C, Cammack, Richard, Friedrich, Bärbel & Armstrong, Fraser A (2005). Electrochemical definitions of O_2 sensitivity and oxidative inactivation in hydrogenases. *Journal of the American Chemical Society*, 127(51), 18179–18189.

Waldron, Kevin J & Robinson, Nigel J (2009). How do bacterial cells ensure that metalloproteins get the correct metal? *Nature Reviews Microbiology*, 7(1), 25–35.

Wang, Weixue, Wang, Ke, Liu, Yi-Liang, No, Joo-Hwan, Li, Jikun, Nilges, Mark J & Oldfield, Eric (2010). Bioorganometallic mechanism of action, and inhibition, of IspH. *Proceedings of the National Academy of Sciences*, 107(10), 4522–4527.

Ward, Jesse, Ollmann, Emily, Maxey, Evan & Finney, Lydia A (2014). X-ray absorption spectroscopy of metalloproteins. In *Metalloproteins*, S. 171–187. Springer.

Warren, Jeffrey J, Lancaster, Kyle M, Richards, John H & Gray, Harry B (2012). Inner-and outer-sphere metal coordination in blue copper proteins. *Journal of inorganic biochemistry*, 115, 119–126.

Webert, Holger, Freibert, Sven-Andreas, Gallo, Angelo, Heidenreich, Torsten, Linne, Uwe, Amlacher, Stefan, Hurt, Ed, Mühlenhoff, Ulrich, Banci, Lucia & Lill, Roland (2014). Functional reconstitution of mitochondrial Fe/S cluster synthesis on Isu1 reveals the involvement of ferredoxin. *Nature communications*, 5(1), 1–12.

White, Malcolm F & Dillingham, Mark S (2012). Iron–sulphur clusters in nucleic acid processing enzymes. *Current opinion in structural biology*, 22(1), 94–100.

Wieckowski, Beata M, Hegemann, Julian D, Mielcarek, Andreas, Boss, Linda, Burghaus, Olaf & Marahiel, Mohamed A (2015). The PqqD homologous domain of the radical SAM enzyme ThnB is required for thioether bond formation during thurincin H maturation. *FEBS letters*, 589(15), 1802–1806.

Wijma, Hein J, MacPherson, Iain, Farver, Ole, Tocheva, Elitza I, Pecht, Israel, Verbeet, Martin Ph, Murphy, Michael EP & Canters, Gerard W (2007). Effect of the methionine ligand on the reorganization energy of the type-1 copper site of nitrite reductase. *Journal of the American Chemical Society*, 129(3), 519–525.

Williams, Colin H, Stillman, Timothy J, Barynin, Vladimir V, Sedelnikova, Svetlana E, Tang, Yue, Green, Jeffrey, Guest, John R & Artymiuk, Peter J (2002). *E. coli* aconitase B structure reveals a HEAT-like domain with implications for protein–protein recognition. *nature structural biology*, 9(6), 447–452.

Winn, Martyn D, Ballard, Charles C, Cowtan, Kevin D, Dodson, Eleanor J, Emsley, Paul, Evans, Phil R, Keegan, Ronan M, Krissinel, Eugene B, Leslie, Andrew GW, McCoy, Airlie *et al.* (2011). Overview of the CCP4 suite and current developments. *Acta Crystallographica Section D: Biological Crystallography*, 67(4), 235–242.

Wofford, Joshua D, Bolaji, Naimah, Dziuba, Nathaniel, Outten, F Wayne & Lindahl, Paul A (2019). Evidence that a respiratory shield in *Escherichia coli* protects a low-molecular-mass FeII pool from O_2-dependent oxidation. *Journal of Biological Chemistry*, 294(1), 50–62.

Wolff, Murielle, Seemann, Myriam, Bui, Bernadette Tse Sum, Frapart, Yves, Tritsch, Denis, Estrabot, Ana Garcia, Rodríguez-Concepción, Manuel, Boronat, Albert, Marquet, Andrée & Rohmer, Michel (2003). Isoprenoid biosynthesis via the methylerythritol phosphate pathway: the (E)-4-hydroxy-3-methylbut-2-enyl diphosphate reductase (LytB/IspH) from *Escherichia coli* is a [4Fe–4S] protein. *FEBS letters*, 541(1-3), 115–120.

Xu, Feng (1996). Oxidation of phenols, anilines, and benzenethiols by fungal laccases: correlation between activity and redox potentials as well as halide inhibition. *Biochemistry*, 35(23), 7608–7614.

Xu, Feng, Berka, Randy M, Wahleithner, Jill A, Nelson, Beth A, Shuster, Jeffrey R, Brown, Stephen H, Palmer, Amy E & Solomon, Edward I (1998). Site-directed mutations in fungal laccase: effect on redox potential, activity and pH profile. *Biochemical Journal*, 334(1), 63–70.

Xu, Feng, Palmer, Amy E, Yaver, Debbie S, Berka, Randy M, Gambetta, Gregory A, Brown, Stephen H & Solomon, Edward I (1999). Targeted mutations in a Trametes villosa laccase axial perturbations of the T1 copper. *Journal of Biological Chemistry*, 274(18), 12372–12375.

Xu, Feng, Shin, Woonsup, Brown, Stephen H, Wahleithner, Jill A, Sundaram, Uma M & Solomon, Edward I (1996). A study of a series of recombinant fungal laccases and bilirubin oxidase that exhibit significant differences in redox potential, substrate specificity, and stability. *Biochimica et Biophysica Acta (BBA)-Protein Structure and Molecular Enzymology*, 1292(2), 303–311.

Xu, Xiang Ming & Møller, Simon G (2008). Iron–sulfur cluster biogenesis systems and their crosstalk. *Chembiochem*, 9(15), 2355–2362.

Yan, Robert, Adinolfi, Salvatore & Pastore, Annalisa (2015). Ferredoxin, in conjunction with NADPH and ferredoxin-NADP reductase, transfers electrons to the IscS/IscU complex to promote iron–sulfur cluster assembly. *Biochimica et Biophysica Acta (BBA)-Proteins and Proteomics*, 1854(9), 1113–1117.

Yan, Robert, Konarev, Petr V, Iannuzzi, Clara, Adinolfi, Salvatore, Roche, Béatrice, Kelly, Geoff, Simon, Léa, Martin, Stephen R, Py, Béatrice, Barras, Frédéric *et al.* (2013). Ferredoxin competes with bacterial frataxin in binding to the desulfurase IscS. *Journal of Biological Chemistry*, 288(34), 24777–24787.

Yanagisawa, Sachiko & Dennison, Christopher (2005). Reduction potential tuning at a type 1 copper site does not compromise electron transfer reactivity. *Journal of the American Chemical Society*, 127(47), 16453–16459.

Yokoyama, Nao, Nonaka, Chihiro, Ohashi, Yukari, Shioda, Masaharu, Terahata, Takuya, Chen, Wen, Sakamoto, Kotomi, Maruyama, Chihiro, Saito, Takuya, Yuda, Eiki *et al.* (2018). Distinct roles for U-type proteins in iron–sulfur cluster biosynthesis revealed by genetic analysis of the *Bacillus subtilis* sufCDSUB operon. *Molecular microbiology*, 107(6), 688–703.

Yoon, Taejin & Cowan, JA (2003). Iron-sulfur cluster biosynthesis. Characterization of frataxin as an iron donor for assembly of [2Fe–2S] clusters in ISU-type proteins. *Journal of the American Chemical Society*, 125(20), 6078–6084.

Yuda, Eiki, Tanaka, Naoyuki, Fujishiro, Takashi, Yokoyama, Nao, Hirabayashi, Kei, Fukuyama, Keiichi, Wada, Kei & Takahashi, Yasuhiro (2017). Mapping the key residues of SufB and SufD essential for biosynthesis of iron-sulfur clusters. *Scientific reports*, 7(1), 1–12.

Yuvaniyama, Pramvadee, Agar, Jeffrey N, Cash, Valerie L, Johnson, Michael K & Dean, Dennis R (2000). NifS-directed assembly of a transient [2Fe–2S] cluster within the NifU protein. *Proceedings of the National Academy of Sciences*, 97(2), 599–604.

Zerva, Anastasia, Simić, Stefan, Topakas, Evangelos & Nikodinovic-Runic, Jasmina (2019). Applications of microbial laccases: patent review of the past decade (2009–2019). *Catalysts*, 9(12), 1023.

Zhao, Yukun, Lin, Junqi, Liu, Yongdong, Ma, Baochun, Ding, Yong & Chen, Mindong (2015). Efficient light-driven water oxidation catalyzed by a mononuclear cobalt (iii) complex. *Chemical Communications*, 51(97), 17309–17312.

Zheng, Limin, Cash, Valerie L, Flint, Dennis H & Dean, Dennis R (1998). Assembly of iron-sulfur clusters identification of an iscSUA-hscBA-fdx gene cluster from Azotobacter vinelandii. *Journal of Biological Chemistry*, 273(21), 13264–13272.

Declaration of Contributions

Maturation of [4Fe–4S] cluster containing proteins *in vivo* and *in vitro*

Steffen Mielenbrink[a,†], Hannah Rosenbach[a,†], Melissa Jansing[a], Sabine Metzger[d,e], and Ingrid Span[a,*]

Submitted to: **Metallomics**
Journal Impact Factor (2020): 3.796
Contribution: 40%

S.M., H.R., and I.S. designed the experiments. S.M. supervized and assisted M.J. in performing protein isolation and electronic absorption spectroscopy. S.M. performed CD measurements. Sabine Metzger performed ICP-MS. S.M., H.R., and I.S. finalized the manuscript.

Evidence for the formation of artificial cobalt-sulfur clusters in proteins

Steffen Mielenbrink[a], Sabine Metzger[d,e], and Ingrid Span[a,*]

To be submitted to: **Journal of American Chemical Society**
Journal Impact Factor (2019): 14.612
Contribution: 80%

S.M. and I.S. designed the experiments. S.M. performed all experiments. S.M. prepared samples for ICP-MS. S.M. and I.S. wrote the manuscript. Sabine Metzger performed ICP-MS. All authors commented on the manuscript.

Influence of the T1 Cu axial ligand on kinetic, spectral, and structural properties of the laccase Ssl1 from *Streptomyces sviceus*

Anna Olbrich[b,†], Steffen Mielenbrink[a,†], Vivian P. Willers[b], George E. Cutsail III[c], James A. Birrell[c], Ingrid Span[a,*], and Vlada B. Urlacher[a,*]

To be submitted to: **Int. J. Biol. Macromol.**
Journal Impact Factor (2020): 5.162
Contribution: 35%

A.C.O., S.M., V.B.U., and I.S. designed the experiments. A.C.O, S.M., V.P.W., G.E.C., and I.S. collected all data. A.C.O., S.M., J.A.B., and I.S. did data analysis and interpretation and drafted the manuscript. All authors commented on the manuscript.

[a] Institut für Physikalische Biologie, Heinrich-Heine-Universität Düsseldorf, Universitätsstr. 1, 40225 Düsseldorf, Germany
[b] Institut für Biochemie, Heinrich-Heine-Universität Düsseldorf, Universitätsstr. 1, 40225 Düsseldorf, Germany
[c] Max Planck Institute for Chemical Energy Conversion, Stiftstr. 34-36, 45470 Mülheim an der Ruhr, Germany.
[d] MS-Platform Biocenter, Cluster of Excellence on Plant Science (CEPLAS), University of Cologne, Albertus-Magnus-Platz, 50923 Cologne, Germany.
[e] IUF-Leibniz Research Institute for Environmental Medicine, Heisenberg-Group - Environmentally-Induced Cardiovascular Degeneration, Mass Spectrometry Core Unit, Auf'm Hennekamp 50, 40225 Düsseldorf, Germany.

[†] equally contributed
* corresponding authors

Ingrid Span: ingrid.span@hhu.de; +(49) (0)211 81-15582
Institut für Physikalische Biologie, Heinrich-Heine-Universität Düsseldorf, Universitätsstr. 1, 40225 Düsseldorf, Germany

Vlada B. Urlacher: vlada.urlacher@hhu.de; +(49) (0)211 81-13687
Institut für Biochemie, Heinrich-Heine-Universität Düsseldorf, Universitätsstr. 1, 40225 Düsseldorf, Germany

Erklärung

Ich versichere an Eides statt, dass die Dissertation von mir selbständig und ohne unzulässige fremde Hilfe unter Beachtung der „Grundsätze zur Sicherung guter wissenschaftlicher Praxis an der Heinrich-Heine-Universität Düsseldorf“ erstellt worden ist.

Die Dissertation wurde in der vorgelegten oder in ähnlicher Form noch bei keiner anderen Institution eingereicht. Ich habe bisher keine erfolglosen Promotionsversuche unternommen.

Düsseldorf, 01.06.2021
Ort, Datum

Steffen Mielenbrink

Danksagung

Zu allererst möchte ich mich bei meiner Erstgutachterin Frau Jun.-Prof. Dr. Ingrid Span für die Möglichkeit einer Promotion in ihrer Arbeitsgruppe bedanken. Durch sie hatte ich die Möglichkeit an spannenden und innovativen Projekten in einer menschlich herausragenden Gruppe zu arbeiten. Konstruktive Kritik im richtigen Maße und das Fordern und Fördern von außerfachlichen Fähigkeiten spielte dabei eine besondere Rolle.

Zusätzlich bedanke ich mich bei meinem Zweitgutachter Herrn Prof. Matias Zurbriggen für konstruktive Gespräche und Diskussionen nach Präsentationen zum Fortschrittsbericht, sowie für ein spannendes und faires Kartrennen nach Feierabend. Herrn Prof. Dieter Willbold danke ich für die Bereitstellung von Verbrauchsmaterialien und den institutionellen Räumlichkeiten.

Danken möchte ich auch meinen Kooperationspartnern innerhalb und außerhalb des IPB, mit denen zusammen ich spannende Projekte bearbeiten und abschließen durfte. Alle haben ihren Teil zu dieser erfolgreichen Arbeit beigetragen. Besondere Erwähnung verdienen hier Dr. Sabine Metzger, Prof. Dr. Vlada Urlacher, Anna Olbrich, Dr. James Birrell, Prof. Dr. George E. Cutsail III, Dr. Hannah Rosenbach und Melissa Jansing.

Außerdem möchte ich mich bei all meinen Kollegen vom Institut vor allem für die schönen und unvergesslichen Momente außerhalb des Laboralltags bedanken. Besonders erwähnen möchte ich Herrn apl. Prof. Dr. Ing. Gerhard Steger, der mein längster Begeleiter am Institut war und mir nach meiner Masterarbeit unter seiner Leitung auch außerwissenschaftlich mit Rat, Tat, spannenden und interessanten Gesprächen, sowie Reiserouten und Empfehlungen zur Seite stand.

In großem Maße sind Astrid Wies, Barbara Schulten und Elke Reinartz für meine Zeit am Insitut eine Bereicherung gewesen, sei es bei der Abwicklung von Verwaltungsfragen oder dem täglichen Laborbedarf, insbesondere aber auf der persönlichen Ebene.

Ganz besonders dankbar bin ich meiner Freundin Hannah, meinen Eltern, meiner Schwester und auch Hannahs Eltern für die bedingunglose Unterstützung, konstruktive Gespräche und ununterbrochenen Zuspruch vor, während und nach dieser turbulenten Zeit. Hannah trug hier eine besonders große Last, sowohl hier vor Ort, als auch in der Ferne. Danke!